Protein translocation across the Gram negative bacterial membrane

A Thesis submitted by

Wanatchaporn Arunmanee

For the Degree of Doctor of Philosophy

Institute for Cell and Molecular Biosciences

Newcastle University

January 2015

Abstract

Gram-negative bacteria are becoming increasingly resistant to many antibiotics. Unlike other bacteria, gram-negative bacteria have an additional membrane, the so-called outer membrane, which protects them from harmful agents. This membrane is highly asymmetric and contains tightly-packed lipopolysaccharides (LPS) in the outer leaflet and phospholipids in the inner leaflet. This thesis describes a study of the outer membrane protein F (OmpF) which is the most abundant porin present in the outer membrane of *Esherichia coli*. OmpF plays a key role in the organization of outer membrane and is also a receptor and translocator for colicins, which are antibacterial toxins. The aim of this project is to better understand the defensive barrier of gram-negative bacteria and find routes to pass through it by studying the interaction of OmpF with colicin N (ColN) and LPS. The solution structure of ColN and the OmpF-ColN complex in neutral detergents, studied by AUC and small-angle scattering (SAS), indicated that translocation and receptor binding domain of ColN (ColN-TR) became more compact when binding to outside of OmpF. Furthermore, OmpF in complex with the protein TolA, which forms part of the ColN translocon complex, was also studied by SAS. It showed that TolA bound to OmpF also became more compact though TolA remains a flexible structure. Furthermore, the interaction of OmpF with LPS was studied. Mutagenesis of positively-charged residues on OmpF was used to disrupt its electrostatic interaction with LPS. The findings suggested that OmpF has two LPS-binding sites and that OmpF binds to LPS via the minimal Lipid A moiety. This was supported by SAS data. Dynamic light scattering experiments indicated that OmpF, LPS and divalent cations form larger-scale structures, which are reminiscent of the outer membrane of bacteria. Alternative approaches for studying OmpF in amphipol (APol) and nanodisc were also utilised. OmpF/APol assembled as filaments in the absence of free APol but these converted into 2D arrays in the presence of LPS and calcium ions. OmpF could be incorporated into Nanodiscs, significantly increasing their diameters compared to empty Nanodiscs.

Acknowledgement

I would like to thank Prof. Jeremy Lakey for his continuous support of my Ph.D. study and research, warm guidance, expert advice and never ending encouragement throughout the years. I would not have made it to the end without his kind understanding.

All members of the Lakey research group from past and present, Dr. Ana Roque, Dr. Yan Huang, Hannah Alfonsa, Daria Stroukova, Alysia Davies and Tim Robson are thanked for their friendship, good advice and collaboration. They have made the lab a better and more enjoyable place to work. Dr. Chris Johnson and Dr. Andrei Soliakov are thanked for their knowledge and kind guidance. I would also like to thank Dr. Helen Waller for her knowledge and support throughout my study. She provided everything I need for running the experiments. She is always there to help me when I am faced with problems.

Collaborators in the small-angle scattering project, Dr. Alexandra Solovyova, Dr. Richard Heenan and Dr. Sarah Roger for help with running experiments and analysing the data. I would also like to thank STFC and ILL/ESRF for beamtime.

In addition, a thank you to Newcastle University's Electron Microscopy Research Services especially to Prof. J. Robin Harris for help with preparing and running samples under TEM.

I gratefully acknowledge the DPST Scholarship from the Royal Thai Government (RTG) that made my Ph.D. work possible.

Finally, I would like thank to my family and Naray Pewnim for their love and encouragement. For my parents who supported me to study the sciences and gave me a chance to pursue my dream of studying abroad even though I have to stay far away from home. I would also like to thank Naray for his kind support and patience during tough times especially in the final year of my study. I will always remember our good times we spent together in the UK and Europe.

Table of Contents

Abstract ..... **i**

Acknowledgement ..... **ii**

Table of Contents ..... **iii**

List of Figures ..... **vii**

List of Tables ..... **xi**

Abbreviation ..... **xiii**

Chapter 1 Introduction **1**

1.1 The outer membrane of gram-negative bacteria 1

1.1.1 Porins 3

1.1.2 Assembly of outer membrane proteins into the outer membrane 8

1.1.3 Lipopolysaccharides 14

1.2 Colicins 15

1.2.1 Structure and function relationship of Colicin N 17

1.2.2 Colicin N translocation across outer membrane 20

1.3 Alternative techniques for protein structure determination 22

1.4 Stabilising membrane proteins 28

1.5 Aim 30

Chapter 2 Materials and Methods **32**

2.1 Materials 32

2.1.1 Chemicals 32

2.1.2 Bacterial strains 32

2.2 General and biochemical protocols 33

2.2.1 Gel filtration chromatography 33

2.2.2 Ion exchange chromatography 33

2.2.3 Reconstitution of OmpF into Amphipols 34

2.2.4 Reconstitution of OmpF into Nanodiscs 35
2.2.5 Lipopolysaccharide Preparation 36
2.2.6 Sodium dodecylsulphate polyacrylamide gel electrophoresis……36
2.2.7 Western blotting 36
2.2.8 UV Spectrophotometry of proteins and DNA 37
2.3 Molecular biological techniques 38
2.3.1 Transformation of competent E. coli cells 38
2.3.2 Polymerase chain reaction (PCR) 38
2.3.3 In-Fusion HD cloning 39
2.3.4 Site-directed mutagenesis by polymerase chain reaction 41
2.4 Protein expression and purification 43
2.4.1 Expression of Histidine-tagged Colicin N-TR 43
2.4.2 Expression of Histidine-tagged TolA II-III 44
2.4.3 Expression of Histidine-tagged membrane scaffold proteins (MSP1E3D1) 44
2.4.4 Purification of Histidine-tagged proteins 44
2.4.5 Expression of wild-type OmpF 45
2.4.6 Production of deuterated OmpF 45
2.4.7 Production of mutant OmpF proteins 46
2.4.8 Extraction of OmpF from the outer membrane 46
2.4.9 Expression and isolation of OmpF inclusion bodies 47
2.4.10 Preparation of refolded OmpF 48
2.5 Biophysical methods 48
2.5.1 Analytical ultracentrifugation (AUC) 48
2.5.2 Dynamic light scattering (DLS) 49
2.5.3 Matrix assisted laser desorption/ionisation – time of flight - mass spectrometry (MALDI-TOF MS) 49

2.5.4 Small angle x-ray scattering (SAXS) 50
2.5.5 Small angle neutron scattering (SANS) 51
2.5.6 Transmission electron microscopy (TEM) 54
Chapter 3 Structural studies of the Colicin N translocon complex by small-angle neutron scattering 55
3.1 Introduction 55
3.2 Results 57
3.2.1 Protein production and purification 57
3.2.2 Match point determination of deuterated components 61
3.2.3 Examining on the deuteration level of deuterated protein 69
3.2.4 Understanding the solution behaviour of ColN-TR. 71
3.2.5 Uncovering the structure of OmpF/ColN-TR complex in neutral detergents by small-angle scattering 75
3.2.6 Structural characterisation of TolA II-III in solutions 79
3.2.7 Investigating the interaction of TolA II-III with OmpF in SDS 84
3.3 Discussion 89
Chapter 4 OmpF/LPS binding studies 94
4.1 Introduction 94
4.2 Results 97
4.2.1 Preparation of LPS-free OmpF 97
Production of Inclusion bodies 97
Refolding OmpF 99
4.2.2 OmpF/LPS in vitro binding studies 101
The OmpF/LPS complex formation studied by SDS-PAGE 101
The effect of divalent cations on LPS-LPS interaction studied by dynamic light scattering 105

Characterising the OmpF/LPS complex by small-angle x-ray scattering 107
4.2.3 Probing for LPS-binding sites of OmpF 110
Site-directed mutagenesis on the LPS binding sites of OmpF 110
The effect of OmpF mutagenesis on maturation of OmpF in *E. coli* 112
Characterising the OmpF/LPS complex by small-angle neutron scattering 119
4.3 Discussion 125
Chapter 5 Using novel approaches to study OmpF in native conditions 131
5.1 Introduction 131
5.2 Results 133
5.2.1 Incorporation of OmpF into Amphipols A8-35 133
Self-association of OmpF/APol complexes as filaments in the absence of free APol 133
Maturation of OmpF/APol filaments 136
Uncovering the solution structure of OmpF/APol complexes by SANS 138
The effect of LPS on the formation of OmpF/APol filaments 144
Study of the interaction of colicin N with OmpF/APol filaments 147
5.2.2 Analysis of OmpF inserted into model membranes, nanodiscs ...148
Expression and purification of membrane scaffold proteins 148
The preparation of nanodiscs 150
Examining the structure of OmpF reconstituted into nanodiscs 153
5.3 Discussion 161
Chapter 6 Conclusions and Future work 164
References 168

List of Figures

Figure 1.1 Overview of gram-negative bacterial cell envelope.....2
Figure 1.2 High resolution structures of outer membrane proteins in different families from *E. coli*.....6
Figure 1.3 Crystal structure of OmpF determined at 2.4 Å resolution. 7
Figure 1.4 The diagram shows the channel constriction by loop 3 acidic residues and barrel wall basic residues of wild-type OmpF. 8
Figure 1.5 Schematic of biogenesis and chaperoning for outer membrane proteins in *E. coli*.....12
Figure 1.6 Structure and biosynthesis of core oligosaccharide of rough LPS in *E. coli* K-12.....15
Figure 1.7 Domain composition of colicins found in both pore forming and nuclease colicins.....17
Figure 1.8 Crystal structure of colicin N (PDB code: 1A87).. 18
Figure 1.9 Crystallographic structures of pore-forming colicins (Ia, N and B) compared to nuclease colicins (E3).. 19
Figure 1.10 Schematic of the translocation pathway of colicin N across OM. The route of Colicin N. 22
Figure 1.11 Schematic illustration of a standard SAS experiment 24
Figure 1.12 Theoretical scattering profiles and P(r) functions from simple geometrical shapes. 26
Figure 1.13 Contrast variation technique used to study the binary complex in small angle neutron scattering 27
Figure 2.1 Schematic representation shows the trapping of OmpF with amphipols adapted from Zoonens *et al*.....35
Figure 2.2 Overview of In-Fusion HD cloning technique. 40
Figure 2.3 Schematic representation of site-directed mutagenesis approach...42
Figure 3.1 SDS-PAGE of dOmpF preparations from *E. coli* BE3000. 58
Figure 3.2 SDS-PAGE of ColN-TR expression and purification. 59
Figure 3.3 Purification of ColN-TR by cation exchange chromatography.....60
Figure 3.4 SDS-PAGE analysis of TolA II-III expression and purification. 61

Figure 3.5 Structure and chemical composition of hydrogenated and deuterated detergents.. 63
Figure 3.6 SANS data for h/d OG mixture in four D_2O solutions.. 67
Figure 3.7 Experimental determinination of contrast match point of deuterated OmpF by SANS. 69
Figure 3.8 MALDI-TOF-MS of full length hydrogenated and deuterated OmpF. 70
Figure 3.9 Sedimentation velocity of ColN-TR. 71
Figure 3.10 SAXS data for ColN-TR. 72
Figure 3.11 EOM analysis of ColN-TR.. 74
Figure 3.12 SANS data for dOmpF/ColN-TR complexes in 1% h/d OG. 76
Figure 3.13 Stuhrmann analysis of dOmpF/ColN-TR complex. 78
Figure 3.14 The structure of TolA from *E. coli.* 79
Figure 3.15 Sedimentation velocity of TolA II-III.....80
Figure 3.16 SAXS data for TolA II-III.....81
Figure 3.17 Theoretical SAXS profiles of TolA II-III models generated from CRYSOL fitted against the experimental SAXS profiles. 82
Figure 3.18 EOM analysis of TolA II-III. 83
Figure 3.19 SDS-PAGE of OmpF/TolA II-III complex.....85
Figure 3.20 SANS data for dOmpF/TolA II-III complexes in 1% h/d SDS. 86
Figure 3.21 Stuhrmann analysis of dOmpF/TolA II-III complex.....88
Figure 3.22 Proposed model for OmpF/TolA II-III complex in solution. 88
Figure 3.23 Comparison between the possible model of OmpF/TolA complexes and the crystal structure of TolC. 93
Figure 4.1 Proposed LPS binding sites for OmpF.....95
Figure 4.2 Crystal structure of FhuA with bound LPS 96
Figure 4.3 Expression and identification of OmpFΔSS (WT OmpF without signal sequence) from inclusion bodies 98
Figure 4.4 Purification of OmpFΔSS using anion exchange chromatography. .99
Figure 4.5 The SDS-PAGE analyses of refolded OmpFΔSS in the presence of DG and DDM.. 100
Figure 4.6 Crystallographic structure of refolded OmpF.. 101
Figure 4.7 *In vitro* study of LPS-free OmpF binding to Ra-LPS. 103

Figure 4.8 Interaction of OmpF with Ra-LPS in the presence and absence of divalent cations. 104
Figure 4.9 Size distribution of OmpF/Ra-LPS and Ra-LPS determined by DLS and expressed by volume in solution with and without divalent cations.. 106
Figure 4.10 Size distribution of OmpF/Ra-LPS in solution by DLS and expressed as volume as a function of Ca^{2+} concentration. 107
Figure 4.11 Scattering data for OmpF with and without LPS.. 109
Figure 4.12 Localisation of basic residues on OmpF trimer and SDS-PAGE analysis of OmpF mutants. 111
Figure 4.13 SDS-PAGE of GlnA OmpF preparations from *E. coli* BZB1107…114
Figure 4.14 SDS-PAGE of Gln B OmpF preparations from *E. coli* BZB1107.. 115
Figure 4.15 SDS-PAGE analysis for OmpF mutants expressed as inclusion bodies. 117
Figure 4.16 SDS-PAGE analysis of OmpF/LPS complexes at 1:5 OmpF/LPS molar ratio in the presence and absence of divalent cations.. 118
Figure 4.17 Experimental determination of contrast match point of Ra-LPS by SANS.. 120
Figure 4.18 SANS data for dOmpF/Ra-LPS complexes in 0.5% h/d SDS.. 120
Figure 4.19 Stuhrmann analysis of dOmpF/Ra-LPS complex.....121
Figure 4.20 Three possible models of OmpF/LPS complexes.. 122
Figure 4.21 Theoretical SANS profiles of OmpF/LPS model generated from CRYSON fitted against the experimental SANS profiles.....124
Figure 4.22 Sequence alignment of proteins demonstrating the homology between OmpF from *E. coli* and OmpC from *Enterobacter cloacae.*. 129
Figure 4.23 Conserved residues of OmpF having a direct contact with LPS.. 130
Figure 5.1 Structure of amphipol (A8-35).. 131
Figure 5.2 Schematic representation of nanodisc structure.. 132
Figure 5.3 Elution profiles of OmpF/APol complexes formed at different OmpF/APol w/w ratios and amphipols A8-35.....134
Figure 5.4 Removal of free APol by SEC led to the self-organisation of OmpF/APol complexes as filaments. 135
Figure 5.5 Progression of filament formation by OmpF/Apol complexes after depletion of free APol 137

Figure 5.6 SANS data for free hAPol. 140
Figure 5.7 SANS data for each component of OmpF/APol complexes after removing free APol by SEC. 141
Figure 5.8 SANS data for the whole OmpF/APol complexes after removing free APol by SEC.. 143
Figure 5.9 Effect of Lipopolysaccharides on the structure of OmpF/APol complexes without free Apol. 146
Figure 5.10 SEC profiles of OmpF/ColN/APol complexes at various OmpF/ColN molar ratios. 147
Figure 5.11 EM study of OmpF/ColN/APol complexes at 3:1 OmpF/ColN molar ratio. 148
Figure 5.12 SDS-PAGE of MSP1E3D1 expression and purification.. 149
Figure 5.13 MALDI-TOF MS of trypsin digested MSP1E3D1. 150
Figure 5.14 Analysis of OmpF-inserted nanodisc by gel filtration and SDS-PAGE.. 151
Figure 5.15 TEM images of OmpF-loaded nanodiscs. 152
Figure 5.16 Analysis of nanodiscs by SEC and DLS. 154
Figure 5.17 Study on empty and OmpF DMPG nanodiscs by EM. 155
Figure 5.18 Sedimentation coefficient distribution c(s) of nanodiscs. 156
Figure 5.19 SAXS data for empty DMPG nanodiscs. 157
Figure 5.20 SAXS data for OmpF in DMPG nanodiscs. 158
Figure 5.21 SANS data for empty and OmpF DMPG nanodiscs. 160

List of Tables

Table 1.1 Families of porins from *E. coli*. 4
Table 1.2 Summary of receptors, translocators and cytotoxic activity of known colicins. 16
Table 1.3 Classification of detergents used in the solubilisation of membrane proteins 29
Table 2.1 List of specialist chemicals and respective suppliers 32
Table 2.2 Bacterial strains for the expression of protein in this study 33
Table 2.3 The theoretical extinction coefficients and molecular weights of proteins used for the determination of protein concentrations. 38
Table 2.4 PCR reaction mixture 39
Table 2.5 PCR reaction conditions....39
Table 2.6 Sequences of oligonucleotides primers used for In-Fusion cloning of OmpF 41
Table 2.7 In-Fusion cloning reaction mixture 41
Table 2.8 Sequences of oligonucleotides primers used for site directed mutagenesis of OmpF. Mutation sites are highlighted in red. 43
Table 2.9 Recipe of minimal media for the production of deuterated OmpF (Meilleur *et al.*, 2009). 46
Table 2.10 The ratio of octyl glucosides in all D_2O solution used in SANS study 52
Table 3.1 List of samples for the structural studies by SAXS and SANS 56
Table 3.2 Coherent neutron scattering length of atoms for SLD calculation. 64
Table 3.3 Parameters of detergents for determining contrast match point....65
Table 3.4 Ratio of octyl glucosides in all D_2O solution used in SANS study 66
Table 3.5 Summary of structural parameters for dOmpF/ColN-TR complexes, 77
Table 3.6 Summary of all parameters derived from Guinier plot and P(r) function for OmpF/TolA II-III complexes. 87
Table 4.1 Summary of all parameters derived from Guinier plot and P(r) function for OmpF and OmpF/LPS complexes in the presence of DDM 110
Table 4.2 List of OmpF mutants in this study 112

Table 4.3 Summary of OmpF mutants created by In-Fusion cloning technique. 113
Table 4.4 Summary of the expression and maturation *in vivo* of OmpF mutants. 116
Table 4.5 Summary of goodness of fit of various OmpF/LPS models to experimental data obtained from CRYSON 123
Table 5.1 Summary of SAXS structural parameters for empty and OmpF nanodiscs by Guinier approximation and P(r) function.....158
Table 5.2 Summary of SANS structural parameters for empty and OmpF nanodiscs by Guinier approximation and P(r) function.....160

Abbreviation

APol	Amphipol
AUC	Analytical Ultracentrifugation
CMC	Critical micelle concentration
CMP	Contrast match point
DDM	Dodecyl maltoside
DLS	Dynamic light scattering
DMPC	1,2-dimyristoyl-sn-glycero-3-phosphocholine
DMPG	1,2-dimyristoyl-sn-glycero-3-phospho-(1'-rac-glycerol)
DG	n-dodecyl-β-D-glucopyranoside
EM	Electron Microscopy
LB	Luria-Bertani
LPS	Lipopolysaccharides
IB	Inclusion bodies
IM	Inner Membrane
IMP	Inner Membrane Protein
IPTG	isopropyl β-D-thiogalactoside
ITC	Isothermal Titration Calorimetry
MSP	Membrane scaffold protein
MP	Membrane protein
NMR	Nuclear Magnetic Resonance
OBS	OmpF Binding Site
octyl-POE	Octyl-polyoxyethylene

OG	Octyl glucoside
OM	Outer Membrane
OMP	Outer Membrane Protein
SAS	Small Angle Scattering
SANS	Small angle neutron scattering
SAXS	Small angle x-ray scattering
SDS	Sodium dodecylsulfate
SEC	Size exclusion chromatography
SLD	Scattering length density
SPR	Surface Plasmon Resonance
WT	Wild type
TEM	Transmission electron microscopy
TOF	Time of flight

Chapter 1 Introduction

1.1 The outer membrane of gram-negative bacteria

The cell envelope of gram-negative bacteria, such as *Escherichia coli* and *Pseudomonas aeruginosa,* is different from other types of bacteria as shown in Figure 1.1. Gram-negative bacterial cells are surrounded by two lipid bilayers which are called the inner and outer membranes. The inner membrane is the cytoplasmic membrane containing phosphatidylethanolamine (70-80%), phosphatidylglycerol and cardiolipin evenly distributed in both leaflets (Koebnik *et al.*, 2000). In contrast to the inner membrane, the outer membrane is highly asymmetric as the leaflets contain different lipid compositions. The outer leaflet is composed of lipopolysaccharides (LPS) only whereas the lipid composition of inner leaflet is the same as the cytoplasmic membrane. The compartment between these two lipid bilayer membranes is the periplasm, which contains the peptidoglycan layer.

The outer membrane is considered as a defensive barrier of gram-negative bacterial cells. It protects the cells from harmful agents such as proteases, bile salts, antibiotics as well as toxins. In addition to serving as a barrier, the outer membrane is responsible for transporting small hydrophilic solutes including nutrients from the environment into and out of the cell. This membrane is often described as leaky as a large number of channel-forming proteins called 'Porins' allow non-specific permeability of water soluble molecules < 600 Da across the membrane (Rosenbusch, 1974; Jaroslawski *et al.*, 2009).

Apart from porins in *E. coli*, there are other integral membrane protein families such as the TonB-dependent receptors and small β-barrel anchors. The outer membrane proteins in the TonB-dependent receptor family play a key role in the uptake of large substrates such as iron-siderophore complexes or vitamin B_{12}. The import of these substrates across the outer membrane is energy dependent. Examples of a protein from this family are FhuA and BtuB. (Nikaido, 2003). On the other hand, the function of proteins in the small β-barrel anchor

family does not involve substrate transport. For example, OmpA is one of the major outer membrane proteins of *E. coli*. The role of OmpA is to maintain the integrity of the bacterial cell surface. It has a specific interaction with the peptidoglycan layer to form the linkage between the outer membrane and the peptidoglycan layer in the periplasm (Demot and Vanderleyden, 1994; Koebnik, 1995). Another integral membrane protein of this type is OmpX. It belongs to a highly-conserved bacterial protein family which promotes the adhesion of bacteria to mammalian cells and protects bacteria from the immune system (Heffernan *et al.*, 1994).

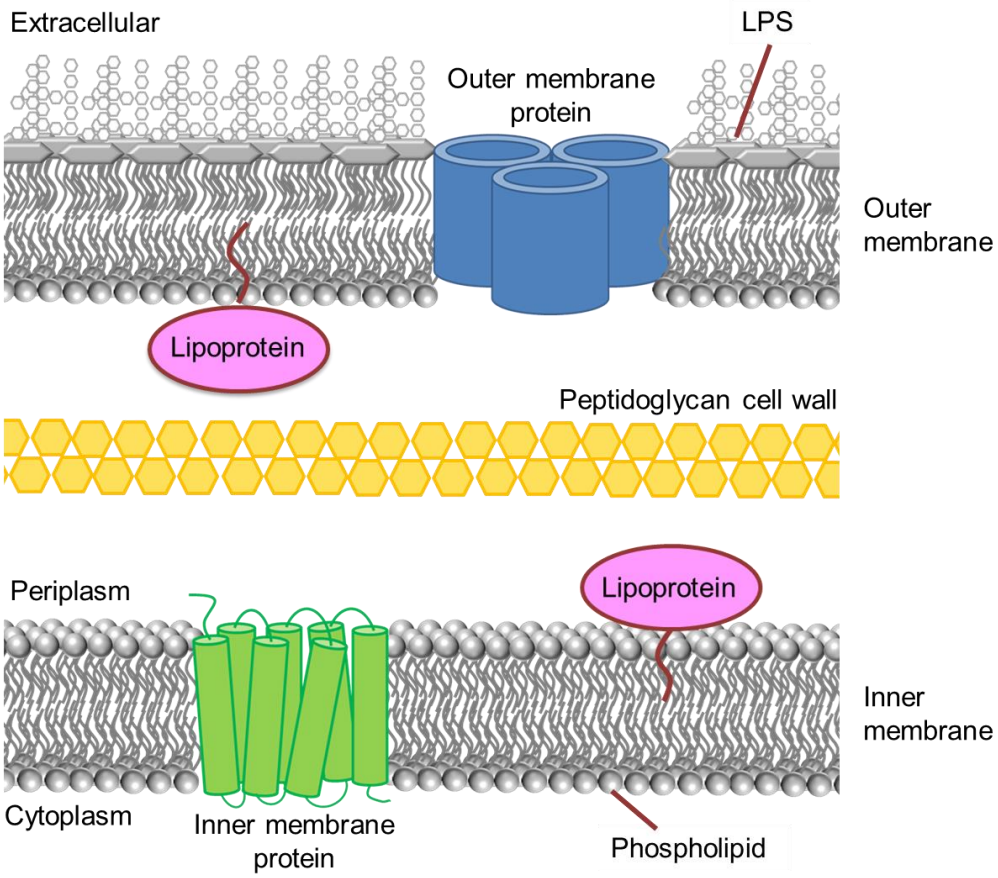

Figure 1.1 Overview of gram-negative bacterial cell envelope. It is composed of two lipid bilayer membranes separated by the periplasmic space.

1.1.1 Porins

Among integral membrane proteins in the *E. coli* outer membrane, the channel-forming proteins or porins, are the most abundant. The *E. coli* porin protein was first isolated by Rosenbusch in 1974 (Rosenbusch, 1974). However, the term porin was not proposed to describe this class of proteins until 1976 when Nakae discovered their channel forming properties (Nakae, 1976). Porins are exploited by antibacterial agents such as bacteriophages and bacteriocins to enter the cells as they are exposed at the cell surface. Porin-like proteins can be commonly found in every species of gram-negative bacteria. In addition to the outer membrane, porins were discovered in mitochondria (Schein *et al.*, 1976; Zalman *et al.*, 1980) and peroxisomes from eukaryotes (Reumann *et al.*, 1995; Reumann *et al.*, 1996; Reumann *et al.*, 1998). This similarity derives from the probable common origin of these organelles and bacteria through the endosymbiotic theory of eukaryotic evolution (Zimorski *et al.*, 2014). However, in this study, we only focus on porins found in the outer membrane of *E. coli*.

Families of porins

There are two families of porins present in the outer membrane of *E. coli*. They can be separated into two categories, specific and non-specific/general porins (Table 1.1). The general porins are expressed at high levels, hence general porins are the most abundant integral membrane proteins found in the outer membrane of *E. coli*. The characteristic feature of general porins is that they show no particular substrate specificity. General porins allow the influx and efflux of small and hydrophilic molecules. The molecules, up to 600 Da, can diffuse through the general porins which include OmpF, OmpC and PhoE. They form homotrimers in the outer membrane and share 70% sequence similarity. Even though they are similar in structure and sequence, they differ in the preference for charge and size of solute passing through their pores. OmpF and OmpC prefer cations over anions but PhoE prefers anions. OmpF pores are less cation selective than OmpC. In contrast to general porins, specific porins are expressed for the uptake of specific substrate. The best-studied example is

maltoporin (LamB) which is specific to the diffusion of maltooligosaccharide. The specificity of maltoporin was confirmed by the liposome swelling assay. It showed a higher uptake rate for maltose and maltodextrins compared to sucrose (Luckey and Nikaido, 1980).

The expression of porins is regulated by several environmental parameters. PhoE expresses only in the shortage of phosphate and has been termed Phosphoporin (Tommassen and Lugtenberg, 1982). In case of OmpF and OmpC, high osmotic strength and high temperature up regulate the production of OmpC (which is also called Osmoporin) but these conditions repress the production of OmpF (Pratt *et al.*, 1996). The expression of Maltoporins (LamB) also depends on environmental conditions. Under carbohydrate-starving conditions, the production of LamB is strongly activated (Death *et al.*, 1993).

Table 1.1 Families of porins from *E. coli*.

Families of porins	Example	Function	Regulation of expression
Non-specific/general	OmpF	Cation transport	Low osmotic strength and low temperature
	OmpC	Cation transport	High osmotic strength and high temperature
	PhoE	Anion transport	Phosphate-starvation
Specific	LamB	Maltose and Maltodextrin uptake	Carbohydrate-starvation

Structures of porins

The first high-resolution structure of porins at 1.8 Å, resolved by x-ray crystallography, was from *Rhodobacter capsulatus* (Weiss *et al.*, 1991; Weiss and Schulz, 1992). Soon after this first structure was published, the structures of OmpF and PhoE from *E. coli* were elucidated by x-ray crystallography at the resolution of 2.4 Å and 3.0 Å (Cowan *et al.*, 1992). The crystal structures of

several porins from *E. coli* have been reported such as OmpC at 2.0 Å (Basle *et al.*, 2006) and LamB at 3.1 Å (Schirmer *et al.*, 1995). Figure 1.2 displays the high resolution structures of *E. coli* outer membrane proteins from different families.

As predicted earlier by Jeanteur *et al* (Jeanteur *et al.*, 1991), the porin structure contains a 16 stranded β-barrel for general porins and 18 stranded β-barrel for specific porins (LamB). Other outer membrane proteins, OmpA and FhuA form 8 and 22 stranded β-barrel. The β-strands of porins are tilted and this helps to generate and stabilise the water filled transmembrane channel. Each transmembrane strand is connected by short turns at the periplasmic side whereas long flexible loops connect the β-strands at the external side. The long loop on the extracellular side can fold back into the water-filled channel of porins. Loop three enters and constricts the barrel and this is called the eyelet region. In these pore-forming β-barrels the interior of the barrel is tightly covered with more hydrophilic residues when compared to the exterior of the barrel which faces the hydrophobic membrane. These residues control diffusion through the porins. The size of the eyelet region varies depending on the specificity of porins. The top view of outer membrane proteins in Figure 1.2 reveals that the general porin (OmpF) with no specific substrate forms a larger pore than the specific porin (LamB) (Schirmer *et al.*, 1995).

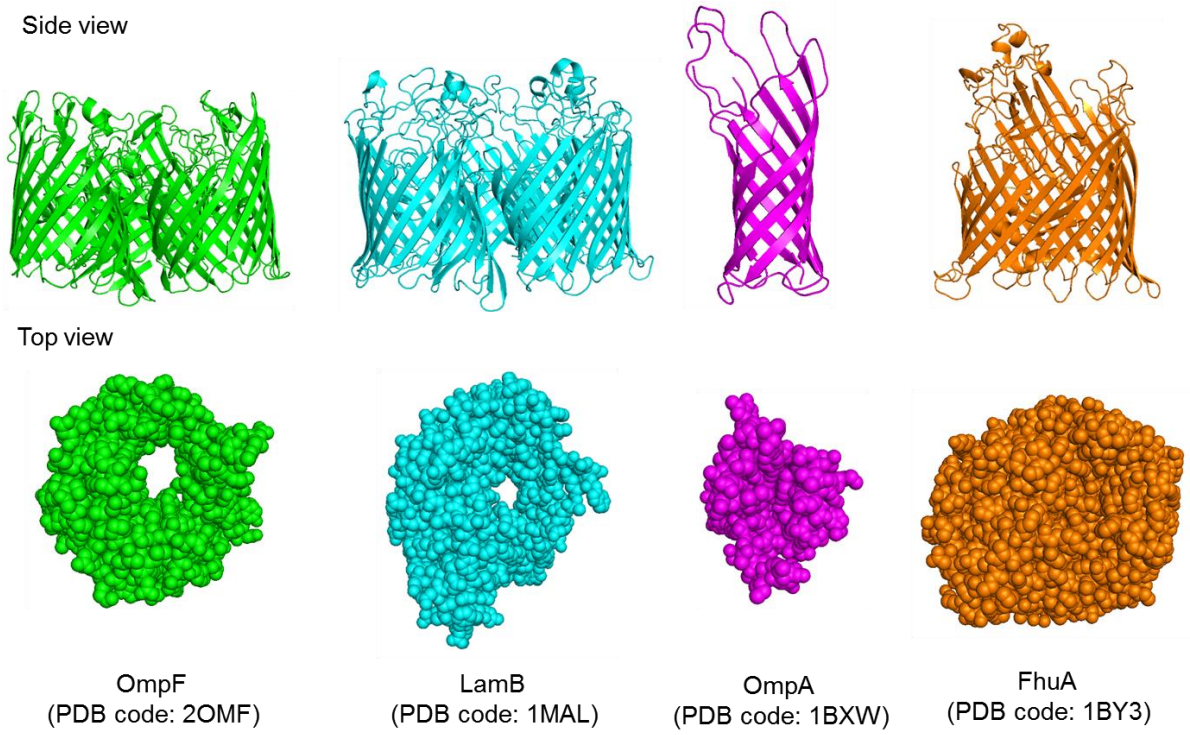

Figure 1.2 High resolution structures of outer membrane proteins in different families from *E. coli*. Upper views are side views of OmpF and LamB as trimers and OmpA lacking its periplasmic domain. The upper part of proteins faces the extracellular side. The lower space filling views are of monomers for all the proteins. View from the extracellular side onto the monomer of proteins.

Structure and function of OmpF

OmpF (or Matrix Porin) is the major porin of the *E. coli* outer membrane (Rosenbusch, 1974) and as discussed earlier, it is a member of the general porin family which allows the non-specific diffusion of small hydrophilic molecules across the outer membrane. OmpF is also a receptor and a translocator of several bacteriocins (Evans *et al.*, 1996a; Cascales *et al.*, 2007). OmpF is a symmetric trimer composed of three copies of a 340-residue monomeric unit whose structure is a β-barrel of 16 amphipathic β-strands (Figure 1.3a) (Cowan *et al.*, 1992). There are 8 extended loops on the extracellular side of the barrel monomer and 8 tight turns on the periplasmic side. In contrast to the other extended loops, the third loop (L3) connects β-strands 5 and 6 and folds inside the OmpF barrel to narrow the channel (Figure 1.3b shown in cyan). The longest dimension of the eyelet region is about 11 Å.

Loop 2 (Figure 1.3b shown in red) bending over to the adjacent monomer is essential for OmpF stability (Phale *et al.*, 1998).

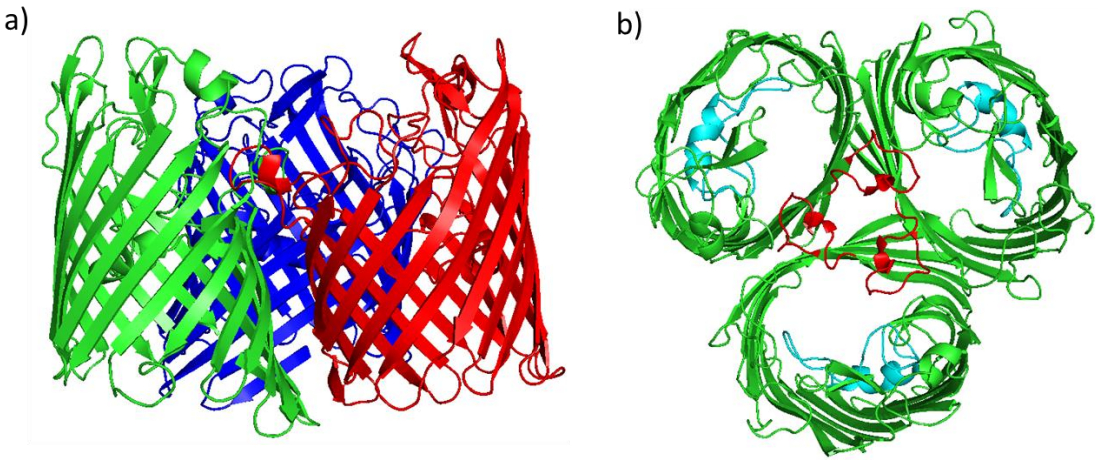

Figure 1.3 Crystal structure of OmpF determined at 2.4 Å resolution (PDB code: 2OMF). a) side view. OmpF is a homotrimer whose monomer is represented by each colour. b) top view. Latching loop 2 in red, eyelet loop 3 in cyan.

Due to the fact that this long polypeptide loop narrows the pore to create the constricted region within the OmpF pore, L3 influences permeability properties such as channel diameter and electrostatic properties. The acidic residues, Asp113, Glu117 and Asp121 in this loop, and the basic residues Lys16, Arg42, Arg82 and Arg132 on the barrel wall protrude and lead to a restriction in the size of channel (Figure 1.4). The influence of these charges on ionic conductance as well as colicin interaction was studied by mutation (Phale *et al.*, 2001; Bredin *et al.*, 2003). They revealed that ion diffusion across the porin is dependent on pore geometry and charge. Additionally, Asp113 appeared to be essential for Colicin A activity whereas Colicin N activity is influenced by Asp121.

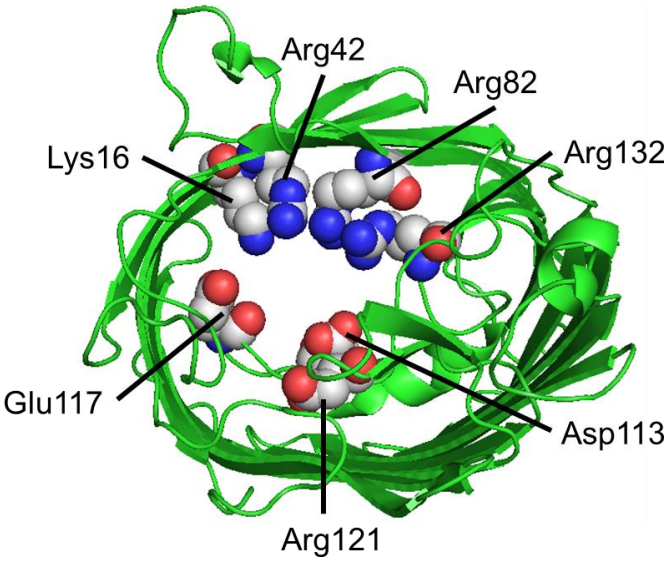

Figure 1.4 The diagram shows the channel constriction by loop 3 acidic residues and barrel wall basic residues of wild-type OmpF. View from the extracellular side onto the OmpF monomer. Carbon, nitrogen and oxygen atoms are shown in white, blue and red, respectively.

1.1.2 Assembly of outer membrane proteins into the outer membrane

Integral membrane proteins in gram negative bacteria are synthesized in the cytosol. To reach their site of action, these membrane proteins must be targeted and assembled into the membrane. When they are folded into the correct conformations in the membrane, they are able to function properly. Integral membrane proteins are classified into two types based on their location in the membrane. Two classes of gram negative bacterial membrane proteins are inner membrane proteins (IMP) and outer membrane proteins (OMP).

The assembly of IMP is not as complicated as that of OMP as IMP inserts and folds within one membrane. IMPs are directed to the inner membrane (IM) using the SRP-targeting pathway. The process is then followed by the insertion into the membrane using SecYEG translocase and YidC insertase embedded within the IM (Dalbey *et al.*, 2011). The folding of IMP is assisted by YidC and phospholipid phosphatidylethanolamine (PE) (Dalbey *et al.*, 2011). In contrast to the assembly of IMPs, that of OMPs is a unique case as OMPs must cross the IM and fold in the outer membrane (OM). In the following sections, the

assembly of OMPs will be described in detail (For a recent review, see (McMorran *et al.*, 2014)). Understanding the OMP biogenesis would help to explain why the disruption of OmpF-LPS interaction has an effect on the assembly of OmpF (see Chapter 4).

Transporting OMP across the periplasm

Synthesised OMPs in an unfolded state are directed to IM by the aid of the molecular chaperone SecB (Driessen and Nouwen, 2008). The translocation of OMPs across IM is mediated by the same translocation complex as IMPs, SecYEG (Rapoport, 2007; Driessen and Nouwen, 2008). Prior to insertion and folding into OM, secreted OMPs in non-native conformations are protected by periplasmic folding factors during their transit through the periplasm. (Mogensen and Otzen, 2005). These folding factors are proteins which facilitate OMP biogenesis by stabilizing unfolded OMPs (chaperones), catalyzing rate-determining steps in OMP folding (folding catalysts), and serving as proteases (Mogensen and Otzen, 2005). To date, the well-characterised periplasmic folding factors are SurA, Skp and DegP which are known as the key periplasmic assistants of OMP biogenesis. It is believed that there are two parallel chaperone pathways for OMP assembly; SurA and Skp/DegP pathways (Sklar *et al.*, 2007; Denoncin *et al.*, 2012).

SurA is a periplasmic chaperone first identified in 1990 as a protein required for the survival of *E. coli* during the stationary phase (Tormo *et al.*, 1990). It was shown to take part in OMP biogenesis since a defect in OMP folding was caused by the lack of SurA *in vivo.* The OMP folding was observed utilising a trypsin sensitivity assay as folded OMPs are less susceptible to trypsin degradation than unfolded OMPs (Lazar and Kolter, 1996). The decrease in the production of several OMPs including OmpF was also found in *surA* deleted strains (Merdanovic *et al.*, 2011). The binding motif of SurA is an aromatic rich sequence containing an Ar-X-Ar motif investigated by binding studies with peptide sequences (Bitto and McKay, 2003; Hennecke *et al.*, 2005). SurA recognises OMPs using this motif, which is mostly present in the C-terminal

regions of OMPs (Merdanovic *et al.*, 2011). The specificity of SurA binding to unfolded OMPs was also shown by competitive ELISA (Bitto and McKay, 2004).

Skp (17 kDa protein) also serves as a periplasmic chaperone assisting in the OMP biogenesis pathway. The lack of Skp *in vivo* moderately reduced the amount of OMPs (Chen and Henning, 1996). It was recently reported that Skp interacts strongly with unfolded OMPs (Qu *et al.*, 2007). The Skp/DegP deleting strain displayed the accumulation of protein aggregates in the periplasm. This suggests that Skp protects OMPs from aggregation before folding (Schafer *et al.*, 1999). Additionally, a putative LPS-binding site on Skp, similar to that of FhuA, was determined because Skp possesses a cluster of basic side chains which could interact strongly with an anionic molecule (Walton and Sousa, 2004).

There is conclusive evidence supporting the hypothesis of parallel pathways in OMP assembly. Either *surA* or *skp* deleting mutants are viable, but mutants lacking in SurA/Skp and SurA/DegP are not viable. Therefore, it was concluded that SurA and Skp are not essential and these SurA and Skp/DegP pathways are redundant (Rizzitello *et al.*, 2001). Although these pathways have the same function in OMP assembly, SurA pathway is thought to be the primary chaperone for OMP transport while Skp/DegP can rescue OMPs from the normal pathway under stressful conditions (Sklar *et al.*, 2007). Sklar and colleagues showed that major OMPs preferred SurA to Skp/DegP pathways. They monitored the rate of OMP assembly and found that the OMPs in *skp/degP* mutant folded faster than those in *surA* mutant. Moreover, depletion of SurA led to a massive decrease in OM density whereas lack of Skp and DegP showed no effect on OM composition (Sklar *et al.*, 2007). Recently, these findings were also confirmed by Denoncin *et al.,* 2012. They demonstrated by proteomics that depletion of SurA has a strong effect on the levels of OMPs while removal of Skp has no impact (Denoncin *et al.*, 2012).

Inserting into the outer membrane

To insert and fold into the OM, OMPs are delivered to the BAM (β-barrel assembly machinery) complex by periplasmic chaperones. The BAM complex is responsible for OMP assembly into the OM. The BAM complex in *E. coli* is a hetero-oligomer consisting of a large β-barrel OMP, BamA and four lipoproteins, BamB, C, D, and E (Knowles *et al.*, 2009). BamA is an essential protein found in all gram-negative bacteria. It plays a vital role in OMP assembly. Removal of BamA is lethal to bacterial cells due to the accumulation of aggregated OMPs in the periplasm (Voulhoux *et al.*, 2003). The structure of bacterial BamA contains an N-terminal soluble region and a C-terminal β-barrel domain. The N-terminal soluble region has five polypeptide transport-associated (POTRA) domains (K. H. Kim *et al.*, 2012). The crystal structures of POTRA 1-4 showed they have identical folds despite no sequence similarity. POTRA serves as a scaffold for the binding of lipoproteins to BamA leading to the formation of the BAM complex (S. Kim *et al.*, 2007). Among the four lipoproteins (BamB, C, D, and E), only BamD is essential for cell viability in *E. coli.* BamD binds to BamA using POTRA 5 and the activity of BamA is controlled by BamD (K. H. Kim *et al.*, 2012; Ricci *et al.*, 2012; Rigel *et al.*, 2013). For these reasons, BamD is also important in the assembly of OMPs.

Several mechanisms of OMP assembly via the BAM complex have been proposed however it is still controversial. One of them suggested that the formation of BamA oligomer may generate a pore in the OM which OMP can insert. Alternatively, OMPs may cross the OM and insert into the OM from the extracellular side or OMPs may exploit BamA as a scaffold for the formation of β-sheet during its folding (K. H. Kim *et al.*, 2012). However, recent crystallographic structures of BamA from two distinct organisms indicated that the barrel domain of BamA has an interior cavity which is large enough for OMP entry. The OMP then exits the cavity into the OM using the lateral gate of BamA predicted by molecular dynamics simulations (Noinaj *et al.*, 2013). A lateral opening of BamA barrel domain is essential for BamA function as the inhibition of lateral opening by disulphide crosslinking led to a loss of BamA function. The

formation of substrate exit pore above the lateral gate is also required for BamA function (Noinaj *et al.*, 2014). According to these recent evidences, Noinaj and colleagues has proposed the mechanism of OMP folding by BAM complex. The unfolded OMPs are delivered to BAM complex and then interact with the POTRA domains. After entering into the barrel domain of BamA, the unfolded OMPs insert into the lateral gate and form β-strands. The formation of loops take place at the substrate exit pore. Once the formation of strands and loops completes, folded OMPs are released into the OM (Noinaj *et al.*, 2014). Figure 1.5 displays the pathway of OMP assembly from cytosol to OM.

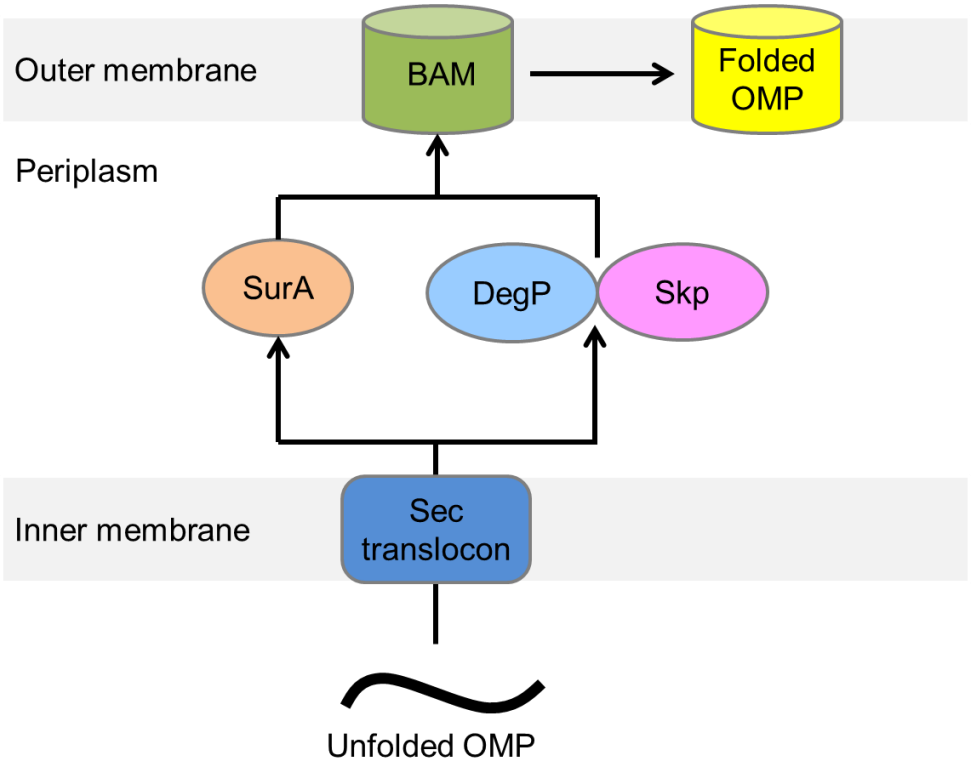

Figure 1.5 Schematic of biogenesis and chaperoning for outer membrane proteins in *E. coli*. Unfolded outer membrane proteins (OMPs) synthesised in the cytosol are targeted to SecYEG for translocation across the inner membrane. To transport through the periplasm, OMPs are assisted by periplasmic chaperones from two parallel pathways, SurA and Skp/DegP. OMPs are then directed to the BAM complex which helps the insertion and folding into the outer membrane. Adapted from (Knowles *et al.*, 2009).

Role of LPS on the assembly of outer membrane proteins

The impact of LPS on OMP biogenesis is taken into consideration because mutants expressing truncated LPS showed the reduction of OMP levels in *E. coli* and *Salmonella typhimurium*. LPS is thought to be a molecular chaperone aiding the assembly of porins (Bos *et al.*, 2007). This is supported by several studies of OMP assembly *in vitro* and *in vivo.* The inhibition of OmpC and OmpF biogenesis was observed when blocking fatty acid synthesis by cerulenin. (Ried *et al.*, 1990). Consistent with this, the amount of porins decreased in mutants producing deep rough LPS (Sen and Nikaido, 1991). In addition to the decrease in the production of porins, the rate of OmpF and LamB assembly became slower in mutants of *E. coli* K-12 expressing deep rough LPS. The molecule of deep rough LPS lacks most of oligosaccharide parts (Laird *et al.*, 1994). *In vitro* folding of some OMPs also requires LPS. For example, the mature trimeric conformation of OmpF successfully folded in the presence of LPS (Sen and Nikaido, 1990), the trimerisation of OmpF did not occur when using deep rough LPS (Sen and Nikaido, 1991), and the folding of PhoE monomer, appearing to be an assembly intermediate, was facilitated by LPS in the presence of detergents and divalent cations (deCock and Tommassen, 1996).

As a putative LPS binding site was discovered in the high resolution structure of Skp (Walton and Sousa, 2004), LPS may be involved in the Skp pathway of OMP assembly. It has been shown that the folding of OmpA into lipid bilayers requires both Skp and LPS (Bulieris *et al.*, 2003). The conformation of OmpA in OmpA/Skp complex changed upon binding to LPS. This aided the insertion and folding of OmpA into the membrane (Qu *et al.*, 2009). However, a putative LPS binding site of Skp was also found in *N. meningitides* but OMP biogenesis in this organism does not depend on LPS (Bos *et al.*, 2007). Therefore, further studies on the role of LPS in this pathway of OMP assembly are still required.

1.1.3 Lipopolysaccharides

In early studies, LPS was known to be one of the components in the cell envelope of gram-negative bacteria and the improvement of sucrose gradient centrifugation for the separation of the OM and IM showed that LPS was only found in the OM (Osborn *et al.*, 1972a). This is followed by the localisation of LPS on the outer leaflet of OM, hence LPS is the main lipid of the outer leaflet of OM found in all gram negative bacteria (Muhlradt and Golecki, 1975; Kamio and Nikaido, 1976). The LPS structure is comprised of three parts: lipid A, a highly conserved oligosaccharide core and a long repeating oligosaccharide (O-antigens). The structures of O-antigens are variable even within the same species (Raetz and Whitfield, 2002). LPS is categorised into smooth LPS and rough LPS. Smooth LPS contains a repeating O-antigen unit but rough LPS does not. The structure of rough LPS is shown in Figure 1.6. Lipid A has several saturated fatty acid chains which give rise to tight-packing of LPS compared to normal phospholipids (Ruiz *et al.*, 2009). The packing of LPS is mediated by divalent cations such as calcium and magnesium ions. This tightly-packed LPS leads to the low fluidity and permeability of OM which prevents the diffusion of hydrophobic molecules such as antibiotics and detergents (Ruiz *et al.*, 2009).

LPS has been shown to be essential for cell viability. Mutants expressing LPS defects were more sensitive to antibiotics (Tamaki *et al.*, 1971; Sanderson *et al.*, 1974; Vaara, 1993). The KDO_2-lipid A was the shortest LPS required for bacteria survival (Raetz and Whitfield, 2002). Osborn *et al* demonstrated that the biosynthesis of LPS in *Sallmonella typhimurium* occurs in the IM (Osborn *et al.*, 1972b). The pathway of LPS biogenesis known as the Raetz pathway was characterised by Raetz and colleagues. The KDO_3-lipid A is synthesised in the cytoplasm. Then, the sugars in the core oligosaccharides of LPS are added sequentially by enzymes at the inner leaflet of IM. Figure 1.6 represents the collection of genes involved in the assembly of core oligosaccharides of LPS in *E. coli* K-12. These genes are encoded for the enzymes which are responsible for the addition of sugar moieties to the core oligosaccharide of LPS (Johnson *et al.*, 2014). All components of LPS transport across the IM as rough LPS and

O-antigen. The ligation of rough LPS to O-antigen then takes place at the outer leaflet of the IM. Finally, full-length LPS is delivered to the OM (For a review see (Ruiz *et al.*, 2009)).

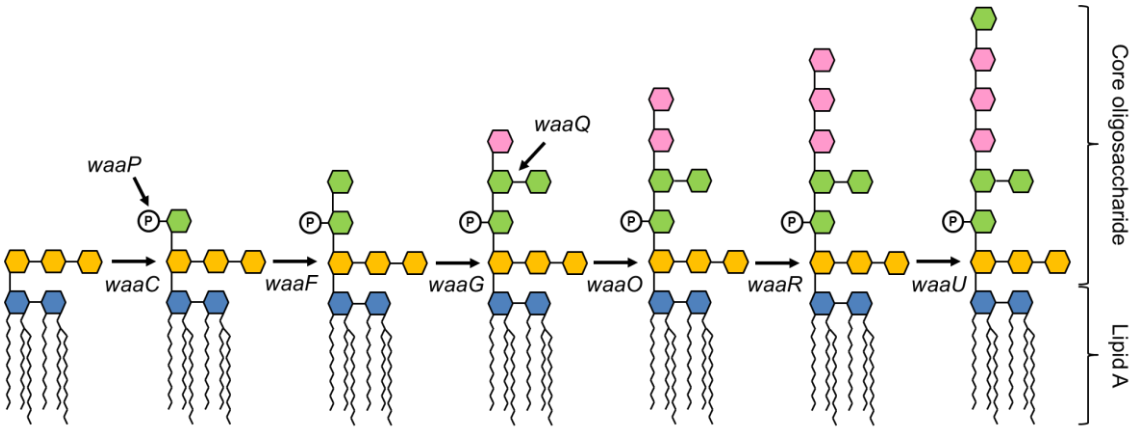

Figure 1.6 Structure and biosynthesis of core oligosaccharide of rough LPS in *E. coli* K-12. The rough LPS is composed of lipid A and core oligosaccharide. The sequential addition of sugar moieties in the core oligosaccharide starts from left to right using enzymes at the inner leaflet of the IM. The genes shown in italics are encoded for heptosyltransferase (*waaC, waaF*, *waaQ* and *waaU*), LPS kinase (*waaP*) and glycosyltransferase (*waaG, waaO* and *waaR*). Hexagons (Blue: glucosamine; yellow: 3-deoxy-oct-2-ulosonic-acid (KDO); green: heptose; pink: glucose), lines and circles stand for the sugar molecules, acyl chains and phosphates, respectively.

1.2 Colicins

Colicins are bacteriocins produced and secreted by some strains of *Escherichia coli* that can kill other sensitive *E. coli* strains (for recent reviews see (Cascales *et al.*, 2007; Jakes and Cramer, 2012; Y. C. Kim *et al.*, 2014)). Competing bacterial cells were killed either by degrading the host nucleic acid or by forming a voltage gated channel in the inner bacterial membrane. In order to kill the bacterial cells, colicins must cross the OM of the target cells to reach their site of action within the IM. The OM is well-known for its ability to protect *E. coli* from antibiotics.

Colicins are classified into two major groups based on the nature of their lethal activity (nuclease and pore-forming colicins) or by their pathways through OM

(Tol systems for Group A colicins and Ton systems for Group B colicins) (Braun *et al.*, 2002; Cascales *et al.*, 2007). The colicin translocation across the OM via Tol systems employs proteins from Tol family (TolQ, TolR, TolA, TolC and TolB) whereas colicin imports via the Ton system require proteins TonB, Exbb and ExbD (Table 1.2).

Table 1.2 Summary of receptors, translocators and cytotoxic activity of known colicins.

Colicins	Receptor	Translocator	Mode of action
Group A			
ColA	BtuB	OmpF,TolQ,TolR, TolA and TolB	Pore-former
ColE2, ColE7, ColE8 and ColE9	BtuB	OmpF,TolQ,TolR, TolA and TolB	DNase activity
ColE3, ColE4 and ColE6	BtuB	OmpF,TolQ,TolR, TolA and TolB	RNase activity
ColE1	BtuB	TolC, TolA and TolQ	Pore-former
ColE5	BtuB	OmpF,TolQ,TolR, TolA and TolB	RNase activity
ColN	LPS	OmpF,TolQ,TolR, and TolA	Pore-former
ColK	Tsx	OmpF,TolQ,TolR, TolA and TolB	Pore-former
ColS4	OmpW	OmpF,TolQ,TolR, TolA and TolB	Pore-former
Group B			
Col5-Col10	Tsx	TolC, TonB, ExbB and ExbD	Pore-former
ColIa and ColIb	Cir	Cir, TonB, ExbB and ExbD	Pore-former
ColB	FepA	TonB, ExbB and ExbD	Pore-former
ColD	FepA	TonB, ExbB and ExbD	RNase activity
ColM	FhuA	TonB, ExbB and ExbD	Inhibition of peptidoglycan synthesis

The colicin mechanism of action is performed by three functional domains; (i) the receptor binding domain (R-domain) binds to a specific receptor on the

bacterial cell surface. (ii) The translocation domain (T-domain) inserts into the periplasm and binds to the periplasmic or IM receptor to facilitate the entry of toxic domains. (iii) The C-terminal toxic domains (these are the pore forming domains in the pore-forming colicins we study and from here on are referred to as the P-domain) translocate into the IM. The general domain organisation for both pore-forming and nuclease colicins is illustrated in Figure 1.7. In general, the receptor and translocator of colicins, which are proteins located in or near the OM, are required for the recognition and translocation. Some types of colicins use two different OMPs as their receptor and translocator whereas others use only one protein such as ColIa which uses Cir (Jakes and Finkelstein, 2010).

Figure 1.7 Domain composition of colicins found in both pore forming and nuclease colicins. T, R, C and P stands for translocation, receptor-binding, C-terminal toxic and pore forming domains, respectively.

Colicins that use Tol family proteins are assigned to class A whilst those which use Ton are in class B. Table 1.2, colicin N (ColN) requires a single outer membrane protein, OmpF, for its translocation and LPS for a receptor (Elkouhen *et al.*, 1993; Jeanteur *et al.*, 1994; Baboolal *et al.*, 2008; Johnson *et al.*, 2014) and belongs to a Group A pore-forming colicin. ColN provides a simple model to study how colicins enter their target bacterium due to the fact that it not only has the smallest size (385 amino acids) of all colicins but also similar properties and functions to other pore-forming colicins.

1.2.1 Structure and function relationship of Colicin N

Even though ColN contains a relatively short polypeptide chain, it is composed of the same three components as all pore-forming colicins, translocation domain (T-domain), receptor-binding domain (R-domain) and pore-forming domain (P-domain). The high-resolution crystal structure of ColN, containing R and P-

domains (missing the first 90 residues of T domain) at 3.1 Å was first elucidated by Vetter *et al* (Vetter *et al.*, 1998).

The structure of ColN is illustrated in Figure 1.8. The pore-forming domain of ColN or toxic domain can form ion channels in the cytoplasmic membrane of sensitive cells resulting in an efflux of cytoplasmic potassium ions (Vandergoot *et al.*, 1993; Jeanteur *et al.*, 1994). Its crystallographic structure consists of a bundle of ten α-helices arranged in such a way that two amphipathic layers wrap around the hydrophobic helical hairpin formed by α helices 8 and 9 in order to maintain its solubility in aqueous solution. This structural organization of pore-forming domains is conserved in other pore-forming colicins such as colicin A, B, Ia and E1 (Parker *et al.*, 1989; Elkins *et al.*, 1997; Wiener *et al.*, 1997; Hilsenbeck *et al.*, 2004). The comparison of P-domains of several colicins is displayed in Figure 1.9. It is shown that the structure of the toxic domain from nuclease colicin E1 is noticeably diffierent from the α-helical bundle structure of P-domain from pore-forming colicins.

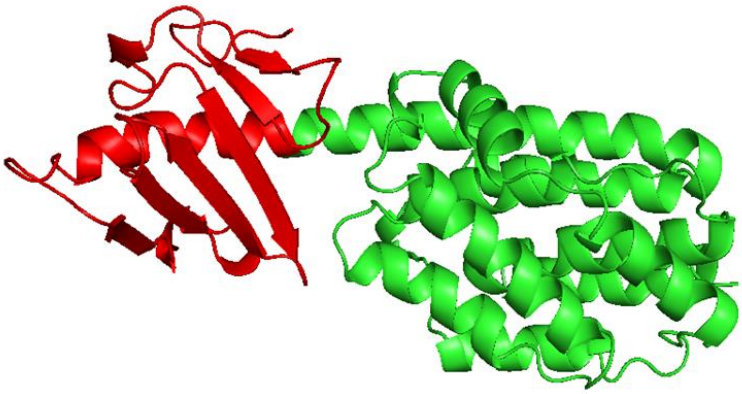

Figure 1.8 Crystal structure of colicin N (PDB code: 1A87). The structure only shows the receptor-binding (red) and pore-forming domains (green). The translocation domain (first 90 amino acids) is missing.

In spite of the fact that the P-domain of ColN shares sequence similarity to the other pore-forming colicins, the R-domain of ColN shares no significant similarity to the other colicins. The receptor-binding domain of ColN, is

composed of a six-stranded sheet surrounding an extension of α-helix 1 from P-domain (Figure 1.8).

The N-terminal translocation domain or T-domain of ColN was first defined by Elkouhen *et al* (Elkouhen *et al.*, 1993). The T-domain plays a vital role in the translocation of ColN through OM by binding to TolA which spans the periplasm and the cytoplasmic membrane. The T-domain of ColN exhibits an intrinsically disordered structure which is confirmed by CD, NMR, FRET and X-ray crystallography studies (Raggett *et al.*, 1998; Vetter *et al.*, 1998; Anderluh *et al.*, 2003; Anderluh *et al.*, 2004).

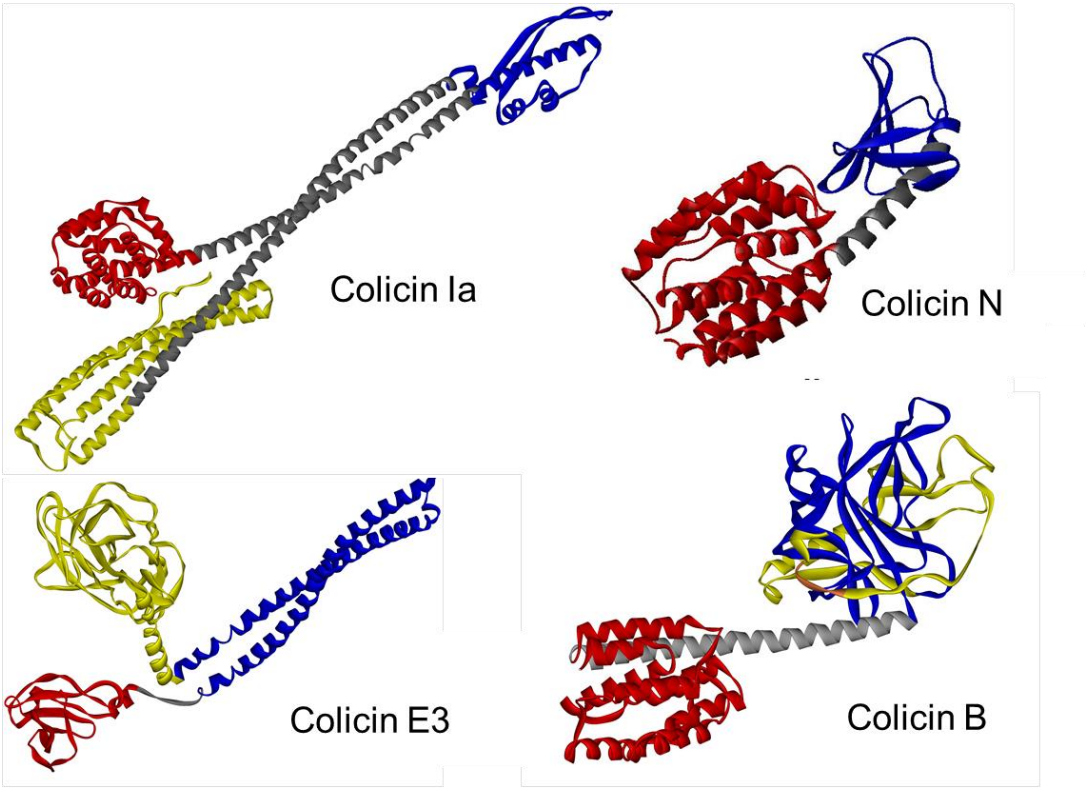

Figure 1.9 Crystallographic structures of pore-forming colicins (Ia, N and B) compared to nuclease colicins (E3). The toxic, receptor-binding and translocation domains of all colicins are shown in red, blue and yellow, respectively. (PDB codes for ColIa, 1CII; ColB, 1RH1; ColE3, 1JCH; ColN, 1A87). Translocation domains are flexible and often only partially resolved. In the case of the colicin N model no yellow translocation domain is present.

1.2.2 Colicin N translocation across outer membrane

To understand how ColN enters into bacterial cells, the interaction of ColN with proteins involved in the translocation process has been extensively studied. On the cell surface, OmpF was thought to be the receptor of ColN however isothermal calorimetric study (ITC) indicated that the R-domain is weakly bound to OmpF (Evans *et al.*, 1996a; Evans *et al.*, 1996b). Interestingly, Sharma *et al* has shown the minimum LPS length required for ColN cytotoxicity by a genome wide screen (Sharma *et al.*, 2009). It was suggested that LPS was essential for ColN activity and led to the hypothesis that ColN may be interacting with LPS. Recently, the interaction of R-domain with LPS was confirmed by ITC, SPR and NMR. It showed that the R-domain binds to the terminal glucose and heptose moieties (and phosphates) of the inner core of LPS (Johnson *et al.*, 2014). ColN now becomes unique among other colicins as it exploits LPS, the ubiquitous molecule of the bacterial surface, as a receptor. Therefore, it is now clear that only the T-domain binds to OmpF. This is supported by ITC studies on the binding of T-domain, TR-domain and wild type ColN to OmpF. It was demonstrated that the binding affinity to OmpF among these ColN constructs were nearly identical hence implying that the T-domain is responsible for OmpF interaction (Johnson *et al.*, 2013). The OmpF binding site (OBS) was also discovered at the extreme N terminus of the flexible T-domain (Johnson *et al.*, 2013). However, only one OBS was found in ColN while two OBSs were identified in ColE9 (Housden *et al.*, 2010). It has been shown that these OBSs guide ColE9 T-domain through OmpF channel (Housden *et al.*, 2013).

As ColN uses the Tol system as the import pathway, the interaction of ColN with TolA was also investigated. The Tol system consists of five proteins TolQ, R, B and A and Pal (peptidoglycan associated lipoprotein). The binding of T-domain to TolA is needed to trigger toxic domain translocation to IM of bacterial cells. TolA spans the inner membrane via a single alpha helix (domain I). TolA also comprises two periplasmic domains; domain II which has been shown to interact with OmpF is predicted to be a long α helix (Derouiche *et al.*, 1996) and Domain III, the only domain with a crystallographic structure, is known to

interact with T-domain of ColN (Raggett *et al.*, 1998; Gokce *et al.*, 2000). The binding of TolA III to ColN was examined by NMR. ColN appeared to interact with TolA III in a similar manner to the G3P protein of bacteriophage Fd but not ColA (which also uses the Tol system). The TolA-binding epitope was also identified within T-domain (Raggett *et al.*, 1998; Gokce *et al.*, 2000; O. Hecht *et al.*, 2009).

According to the information about ColN interaction with its partners, the mechanism of translocation across the outer membrane is shown in Figure 1.10. To target the cell, the R-domain directs to the inner core of LPS close to cell surface. The T-domain binds to OmpF using OBS and threads through the OmpF channel. When it reaches the periplasm, T-domain interacts with TolA III via the TolA-binding epitope. This interaction mediates the import of P-domain into the periplasm. The P-domain transports across the periplasm and then generates the voltage gated channel in the IM. However, the pathway of the P-domain through the OM is not well-understood. There are two proposed routes, the translocation of P-domain occurs either at the OmpF-Lipid interface (Bainbridge *et al.*, 1998; Baboolal *et al.*, 2008; Clifton *et al.*, 2012) or through the barrel lumen (Kleanthous, 2010).

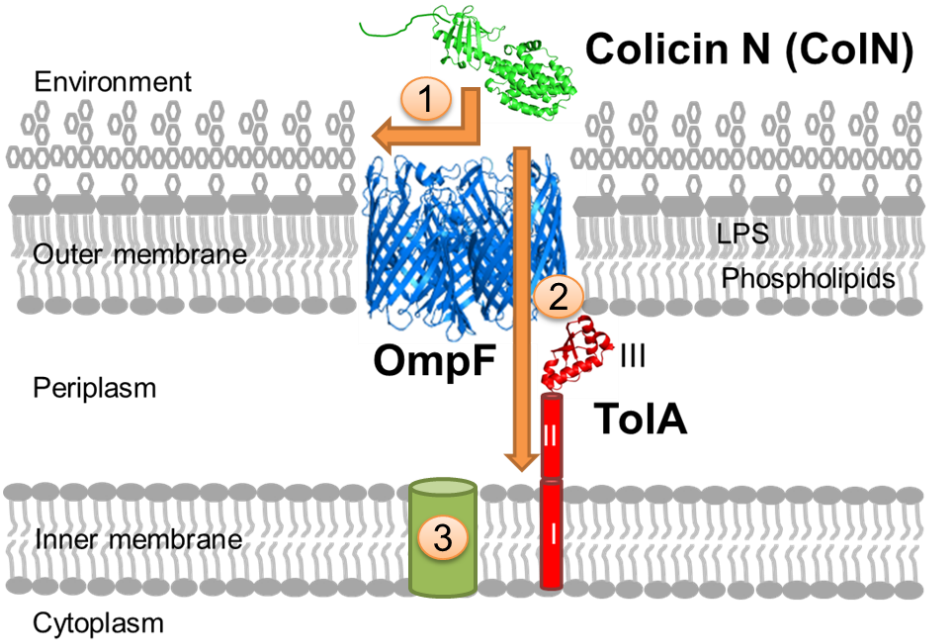

Figure 1.10 Schematic of the translocation pathway of colicin N across OM. The route of Colicin N (green, PDB code: 1A87) entry into gram negative bacteria requires the interaction with LPS, OmpF (blue, PDB code: 2OMF) and TolA (red, PDB code for TolA III: 3QDP). Firstly, the receptor-binding domain targets the inner core of LPS on the bacterial cell surface. Next, the translocation domain inserts into OmpF lumen and then interacts with TolA III in order to facilitate the translocation of pore-forming domain. The pore-forming domain ultimately crosses the outer membrane and forms an ion channel in the inner membrane causing cell death.

1.3 Alternative techniques for protein structure determination

The determination of protein structure gives invaluable information of how each protein functions in bioorganisms. X-ray crystallography and nuclear magnetic resonance (NMR) are now widely used techniques for the elucidation of three-dimensional structure of proteins. The protein structures recorded in protein data banks are mostly derived from these two techniques. X-ray crystallography provides the atomic and molecular structure from protein crystals whereas NMR is used to study the structure and dynamics of protein in solution. However, each method has advantages and disadvantages. The limitations of x-ray crystallography are 1) the difficulty in growing protein crystals, 2) the limitation in observing the flexibility of proteins and 3) providing the structure in one conformation due to the crystal constraint. In the case of NMR, the molecular

size of proteins characterised by NMR is limited to less than 70 kDa. Due to these limitations, scientists seek for an alternative way to study the structure and dynamics of proteins. In this present study, we wish to investigate the interaction of a large outer membrane protein (OmpF, 111 kDa) with LPS and the flexible proteins (ColN and TolA). As these complexes are too large for NMR study and difficult to crystallise due to the flexibility, we have used alternative methods to study them.

Due to recent developments of instrumentation and image processing software, cryo-electron microscopy (cryo-EM) of single particles or 2D crystals has become a useful method for the determination of complex molecular structure at atomic scale resolution. Advances in new detector hardware has substantially improved the resolution of cryo-EM (For a recent review see (Milne *et al.*, 2013)). The advantages of cryo-EM over X-ray crystallography are 1) crystals are not required and 2) proteins are in a nearly-native environment. Recently, ordered structures such as viruses or 2D crystals can approach resolutions of 3Å which allows for the definition of secondary structures and the larger side chains. Even with single particles, membrane proteins such as the γ-secretase can be resolved to 4.5 Å (Lu *et al.*, 2014).

Small angle scattering (SAS) is another promising technique exploited for the study of large-scale structure in solutions. It also offers the possibility of analysis of disordered systems. SAS has been introduced to study macromolecules in solution for more than 80 years. In the early days, SAS of biological macromolecules was used to determine a simple structural parameter such as radius of gyration. Due to the development of faster and more sensitive instruments, easy to use software for data analysis and interpretation, and the availability of instrumentation, SAS has now become widely used to study biological molecules in solution. SAS is often used as a complementary technique to other biophysical techniques especially x-ray crystallography. (For recent reviews about SAS see (Jacques and Trewhella, 2010; Mertens and Svergun, 2010)).

Basics of small-angle scattering

According to the basic principles of quantum mechanics, x-rays and neutrons show a wave-like character as well as a particle-like behaviour. When x-rays and neutrons pass through a particle, they interact with the atoms of the particle and generate secondary wavelets. These wavelets interfere each other constructively and destructively resulting in the diffraction pattern from the particle. X-rays are an electromagnetic radiation which interacts with the electron clouds of each atom whereas neutrons are neutral particles which are scattered by atomic nuclei. Figure 1.11 shows a typical SAS experiment. A beam of X-rays or neutrons with a narrow band of wavelength is directed at the sample of proteins in solution. X-rays and neutrons interact with proteins and then they are scattered. The scattered radiation is recorded on a detector while the transmitted radiation is absorbed by a beamstop.

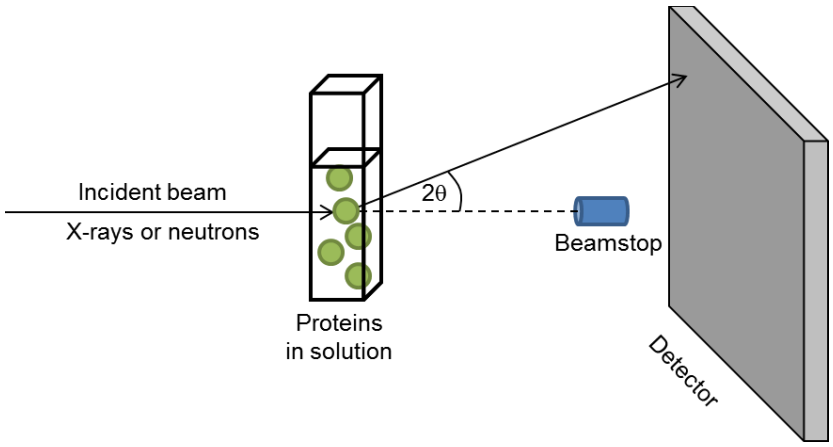

Figure 1.11 Schematic illustration of a standard SAS experiment

For simplicity, the scattering pattern is defined as intensity (I) as a function of the momentum transfer, Q.

$$Q = \frac{4\pi sin\theta}{\lambda}$$

Where θ is half the angle between the incident and scattered beams (see Figure 1.11) and λ is the wavelength of the incident beam. In most SAS experiments,

but not “white beam” time-of-flight small angle neutron scattering (TOF-SANS), λ is usually constant hence Q depends only on the scattering angle. The scattering profile from SAS is presented as I(Q) versus Q.

Small angle scattering data analysis

The initial analysis of scattering data is to determine the simple structural parameters such as radius of gyration, R_g, and the forward scattering intensity, I(0). These two parameters are directly related to particle size and shape. R_g refers to the root-mean-squared distance between all elemental scattering volume and the centre of mass. I(0) is defined as the scattering intensity at zero angle (at the beamstop). I(0) is directly dependent on the molecular mass of particle. The Guinier approximation is used to estimate these values by the equation below.

$$I(Q) = I(0)e^{\frac{-Q^2R_g^2}{3}}$$

Therefore, R_g and I(0) are a slope and the y-intercept from a linear fit of In[I(Q)] versus Q^2 for $QR_g < 1.3$. The linear Guinier plot is also an indicator of high sample quality which is free of aggregates. The Guinier analysis estimates R_g and I(0) from the scattering profiles at low angle. To precisely determine R_g and I(0) from the entire scattering profile, the interatomic distance distribution function P(r) is used to calculate them.

The P(r) function is a real space representation of scattering data. It is computed by the indirect Fourier transformation of the scattering curve using GNOM (Svergun, 1992). This is due to the fact that as the range of scattering data is present from minimum q to maximum q, direct Fourier transformation of the scattering curve from the limited number of data points is not possible. P(r) describes the probable frequency of interatomic distance (r) within the particle. P(r) provides not only the simple structural parameters such as R_g, I(0) and the maximum linear dimension (D_{max}) but also information about the shape, symmetry and domain structure within the particle. Mertens and Svergun have

shown the effect of particle shape on the scattering profiles and P(r) functions (Figure 1.12) (Mertens and Svergun, 2010). The consistency of R_g estimated from Guinier approximation and P(r) function indicates an aggregate-free sample and the correct assigned D_{max}.

Furthermore, SAS can indicate the folded/unfolded state of proteins. The Kratky plot can be used to represent the compactness of proteins from the scattering profiles by plotting $Q^2I(Q)$ versus Q. A folded protein gives a bell-shaped curve while the unfolded protein shows a continuous rise at high Q range. An extended tail of P(r) function is also an indication of unfolded proteins.

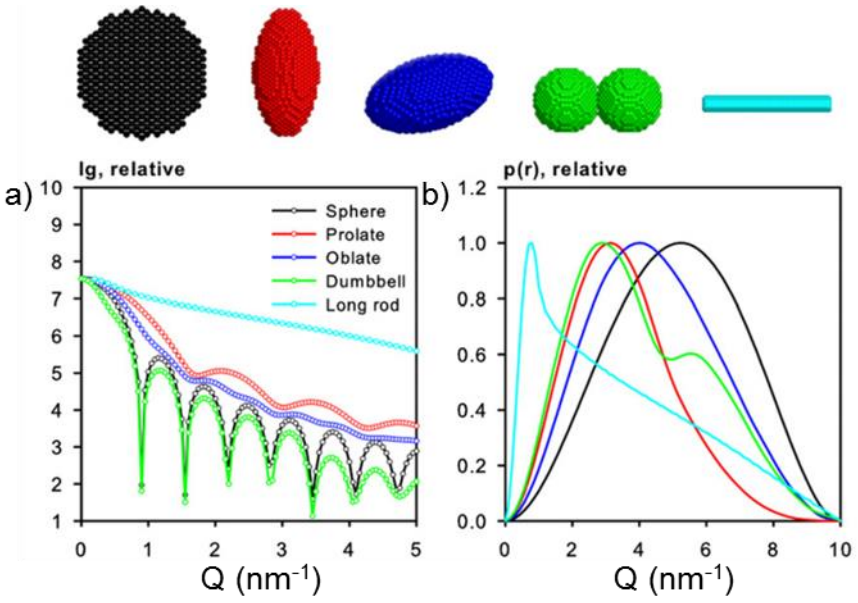

Figure 1.12 Theoretical scattering profiles and P(r) functions from simple geometrical shapes. The models used for the calculation are displayed above the plots. Plots taken from (Mertens and Svergun, 2010).

Contrast variation

Even though small angle x-ray scattering (SAXS) is similar to small angle neutron scattering (SANS), one of the key advantages of SANS over SAXS is the use of contrast variation method to study the structure of biomolecules. Due

to the difference between hydrogen and deuterium, in neutron scattering power, it is feasible to have different contrasts for each component of biological complexes if one component is deuterated. The contrast variation allows us to observe the individual component of complexes or the entire complexes. The neutron scattering experiment using this approach is achieved by recording SANS data in solvents with different ratios of H_2O:D_2O. At certain H_2O:D_2O, the scattering contributions of each component in complexes are varied. When the scatter of solvent is equal to that of one component, it is invisible to neutrons. Figure 1.13 shows how the contrast variation approach works.

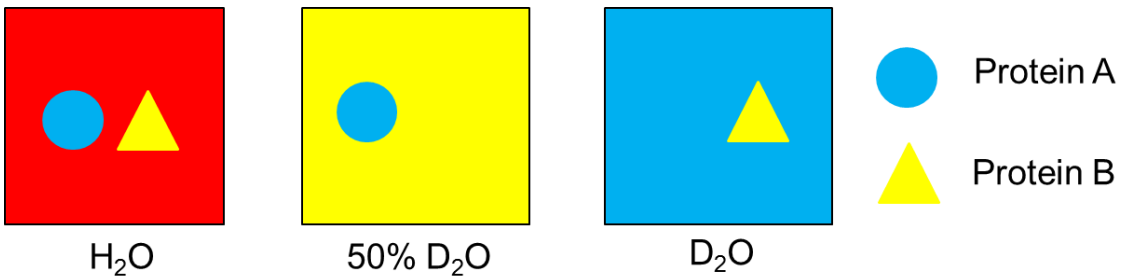

Figure 1.13 Contrast variation technique used to study the binary complex in small angle neutron scattering. Protein A and B are in different colours as one of them is deuterated. The data are recorded in solutions containing different H_2O:D_2O ratio. The solutions in each ratio represent in different colour. The scatter of A is equal to that of D_2O but the scatter of B is equal to that of 50% D_2O. Therefore, both A and B can be observed in H_2O whereas either A or B is visible to neutrons in 50% D_2O or 100% D_2O.

Modelling from scattering data

The modelling of biological molecules from SAS data can be achieved in three different ways, *ab initio* modelling, rigid body modelling, and ensemble optimisation methods. Most modelling software used in this study comes from the ATSAS suite pioneered by the Svergun research group at EMBL Hamburg (Petoukhov *et al.*, 2012). The *ab initio* method uses dummy atoms to reconstruct a molecular shape based on the scattering data alone. The disadvantage of this method is that several shapes generated from this method are able to fit the data equally well. Therefore, the molecular shape from *ab initio* modelling must be supported by results obtained by other techniques. In

contrast to the *ab initio* method, rigid body modelling exploits the availability of high resolution structures of proteins, for example separate subunits of a complex, from X-ray crystallography. It generates the theoretical scattering data from the high-resolution structure and which is then compared to the experimental data. Additionally, rigid body modelling offers the possibility to model flexible loops or inter domain linkers missing in the crystal structure. The last approach is ensemble optimisation method for flexible systems. A pool of models is randomly generated according to the sequence and structural information of the protein. The program then chooses an ensemble of conformations and fits the averaged theoretical scattering data from an ensemble of conformations to the experimental data.

1.4 Stabilising membrane proteins

The difficulty in studying membrane proteins (MP) is to stabilise and solubilise them once removed from the natural lipid environment. To handle MP in aqueous solution, MPs require the system that matches their hydrophobic region and retains their solubility in solution. Conventionally, MPs are isolated from lipid membranes and solubilised using detergents. The structure determination and functional study of MPs are performed in the form of MP/detergent complexes. Thus, there is no doubt that detergents are a useful tool for MP characterisation.

Detergents are amphipathic molecules consisting of hydrophobic chains (tails) and hydrophilic head groups. They are able to form micelles in solutions. MPs can be solubilised in micelles which mimic the structure of biomembranes. Detergents are classified into 4 major categories which are ionic detergents, bile acid salts, non-ionic detergents and zwitterionic detergents (Table 1.3). The general properties of detergents are taken into consideration in order to select a suitable detergent for studying certain MP. The most important property is critical micelle concentration (CMC) which is defined as the lowest concentration which detergents are able to form micelles. The CMC is dependent on hydrophobic, hydrophilic groups and salt concentrations. The

increase in the length of the hydrocarbon chain leads to a decrease in CMC. Detergents with saturated hydrocarbon chains have lower CMC than ones with unsaturated hydrocarbon chains. Detergents with charged head group tend to have higher CMC than uncharged ones. The CMC of ionic detergents is also affected by the presence of salts in the solutions. The high salt concentration reduces the CMC of detergents. The detergents with low CMC are usually considered as mild detergents such as octyl glucoside and dodecyl maltoside due to the fact that they disrupt protein-lipid and lipid-lipid interactions rather than protein-protein interactions.

Table 1.3 Classification of detergents used in the solubilisation of membrane proteins

Classes	Head groups	Tails	Example	Properties
Ionic	Cationic or anionic	hydrophobic chain or steroidal backbone	Sodium dodecyl sulphate (SDS)	deactivating
Bile acid salts	Cationic or anionic	rigid steroidal group	Sodium cholate, sodium deoxycholate	Relatively mild
Non-ionic	Uncharged	hydrophobic chain or steroidal backbone	Octyl glucoside (OG), dodecyl maltoside (DDM), octyl-POE	Mild and non-denaturing
Zwitterionic	Uncharged	hydrophobic chain or steroidal backbone	CHAPS, CHAPSO	Less deactivating than ionic but more than non-ionic

However, detergents sometimes destabilise MPs in solution. This has prompted scientists to seek for alternative platforms to study MPs. These platforms can stabilise MPs as well as keep MPs soluble in solutions. This study will focus on the two novel systems; amphipols and nanodiscs. Amphipols are amphipathic polymers which stabilise MPs by absorbing onto the hydrophobic region of MPs (Tribet *et al.*, 1996). Nanodiscs are segments of lipid bilayers surrounded by

membrane scaffold proteins (Bayburt *et al.*, 2002). These two approaches are exploited to perform both structural and functional of MPs in near native conditions. The advantages of using amphipols and nanodiscs over conventional detergents are 1) amphipols has high affinity to MPs hence MPs are stabilised in nearly absence of free amphipols, 2) MPs inserted into nanodiscs are in lipid environment which is extremely similar to biological membranes and 3) nanodiscs have controlled size which is suitable for structural studies in solutions (Jean-Luc Popot, 2010).

1.5 Aim

The aim of this project is to understand the outer membrane of *E. coli* and search for entry routes across the outer membrane. The characterisation of OmpF interacting with ColN, TolA and LPS was carried out using biophysical techniques such as electron microscopy, small-angle scattering, analytical ultracentrifugation as well as other techniques. Since OmpF is not soluble in aqueous solutions the complexes will be studied in several platforms such as detergents, amphipols, and nanodiscs. The following studies were carried out:

1) The interaction of OmpF in complex with ColN and TolA was studied by small angle scattering. These proteins are involved in the translocation of ColN across the outer membrane. A study of these interactions could allow us to gain a better understanding of how ColN enters into gram-negative bacterial cells and triggers cell killing by delivering its toxic domain to the inner membrane.

2) The elucidation of OmpF-LPS interaction was carried out in order to understand the outer membrane organization of *E. coli*. The localisation of the LPS binding site on OmpF was also examined by mutagenesis and small-angle scattering.

3) OmpF stabilisation in two new platforms was investigated to seek alternative approaches of studying the OmpF-ColN complex. The structural studies of

OmpF incorporated in amphipols and nanodiscs were performed by small angle scattering and transmission electron microscopy.

As a result, the knowledge gained from these experiments has the potential to reveal the weak points of bacterial cells that could be exploited by new antibacterial drugs.

Chapter 2 Materials and Methods

2.1 Materials

2.1.1 Chemicals

Most chemicals were obtained from either Sigma-Aldrich Company Ltd. or Melford (UK) except for specialist chemicals which were purchased from suppliers listed in Table 2.1.

Table 2.1 List of specialist chemicals and respective suppliers

Chemical	Supplier
octyl-polyoxyethylene (octyl-POE)	Enzo
Lipopolysaccharide (LPS)	Sigma Aldrich
Bug-Buster protein extraction reagent	Novagen
n-dodecyl-b-D-glucopyranoside (DG), deuterated octyl glucoside (OG)	Anatrace
deuterium oxide, deuterated sodium dodecylsulfate (SDS)	Cambridge Isotope Laboratories
n-dodecyl-b-D-maltoside (DDM)	Melford
Bio-Beads-SM2	Bio-Rad
Amphipol A8-35 (APol)	kind gift from J.L. Popot Institut de Biologie Physico-Chimique, CNRS, Paris, France

2.1.2 Bacterial strains

Bacterial strains were obtained from Invitrogen except *E. coli* BZB1107 and *E. coli* BE3000 which were kind gifts from J. Rosenbusch and T. Schirmer. The genotype and reference of each strain are shown in Table 2.2. Mach I was routinely used as a host for cloning and plasmid DNA purification. BZB1107 is an OMP deficient strain used in most OmpF expressions while BE3000

produces only OmpF plus PhoE (Phosphoporin) and LamB (Maltoporin), which can be both suppressed by addition of glucose and phosphate to the media, respectively.

Table 2.2 Bacterial strains for the expression of protein in this study

Strain	Genotype	Reference
E. coli BZB1107	*OmpF::*Tn5 (Kan^r)	(Lupi *et al.*, 1989)
E. coli BE3000	*OmpA*$^-$ *(BZB6/3)*	(Garavito and Rosenbusch, 1986)
E. coli BL21 (DE3)	F- *ompT hsdS*$_B$*(*r_B^-*,* m_B^-*) gal dcm (DE3)*	(Studier *et al.*, 1990)
E. coli BL21-AI	F- *ompT hsdS*$_B$ ($r_B^-m_B^-$) *gal dcm araB::T7RNAP-tetA*	Invitrogen
E. coli MachI	F– Φ80*lacZ*ΔM15 *ΔlacX74 hsd*R(r_K^-, m_K^+) Δ*rec*A1398 *end*A1 *ton*A	Invitrogen

2.2 General and biochemical protocols

2.2.1 Gel filtration chromatography

Unless otherwise stated, all size exclusion chromatography was performed using an ÄKTA purification system (GE Healthcare). 100 µl of sample was injected into a Superose 12 10/300 GL column which was previously equilibrated with a running buffer until a stable baseline was established. To remove small particles from buffers, all buffers were filtered through a 0.22 µm filter before use. The elution at a flow rate of 0.5 ml/min was carried out at room temperature and the absorbance at 280 nm was measured to detect the protein.

2.2.2 Ion exchange chromatography

Ion exchange chromatography was performed using an ÄKTA purification system (GE Healthcare). A 1-ml HiTrap Q Sepharose and a Mono S 5/50 GL column were used for anion and cation exchange chromatography, respectively. The column was equilibrated with a low ionic strength buffer until a stable baseline was reached. Samples were injected into the column and washed

using the same buffer for at least 5 times the column volume. The bound proteins were then eluted using a salt gradient. The protein-containing fractions were then collected and the proteins monitored by measuring $A_{280.}$

2.2.3 Reconstitution of OmpF into Amphipols

The preparation of membrane protein/amphipol complexes (Figure 2.1) has been previously described by Zoonens *et al* (Zoonens *et al.*, 2005). In brief, the stock of APol A8-35 at 20 mg/ml in water was stirred using a magnetic stirrer overnight at room temperature before use. The APol was added to detergent-solubilised OmpF at a 1:10 OmpF/APol weight ratio in 20 mM phosphate buffer, pH 7.9, 100 mM NaCl, 0.5% (v/v) octyl POE. The mixture was then incubated for 15 min at room temperature. After the 15 min incubation, detergents were removed by incubating the mixture with wet polystyrene Bio-Beads in a 1:10 detergent/beads weight ratio at room temperature for 3 h. The Bio-Beads were pre-washed with methanol and deionised water. The removal of the polystyrene beads was acheived by centrifugation for 5 min at room temperature. In case of OmpF/ColN/APol complexes, ColN was added at a 3:1 OmpF/ColN molar ratio after the removal of biobeads and incubated for 15 min. The samples were then ready to be further analysed by other techniques.

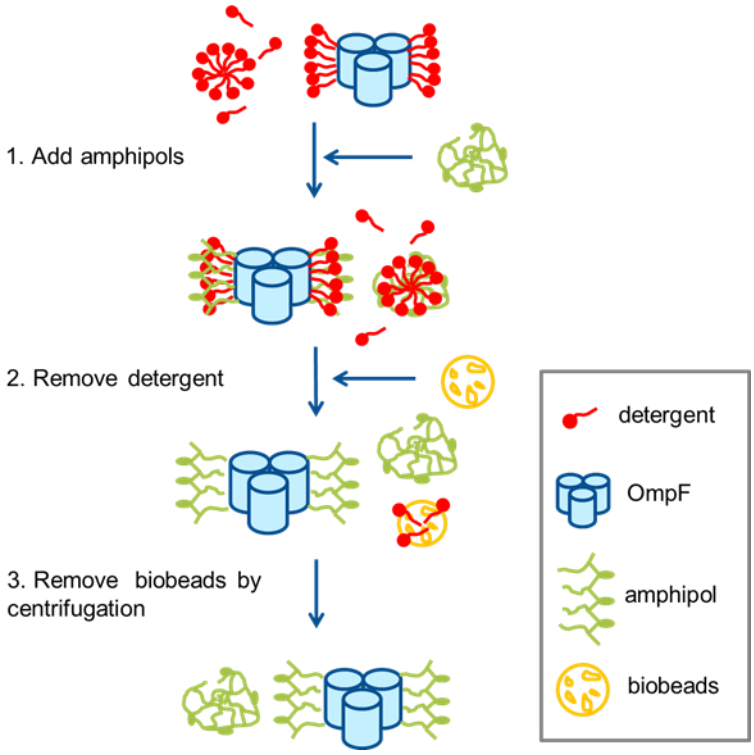

Figure 2.1 Schematic representation shows the trapping of OmpF with amphipols adapted from Zoonens *et al* (Zoonens *et al.*, 2005).

2.2.4 Reconstitution of OmpF into Nanodiscs

The incorporation of membrane protein into nanodiscs was previously described by Ritchie *et al* (Ritchie *et al.*, 2009). DMPC and DMPG stock solutions were prepared in 20 mM Tris-HCl pH 7.4, 0.1 M NaCl, 0.5 mM EDTA, 5% octyl-POE to give a final lipid concentration of 50 mM. The solutions were heated under hot tap water and sonicated in an ultrasonic bath until the solution is clear. MSP1E3D1/lipid at a 1:140 molar ratio for empty nanodiscs and MSP/OmpF/lipid at a 2:3:280 molar ratio for OmpF nanodiscs were mixed in the same buffer without detergents. The samples was incubated for 1 h at 30^{o}C using a water bath. After the incubation, detergents were removed by incubating with wet (see Amphipol section above) Bio-Beads (adding 500 mg/ml of solution) for 3 h at room temperature. After the removal of detergents, Bio-Beads were removed by centrifugation for 10 min at 4^{o}C. The nanodiscs were then ready for further analysis.

2.2.5 Lipopolysaccharide Preparation

LPS and lipid A (protein impurities < 3%) were dissolved in 20 mM Tris-HCl, pH 7.4, 300 mM NaCl supplemented with 0.5% octyl-POE or 0.5% SDS or to give a final concentration of 2 mg/ml. The LPS solution was then sonicated in a water bath for 20 min and temperature cycled 6 times between 4 and 70^{o}C. The resulting solution was kept at 4^{o}C overnight before use.

2.2.6 Sodium dodecylsulphate polyacrylamide gel electrophoresis (SDS-PAGE)

Analysis of proteins using SDS-PAGE followed standard procedures from Laemmli (Laemmli, 1970). The discontinuous gel is used in the experiment and contains 10% or 12% (v/v) acrylamide for resolving gels and 6% (v/v) for stacking gels, unless otherwise stated. The protein samples were prepared by mixing 20 – 50 µl of protein solutions in the range of 0.3 to 1.5 mg/ml into the sample loading buffer (15% (v/v) glycerol, 0.125 M Tris, 2% (w/v) SDS, 0.1% (w/v) bromophenol blue, 1% (v/v) 2-Mercaptoethanol, pH 6.8) at 1:1 ratio. The samples were then boiled at 95^{o}C for 10 min and 5 – 20 µl of samples were loaded onto the stacking gel. The SDS-PAGE was performed at 50 mA in Mini-PROTEAN II, the vertical electrophoretic cell from Bio-Rad and 0.025 M Tris, 0.192 M glycine, 0.1% SDS, pH 8.0 were used as a running buffer. The protein bands were visualised by immersing in a staining solution (0.05% Coomassie Brilliant Blue, 10 % (v/v) glacial acetic acid, 10% (v/v) propan-2-ol) for 15 min and followed by placing in destaining solutions (the same solution without Coomassie Brilliant Blue) until the bands developed. The protein sizes were determined by comparing to the standard markers (Precision Plus Protein Prestained Standards dual colour from Bio-Rad).

2.2.7 Western blotting

Protein samples were first electrophoretically separated in a SDS-PAGE gel. Prior to protein transfer, the nitrocellulose membrane and blotting papers were previously soaked with transfer buffer (10 mM CAPS buffer, pH 11, 20% (v/v) MeOH) for 10 min. The protein bands from SDS-PAGE gels were blotted onto a

nitrocellulose membrane at 20 V for 30 min using a semi-dry transfer technique (a BioRad semi-dry electroblotter). Next, the membrane was incubated with PBS (10 mM phosphate buffer, 2.7 mM KCl, 137 mM NaCl, pH 7.4) containing 5% (w/v) milk powder at room temperature for 3 h. The membrane was rinsed with PBS three times and incubated overnight at 4^{o}C with the fresh PBS/milk buffer supplemented with 0.05% (v/v) Tween and the primary antibody specific to the target protein (diluted 1/1000). The buffer with the primary antibody was removed by washing the membrane with PBS buffer. After washing the membrane 3 times, it was incubated with fresh PBS/milk buffer containing the secondary antibody (diluted 1/1000). The secondary antibody is a horseradish peroxidase-conjugated antibody specific for the first antibody class. The wash step with PBS was repeated three times. For the detection, 4-chloro-1-naphol, a substrate of peroxidase, was used to react with the secondary antibody resulting in an insoluble and stable violet dye. 30 mg 4-chloro-napthol, 10 ml MeOH and 60 µl of H_2O_2 in 50 ml of developing buffer (50 mM Tris, 137 mM NaCl, 0.7 mM Na_2HPO_4, pH 7.2) was added to the membrane and incubated for a few min. Once the bands develop, the reaction was stopped by washing with deionised water.

2.2.8 UV Spectrophotometry of proteins and DNA

The concentration of proteins and DNA was routinely measured using a Nanodrop ND-1000 at 260 nm for DNA and 280 nm for proteins. All protein concentrations were estimated using the Beer-Lambert Law:

$$A = \varepsilon cl$$

Where ε is the molar extinction coefficient (M^{-1} cm^{-1}) (cf. Table 2.3), c is the concentration of proteins (M^{-1}) and l is light path (cm).

Table 2.3 The theoretical extinction coefficients and molecular weights of proteins used for the determination of protein concentrations.

Protein	Molecular weight (kDa)	Extinction coefficient at 280 nm (M^{-1} cm^{-1})
OmpF	37.08	48500
ColN-TR	20.75	26030
TolA II-III	39.66	7580
MSP1E3D1	32.60	29910

2.3 Molecular biological techniques

2.3.1 Transformation of competent E. coli cells

E. coli competent cells were produced by pre-treatment with a frozen storage buffer (10 mM Potassium acetate, pH 6.2, 100 mM KCl, 50 mM $CaCl_2.2H_2O$, and 10% (w/v) glycerol) and kept at -80^{o}C. Prior to transformation, cells were removed from the -80^{o}C freezer and thawed on ice. Once thawed, 2-5 µl of plasmid DNA (5 ng to 100 ng) were added to the cells and incubated for 30 min on ice. After 30-min incubation, the transformation tube was placed in a 42^{o}C water bath for 2 min in order to heat-shock cells and then left it on ice for further 5 min. 250 µl of LB were added to the cells and grew for 1 h at 37^{o}C. Transformed cells were then plated onto LB agar plates containing appropriate antibiotics.

2.3.2 Polymerase chain reaction (PCR)

Polymerase chain reaction was performed in order to amplify or mutate the genes for the proteins used in this study. The primers were synthesised by Eurofins Genomics. The DNA polymerase used in this study was *PfuUltra* high-fidelity DNA polymerase from Agilent Technologies. The PCR reaction was performed by mixing the components in Table 2.4 and using the conditions in Table 2.5.

Table 2.4 PCR reaction mixture

Component	Volume (μl)	Final Concentration
10 μM forward primer	1	0.2 μM
10 μM reverse primer	1	0.2 μM
10X buffer for *PfuUltra* polymerase	5	1X
2 mM dNTPs	5	0.2 mM
Plasmid DNA template (10 ng/μl)	1	0.2 ng/μl
PfuUltra polymerase (2.5 U/μl)	1	0.05 U/μl
Nuclease free water (autoclaved)	36	-
Total	50	-

Table 2.5 PCR reaction conditions

Segment	Number of cycles	Target size	
		≤ **1000 bp**	**> 1000 bp**
1	1	95^{o}C for 2 min	
2	30	95^{o}C for 30 s	
		Lowest primer Tm^{o}C for 30 s	
		72^{o}C for 1 min	72^{o}C for 1 min per kb
3	1	72^{o}C for 10 min	

2.3.3 In-Fusion HD cloning

In-Fusion HD cloning offers a new cloning technique without restriction digestion, phosphatase treatment and ligation. A broad range of DNA fragments can be cloned into any location within any vector using In-Fusion enzyme which recognises 15 bp overlap at the end of the fragment and the vector. This cloning method is based on sequence and ligation independent cloning (SLIC) (Li and Elledge, 2007). The outline of In- Fusion HD method is illustrated in Figure 2.2.

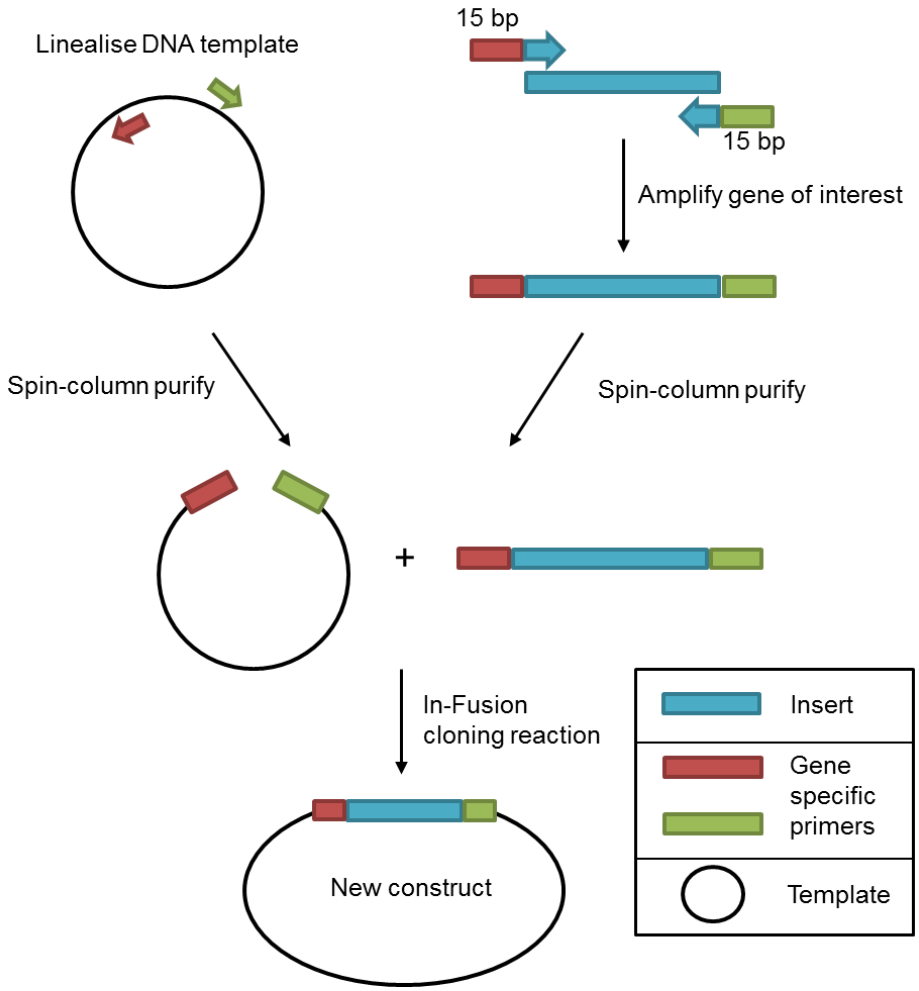

Figure 2.2 Overview of In-Fusion HD cloning technique. (Adapted from In-Fusion HD cloning instruction manual (Clontech Laboratories, Inc))

In brief, a linearised DNA template is generated by inverse PCR. The PCR mixture and conditions are described in section 2.3.2. PCR primers for the gene of interest with the addition of 15 bp complementary to the template were designed (cf. Table 2.6). The gene of interest was amplified by PCR. The DNA templates in both reactions were selectively digested by *DpnI* restriction enzyme for 1 h at 37^{o}C. The linearised vector and insert were purified using the spin-column method in the QIAquick PCR Purification kit from QIAGEN. Next, linearised vector and insert were mixed with In-Fusion HD enzyme premix (cf. Table 2.7). The reaction was incubated for 15 min at 50^{o}C and then placed on ice. This reaction mimics *in vivo* homologous recombination by using

exonuclease to generate single-stranded DNA overhangs in insert and vector. After annealing of vector and insert, the new construct was then transformed into competent cells.

Table 2.6 Sequences of oligonucleotides primers used for In-Fusion cloning of OmpF

Primer name	Sequence (5' to 3')
A site amplification forward	TAGATCTGTACGGTAAAGCTGTCGGTCTGC
A site amplification reverse	CGCGTCGTACTTCAGACCAGTAGCCCACTG
A site linearisation forward	CTGAAGTACGACGCGAACAACATC
A site linearisation reverse	TACCGTACAGATCTACTTTGTTGCC
B site amplification forward	AACAACATCTACCTGGCAGCGAACTACGGT
B site amplification reverse	GATACCCACAGCAACGGTGTCGTCTGAACC
B site linearisation forward	GTTGCTGTGGGTATCGTTTACC
B site linearisation reverse	CAGGTAGATGTTGTTCGCGTC

Table 2.7 In-Fusion cloning reaction mixture

Component	Cloning Reaction (μl)
Insert (100 ng/μl)	1
Linearised vector (50 ng/μl)	1
5X In-Fusion HD enzyme premix	1
Deionised water	2

2.3.4 Site-directed mutagenesis by polymerase chain reaction

The overview of site-directed mutagenesis method is shown in Figure 2.3. In brief, plasmid DNA containing the gene of interest was used as a template in a thermocycling reaction. The mutagenic primers containing an appropriate

mutation were designed and annealed to DNA template. The sequences of mutagenic primers used in this study are summarised in Table 2.8. The extension of primers and amplification of DNA were carried out using the *PfuUltra* high-fidelity DNA polymerase. The DNA templates were then digested by *DpnI* restriction enzyme at 37^{o}C for 1 h leaving the synthetic DNA with desired mutation intact. Finally, the synthetic DNA can be used for transformation into the appropriate host bacteria. The PCR mixture and conditions are described in section 2.3.2.

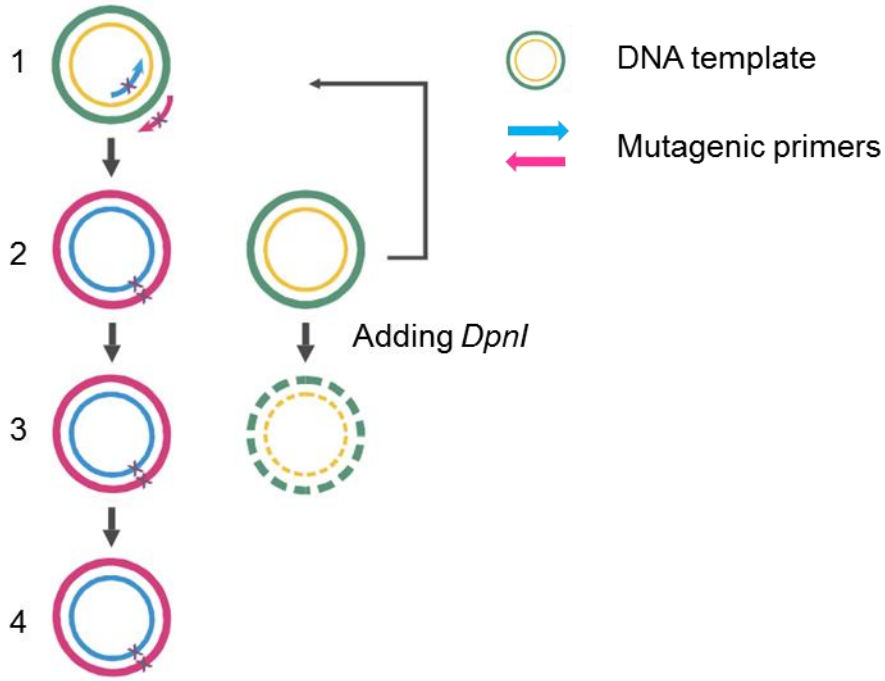

Figure 2.3 Schematic representation of site-directed mutagenesis approach. 1) Anneal mutagenic primers to DNA template. The primers contain the mutation at central point 2) *PfuUltra* DNA polymerase extend primers 3) Remaining DNA template was digested using *DpnI* restriction enzyme 4) DNA with desired mutation can be used for transformation (Adapted from QuikChange instruction manual (Stratagene)).

Table 2.8 Sequences of oligonucleotides primers used for site directed mutagenesis of OmpF. Mutation sites are highlighted in red.

Primer name	Sequence (5' to 3')
K25Q forward	CTG CAT TAT TTC TCC CAA GGT AAC GGT GAA AAC
K25Q reverse	GTT TTC ACC GTT ACC TTG GGA GAA ATA ATG CAG
K160Q forward	GTT CAG TAC CTG GGT CAA AAC GAG CGT GAC AC
K160Q reverse	GT GTC ACG CTC GTT TTG ACC CAG GTA CTG AAC
K209Q K210Q forward	CTT GGC AAC GGT CAA CAA GCT GAA CAG TGG
K209Q K210Q reverse	CCA CTG TTC AGC TTG TTG ACC GTT GCC AAG
K277Q forward	CC ATC GCT TAC ACC CAA TCT AGA GCG AAA GAC
K277Q reverse	GTC TTT CGC TCT AGA TTG GGT GTA AGC GAT GG
K279Q K281Q forward	GCT TAC ACC AAA TCT CAA GCG CAA GAC GTA GAA GGT ATC GG
K279Q K281Q reverse	CC GAT ACC TTC TAC GTC TTG CGC TTG AGA TTT GGT GTA AGC

2.4 Protein expression and purification

2.4.1 Expression of Histidine-tagged Colicin N-TR

Truncated colicin N with a C-terminal His-Tagged (-SSHHHHHH) (ColN-TR) was expressed from *E. Coli* BL21-AI with the plasmid pET3a. Selected transformed cells from overnight culture were grown in LB (Luria-Bertani) medium containing 100 µg/ml ampicillin at 37 °C. At OD_{600} = 0.6, L-arabinose was added to cell culture to a final concentration of 0.2% (v/v) and cells were then grown for a further 3 h. To harvest cells, the cell culture was centrifuged for 10 min at 8,000 g at 4^{o}C.

2.4.2 Expression of Histidine-tagged TolA II-III

Truncated TolA II-III with an N-terminal His-tag was expressed from *E. Coli* BL21-AI as a host with the plasmid pET8c. Selected transformed cells from overnight culture were grown in LB (Luria-Bertani) medium containing 100 µg/ml ampicillin at 37 °C. At OD_{600} = 0.6, L-arabinose was added to cell culture to a final concentration of 0.2% (v/v) and cells were then grown for a further 3 h. To harvest cells, the cell culture was centrifuged for 10 min at 8,000 g at 4^{o}C.

2.4.3 Expression of Histidine-tagged membrane scaffold proteins (MSP1E3D1)

Membrane scaffold protein with an N-terminal His-tags (MSP1E3D1) was expressed using the pET expression system using *E. Coli* BL21(DE3) as a host. Selected transformed cells from overnight culture were grown in LB (Luria-Bertani) medium containing 30 µg/ml Kanamycin at 37 °C. At OD_{600} = 0.6, IPTG (isopropyl β-D-thiogalactoside) was added to the cell culture to a final concentration of 1 mM. After growing for 3 h, cells were harvested by centrifugation for 10 min at 8,000 g at 4^{o}C.

2.4.4 Purification of Histidine-tagged proteins

The cell pellet harvested by centrifugation was resuspended in Ni column loading buffer (50 mM sodium phosphate buffer, pH 8.0, 300 mM NaCl, 10 mM imidazole) and then disrupted by sonication on ice for 15 min. To remove unbroken cells and cell debris, the resulting suspension was centrifuged at 17,000 g at 4^{o}C. The clarified supernatant was loaded on to a Ni-NTA (nickel-nitriloacetic acid) column previously equilibrated in Ni column loading buffer. The removal of non-specifically bound proteins was done by washing the column twice with Ni column wash buffer (50 mM sodium phosphate, pH 8.0, 300 mM NaCl, 25 mM imidazole). Bound protein was eluted using a 25-250 mM imidazole gradient collecting 5 ml fractions. Protein containing fractions were then dialysed twice against 50 mM sodium phosphate buffer, pH 7.4, 300 mM NaCl.

2.4.5 Expression of wild-type OmpF

WT OmpF was produced from *E. coli* BE3000 (Garavito and Rosenbusch, 1986). Cells were grown in 2 x 50 ml in LB (Luria-Bertani) medium at 37 °C overnight. The cells from the overnight culture were then harvested by centrifugation at 8,000 g at room temperature and resuspended into 10 ml of fresh LB medium. 10 ml of cell culture was inoculated into a 1.5-litre fermentation vessel in a Minifors fermenter (INFORS) at 37^{o}C using glucose as a carbon source. During cell growth, a pH of 7.3 was maintained by adding 10% (w/v) NaOH. The measurement of OD_{600} by a UV-1800 UV spectrophotometer (Shimadzu) was performed to monitor the cell growth. When the OD_{600} reached at least 10.0, the cells were harvested by centrifugation at 8,000 g for 10 min at 4^{o}C.

2.4.6 Production of deuterated OmpF

The deuterated OmpF was produced from *E. coli* BE3000 (Garavito and Rosenbusch, 1986). Cells were first adapted onto a hydrogenated, solid minimal medium plate and followed by growth on a 85% D_2O minimal medium plate (Artero *et al.*, 2005). The recipe for minimal media is shown in Table 2.9. Once colonies grew on the plate (which normally takes a few days due to the slower growth of the cells), selected larger colonies were grown in 50 ml of 85% D_2O minimal liquid medium. Once growth is established overnight, these cells were inoculated at 1:20 ratio into 2 x 50 ml of fresh 85% D_2O minimal liquid medium. This step was repeated three times in order to increase the initial growth rate. Cells were harvested by centrifugation at 8,000 g at room temperature and resuspended into 10 ml of fresh 85% D_2O minimal liquid medium. This cell culture was then inoculated into the 1.5 L fermenter as previously described in section 2.4.5.

Table 2.9 Recipe of minimal media for the production of deuterated OmpF (Meilleur *et al.*, 2009).

Component	Concentration
$(NH_4)_2SO_4$	3.45 g/L
KH_2PO_4	0.78 g/L
$Na_2HPO_4.2H_2O$	3.24 g/L
$(NH_4)_2$-H-citrate	0.25 g/L
$MgSO_4.7H_2O$*	0.13 g/L
Trace metal solution**	0.5 ml/L
Glycerol	2.5 g/L

* $MgSO_4.7H_2O$ is added last otherwise it will precipitate.

**Trace metal solution contains 0.5 g/L $CaCl_2.2H_2O$, 16.7 g/L $FeCl_3.6H_2O$, 0.18 g/L $ZnSO_4.7H_2O$, 0.16 g/L $CuSO_4.5H_2O$, 0.15 g/L $MnSO_4.4H_2O$, 0.18 g/L $CoCl_2.6H_2O$, 20.1 g/L EDTA.

2.4.7 Production of mutant OmpF proteins

OmpF mutants were expressed in the outer membrane of a porin deficient strain, *E. coli* BZB1107 from the plasmid pMS119 encoding the desired mutant *ompF* gene. Transformed cells were grown at 37ºC in LB (Luria-Bertani) medium supplemented with 100 µg/ml ampicillin, 30 µg/ml kanamycin and 0.2% (v/v) glucose in order to inhibit the expression of another outer membrane protein, LamB. PhoE porin expression is suppressed by the phosphate present in the media. When the OD_{600} of the cell culture reached 0.6, IPTG (final concentration of 1 mM) was added to induce protein expression and grown for a further 3 h. Cells were harvested by centrifugation at 8,000 g for 10 min at 4 ºC.

2.4.8 Extraction of OmpF from the outer membrane

The cell pellet was resuspended in 20 mM sodium phosphate, pH 6.8 and supplemented with DNase (10µg/ml) and RNase (10µg/ml). The cells were lysed by sonication of the cells on ice for 15 min. To remove unbroken cells

and cell debris, the suspension was centrifuged at 3,000 g for 15 min. After removing the pellet containing unbroken cells and cell debris, the supernatant was centrifuged at 40,000 rpm for 1 h in a 45-Ti rotor on a Beckman L7-80 ultracentrifuge in order to isolate the membrane pellet. The membrane pellet obtained was resuspended in wash buffer (20 mM Tris, 2% (w/v) SDS, pH 7.4) and then homogenised at 55ºC for 1 h. The solution was centrifuged at 40,000 rpm for 1 h in a 45-Ti rotor on a Beckman L7-80 ultracentrifuge and then the supernatant was discarded. The wash step was repeated twice. The extraction of OmpF from the remaining membrane pellet was carried out by incubating and homogenising the pellet in wash buffer with additional 500 mM NaCl. After incubation for 1 h at room temperature, the extract was centrifuged at 40,000 rpm for 1 h in a 45-Ti rotor on a Beckman L7-80 ultracentrifuge. The extraction was repeated once to increase the yield of OmpF. The supernatant containing SDS solubilised OmpF was dialysed against 5 mM $NaHCO_3$, 0.1% (w/v) SDS overnight at 37 ºC. The precipitation of OmpF (to concentrate or change detergent) was achieved by mixing cold ethanol, pre-chilled at -80 ºC, with OmpF samples to give a final ethanol concentration of 90% (v/v). This solution was then incubated at -20 ºC overnight. To isolate the precipitated OmpF pellet, the solution was centrifuged at 17,000 g for 1 h. The OmpF pellet was dried under a stream of air. OmpF was recovered by resuspension in 20 mM Tris-HCl, pH 7.5, 300 mM NaCl containing an appropriate detergent such as OG or octyl-POE.

2.4.9 Expression and isolation of OmpF inclusion bodies

OmpF inclusion bodies were expressed in *E. coli* BZB1107 from a pMS119 plasmid in which the *ompF* signal sequence (residues 1–22) plus the initial Ala23 residue is replaced by a single methionine residue to give a new start codon. Inclusion bodies were purified by BugBuster solution (Novagen) and solubilised with the denaturation buffer (50 mM sodium phosphate, pH 8.0, 300 mM NaCl, and 6 M guanidine HCl) and dialysed into 50 mM Bis-Tris, pH 7.0, 6 M urea at room temperature. Proteins extracted from inclusion bodies were purified using anion exchange chromatography in a 1-ml HiTrap Q Sepharose column. The proteins were eluted using a salt gradient.

2.4.10 Preparation of refolded OmpF

This was performed as in Visudtiphole *et al* with slight modification (Visudtiphole *et al.*, 2005). The purified OmpF from inclusion bodies was refolded by a 20x dilution in 50 mM Tris-HCl, pH 8.0, 1 mM DTT (dithiothreitol) and 0.1 mM EDTA containing the mixture of 1% (w/v) DG (n-dodecyl-β-D-glucopyranoside) and 0.4% (w/v) DDM (n-dodecyl-β-D-maltoside). After a stationary incubation at 37ºC for at least 3 days, the sample was precipitated by mixing 1:9 with cold ethanol (see above) and then the refolded trimeric OmpF was recovered by resuspending in 20 mM Tris-HCl, pH 7.4, 0.5% (v/v) Octyl POE. To completely exchange the refolding detergents to another detergent, the buffer exchange was achieved by anion exchange chromatography using a 1-ml HiTrap Q Sepharose column equilibrated with 20 mM Tris-HCl, pH 7.4, 0.5% (v/v) octyl POE. The refolded OmpF were eluted using a salt gradient.

2.5 Biophysical methods

2.5.1 Analytical ultracentrifugation (AUC)

Protein samples (400 μl) at the concentration of 0.3 – 1.5 mg/ml in buffer were analysed by Dr A Solovyova at Newcastle University Protein and Proteome Analysis (NUPPA). Sedimentation velocity (SV) experiments were conducted in a Beckman Coulter (Palo Alto, CA) ProteomeLab XL-I analytical ultracentrifuge using absorbance at 280 nm and interference optics. All runs were performed at 4^{o}C at a rotor speed of 48,000 rpm. The samples were loaded onto double sector aluminium-epon centerpieces. The SEDNTERP software programme was used to estimate the partial specific volume ($\bar{v}$) of protein from its sequence and the buffer density and viscosity at 4^{o}C (Laue *et al.*, 1992). Data were analysed with SEDFIT software programme (Schuck, 2000). The experimental sedimentation coefficients (s) were corrected to $s_{20,w}$ representing an s value in a standard condition of water at 20^{o}C. The $s_{20,w}$ values were calculated using the standard correction equation (Lebowitz *et al.*, 2002).

$$s_{20,w} = s_{T,B}\left(\frac{\eta_{T,B}}{\eta_{20,w}}\right)\frac{(1-\bar{\nu}\rho)_{20,w}}{(1-\bar{\nu}\rho)_{T,B}}$$

where T and B represent the temperature and buffer of experimental conditions, and 20,w indicates standard conditions. $\bar{\nu}$ is the partial specific volume of the protein, η is the viscosity of the solution, and ρ is the density of the solution.

2.5.2 Dynamic light scattering (DLS)

DLS measurements were performed with Zetasizer Nano (Malvern instrument Ltd.). 50 µl of protein at 0.1-0.5 mg/ml in 45 µl quartz glass cuvette (Hellma 105.251-QS) was measured at 25^{o}C or 30ºC in triplicates. Size measurements and data analysis were performed by Zetasizer software.

2.5.3 Matrix assisted laser desorption/ionisation – time of flight - mass spectrometry (MALDI-TOF MS)

All samples were sent to Dr J Gray and Dr A Solovyova at Biological Mass Spectrometry unit (Pinnacle) at Newcastle University. The mass spectra were measured on an Applied Biosystems Voyager V5. The two types of measurements performed are as follows.

- Peptide mass-fingerprint (PMF)

The unknown proteins from the sample in form of a SDS-PAGE gel slice were eluted and digested into smaller peptides by trypsin which cleaves the protein at lysine and arginine side chains. After proteolysis, a protein solution was mixed with matrix media (α-cyano-4-hydroxycinnamic acid (CHCA)). Calibration mixture 2 from ABSciex (Warrington, UK) was used to calibrate the machine. The masses of peptides were analysed by the programme Mascot using the peptide mass query tool. Next, the experimental trypsin fingerprint was compared to the fingerprint from the SwissProt database in order to search for potential matches to the unknown protein.

- Intact protein mass

The protein samples in solution were passed through a desalting column to exchange the buffer and remove salts. The samples were then solubilised in 60% (v/v) acetonitrile and 0.1% (v/v) trifluoroacetic acid. The sinapinic acid at 10 mg/ml in 30% (v/v) acetonitrile and 0.1% (v/v) trifluoroacetic acid was used as a matrix to mix with the samples. The instrument was calibrated using bovine carbonic anhydrase (BCA) with a molecular weight of 30 kDa.

2.5.4 Small angle x-ray scattering (SAXS)

Sample preparation

- ColN-TR and TolA II-III

Proteins at a concentration of 0.5 – 10 mg/ml were dialysed against 50 mM sodium phosphate, pH 7.4, 300 mM NaCl since colicin domains are insoluble in low salt conditions. The measurements were performed with at least 3 concentrations of proteins.

- OmpF/LPS

The LPS-free OmpF, LPS-added OmpF (adding Ra-LPS to LPS-free OmpF at a 1:5 OmpF/LPS molar ratio) and WT OmpF were passed through a Superose 12 column equilibrated with 10 mM Tris-HCl, pH 8.0, 150 mM NaCl and 0.2% (w/v) DDM. The protein-containing fractions collected from SEC were measured on the SAXS beamline using the column running buffer as a background.

- Nanodiscs

The preparation of nanodiscs was as previously described in section 2.2.4. The samples were purified using gel filtration chromatography with a Superose 12 column equilibrated with 20 mM Tris-HCl pH 7.4, 0.1 M NaCl, 0.5 mM EDTA. The fractions collected from SEC were concentrated using a Vivaspin concentrator (Sartorius Stedim Biotech) with 10 kDa molecular weight cut-off. The samples were then centrifuged for 15 min at 4^{o}C prior to a SAXS

measurement. The running buffer was used for a background subtraction. The concentration of samples was 0.5 to 1.0 mg/ml.

Data collection

SAXS data were collected on ESRF BM29 and Diamond B21 beamlines with different setups as shown below. The data reduction and buffer subtraction were performed using the software on site. The data analysis and modeling were carried out using the ATSAS software suite (Petoukhov *et al.*, 2012).

- Beamline BM29 at ESRF, Grenoble, France.

SAXS data were collected at 1 Å wavelength with a sample-to-detector distance of 2.85 m covering a Q range of 0.05 – 0.45 $Å^{-1}$. The automated sample changer was used to handle the samples. The samples stored in 1.5 ml Eppendorf tubes were automatically injected into a 1.8 mm diameter quartz capillary and measured at 4^{o}C.

- Beamline B21 at Diamond, Harwell, UK

SAXS data were collected using an x-ray beam with a wavelength of 1 Å, and the distance from the sample to detector was 4 m, covering a Q range from 0.015 – 0.3 $Å^{-1}$. The samples were in a 96-well plate and handled by an automated sample changer. The measurements were conducted at 4^{o}C and 25^{o}C.

2.5.5 Small angle neutron scattering (SANS)

Sample preparation

- OmpF/ColN-TR

50 mM sodium phosphate buffer, pH 7.4, 300 mM NaCl was made at 4 different H_2O/D_2O ratios (16 %, 41%, 77% and 100 % D_2O). Octyl glucosides (OG) in three different forms (hydrogenated OG (h-OG), tail-deuterated OG (d17-OG) and fully-deuterated OG (d24-OG)) were added to the buffer at certain ratios

(Table 2.10) to give the final concentration of 2% (w/v) h/d OG. By mixing h- and d-OG using these ratios, the scattering length densities (SLD) of OG are equal to the SLDs of all solvents. The buffers with 2% (w/v) h/d OG were used to solubilise the dOmpF pellet from ethanol precipitation. The dOmpF in the buffer with 2% (w/v) h/d OG was mixed with ColN-TR in the buffer without OG at a 1:1 dOmpF/ColN-TR molar ratio. This formed complexes at 1% (w/v) h/d OG in the buffer and these were then dialysed against the same buffer with 1% (w/v) h/d OG. Dialysis confirms the buffer composition and provides a reference buffer which is identical to the sample buffer.

Table 2.10 The ratio of octyl glucosides in all D_2O solution used in SANS study

%D_2O	Percentage of each OG forms in OG buffer		
	h-OG	d17-OG	d24-OG
16	100	0	0
41	58	42	0
77	0	94	6
100	4	0	96

- OmpF/TolA II-III

50 mM sodium phosphate buffer, pH 7.4, 300 mM NaCl was made at two different H_2O/D_2O ratios (13 % (v/v) and 100 % (v/v) D_2O). Hydrogenated SDS (h-SDS) was added to 13% D_2O buffer (which has the same SLD as h-SDS) to give a final concentration of 1% (w/v) while 5% (w/v) h-SDS and 95% (w/v) deuterated SDS were added to 100% D_2O buffer to give a final concentration of 1% (w/v) h/d-SDS with the same SLD as D_2O. These two solutions were used as the stock solutions to prepare 41% and 90% D_2O buffer in which the SLD of SDS is always matched to the solvent. Eventually, there are four solutions containing 1% (w/v) SDS used in this experiment, 13%, 41%, 90% and 100 % D_2O solutions. In order to form complexes between dOmpF and domain II-III of TolA, dOmpF pellets from ethanol precipitation as described above were resuspended in each of the D_2O buffers and then formed complexes with TolA II-III (in the same buffer without SDS) at a 1:1 OmpF/TolA

molar ratio. Therefore, the binary complexes are in 13, 41, 90 and 100 % (v/v) D_2O solutions containing 0.5% (w/v) h/d-SDS as TolA II-III were in the same buffer without SDS. After mixing altogether, each sample was dialysed against 13, 41, 90 and 100% (v/v) D_2O solutions in the presence of 0.5% (w/v) h/d-SDS.

- OmpF/LPS

The natural LPS was removed from dOmpF using size exclusion chromatography as previous attempts in our group to refold d-OmpF were unsuccessful. A Superose 12 column was equilibrated with 20 mM Tris, pH 7.5, 300 mM NaCl, 10 mM EDTA and 0.5% octyl-POE. The purified dOmpF was then used to form complexes by incubation with Ra-LPS at a 1:5 dOmpF/LPS molar ratio at 37^{o}C overnight. To remove unbound and loosely bound LPS, the samples were passed through a Superose 12 column again using the same buffer without EDTA. After SEC, the proteins in the fractions were precipitated by pre-chilled ethanol at 1:9 ratio (90% ethanol in total). The protein pellet was resuspended with 50 mM potassium phosphate, pH 7.5, 150 mM NaCl containing 0.5% h/d SDS in 13%, 27%, 41%, 77% and 100% D_2O and dialysed against the same buffer. The preparation of buffer was the same as the procedure in the preparation of OmpF/TolA II-III complex.

- OmpF/APol

The preparation of OmpF/APol complexes was described in section 2.2.3. The samples were then passed through a Superose 12 column equilibrated with 20 mM sodium phosphate, pH 7.9, 100 mM NaCl. The protein-containing fractions were concentrated using a Vivaspin with 10 kDa molecular weight cut-off and then dialysed against the same buffers in 0%, 23.5%, 77% and 100% D_2O. The final protein concentration in the sample was 2 mg/ml.

- Nanodiscs

The same procedure as the preparation of the nanodiscs sample for SAXS was used but the column running buffer was changed to 20 mM Tris-HCl pH 7.4, 0.1 M NaCl, 0.5 mM EDTA in 100% D_2O.

Data collection

SANS data were recorded on D22 and SAN2D beamlines with different setups as shown below. The scattering data recorded on the detector were reduced to one-dimensional scattering profiles, and the scattering of the buffer was subtracted from the sample profile using the software on site. The data analysis and modeling were carried out using ATSAS suite (Petoukhov *et al.*, 2012).

- D22 beamline at ILL Grenoble, France.

Samples (approx 300 µl) were measured in a 1 mm pathlength quartz cuvette at 6 Å wavelength. The measurements were conducted at 20^{o}C at sample-detector distances of 2, 5.6 and 11.2 m (Q range from 0.03 - 0.33 Å^{-1}).

- SANS2D at ISIS, Harwell, UK

SANS data were recorded with a 4-m sample-to-detector distance covering Q range from 0.005 – 0.75 Å^{-1}. This is a time of flight-SANS instrument using the white beam technique so the wavelengths of the neutrons ranged from 2 – 14 Å. The samples (approx 300 µl) were measured in a 1 mm pathlength quartz cuvette at 20^{o}C.

2.5.6 Transmission electron microscopy (TEM)

Preparation of negatively stained specimens was achieved using the single-droplet Parafilm procedure as described in (Harris, 1997). Samples at the concentration of 50 µg/ml were adsorbed to glow-discharged carbon-coated grids and individually negatively stained with uranyl acetate (2.0% w/v). Micrographs were recorded at 100 kV on a Philips CM100 EM in the Biomedical Microscopy Unit at Newcastle University. Digital images were taken by a 1024x1024 pixel CCD. Sizes of molecules were measured using JMicroVision v1.27 software.

Chapter 3 Structural studies of the Colicin N translocon complex by small-angle neutron scattering

3.1 Introduction

The translocation process of Colicin N (ColN) is one of the key steps in its ability to kill gram negative bacteria. The outer membrane of gram-negative bacteria has an extracellular leaflet of tightly packed lipopolysaccharides (LPS) which help to protect them from antibiotics, bile salts and other external toxic agents. To kill the cells, ColN must cross this barrier to reach the inner membrane of bacteria where it forms a pore resulting in potassium and phosphate efflux (Guihard *et al.*, 1993; Cascales *et al.*, 2007). However, ColN transport across the outer membrane has not been clearly described.

ColN is composed of three domains termed the translocation and the receptor-binding and the pore-forming domains. The first two domains are essential for the interaction of ColN with the bacterial cell surface. The translocation domain (T-domain) interacts with its translocator, OmpF, whereas the receptor binding domain (R-domain) binds to LPS (Johnson *et al.*, 2013; Johnson *et al.*, 2014). Furthermore, the T-domain also interacts with the C-terminal domain of TolA (TolA III) after the T-domain has entered into the periplasm using OmpF (Raggett *et al.*, 1998). The translocation of ColN was previously described in Figure 1.10. Less is known about how TolA interacts with OmpF prior to ColN translocation. The *in vitro* interaction of TolA with OmpF has been reported to require the central domain of TolA (TolA II) for complex formation (Derouiche *et al.*, 1996).

The aim of this study is the structural characterisation of proteins which play a key role in the translocation of ColN. Small angle scattering was employed due to the intrinsic flexibility of ColN-TR and TolA II-III and the difficulty in studying membrane proteins. SAXS is a suitable technique for soluble proteins while SANS is a useful technique for a complex system such as a membrane protein in detergent micelles. Here small-angle neutron scattering (SANS) was utilised

to study the solution structures of OmpF in complex with translocation and receptor binding domains of ColN (ColN-TR) or the C-terminal and central domains of TolA (TolA II-III). Since OmpF is a membrane protein, detergents are required to stabilise it in aqueous solution. The OmpF/ColN-TR complexes were solubilised in the mild detergent, octyl glucoside (OG) because their association has been measured by isothermal titration microcalorimetry (ITC) in neutral detergent (Evans *et al.*, 1996a). The OmpF/TolA II-III complexes were stabilised in SDS as this was used to prepare the published complexes (Derouiche *et al.*, 1996; Dover *et al.*, 2000). The contrast variation technique in the SANS experiment was exploited to observe either individual components or the whole complex by varying H_2O/D_2O content. The solution behaviour of ColN-TR and TolA II-III alone in detergent free solution was also studied by SAXS. Table 3.1 summarises the protein in this study observed by SAXS and SANS.

Table 3.1 List of samples for the structural studies by SAXS and SANS

Proteins	Techniques	Conditions
ColN-TR	SAXS	Phosphate buffer
OmpF/ColN-TR complex	SANS	Phosphate buffer with octyl glucoside (mild detergent)
TolA II-III	SAXS	Phosphate buffer
OmpF/TolA II-III complex	SANS	Phosphate buffer with SDS (ionic detergent)

3.2 Results

3.2.1 Protein production and purification

- Deuterated OmpF

To study the protein complexes by SANS, contrast variation and the selective deuteration of individual components allow us to observe both the whole complex and individual component by varying the D_2O content in the sample. In most of the experiments described here, deuterated OmpF (dOmpF) is used to differentiate it from the other protein components such as ColN or TolA. The deuteration of OmpF was achieved by growing *E. coli* BE3000 cells in 85% D_2O minimal media using glucose as a carbon source. The dOmpF was then extracted from the outer membrane by high-salt buffer and detergents in H_2O. The details were previously described in the Methods Section (Chapter 2 section 2.4.8). Protein samples were taken at each step of the purification and analysed by SDS-PAGE (Figure 3.1). As expected, the SDS-PAGE analysis of the dOmpF extract showed that the single band of dOmpF monomer (heat denatured samples) ran at slightly below 40 kDa whereas native dOmpF trimer shifted to ≈70 kDa. This is the typical feature of *E. coli* porins in which the natively folded trimeric porins migrate more slowly than the denatured monomers, but faster than their 111 kDa size would predict, on SDS-PAGE (Sen and Nikaido, 1990). Some dOmpF were removed in the wash steps due to the loose association with the membrane. In the preparation used here dOmpF was successfully produced with the yield of 74 mg of dOmpF obtained from 1.5-litre D_2O minimal media. There is no need for further OmpF identification as the strain used was well defined. OmpF is the only porin produced by this strain (Garavito and Rosenbusch, 1986).

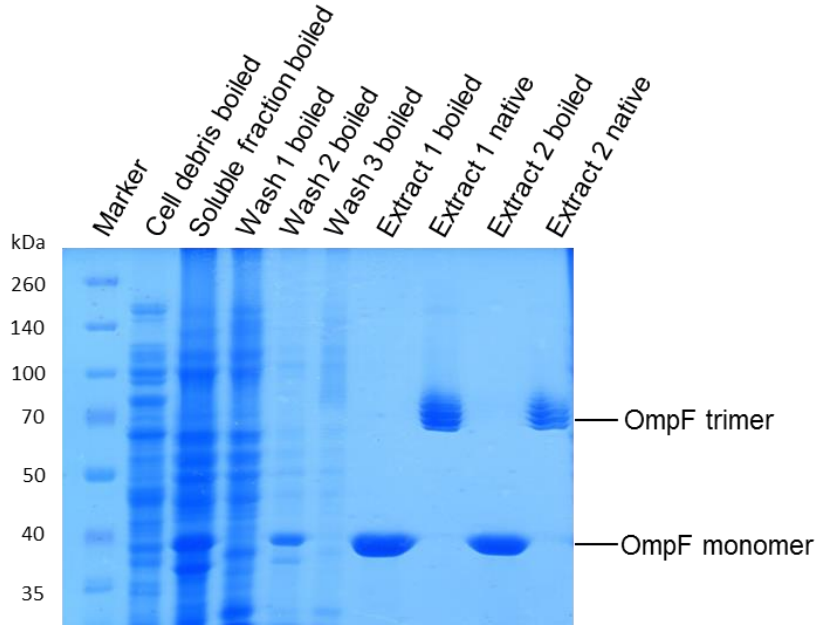

Figure 3.1 SDS-PAGE of dOmpF preparations from *E. coli* BE3000. Samples taken from each stage of purification were visualised on 10% SDS-PAGE gel. Denatured and native dOmpF ran at 40 kDa and 70 kDa, respectively.

- ColN-TR

Truncated ColN comprising translocation and receptor binding domains (ColN-TR) was expressed in *E. coli* BL21-AI from a plasmid encoding a C-terminal His-tagged ColN-TR gene in a pET3a vector. The expression level of ColN-TR was monitored by performing SDS-PAGE of cell lysates from samples taken every hour during cell culture (Figure 3.2a). It was demonstrated that the ColN-TR was expressed from the first hour of induction and migrated on SDS-PAGE at ≈20 kDa. His-tagged ColN-TR was then purified by using a Ni-NTA column. The protein-containing fractions were loaded onto a 12% SDS-PAGE gel in order to assess the purity of the protein (Figure 3.2b).

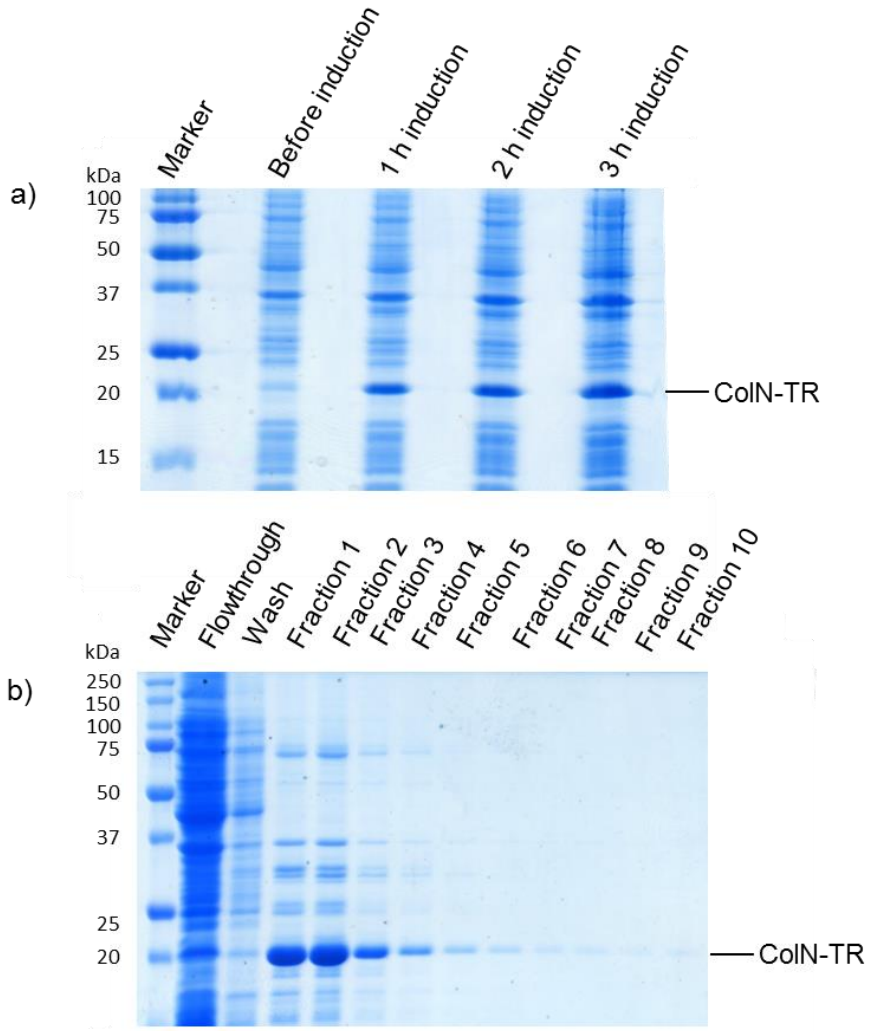

Figure 3.2 SDS-PAGE of ColN-TR expression and purification. a) Samples of cell lysates taken before and after cell induction. The bands corresponding to ColN-TR ran at 20 kDa. b) SDS-PAGE of ColN-TR samples after purifying by His-tagged affinity column. Fractions were 5 ml.

However, there were still significant amounts of contaminants in ColN-TR and further purification was needed. Due to the fact that the theoretical isoelectric point (pI) of ColN-TR is 9.67, ColN-TR was loaded on to a cation exchange column (Mono S 5/50 GL) where it was strongly retained. The pI is the pH where a protein has no net charge. The theoretical pI of protein is the mean of pK values of amino acid composition calculated by the software, ProtParam (Gasteiger *et al.*, 2003). ColN-TR was eluted by a salt gradient as shown in the elution profile in Figure 3.3a. The purity of proteins confirmed by SDS-PAGE showed that most contaminants were removed and the expected bands of

ColN-TR at 20 kDa were clearly seen in all protein-containing fractions (Figure 3.3b).

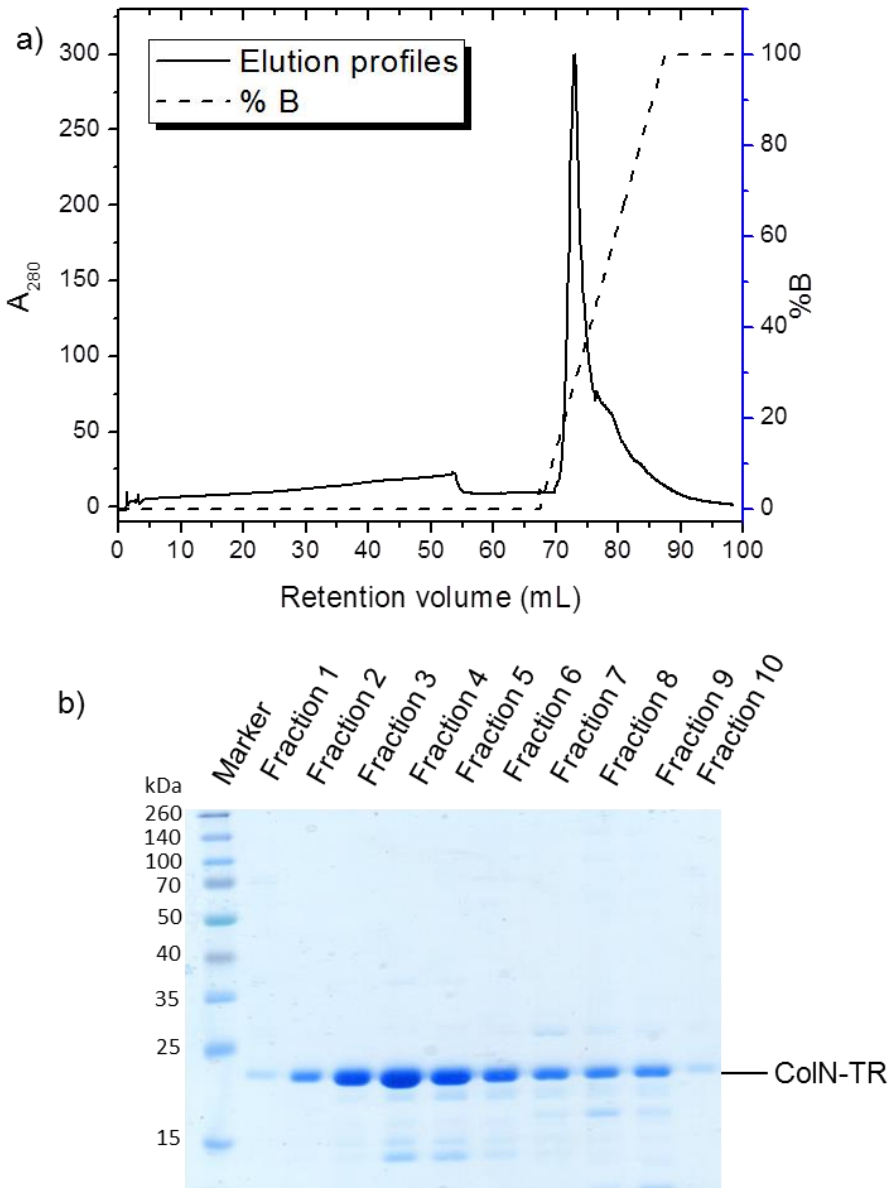

Figure 3.3 Purification of ColN-TR by cation exchange chromatography. a) Elution profile of ColN-TR using Mono S 5/50 GL equilibrated with buffer A (20 mM phosphate buffer, pH 7.5, 150 mM NaCl). A gradient from 0% to 100% of buffer B (20 mM phosphate buffer, pH 7.5, 1 M NaCl) was applied to the column. b) SDS-PAGE of protein-containing fractions taken from Mono S column. Fractions were 5 ml starting at 70 ml.

- TolA II-III

The truncated TolA was constructed in the pET8c expression vector having ampicillin resistance gene. The combined central and C-terminal domains of TolA with a His tag at N-terminus (TolA II-III) were expressed using *E. coli* BL21-AI as a host. Samples of cell culture were collected before and after induction by L-arabinose. The expression of TolA was tested by SDS-PAGE of cell lysates (Figure 3.4a). The samples were run alongside purified TolA II-III which runs at a 50 kDa even though the molecular size of TolA II-III is 39.66 kDa. The proteins were then purified by Ni-NTA column and the purity of TolA II-III was evaluated by SDS-PAGE (Figure 3.4b). According to the SDS-PAGE gel, TolA II-III was relatively clean therefore no further purification step was required.

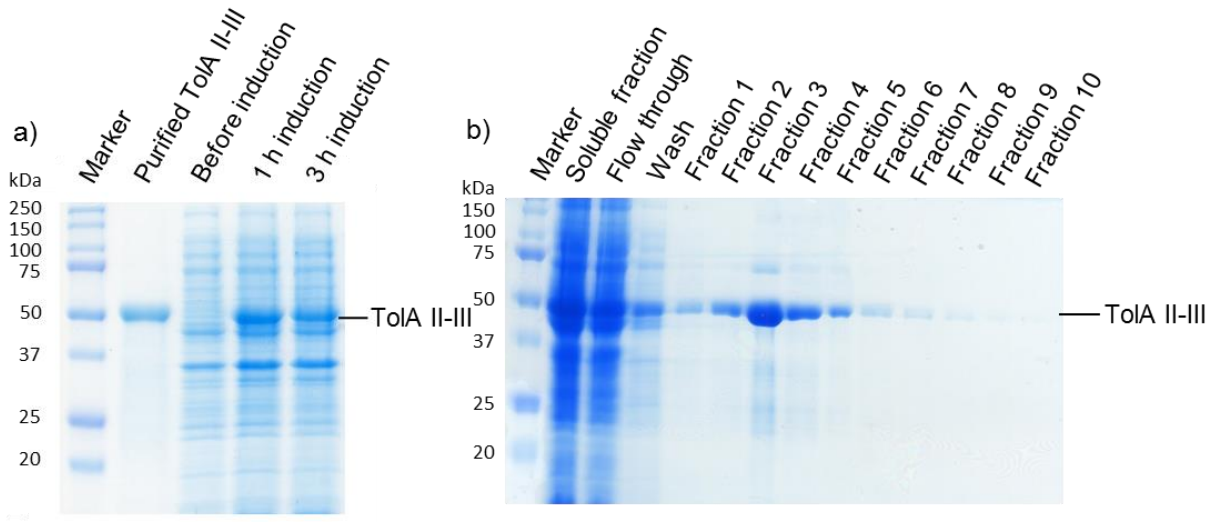

Figure 3.4 SDS-PAGE analysis of TolA II-III expression and purification. a) SDS-PAGE of cell lysates running along with purified TolA II-III showed unfolded TolA II-III ran at 50 kDa. b) The assessment of protein-containing fractions from the Ni-NTA column by SDS-PAGE. Fractions were 5 ml.

3.2.2 Match point determination of deuterated components

The contrast variation technique used in the SANS experiment requires knowledge of the accurate contrast match point (CMP) of each component in the samples. At certain H_2O/D_2O ratio, molecules can be invisible to neutrons.

The CMP is the percentage of D_2O where the scatter of solvent is equal to the scatter of the sample. At CMP, the neutrons cannot distinguish between the scatter of solvent and sample. There are two approaches to determine the CMP of molecules, by calculation or by measurement. The CMP of simple molecules like detergents can be accurately calculated whereas that of proteins must be done experimentally. In this study, we investigated the interaction of deuterated OmpF (dOmpF) in complex with ColN-TR and TolA II-III in the presence of a mixture of hydrogenated and deuterated detergents. The CMP of hydrogenated proteins is known to be at 41% D_2O (Jacrot, 1976). However, the CMP of deuterated proteins and detergents must be determined.

- Contrast match point of detergents by calculation.

As OmpF is a membrane protein, all complexes in the experiment must be handled in the presence of detergents. The detergents form micelles in solution which interfere with the scatter of protein complexes in SANS studies. To solve this problem, a recently developed strategy of mixing hydrogenated and deuterated detergents to match all D_2O contents has been described (Clifton *et al.*, 2012). This allows detergents to be invisible to neutrons and so only protein complexes can be observed. To achieve this, the CMP of both hydrogenated and deuterated detergents must be known. The detergents utilised in this study are the non-ionic detergent, octyl glucoside (OG) and the anionic detergent, sodium dodecyl sulphate (SDS). There are three forms of OG commercially available which are: hydrogenated OG (h-OG), tail-deuterated OG (d17-OG) and fully deuterated OG (d24-OG) (purchased from Anatrace). There are two forms of SDS available which are hydrogenated SDS (h-SDS) and fully deuterated (d-SDS). The structures of detergents in this study are illustrated in Figure 3.5.

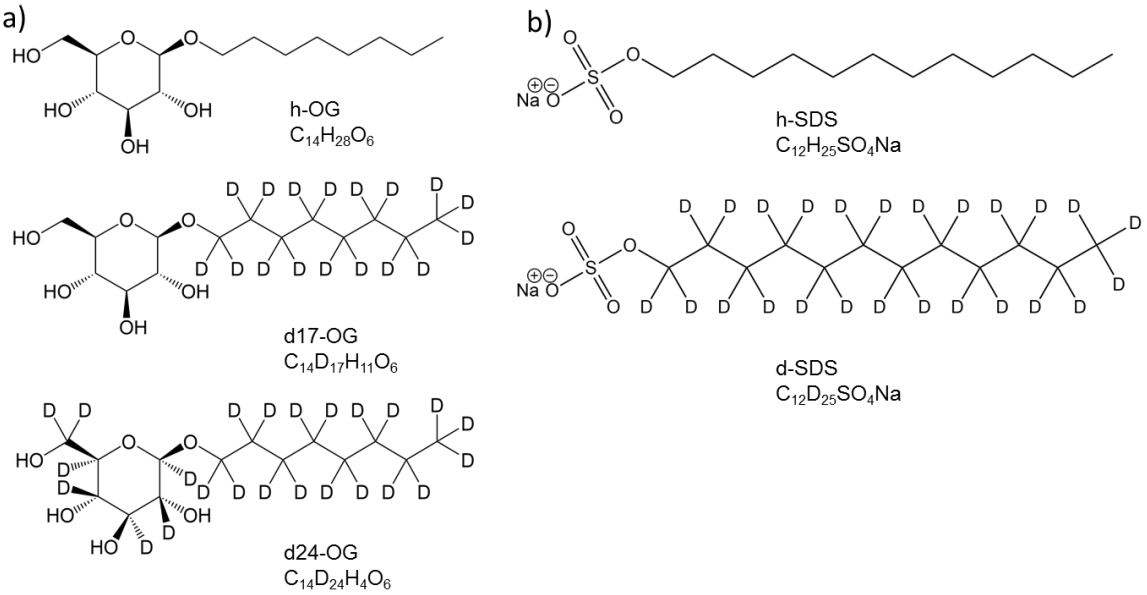

Figure 3.5 Structure and chemical composition of hydrogenated and deuterated detergents. a) Three different forms of OG, h-OG, tail-deuterated OG (d17-OG) and fully deuterated OG (d24-OG) b) two forms of SDS; h-SDS and d-SDS.

To determine the CMP, we need to find the scattering length density (SLD) of the molecule. SLD is the strength of the interaction of neutrons with the nuclei of molecules. It is defined as the sum of coherent scattering lengths of all atoms per unit volume. Therefore, SLD (ρ_N) is given by

$$\rho_N = \frac{\sum b}{V}$$

Where b is the coherent neutron scattering length of atoms in a molecule (cm) and V is the volume of the molecule (cm^3). The coherent neutron scattering length of atoms commonly found in biomolecules are summarised in Table 3.2.

Table 3.2 Coherent neutron scattering length of atoms for SLD calculation.

Atom	b (10^{-12} cm)
H	-0.37409
D	0.6671
C	0.665
O	0.5803
N	0.936
P	0.513
S	0.2847
Na	0.363

The SLD of a molecule is then compared to that of a solvent. This is referred to as contrast. The contrast ($\Delta\rho_N$) is the difference of SLD between molecule (ρ_N) and solvent (ρ_N°).

$$\Delta\rho_N = \rho_N - \rho_N^\circ$$

The CMP is where SLD of a molecule is equal to that of the solvent ($\Delta\rho_N = 0$). This means there is no scattering from the molecule. Thus,

$$\rho_N = \rho_N^\circ$$

Where ρ_N° is simply the sum of the SLD of D_2O and H_2O in solution.

$$\rho_N = \left(x_{D_2O} \times \rho_{D_2O}\right) + \left(\left(1 - x_{D_2O}\right) \times \rho_{H_2O}\right) \quad \text{and}$$

$$x_{D_2O} = \frac{\rho_N - \rho_{H_2O}}{\rho_{D_2O} - \rho_{H_2O}}$$

Where x_{D_2O} is D_2O fraction in the solvent, ρ_{D_2O} is the SLD of D_2O and ρ_{H_2O} is the SLD of H_2O. Therefore, CMP is given by

$$CMP = \frac{\rho_N - \rho_{H_2O}}{\rho_{D_2O} - \rho_{H_2O}} \times 100$$

Following from the equations above, all the parameters used in the calculations and the CMP of the detergents are summarised in Table 3.3

Table 3.3 Parameters of detergents for determining contrast match point

Component	Composition	Mw ($g.mol^{-1}$)	$\bar{V}$ ($cm^3.g^{-1}$)	V (cm^3)	Exchangeable proton	Σb (cm)	ρ_N (x $10^{10} cm^{-2}$)	CMP (%D_2O)
h-OG	$C_{14}H_{28}O_6$	292.4	0.859	4.17×10^{-22}	0	2.316×10^{-12}	0.56	16.0
					4	6.481×10^{-12}	1.55	30.4
d17-OG	$C_{14}D_{17}H_{11}O_6$	309.5	0.830	4.27×10^{-22}	0	2.002×10^{-11}	4.69	75.4
					4	2.418×10^{-11}	5.67	89.4
d24-OG	$C_{14}D_{24}H_4O_6$	316.5	0.780	4.10×10^{-22}	0	2.731×10^{-11}	6.67	103.7
					4	3.147×10^{-11}	7.68	118.3
h-SDS	$C_{12}H_{25}SO_4Na$	288.38	0.863	4.13×10^{-22}	0	1.595×10^{-12}	0.39	13
d-SDS	$C_{12}D_{25}SO_4Na$	313.53	-	-	0	1.095×10^{-11}	6.74	104.8
H_2O	-	18	-	-	-	-	-0.562	-
D_2O	-	20	-	-	-	-	6.404	-

The design of SANS experiments relies on the CMP of detergents used in the sample preparation. In the study of OmpF/TolA complexes, the mixture of h/d SDS is used to stabilise the complexes. The same strategy as previously described in (Clifton *et al.*, 2012). The SANS data of complexes were recorded at 13%, 41%, 90% and 100% D_2O buffers in the presence of 0.5% (w/v) h/d SDS mixture.

However, in the case of OmpF/ColN-TR complexes formed in OG, the strategy was slightly changed. In brief, the measurement was carried out in 16%, 41%, 77% and 100% D_2O solutions. Three forms of OG were mixed at defined ratios to match the OG scattering to the solutions (Table 3.4). These ratios of OG were calculated from the CMP of OG without taking exchangeable protons of OG head into account. All the mixtures of h/d OG in buffer were measured on the SANS beamline against the buffer without OG. The scattering data displayed low signal of OG scatter in all D_2O solutions as the scattering curves were relatively flat (Figure 3.6a).

Table 3.4 Ratio of octyl glucosides in all D_2O solution used in SANS study

%D_2O	**Percentage of each OG forms in 1% OG (w/v) buffer**		
	h-OG	**d17-OG**	**d24-OG**
16	100	0	0
41	58	42	0
77	0	94	6
100	4	0	96

However, the CMPs of h/d OG obtained by estimation and experimental measurements have been recently reported; both of which were different from our calculations (Gabel *et al.*, 2014). By taking exchangeable protons into account, the CMP of each OG form increased significantly as shown in Table 3.3. When we investigated our previous results further by plotting the data on a logarithmic scale, it was found that the residual signals of OG were actually present in the sample, especially in the sample at high D_2O concentration (Figure 3.6b). At 16% and 41% D_2O, the noisy data indicated that there were only tiny signals contributing from the presence of OG while there was a more

obvious OG contribution at 77% and 100% D_2O. The OG and solvent scattering at 16% and 41% D_2O were similar while those at 77% and 100% were different (Figure 3.6c). This confirmed that exchangeable protons were replaced by deuterium at high D_2O concentration and the CMP is considerably changed in high D_2O content. Therefore, the CMPs of OG used in our experiments were underestimated and the scatter of OG was not properly matched to that of the solvent.

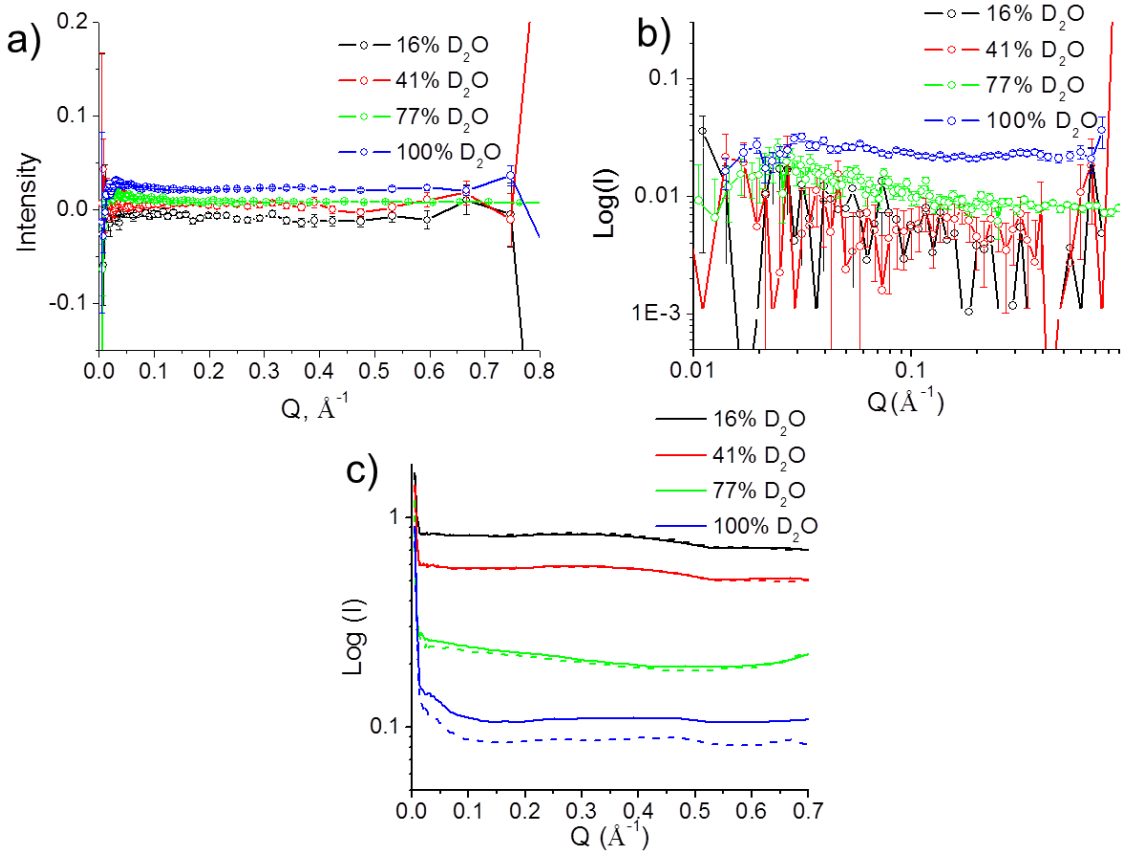

Figure 3.6 SANS data for h/d OG mixture in four D_2O solutions. 1%(v/v) h/d-OG mixture in 50 mM sodium phosphate, pH 7.5, 300 mM NaCl were measured at SANS2D beamline, ISIS. The data is after subtraction of the signal from the buffer without OG. a) absolute scale b) logarithmic scale. c) differences between solvent (dash lines) and OG scattering curves (solid lines).

- Experimental determination of contrast match point

Unlike the composition of detergents, proteins are more complicated due to a large number of exchangeable protons which must be taken into account when calculating CMP. The number of exchangeable protons cannot be accurately estimated because it is dependent on the conformation of proteins which determines which protons are exposed to the surrounding solution. For this reason, determining CMP of proteins using experimental data is more accurate. The aim is to find out at what $\%D_2O$ we would cease to observe any scattering from proteins. In brief, protein scattering curves were recorded over a range of D_2O percentages. The square roots of the normalised I(0) (divided by the concentration of sample, C) obtained from the Guinier approximation of the scattering curve were plotted against D_2O contents. I(0), the forward scattering, is defined as the scattering intensity at zero angle. By fitting a straight line to the data (see Figure 3.7) we find that the Y=0 intercept is the CMP of the protein.

In this study, the scattering curves of OmpF at 2 mg/ml in 5 D_2O solutions were recorded on SANS2D beamline, ISIS, as displayed in Figure 3.7a. It indicated that the scattering intensity of dOmpF declined gradually from 13% D_2O to 85% D_2O and increased at 100% D_2O. This suggested that the CMP of dOmpF should be between 85% and 100% D_2O. This was in good agreement with the plot of $\sqrt{I(0)}/C$ vs $\%D_2O$ as the x intercept (CMP of dOmpF) is equal to 87% D_2O (Figure 3.7b). There were two batches of dOmpF used in our experiment. One, purified without the further purification step gave a CMP of 87% D_2O and the batch purified and passed through a gel filtration column (a Superose 12 using 20 mM potassium phosphate, pH 7.5, 300 mM NaCl, 10 mM EDTA and 0.5% octyl-POE as a running buffer) with a CMP of 77% D_2O, which were used in the studies of the OmpF interaction with TolA II-III and ColN-TR, respectively. The data for the second batch of dOmpF was also illustrated in Figure 3.7c.

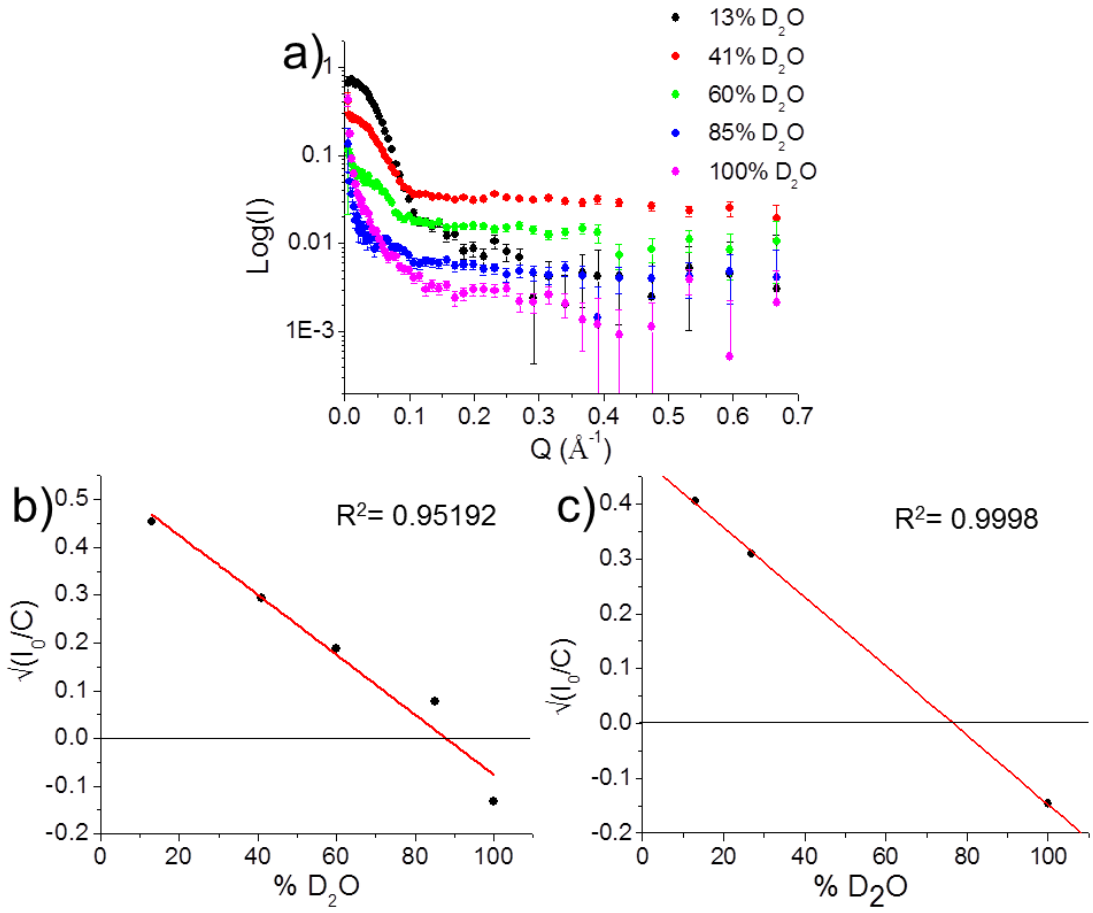

Figure 3.7 Experimental determinination of contrast match point of deuterated OmpF by SANS. a) SANS curve of dOmpF in 50 mM sodium phosphate, pH 7.5, 300 mM NaCl and 0.5% (w/v) h/d SDS as a function of D_2O content. The determination of contrast match point from dOmpF used in b) dOmpF/TolAII-III study and c) dOmpF/ColN-TR study. The linear fitting (lines) of data (symbols) showed the CMPs of dOmpF (x axis intercept) are 87%D_2O and 77%D_2O, respectively.

3.2.3 Examining on the deuteration level of deuterated protein

The deuteration level of deuterated proteins can be determined by mass spectrometry. The molecular mass difference between wild-type protein and deuterated protein results from hydrogen/deuterium replacement. Both hydrogenated and deuterated full-length OmpF were simultaneously analysed by MALDI-TOF-MS to ensure that both proteins were measured under the same conditions. The samples of hOmpF and dOmpF in H_2O solution were sent to the Biological Mass Spectrometry unit (Pinnacle) at Newcastle University. The

mass spectrum was recorded using an Applied Biosystems Voyager V5. OmpF samples were passed through a desalting column to remove detergents and salts. OmpF samples were then solubilised in 60% (v/v) acetonitrile and 0.1% (v/v) trifluoroacetic acid. Bovine carbonic anhydrase (BCA) was used to calibrate the mass and the matrix was sinapinic acid (10 mg/ml in 30% (v/v) acetronitrile and 0.1% (v/v) trifluoroacetic acid). According to the mass spectrum in Figure 3.8, the molecular mass of dOmpF is 38306.85 Da with a mass shift of +1202.82 Da when comparing to hOmpF. This mass shift originated from the replacement of non-labile hydrogen by deuterium in dOmpF. Therefore, the deuteration level of dOmpF is the percentage of non-labile hydrogen replaced by deuterium. There are 1814 non-labile hydrogens present in OmpF hence the deuteration level is (1203/1814) x 100 = 66%. This value is essential for analysing SANS data and modelling protein complexes.

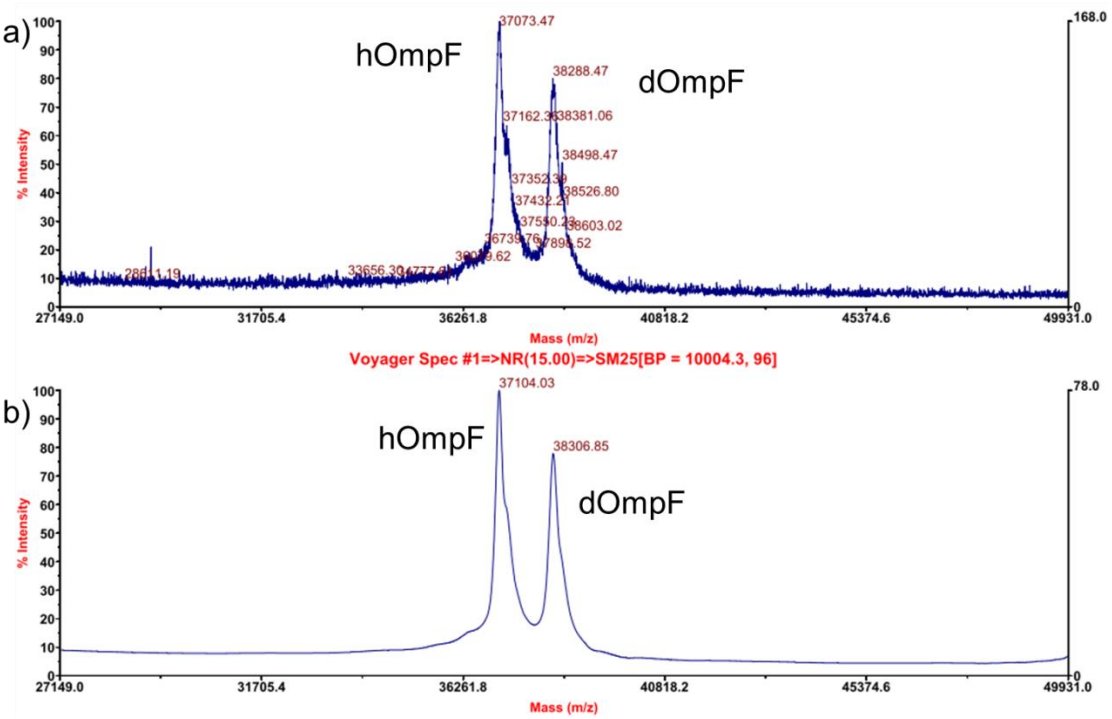

Figure 3.8 MALDI-TOF-MS of full length hydrogenated and deuterated OmpF. a) Raw data b) Processed peaks

3.2.4 Understanding the solution behaviour of ColN-TR.

The translocation domain of ColN (T domain) cannot be seen in the crystal structure of ColN because its structure is intrinsically disordered (Vetter *et al.*, 1998). To gain a better understanding of this disordered domain, we investigated its structure in solution by AUC and SAXS. Truncated ColN comprising of translocation and receptor-binding domains (ColN-TR) was studied as these two domains are essential for the translocation process of ColN. The extreme end of the T-domain has an OmpF binding site (OBS) (Housden *et al.*, 2010; Housden *et al.*, 2013) which enters into the lumen of the OmpF channel (Johnson *et al.*, 2013). Furthermore, the C-terminal pore-forming domain could dominate the interaction as observed in (Clifton *et al.*, 2012).

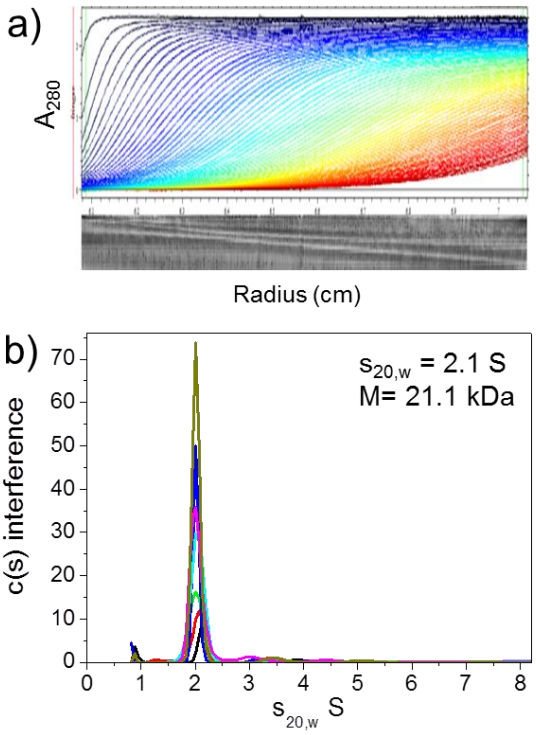

Figure 3.9 Sedimentation velocity of ColN-TR. a) Sedimentation velocity profiles. b) Sedimentation coefficient distributions c(s). ColN-TR at 0.3 – 1.5 mg/ml was in 50 mM sodium phosphate, pH 7.4, 300 mM NaCl.

Prior to performing the small angle scattering experiment, the homogeneity of the sample must be assessed by other techniques. AUC is a tool to monitor the

dispersity, shape and size of macromolecules in solution. AUC experiments were run by Dr A Solovyova of Newcastle University Protein and Proteome Analysis (NUPPA). The sedimentation velocity experiment revealed that ColN-TR was monodisperse in solution as only one major peak at $s_{20,w}$ = 2.1 S was observed corresponding to the molecular mass of the ColN-TR monomer, 21.1 kDa (s value was estimated for buffer viscosity and density at 20^{o}C) (Figure 3.9b). The s value indicated the compact folded structure of ColN-TR, even though the T-domain is flexible and disordered.

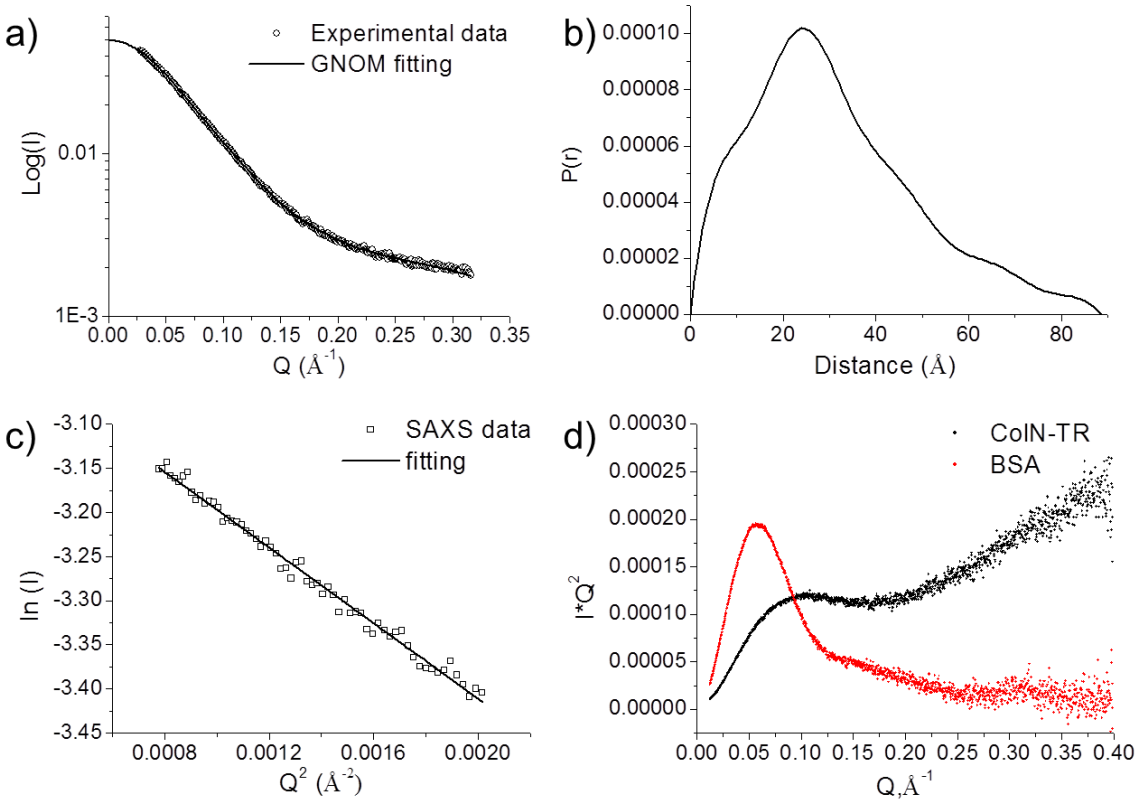

Figure 3.10 SAXS data for ColN-TR. a) SAXS data (symbols) and fitting (line) by GNOM b) Distance distribution functions, P(r), calculated using GNOM c) Guinier analysis d) Kratky plot for ColN-TR comparing to BSA. ColN-TR at 3.85 mg/ml in 50 mM sodium phosphate, pH 7.4, 300 mM NaCl and BSA at 2 mg/ml in water were used in the measurement.

In order to acquire a better understanding of the ColN-TR structure in solution, SAXS was carried out. SAXS curves of ColN-TR at 3.85 mg/ml were collected on beamline B21 at Diamond, Didcot, UK (Figure 3.10a). The pair-distribution function, P(r), obtained by an indirect Fourier transform within GNOM revealed

a D_{max} of 88.6 Å and a R_g of 25.20 ± 0.1 Å. This is consistent with a R_g of 25.3 ± 3.7 Å estimated from the Guinier approximation by PRIMUS (Figure 3.10 b and c) (Svergun, 1992; Konarev *et al.*, 2003). The agreement of R_g value obtained from both methods supported the lack of aggregation in samples. Furthermore, the Guinier plot of the SAXS curve gave a straight line which also confirmed the absence of aggregation in samples. Kratky representations of the SAXS curves were plotted to quickly screen for the degree of compactness of the proteins. A folded protein (BSA) displays a peak, while a disordered protein presents a continuous rise of the curve in the high Q region. The Kratky plot was derived as described in (Durand *et al.*, 2010; Rambo and Tainer, 2011). The scattering curves were plotted as $I(Q)*Q^2$ vs Q. The scattering intensity of a globular protein decreases as Q^{-4} in the large Q region. In Figure 1.10d, the Kratky plot of ColN-TR compared to BSA showed that ColN-TR is partly disordered as the curve indicated both a peak and a continuous rise at high Q. Also, the P(r) function in Figure 3.10b showed extended tails at long distance which is reminiscent of an elongated structure.

Due to the fact that ColN-TR is partly disordered, the data was further analysed by Ensemble Optimisation Method (EOM) (Bernado *et al.*, 2007). EOM is an approach used to characterise the structure of flexible proteins by SAXS. It allows for different protein conformations that can be present in the analysis. A pool of models based on the amino acid sequence of the T-domain and the crystal structure of the R-domain (Vetter *et al.*, 1998) were randomly generated. R-domain was treated as a rigid body connected with 90 dummy residues of T-domain. A generic algorithm then selected an optimized ensemble of conformers from the pool. EOM compares the SAXS experimental scattering with the combined theoretical scattering curve from the best selected conformers. EOM analysis of ColN-TR data created an optimized ensemble (containing 11 models) that fits the experimental data (Figure 3.11a). D_{max} distribution of the optimised ensemble was compared to that of a random pool (Figure 3.11b). It suggested that there were three major species of optimized ensemble which represent various levels of compactness of ColN-TR structure with D_{max} of 65 Å, 100 Å and 150 Å as shown in Figure 3.11d. Therefore, this

supported the notion that ColN-TR has a flexible structure. The sedimentation coefficients of eleven selected models were then calculated using the software, HYDROPRO (de la Torre *et al.*, 2000). Figure 3.11c displays the comparison of sedimentation coefficients of ColN-TR from AUC and SAXS data. The AUC data demonstrated a compact folded ColN-TR with the sedimentation coefficient of 2.1 S. In contrast to AUC analysis, the sedimentation coefficients of selected SAXS-derived models by EOM varied from 1.5 S and 2.0 S.

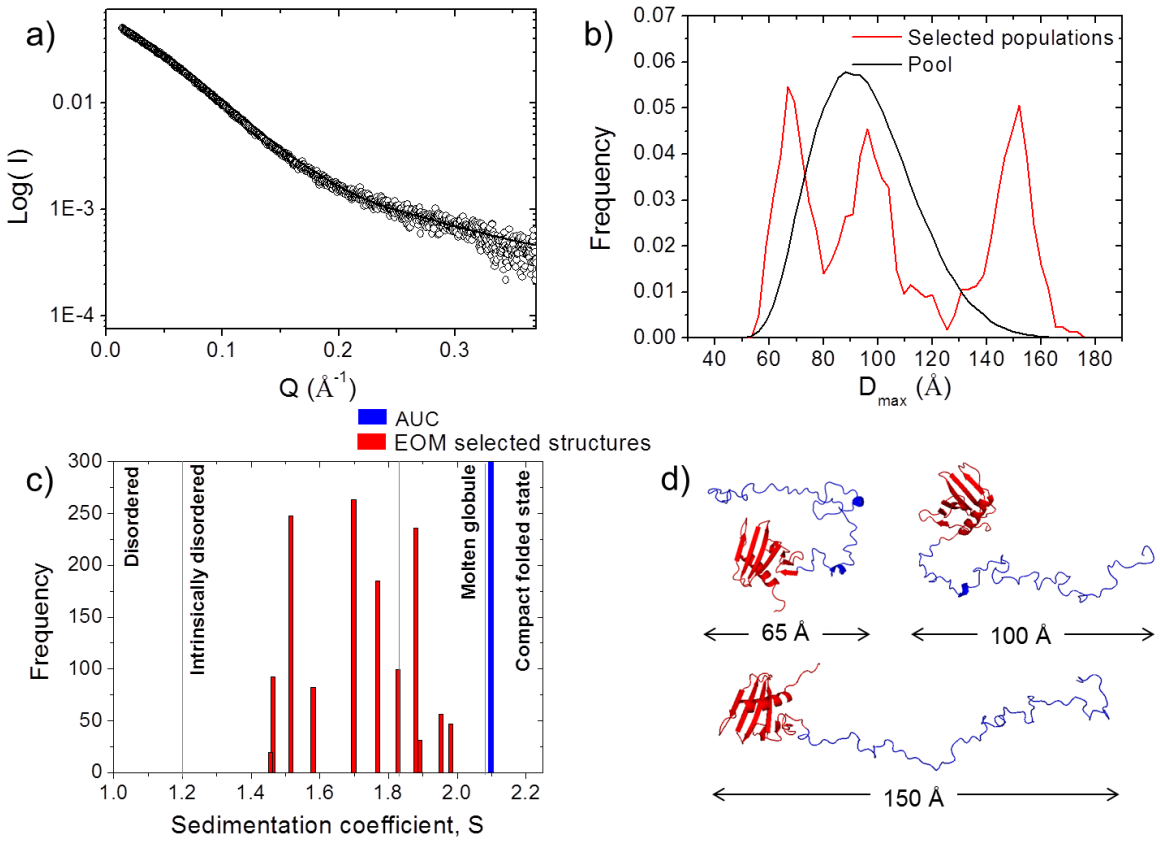

Figure 3.11 EOM analysis of ColN-TR. a) SAXS data (symbols) and fitting (line) generated from EOM. b) D_{max} distributions of the pool structure (black) and selected structure (red) from EOM analysis c) Distribution of sedimentation coefficient obtained from EOM selected structure (red) comparing to AUC data (blue). d) The example of ColN-TR structures from EOM analysis showing the different degrees of compactness. T and R domain of ColN are shown in blue and red, respectively.

3.2.5 Uncovering the structure of OmpF/ColN-TR complex in neutral detergents by small-angle scattering

After binding to LPS via the R-domain (Johnson *et al.*, 2014), the first step of ColN translocation requires the interaction of ColN with OmpF at the bacterial cell surface. The translocation domain of ColN is known to be responsible for this binding. To gain insight into the translocation process of ColN, a structural study of ColN-TR complexed with OmpF was performed by SANS. ITC data has revealed that the ColN-TR binds to OmpF with a K_d of 1.60 μM (Johnson *et al.*, 2013) thus ColN-TR definitely interacts with OmpF at the concentration used in this SANS study (approximately 3 mg/ml or 53 μM). The ColN-TR formed complexes with deuterated OmpF at a 1:1 molecular ratio (3 molecules of ColN-TR per 1 dOmpF trimer) in 50 mM sodium phosphate, pH 7.5, 300 mM NaCl and the mixture of 1% (w/v) h/d OG using the contrast variation technique. Due to the CMP underestimation of OG, pure micelles of detergents in all measured D_2O solutions are visible to neutrons. However, the scattering data was subtracted by the scattering data of the buffer with OG. Thus, the scatter of micelles should not be present in the final scattering profiles but the OmpF-bound detergents are still visible, especially at high D_2O content. The scattering curves of complexes were collected at 16%, 41%, 77% and 100% D_2O on SANS2D beamline, ISIS (Figure 3.12a). The data is after subtraction of the signal from the buffer with OG (Figure 3.12d). Using these D_2O solutions, we observed the complexes differently. At 16% and 100% D_2O, the whole complex was visible to neutrons. At 41% D_2O which is the CMP of ColN-TR, only dOmpF can be seen. At 77% D_2O which is the CMP of dOmpF, only ColN-TR is observed.

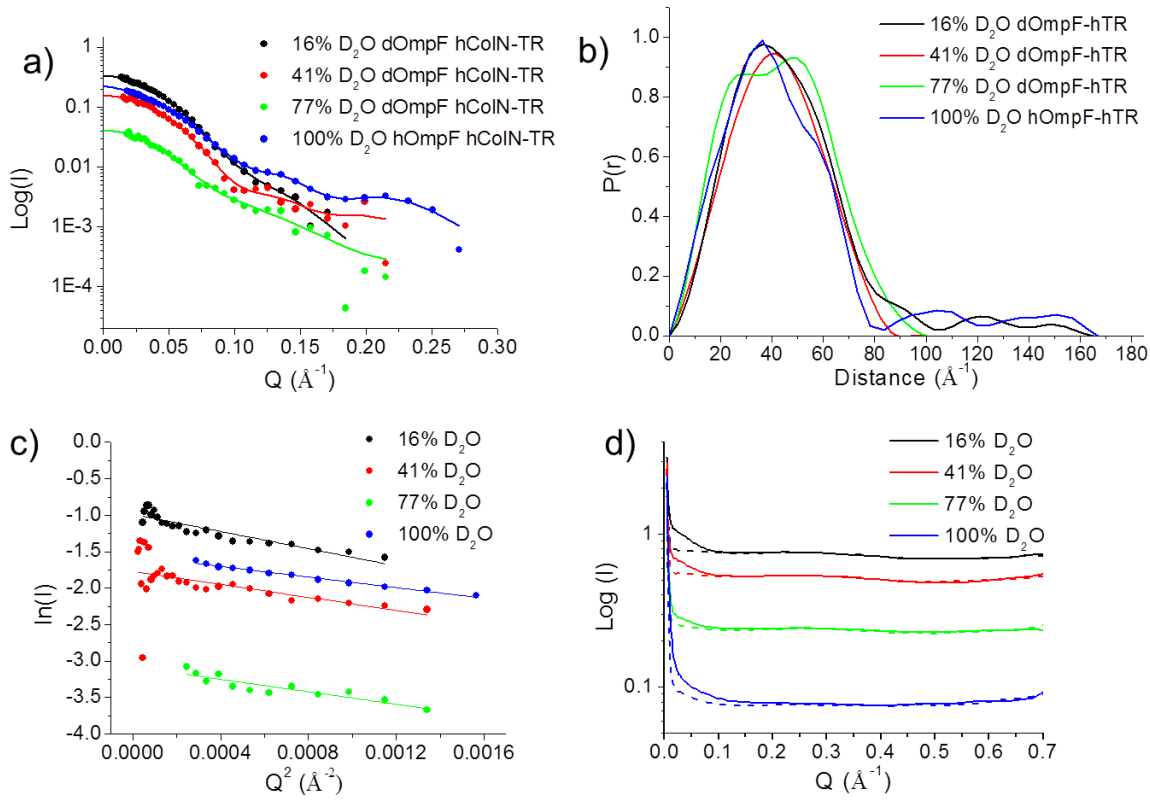

Figure 3.12 SANS data for dOmpF/ColN-TR complexes in 1% h/d OG. a) SANS data (symbols) and fitting (lines) generated by GNOM. b) Distance distribution function, P(r), calculated by GNOM. c) Guinier analysis. d) Scattering curves of samples (solid lines) and buffers with OG (dash lines) before the background subtraction.

In Figure 3.12b, the P(r) function made by the indirect Fourier transforms using GNOM suggested that the smallest P(r) was observed at 41% D_2O whereas the largest P(r) was shown in 16% and 100% D_2O. At 77% D_2O, the P(r) has two maxima which is an indication of a multi-domain structure suggesting more than one molecule of ColN-TR is present in the complexes (see (Clifton *et al.*, 2012)). It confirmed that ColN-TR certainly interacted with OmpF because the particles became larger in the D_2O solutions where both ColN and OmpF are visible. According to Table 3.5 demonstrating R_g and D_{max} from the Guinier plot and P(r) function, R_g values from these two analyses are consistent. The agreement of R_g values is a sign of the proper assignment of D_{max} and the lack of aggregation in samples. The linear behaviour in the Guinier plot of all D_2O

solution also confirmed that the samples are homogenous and free of aggregation.

Table 3.5 Summary of structural parameters for dOmpF/ColN-TR complexes, OmpF and ColN-TR by Guinier approximation and P(r) function. PRIMUS is used for Guinier analysis and GNOM calculated P(r) function.

Sample	Guinier Analysis $0.4<R_gQ<1.3$	P(r) function	
	R_g (Å)	R_g (Å)	D_{max}(Å)
dOmpF:hColN-TR in 16% D_2O (entire complex)	35.0 ± 0.927	37.08 ± 1.713	167.0
dOmpF:hColN-TR in 41% D_2O (OmpF only)	32.0 ± 1.250	31.64 ± 0.350	85.1
dOmpF:hColN-TR in 77% D_2O (ColN-TR only)	35.4 ± 4.383	34.25 ± 1.670	121.2
hOmpF:hColN-TR in 100% D_2O (entire complex)	40.8 ± 0.420	39.35 ± 1.306	167.0
hColN-TR in H_2O	25.3 ± 3.741	25.20 ± 0.069	88.6

To further investigate where ColN-TR interacted with OmpF, Stuhrmann analysis was carried out. This analysis of contrast variation represents the effect of changing solvent scattering density on the R_g of complexes. For this to work, the two components present in complexes must have different scattering length densities and therefore CMP. The variation of R_g as a function of contrast ($\Delta\rho_N$) is given by the Stuhrmann equation (Ibel and Stuhrmann, 1975).

$$R_g^2 = (R_g^2)_{1/\rho\to 0} + \frac{\alpha}{\Delta\rho_N} + \frac{\beta}{\Delta\rho_N^2}$$

where $(R_g^2)_{1/\rho\to 0}$ stands for the R_g at infinite contrast. The analysis can be done by plotting of R_g^2 against $\frac{1}{\Delta\rho_N}$, where R_g is radius of gyration derived from the Guinier plot and contrast ($\Delta\rho_N$) is defined as the difference of scattering length density between protein complexes and solvent. The $\Delta\rho_N$ is calculated from

MULCh (ModULes For The Analysis Of Contrast Variation Data) using the information from Guinier analysis (Whitten *et al.*, 2008). The coefficients, α and β, are obtained from the Stuhrmann plot by fitting a parabola to the experimental data points. The sign of α reveals where the R_g of the lower CMP component compares to the R_g of the higher CMP one. The Stuhrmann analysis of dOmpF/ColN-TR complexes yielded a negative value of α which showed that the lower CMP component (ColN-TR) is on the outside of higher CMP component (dOmpF) (Figure 3.13). However, the error bars on the Stuhrmann plots were relatively large thus this analysis did not provide conclusive evidence for the localisation of ColN-TR on dOmpF.

We attempted to resolve the structure of complexes by *ab initio* and rigid body modelling, however, the models were inaccurate (data not shown). Due to the underestimation of CMP for OG; the OG was not matched in all measured D_2O solutions. Even though the SANS curve were subtracted by the buffer containing OG as the background, there will still be residual signals of OG bound to dOmpF. This leads to a larger complex than provided by the protein alone. Therefore, experiments must be repeated with the correct CMP value.

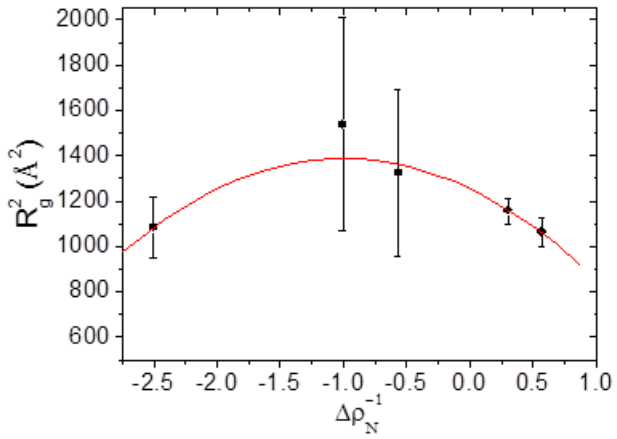

Figure 3.13 Stuhrmann analysis of dOmpF/ColN-TR complex. The reciprocal of the contrast is plotted against the square of the radius of gyration (R_g). The experimental data points are shown as symbols. A parabola fitted to the data is shown in red.

3.2.6 Structural characterisation of TolA II-III in solutions

To date, the high resolution structure of only the C-terminal domain of TolA III has been resolved by X-ray crystallography (Lubkowski *et al.*, 1999). TolA-I is the transmembrane domain which is not included in soluble constructs. TolA II is predicted to consist of long helices and, due to its probable flexibility, solution scattering is the best approach to shed light on the structure of TolA II-III. The solution structure of truncated $TolA_{42-421}$ including central (domain II) and C-terminal domains (domain III) but missing the N-terminal membrane spanning domain (domain I) was examined by SAXS. The schematic representation of TolA domains and localisation of TolA protein in *E. coli* is in Figure 3.14.

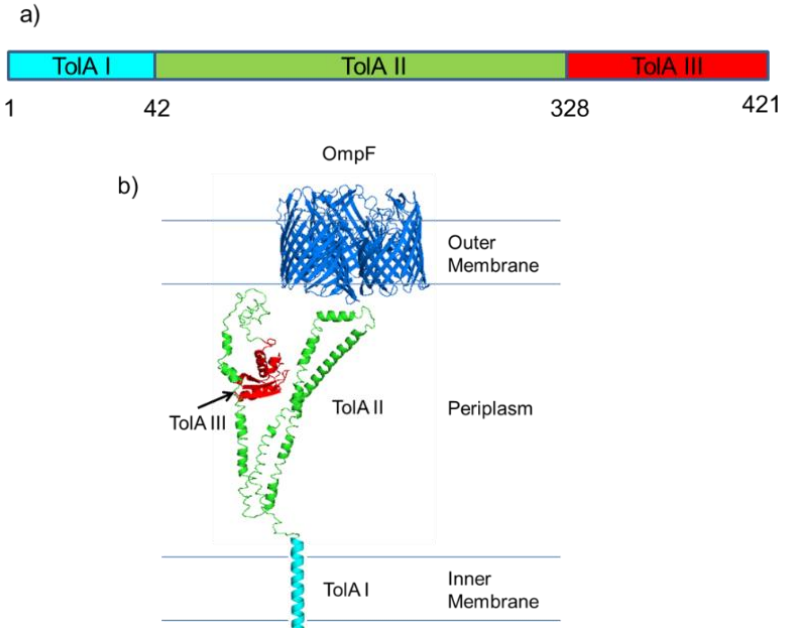

Figure 3.14 The structure of TolA from *E. coli.* a) Schematic of TolA domains b) Periplasmic localisation of TolA proteins. TolA I (cyan) is a transmembrane helix located on the inner membrane. TolA II (green) modeled by I-TASSER (Roy *et al.*, 2010) is assumed to be a long α-helical structure that spans the periplasmic space. TolA III (red) (PDB code: 3QDP) has a globular structure.

Firstly, in order to ensure the homogeneity of TolA II-III, the concentration series of proteins was assessed by AUC. The TolA II-III samples were prepared at various concentrations in 50 mM sodium phosphate buffer, pH 7.4, 300 mM NaCl. According to Figure 3.15, The c(s) distribution of TolA II-III showed a single dominant peak with a sedimentation coefficient ($s_{20,w}$) of 1.534 S in TolA

II-III at all concentrations measured. This means that TolA II-III was present as a single species in solution. The low s value obtained from the experiment gave a clear indication of an elongated structure. The (estimated) s value of globular proteins can be estimated by their molecular weight. The lower experimental s value when comparing to theoretical s value indicates an extended non-globular structure (Lebowitz *et al.*, 2002). The molecular mass of TolA II-III computed from sedimentation velocity experiment is 38.01 kDa which is slightly lower than the theoretical molecular mass of TolA II-III (39.66 kDa). As the AUC data confirmed TolA II-III is homogenous in solution, the TolA II-III sample is suitable for use in solution scattering experiments.

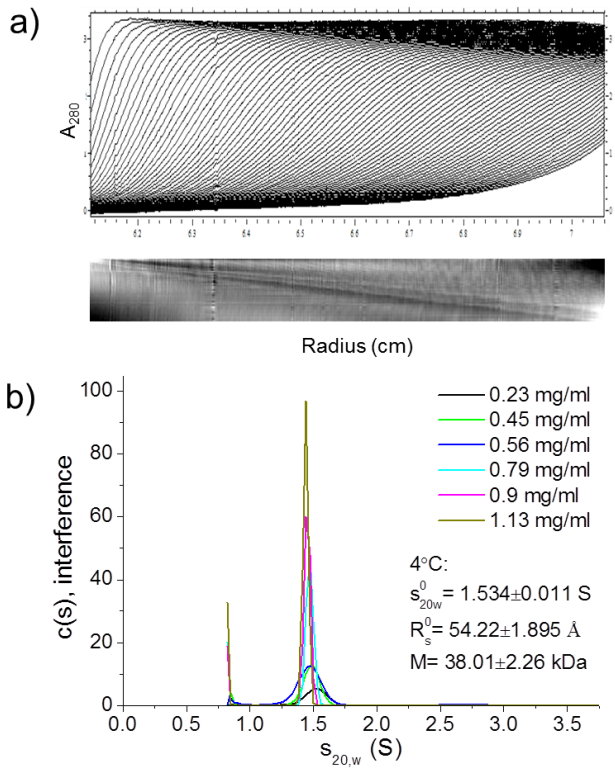

Figure 3.15 Sedimentation velocity of TolA II-III. a) Sedimentation velocity profiles. b) Sedimentation coefficient distributions c(s) at different concentrations. The TolA samples were in 50 mM sodium phosphate, pH 7.4, 300 mM NaCl.

SAXS curve of TolA at 5.3 mg/ml was recorded on the BM29 beamline at ESRF, Grenoble, France (Figure 3.16a). The P(r) showed a sign of an extended tail at the long distance and yielded a D_{max} of 410 Å and a R_g of 118.7 ± 2.09 Å

(Figure 3.16b) whereas a R_g of 45.18 ± 3.70 Å was estimated by the Guinier analysis. The disagreement of R_g between these two analyses indicated TolA II-III possesses an elongated and flexible structure. The Guinier plot appeared to be a straight line which confirmed the homogeneity of TolA II-III in solution (Figure 3.16c). The Kratky plot of TolA lacks a bell-shaped peak when comparing to that of BSA (Figure 3.16d). Having a plateau in Kratky plot also supported that the TolA II-III structure is flexible and elongated.

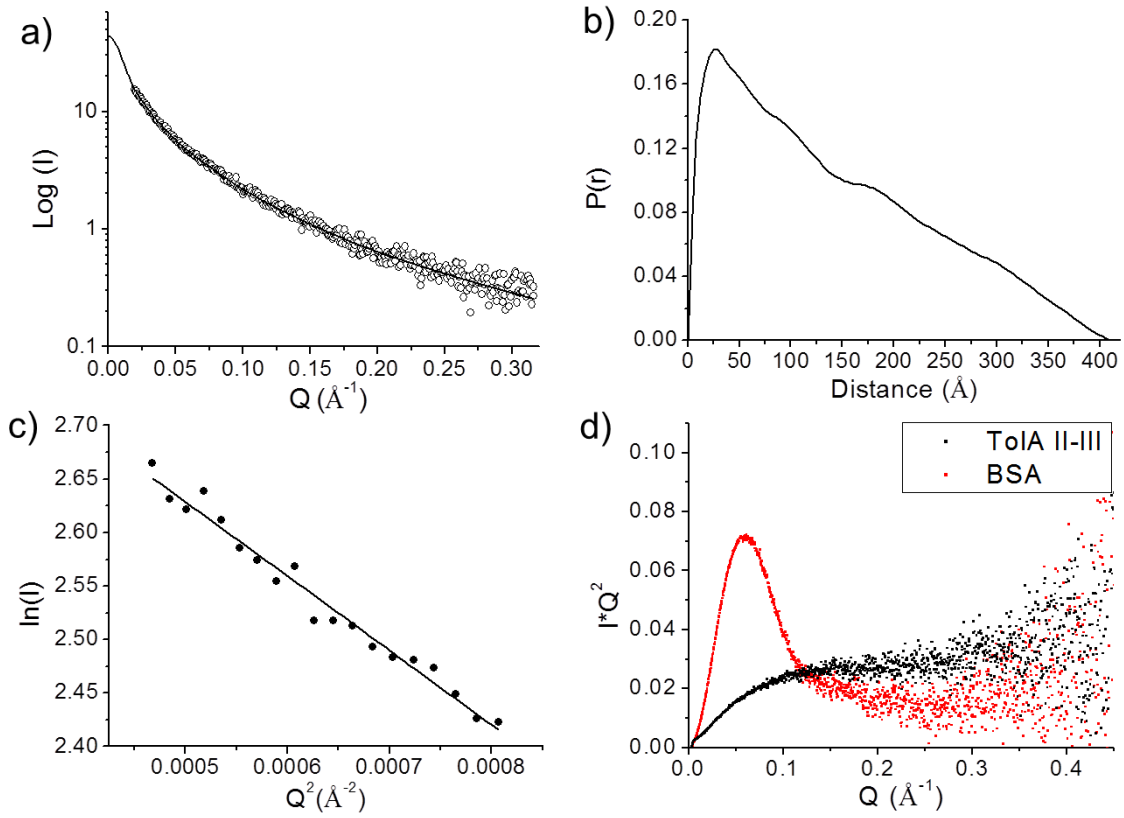

Figure 3.16 SAXS data for TolA II-III. a) SAXS data (symbols) and fitting (line) by GNOM b) Distance distribution functions, P(r), calculated using GNOM c) Guinier analysis d) Kratky plot for TolA II-III compared to BSA. TolA II-III at 5.3 mg/ml in 50 mM sodium phosphate buffer, pH 7.4, 300 mM NaCl and BSA at 2.0 mg/ml in water were used in the measurement.

To further confirm the flexibility of TolA II-III, the SAXS curve was investigated using CRYSOL software (Svergun *et al.*, 1995). CRYSOL is used to compute the theoretical scattering amplitude from atomic structure and compares the theoretical scattering curve to the experimental one. The TolA II structures

modeled by I-TASSER (Roy *et al.*, 2010) were then joined to the crystal structure of TolA III (PDB code: 3QDP) (Figure 3.17d). Three models at different lengths were made and compared to the experimental SAXS curve by CRYSOL (Figure 3.17a, b and c). The best fit was from model 2 which has a maximum length of 190 Å. However, none of these models were a perfect fit to the experimental data because the goodness of fit (χ) was too large (it should be less than 1.1). Therefore, only one conformation is unlikely to truly represent the structure of TolA II-III. It is concluded that TolA II-III is likely to have more than one conformation in solution.

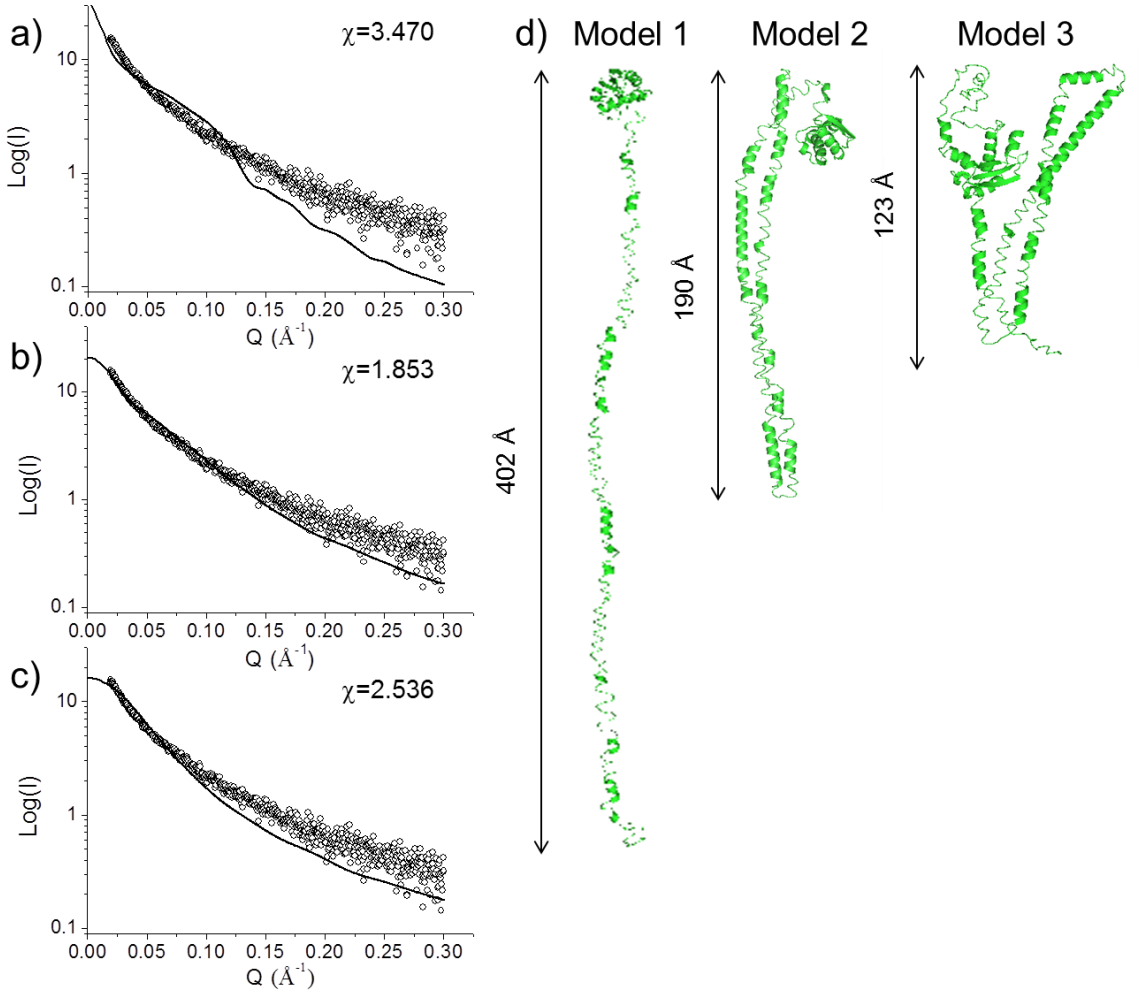

Figure 3.17 Theoretical SAXS profiles of TolA II-III models generated from CRYSOL fitted against the experimental SAXS profiles. Lines and symbols represent CRYSOL fitting and SAXS data, respectively a) Model 1. b) Model 2 and c) Model 3. d) TolA II-III structures modeled by I-TASSER (Roy *et al.*, 2010) and optimised by Coot.

Consequently, to deal with this flexible system, EOM analysis of TolA II-III was carried out. The pool of TolA II-III models based on a sequence of TolA II and the crystal structure of TolA III was randomly created. 295 residues of TolA II were treated as dummy spheres while TolA III was considered as a rigid body. A generic algorithm was used which then chose an opitimised ensemble containing a group of different TolA II-III conformations whose average theoretical scattering curves fit experimental data well. According to Figure 3.18a, the scattering curve obtained from the optimised ensemble almost perfectly fits the experimental data with a χ of 1.05. Comparing R_g and D_{max} distribution to the random pool, it displayed R_g and D_{max} distribution of optimised ensemble shifted towards the larger and extended particle with major peaks at R_g = 75 Å and D_{max} = 200 Å (Figure 3.18c and d).

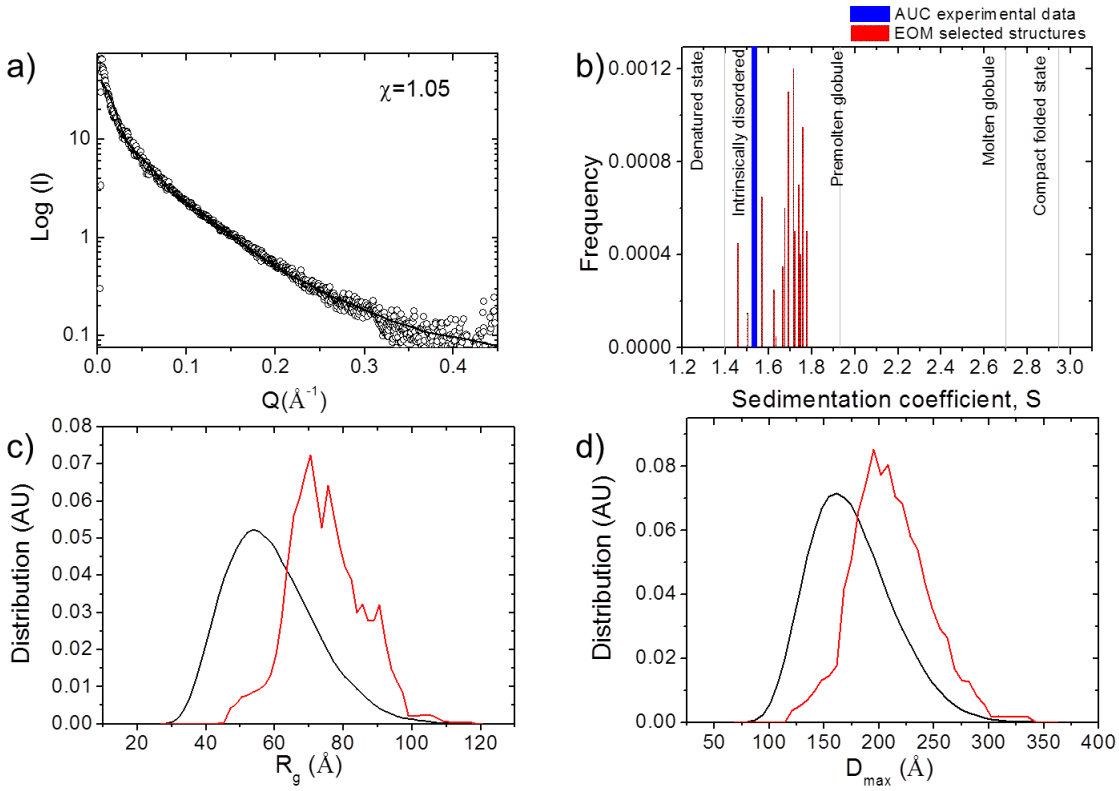

Figure 3.18 EOM analysis of TolA II-III. a) SAXS data (symbols) and fitting (line) generated from EOM. b) Distribution of sedimentation coefficient obtained from EOM selected structure (red) comparing with AUC data (blue). Size and shape distributions of the pool structure (black) and selected structure (red) for EOM analysis c) R_g d) D_{max}

The sedimentation coefficient from models generated by EOM was calculated by HYDROPRO and compared to the sedimentation coefficient obtained from the AUC experiment (Figure 3.18b). The s value from models ranged from 1.4 S to 1.8 S but AUC data showed only one species of TolA II-III with an s of 1.5 S. However, EOM analysis is in a good agreement with CRYSOL analysis. EOM predicted that the major species of TolA II-III is at D_{max} = 200 Å and model 2 with a maximum length of 190 Å best fitted with experimental data by CRYSOL.

3.2.7 Investigating the interaction of TolA II-III with OmpF in SDS

OmpF and TolA are involved in ColN translocation (Y. C. Kim *et al.*, 2014). It is proposed that the T-domain first binds to OmpF and then TolA (Housden *et al.*, 2013; Johnson *et al.*, 2013). The binding to TolA then triggers the entry of ColN into bacterial cells. TolA and OmpF have been shown to form complexes *in vitro* (Derouiche *et al.*, 1996; Dover *et al.*, 2000) but no evidence yet exists for *in vivo* interaction. In order to understand how these two interaction partners of ColN could form complexes prior to the translocation, the structure of *in vitro* OmpF/TolA complexes previously observed in SDS (Derouiche *et al.*, 1996) (Dover *et al.*, 2000) was further studied by small-angle solution scattering. The truncated TolA consisting of domain II and III was used in these experiments because the full length TolA is poorly expressed. The complexes were formed in the presence of 0.5% (w/v) SDS. Firstly, the complexes in SDS were assessed by SDS-PAGE as in Figure 3.19. The native sample of complexes were run along with the purified TolA II-III and OmpF without boiling hence all proteins in the sample were in their native structure. Results showed that the complex band shifted towards higher molecular weight and confirmed that TolA II-III can interact with OmpF *in vitro*. This is in good agreement with Derouiche *et al* and Dover *et al* (Derouiche *et al.*, 1996; Dover *et al.*, 2000). Interestingly, the characteristic OmpF ladder on SDS-PAGE still existed when OmpF formed complexes with TolA II-III. The ladder is caused by LPS tightly bound to the extracellular half of the membrane face of OmpF. It has been previously demonstrated that ColN binding displaces LPS from OmpF at this extracellular part since these complexes do not show a ladder on SDS-PAGE (Baboolal *et*

al., 2008). On the other hand, the existence of a ladder in OmpF/TolA complexes on SDS-PAGE suggested that TolA II-III bound to OmpF elsewhere, perhaps at the periplasmic side. Interestingly, ColN and TolA II also compete for a binding site so this must overlap (Dover *et al.*, 2000).

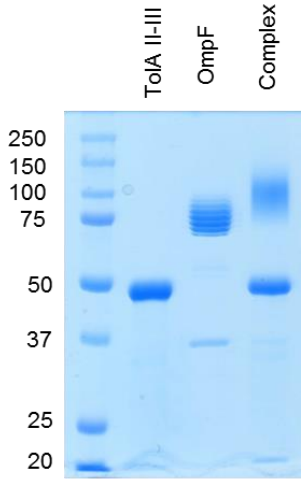

Figure 3.19 SDS-PAGE of OmpF/TolA II-III complex. All samples were prepared without boiling thus proteins were in their native state. Both OmpF and complexes had the ladder features due to the binding of LPS to OmpF. The LPS came from the outer membrane of *E. coli* when purifying OmpF.

The SANS experiments on OmpF/TolA II-III complexes were carried out on SANS2D beamline at ISIS, UK. Using the same technique as the study of OmpF/ColN-TR complex, the dOmpF with the CMP of 87% D_2O formed complexes with TolA II-III at a 1:1 molecular ratio (3 molecules of TolA II-III per 1 molecule of OmpF trimer) in 50 mM sodium phosphate, pH 7.4, 300 mM NaCl and the mixture of h/d SDS. This was done to ensure that the scatter from SDS is matched to all D_2O solutions. The samples were prepared in four D_2O solutions; 13%, 41%, 90% and 100% D_2O. Varying the H_2O/D_2O content in the sample allowed us to observe either the individual component or the whole complex. The whole complex can be seen in 13% and 100% D_2O solutions whereas the dOmpF and TolA II-III were observed at 41% and 90% D_2O, respectively. The scattering curves were recorded and evaluated by the indirect Fourier transform using GNOM (Figure 3.20a). The P(r) distribution function generated by GNOM revealed the smallest P(r) at 41% D_2O when observing

only dOmpF and the largest P(r) at 100% D_2O when observing the entire complex (Figure 3.20b). At 90% D_2O where only TolA II-III is visible, the maximum peak was shifted towards the short distance and the shape of P(r) function was changed. Therefore, it was an obvious indication of TolA II-III forming complexes with dOmpF because the P(r) of complex (at 13% and 100% D_2O) is larger than that of only OmpF (at 41% D_2O). The Guinier plots in Figure 3.20c were linear and confirmed the lack of aggregation in samples.

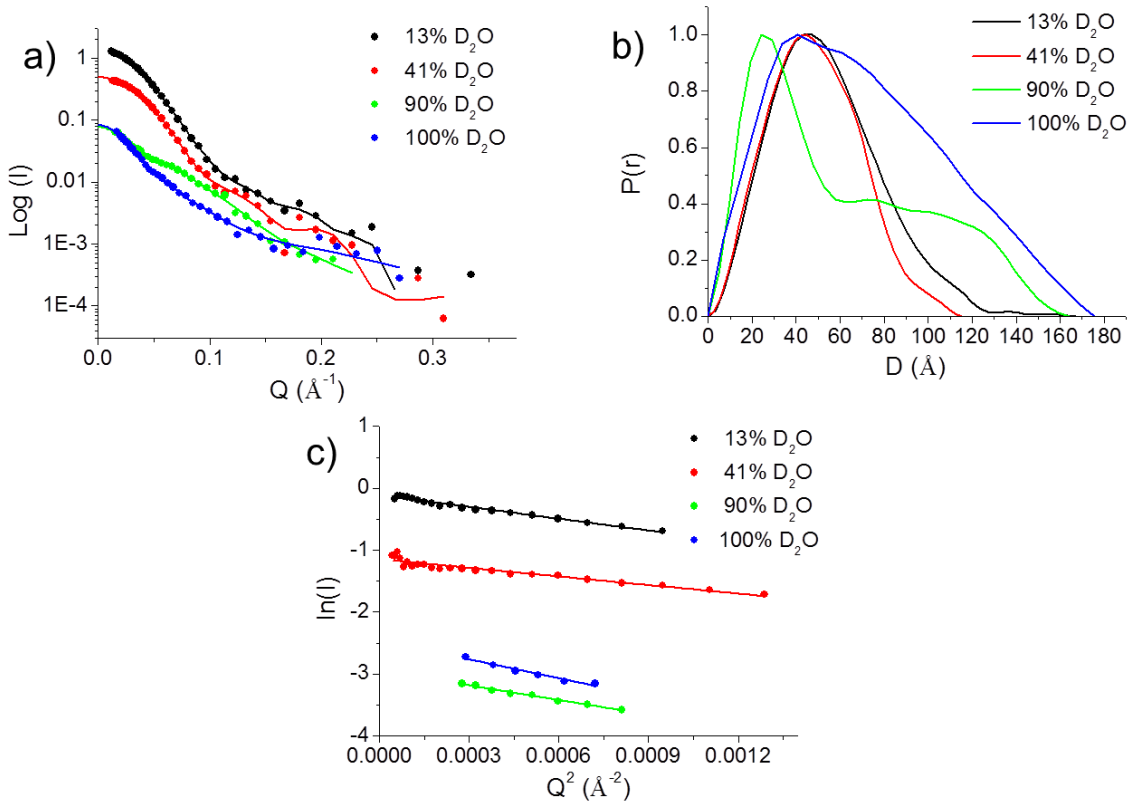

Figure 3.20 SANS data for dOmpF/TolA II-III complexes in 1% h/d SDS. a) SANS data (symbols) and fitting (lines) generated by GNOM. b) Distance distribution function, P(r), calculated by GNOM. c) Guinier analysis

The size parameters, R_g and D_{max}, derived from Guinier and P(r) plots were summarized in Table 3.6. The consistency of the R_g value determined from these two analyses also pointed out that the complexes are monodisperse and the assigned D_{max} values were accurate. When comparing the R_g value of complexes in 90% D_2O (only TolA II-III is visible) to that of TolA II-III in normal buffer studied by SAXS, the R_g values for TolA II-III by itself in the SAXS

experiment were inconsistent due to the flexibility of TolA II-III, however the R_g values of TolA II-III in complex with OmpF in the SANS experiment were consistent. D_{max} of TolA II-III also substantially changed when TolA II-III bound to dOmpF. This indicated that the structure of TolA II-III in complex becomes more compact.

Table 3.6 Summary of all parameters derived from Guinier plot and P(r) function for OmpF/TolA II-III complexes. PRIMUS is used for Guinier analysis and GNOM calculated P(r) function.

Sample	Guinier Analysis $0.4<R_gQ<1.3$	P(r) function	
	R_g (Å)	R_g (Å)	D_{max}(Å)
dOmpF:hTolA in 13% D_2O (entire complex)	41.53±2.792	42.11±0.383	170
dOmpF:hTolA in 41% D_2O (dOmpF only)	35.00±3.236	37.36±0.324	112
dOmpF:hTolA in 90% D_2O (hTolA only)	48.70±3.530	50.50±1.523	167
dOmpF:hTolA in 100% D_2O (the entire complex)	54.70±2.410	56.66±0.964	175.5
hTolA in H_2O	45.18 ± 2.93	118.70 ± 2.09	410.0

The R_g of complexes derived from the initial analysis of SANS data were then utilised for the Stuhrmann analysis. The change of R_g as a function of contrast was evaluated by plotting of R_g^2 against $\frac{1}{\Delta\rho_N}$ and fitting by a parabola curve. R_g and I(0) from the Guinier plot were used as the input in MULCh program in order to calculated $\Delta\rho_N$. This analysis shows the position where TolA II-III is in complex with OmpF. Figure 3.21 shows the Stuhrmann plot for dOmpF/TolA II-III complexes along with the parabola fit with a χ^2 of 0.78. The α value obtained from a fit has a negative sign. The sign of α suggested that TolA II-III is located on the outside of OmpF trimer.

According to the findings from SANS and SDS-PAGE studies, the proposed model of OmpF/TolA II-III complexes is shown in Figure 3.22. TolA II-III is located at the periplasmic side of the OmpF trimer. The length of TolA II-III is derived from the P(r) function at 90% D_2O where only TolA II-III is visible to neutrons.

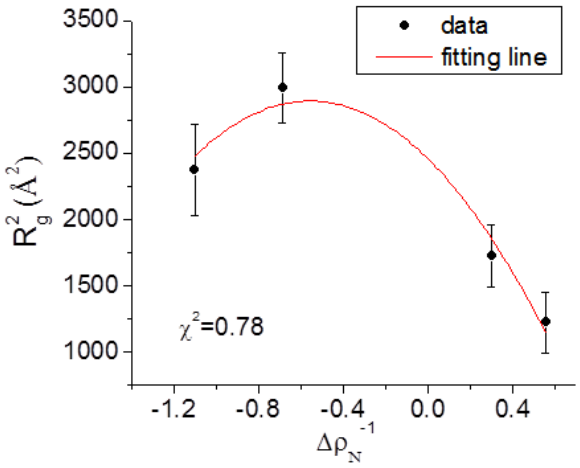

Figure 3.21 Stuhrmann analysis of dOmpF/TolA II-III complex. The reciprocal of the contrast is plotted against the square of the radius of gyration (R_g). The experimental data points are shown as symbols. A parabola fitted to the data is shown in red.

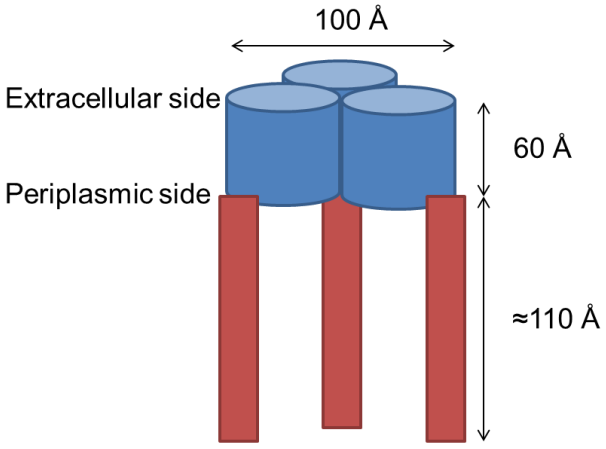

Figure 3.22 Proposed model for OmpF/TolA II-III complex in solution. Three blue cylinders represent the OmpF trimer whose height and diameter are obtained from its crystallographic structure (PDB code: 2OMF). Three red rectangles display TolA II-III with a length of ≈110 Å interacting with OmpF at the periplasmic side.

3.3 Discussion

The mechanism of translocation of ColN through the outer membrane of gram-negative bacteria has not yet been clearly described (Clifton *et al.*, 2012; Jakes, 2014). To understand this process, the structural characterisation of proteins involved in ColN transport is required. The small-angle scattering studies of the proteins were performed with the aim of developing a structural model for translocon complexes. SAXS was used to study the soluble proteins which are each truncated versions of ColN and TolA. On the other hand, SANS was utilised for the complex systems which are OmpF/ColN-TR and OmpF/TolA II-III in the presence of detergents.

Prior to performing small angle scattering experiment, we have expressed and purified deuterated OmpF (dOmpF) which was used for contrast variation techniques in the SANS experiments. Bacterial cells were grown in 85% D_2O minimal media supplemented with glucose as a carbon source. The deuteration level of dOmpF determined by mass spectrometry was 66% D_2O which is almost 20% lower than the D_2O content in the media. It seemed much lower than expected as it normally decreases approximately 10% D_2O as a result of adding unlabelled glucose (Ito *et al.*, 1990; Christie *et al.*, 2012). In the case of our dOmpF production, glucose and 2 ml of NaOH rather than NaOD was added to the cell culture every hour in order to use as a carbon source and maintain the pH. This could be the reason why the deuteration level of dOmpF was only 66% D_2O. Moreover, the CMPs of each component of samples for SANS experiments were required. Most of them were determined correctly except OG because the exchangeable protons of OG must be taken into account for the calculation of CMP, otherwise the determination of CMP should be done experimentally.

The ColN from *E. coli* has been characterised by x-ray crystallography (Vetter *et al.*, 1998). However, this crystal structure of ColN lacked the first 90 amino acids of the translocation domain due to the fact that it possesses an intrinsically disordered structure. The unfolded nature of the T-domain has

already been confirmed by CD and NMR (Raggett *et al.*, 1998; Anderluh *et al.*, 2004). Therefore, non-crystallographic approaches are needed to study this protein in solution. ColN-TR was selected for further study as it plays a vital role in ColN entry into bacterial cells. ColN-TR was chosen rather than T-domain and full length ColN because the T-domain is too small for SANS study and full length ColN is not stable in neutral detergents because the P–domain unfolds and is likely to bind to OmpF itself (Dover *et al.*, 2000; Clifton *et al.*, 2012). AUC is a useful tool to detect the disordered protein as the disordered protein will sediment more slowly than its folded monomer (Salvay *et al.*, 2012). AUC experiments revealed one species of ColN-TR with a compact structure despite having an intrinsically disordered region. This is likely due to the fact that the flexible T-domain has a weak interaction with R-domain as shown by HSQC NMR (Oliver Hecht *et al.*, 2008). The analysis of the SAXS curve by initial data evaluation and EOM indicated that ColN-TR has a partially unfolded structure and there are three major species with different degrees of compactness. These results suggest that the structure of T-domain in ColN-TR remains unstructured as it is in full length ColN. The disagreement between AUC and SAXS data of ColN-TR indicated that ColN-TR has one stable conformation detected by AUC and the other three species appearing in the EOM analysis of SAXS data could be in equilibrium. The AUC data may be dominated by the faster sedimenting species.

The solution structure of ColN-TR studied by AUC and SAXS was then compared to the structure of ColN-TR in complex with OmpF. In SANS experiments on the complexes, ColN-TR interacting with OmpF became more compact as the R_g and D_{max} values of the complexes are only slightly changed from those of OmpF. Furthermore, ColN-TR is bound to OmpF on the outside of OmpF according to the increase in R_g and D_{max} upon ColN-TR binding and the Stuhrmann analysis of SANS data. However, it is not certain that ColN-TR interacts at the periphery of OmpF as a result of the large error bars of the Stuhrmann plots. These large error bars could be derived from the determination of R_g using the Guinier analysis. The Guinier analysis estimates R_g from the data at low Q region whereas the R_g obtained from the P(r) function

is derived from the entire scattering curve. To improve the Stuhrmann analysis of dOmpF/ColN-TR complex, R_g of the complex estimated from the P(r) function may be used as it is more accurate. The underestimation of CMPs of h/d-OG also has an impact on the solution structure of complexes. The size of complexes may become larger as a result of the residual signal from the scattering of mismatched OG. The R_g and D_{max} obtained from this experiment could be slightly larger than they actually are. Our study on the complex in neutral detergents is different from the previous study. The SANS study of full-length ColN with OmpF in SDS demonstrated that C-terminal P-domain was essential for complex-formation, however, our complexes in neutral detergents lacking the P-domain (Clifton *et al.*, 2012) were mediated by the T-domain. The importance of T-domain in complex formation in the presence of neutral detergents was confirmed by ITC (Johnson *et al.*, 2013). It is concluded that the complexes formed in neutral detergents represent the early step of ColN translocation when compared to complexes in SDS.

The structure of the C-terminal domain of TolA (TolA III) in *E. coli* has been solved by x-ray crystallography and NMR (Lubkowski *et al.*, 1999; Deprez *et al.*, 2005; Penfold *et al.*, 2012). The structure of TolA II has not been solved by x-ray crystallography which may indicate problems due to the flexibility of the long helices (Derouiche *et al.*, 1999). Therefore the best way to study this protein is possibly in solution. The sedimentation velocity experiment by AUC indicated that TolA II-III is a single species of extended structure with a sedimentation coefficient of 1.5 S. Even though TolA II-III was predicted as a folded protein, it sedimented more slowly than expected. This is an indication of extended and flexible structure.

However, SAXS of TolA II-III analysed by EOM reported more than one species of TolA II-III present in solution because a good fit to the scattering data requires models with the combination of multiple conformations of the central domain. When comparing our data to the previous study of TolA II-III from *P. aeruginosa* whose R_g is 42.0 Å with 1% error, TolA II-III from *E. coli* is more extended with R_g ranging from 45 Å to 120 Å (Witty *et al.*, 2002). Like the SAXS

study on ColN-TR, AUC data of TolA II-III observed only one conformation of TolA II-III while SAXS data detected several species of TolA II-III. It also confirmed that the AUC technique sees a stable species only. TolA II-III is proposed to span the periplasmic space whose thickness varies from 10 to 50 nm (Graham *et al.*, 1991). The flexibility of TolA II-III in the D_{max} from 10 to 40 nm agrees well with the thickness of periplasmic space.

When TolA II-III was bound to OmpF, the results from SANS study indicated that TolA II-III was more compact as the R_g and D_{max} of TolA II-III decreased dramatically upon binding to OmpF. The complexes were formed by the central domain of TolA probably binding at the periplasmic side of OmpF as observed by SDS-PAGE (Derouiche *et al.*, 1996). The multiple band pattern of OmpF caused by the LPS binding still appeared on SDS-PAGE when TolA II-III interacts with OmpF. This indicated that the binding of TolA did not displace LPS located at the extracellular side of OmpF. SANS data also supported the finding that TolA II-III is at the perimeter of OmpF because the formation of complexes increased the R_g and D_{max} and the Stuhrmann analysis yielded the negative value of α. These studies of complexes *in vitro* could reflect how TolA interacts with OmpF *in vivo*. The structure of the complex could be similar to that of TolC (Koronakis *et al.*, 2000). The function of TolC and OmpF/TolA II-III complexes is to import colicins across the outer membrane. TolC serves as a translocator of colicin E1 (ColE1) whereas the translocators of ColN are OmpF and TolA. When comparing the structure of OmpF/TolA II-III complexes with TolC, OmpF may act as the β barrel domain of TolC located at the outer membrane while TolA II may serve as the α helical barrel domain of TolC spanning the periplasm. This possibility is supported by Schendel and colleagues who showed that ColE1 which requires TolA III and TolC does not need TolA II whilst colicin A and N absolutely require TolA II and cannot use TolC instead (Schendel *et al.*, 1997). It could be possible that the long helices of TolC replace TolA II for ColE1. Figure 3.23 shows the comparison between the structure of TolC and the model of OmpF/TolA complexes.

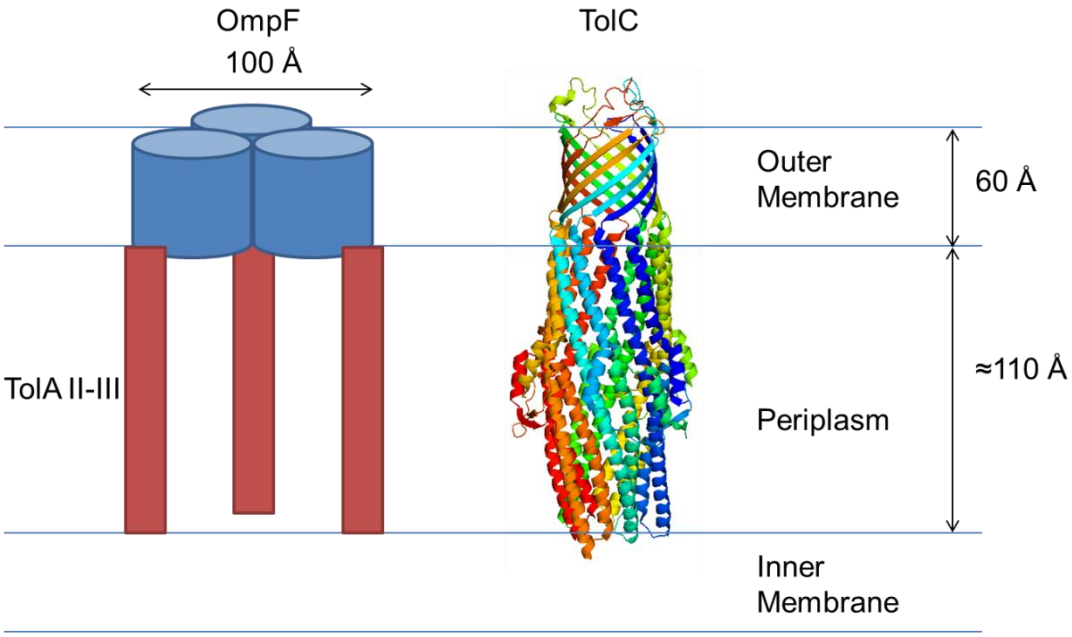

Figure 3.23 Comparison between the possible model of OmpF/TolA complexes and the crystal structure of TolC (PDB code: 1EK9). OmpF trimer (blue cylinders) forms channels in the outer membrane like the β-barrel domain of TolC. Three molecules of TolA II-III (red rectangles) bind to OmpF at the periplasmic side. The α helical structure of TolA II in complex with OmpF may be similar to the α-helical trans-periplasmic tunnel of TolC.

Chapter 4 OmpF/LPS binding studies

4.1 Introduction

To survive in an unpredictable and hostile environment, gram negative bacteria build a sophisticated multilayered cell envelope to protect itself. They are surrounded by two lipid bilayers which form the inner and outer membranes. The outer membrane (OM) is a characteristic feature of gram-negative bacteria which contains phospholipids in the inner leaflet and lipopolysaccharides (LPS) in the outer leaflet which faces the extracellular environment (Nikaido, 2003). The function of the OM is to protect bacterial cells from various toxic molecules such as antibiotics and bile salts.

LPS is a polyanionic molecule which consists of three regions; 1) Lipid A, a glucosamine based lipid, 2) core oligosaccharide, and 3) O-antigen polysaccharide (Raetz and Whitfield, 2002). The negatively charged core oligosaccharide and lipid A interact strongly with divalent cations to reduce the electrostatic repulsion between LPS molecules. This strong lateral interaction between LPS molecules via divalent cations results in the lower fluidity and higher hydrophobicity of OM compared to a typical fluid mosaic phospholipid bilayer. Therefore, LPS is crucial for the structural integrity of the OM (Rietschel *et al.*, 1994).

In addition to LPS, integral membrane proteins with β-barrel structures, such as porins and gated channels are embedded within the OM. Some of them, for example the porins, are extremely abundant. three major porins, OmpF, OmpC and PhoE, are expressed at high levels in the OM of *E. coli* (>10^5 copies per cell) (Rosenbusch, 1974). OmpF, or matrix porin, binds to LPS so tightly that the OmpF-LPS complexes can be observed on SDS-PAGE (Holzenburg *et al.*, 1989). However, little is known about how OmpF interacts with LPS in the OM and this could be very important for the organisation of the OM. The LPS-binding sites of OmpF have been predicted based on negative stain electron micrographs of 2D crystallised OmpF-LPS complexes as shown in Figure 4.1

(Hoenger *et al.*, 1990; Baboolal *et al.*, 2008). It has also been shown that OmpF requires LPS for its correct assembly into OM (Ried *et al.*, 1990; Sen and Nikaido, 1990; Sen and Nikaido, 1991). Recently, Johnson and colleagues discovered that Colicin N, a bacterial toxin produced by *E. coli*, requires both OmpF and LPS to enter the target cells (Johnson *et al.*, 2014). Several antibiotics such as polymyxin and colistin also target LPS and destabilise the outer membrane (Velkov *et al.*, 2010). OmpF and other porins form dense quasi crystalline regions in the outer membrane and the contacts between trimers must contain LPS. For these reasons, it is evident that the OmpF-LPS interaction is key to understanding both the functional and structural integrity of OM.

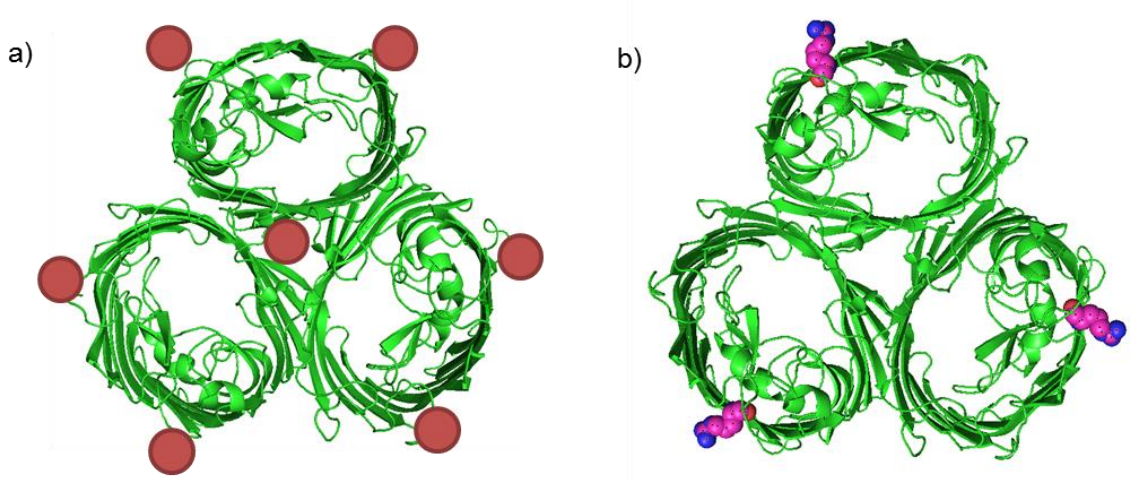

Figure 4.1 Proposed LPS binding sites for OmpF (PDB code: 2OMF). a) Hoenger *et al* proposed two binding sites for each OmpF monomer and one in the middle of OmpF trimer (Hoenger *et al.*, 1990). LPS binding sites are represented by red circle. b) Baboolal *et al* suggested that LPS binds to OmpF near Arg235 (Pink) (Baboolal *et al.*, 2008).

The crystallographic structure of LPS with the integral outer membrane protein, FhuA, is the only structure of outer membrane protein with bound LPS resolved to date (Figure 4.2) (Ferguson *et al.*, 1998). The interaction with 11 charged or polar FhuA residues is responsible for the tight binding of LPS. A structural search of the PDB (Ferguson *et al.*, 2000) showed that four of these side chains

were conserved between known LPS binding proteins. The fatty acid acyl chains of LPS also make contact with hydrophobic residues of FhuA.

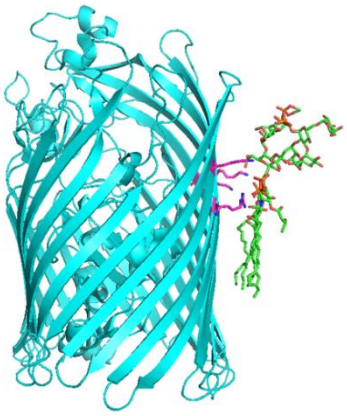

Figure 4.2 Crystal structure of FhuA with bound LPS (PDB code: 1QFG). The conserved LPS-binding motif is coloured magenta and the LPS is in green.

The purpose of this study is to investigate the OmpF-LPS interaction as OmpF and LPS are major components of the OM and likey to determine its stability. This study will shed light on the organisation of OM in gram-negative bacteria. As the OM is a strong protective barrier against antibiotics, the understanding of OmpF-LPS interaction may allow us to find the weak points or Achilles Heel of gram-negative bacteria. Evidence for this comes from the action of colicin N which has been shown to bind to the core region of LPS in the membrane (Johnson *et al.*, 2014), displace tightly bound LPS from the surface of OmpF (Baboolal *et al.*, 2008) and bind to the membrane interface of OmpF in a way that may allow it to cross the outer membrane (Baboolal *et al.*, 2008; Clifton *et al.*, 2012) and reach its target, which is the inner membrane.

Here, the formation of OmpF-LPS complexes was studied by SDS-PAGE, dynamic light scattering (DLS) and small-angle x-ray scattering (SAXS). The LPS-free OmpF, produced by refolding denatured OmpF from inclusion bodies, was used to form defined complexes with selected LPS subtypes. The effect of divalent cations on complex formation was also studied. Furthermore, the LPS binding site was probed by mutagenesis and small-angle neutron scattering (SANS).

4.2 Results

4.2.1 Preparation of LPS-free OmpF

OmpF purified from the outer membrane of *E. coli* is almost always contaminated with LPS. In order to study the interaction of OmpF and LPS, LPS-free OmpF is required. To achieve this, OmpF was expressed in inclusion bodies in *E. coli* rather than the outer membrane and then refolded to the native OmpF trimer *in vitro*.

Production of Inclusion bodies

The pMS119 plasmid containing an *ompF* gene without signal sequence, OmpFΔSS (lacking residues 1-22 and having the mutation A23M to provide a new ATG start codon), was transformed into BZB1107 *E. coli* (ompF::Tn5) as a host as described in Visudthiphole *et al* (Visudtiphole *et al.*, 2005), so that the only OmpF present was in inclusion bodies. The inclusion bodies of OmpFΔSS were isolated and solubilised in a buffer containing 6 M guanidine HCl. The solubilised inclusion bodies were then dialysed into a buffer containing 6 M urea and assessed for purity by SDS-PAGE and western blot running with purified WT OmpF as a standard (Figure 4.3a and b).

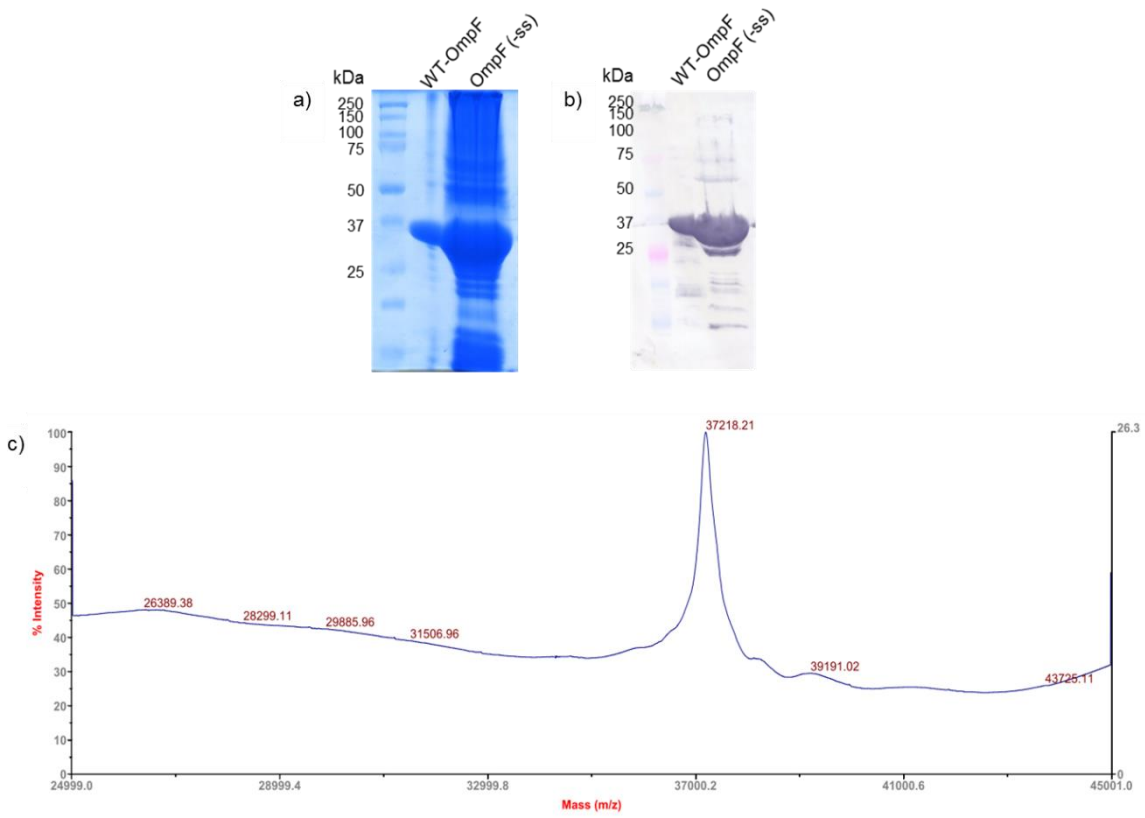

Figure 4.3 Expression and identification of OmpFΔSS (WT OmpF without signal sequence) from inclusion bodies a) SDS-PAGE analysis of OmpF inclusion bodies solubilised in 6 M urea b) Western blot using anti-OmpF antibody (Bainbridge *et al.*, 1998) c) MALDI-TOF MS analysis of OmpFΔSS from inclusion bodies.

The SDS-PAGE and western blot using anti-OmpF antibodies (Bainbridge *et al.*, 1998) indicated that OmpFΔSS from inclusion bodies ran at 37 kDa, as does the monomer of WT OmpF. To confirm that intact OmpFΔSS was expressed, the samples of OmpFΔSS were then further investigated by MALDI-TOF MS without tryptic digestion. The mass spectrum from the SDS-PAGE gel slice of OmpFΔSS from inclusion bodies is illustrated in Figure 4.3c. OmpFΔSS has a molecular mass of 37218.21 Da with 0.12% error when compared to the theoretical molecular mass of 37172.60 Da. The size difference of <46 Da is within experimental error for this approach. Therefore, it indicated that the correct length OmpFΔSS was successfully expressed.

The contaminants were then partly removed by anion exchange chromatography using elution by a NaCl gradient (Figure 4.4a). The protein-containing fractions were tested on SDS-PAGE to confirm the purity of the sample. (Figure 4.4b) The clean OmpF samples were then used for refolding.

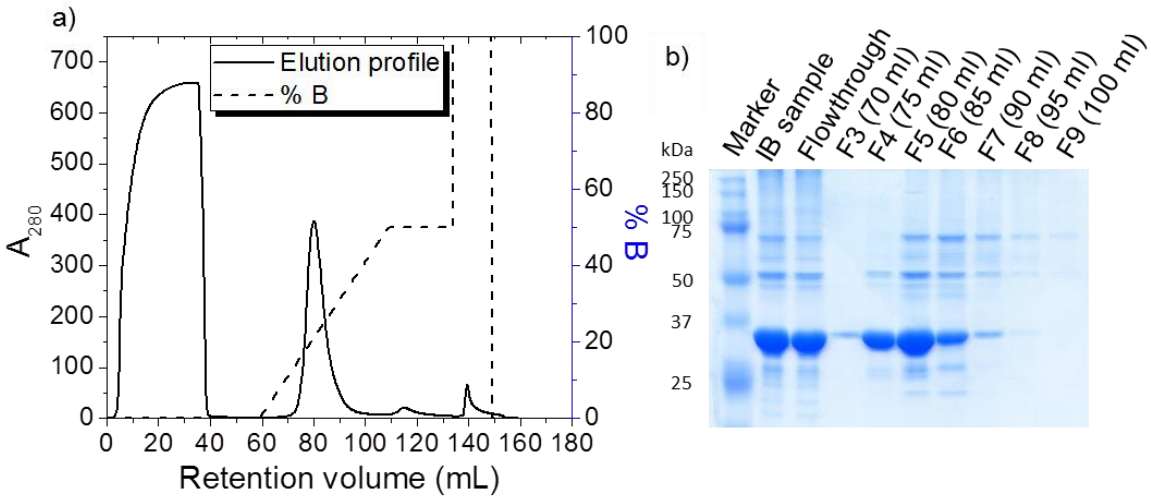

Figure 4.4 Purification of OmpFΔSS using anion exchange chromatography a) Elution profile (line) of the anion exchange 1-ml HiTrap Q Sepharose column equilibrated with buffer A (50 mM Bis-Tris, pH 7.0, 6 M urea) at a flow rate of 0.5 ml/min. A gradient from 0% to 50% of buffer B (50 mM Bis-Tris, pH 7.0, 6 M urea, 1 M NaCl (dash line)) was applied to the column. Fractions are 5 ml and were collected starting at 60 ml. b) SDS-PAGE analysis of protein-containing fractions from anion exchange chromatography. IB stands for inclusion body.

Refolding OmpF

LPS-free OmpF trimers were then produced by refolding urea solubilised OmpFΔSS in the presence of detergent micelles as previously described in Visudtiphole *et al* (Visudtiphole *et al.*, 2005). A mixture of DG (n-dodecyl-*β*-D-glucopyranoside) and DDM (n-dodecyl-*β*-D-maltoside) at 5:2 weight ratio was utilised for OmpF refolding. The purified OmpFΔSS was refolded by a 20x dilution in 50 mM Tris/HCl, pH 8.0, 1 mM DTT (dithiothreitol) and 0.1 mM EDTA containing the mixture of DG and DDM. OmpFΔSS at 1.25 mg/ml was diluted into varied amount of detergents while keeping the ratio of DG:DDM at 5:2.

After a stationary incubation at 37ºC for 3 days, the samples were tested on SDS-PAGE. Figure 4.5a reveals that refolding in 1% (w/v) DG and 0.4% (w/v) DDM gave the highest OmpF trimer yield. After varying the concentration of OmpFΔSS from 1.00 to 2.00 mg/ml, the optimum condition for refolding OmpF was found to be 1.50 mg/ml OmpFΔSS in 1.0% DG and 0.4% DM. The resulting refolded trimers are completely free of LPS as there is no smear band which always appears when running the SDS-PAGE analysis of WT-OmpF. (Figure 4.5a and b) Finally, a second anion exchange chromatography step was performed to exchange the buffer containing DG and DDM (which is poorly soluble) to a buffer containing the desired detergent.

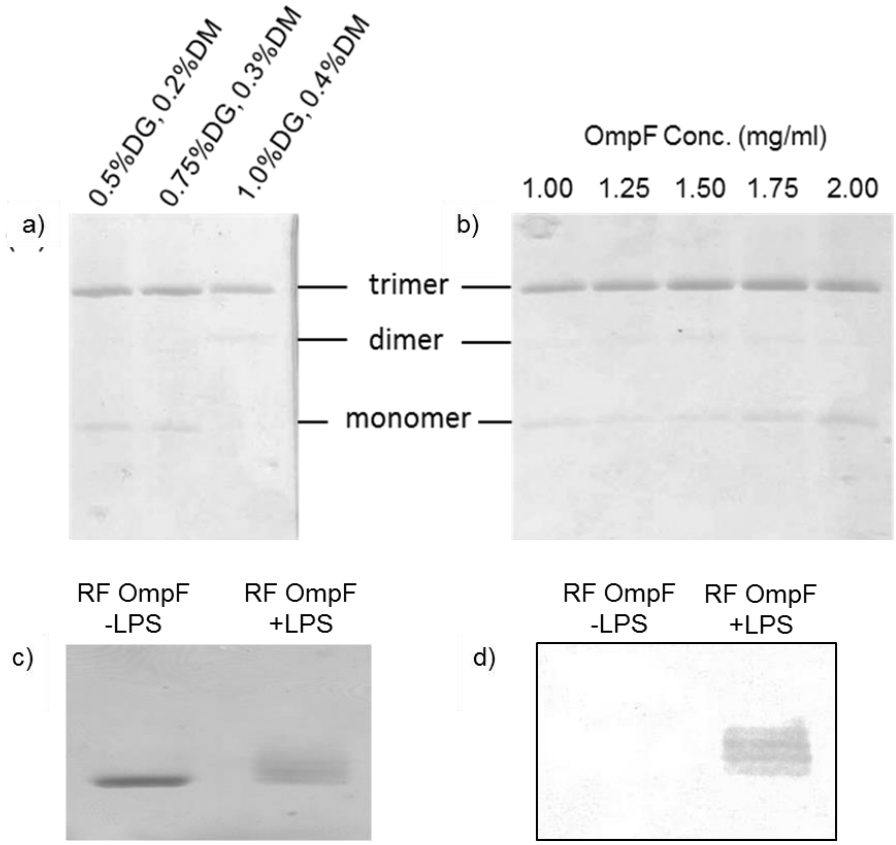

Figure 4.5 The SDS-PAGE analyses of refolded OmpFΔSS in the presence of DG and DDM. a) The comparison of 1.25 mg/ml OmpFΔSS diluted in the refolding buffer containing different concentrations of DG and DDM for 3 days. b) The different concentrations of OmpFΔSS used to refold in 1.0% DG and 0.4% DDM. c) Refolded OmpF (RF OmpF) in the presence and absence of Ra-LPS was assessed on SDS-PAGE. d) Western blot using the anti-LPS antibody WN1 222-5 (Dipadova *et al.*, 1993).

To confirm that refolded OmpF (RF OmpF) is free of LPS, we used the anti-LPS antibody WN1 222-5 (Dipadova *et al.*, 1993). The SDS-PAGE and western blot of RF OmpF with and without Ra-LPS indicated that RF OmpF lacked LPS (Figure 4.5c and d). The formation of stable OmpF trimers visible on SDS-PAGE was shown to be characteristic of fully folded and stable OmpF (Visudtiphole *et al.*, 2005). This is also confirmed by the high resolution structure of refolded OmpF elucidated by x-ray crystallography (Figure 4.6a) (In collaboration with Dr. Arnaud Basle). The structure of refolded OmpF is identical to that of WT OmpF as seen in the superimposition of refolded OmpF and WT OmpF structures (Figure 4.6b).

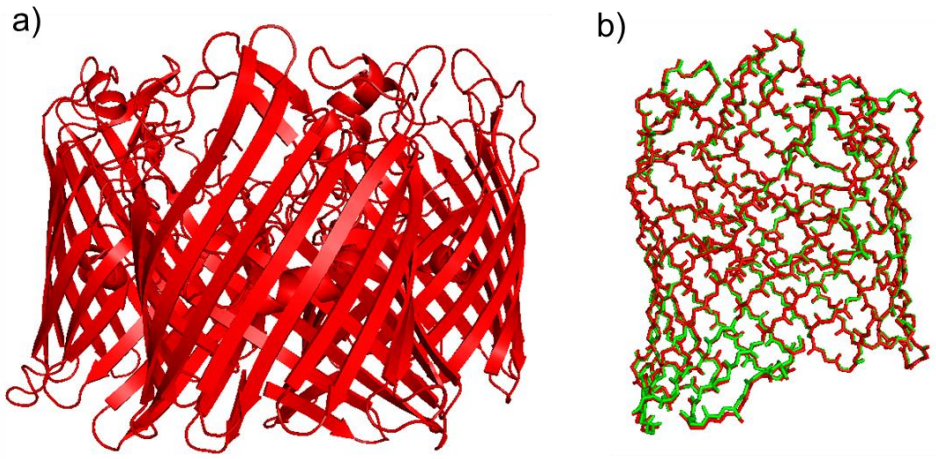

Figure 4.6 Crystallographic structure of refolded OmpF. a) The structure of trimeric refolded OmpF. b) Structural alignment of refolded OmpF monomer (red) and WT OmpF monomer from *E. coli* (green, PDB code: 2OMF).

4.2.2 OmpF/LPS in vitro binding studies

The OmpF/LPS complex formation studied by SDS-PAGE

LPS structure consists of Lipid A, core oligosaccharides and O-antigen oligosaccharides as shown in Figure 4.7a. Basically, LPS can be divided into 2 types which are smooth and rough LPS. Smooth LPS includes O-antigen oligosaccharide but rough LPS does not. Rough LPS is categorised based on the length of oligosaccharides in the core oligosaccharide region. Ra-LPS is the longest rough LPS while Re-LPS is the shortest type. In this experiment, we

observed the formation of OmpF/LPS complexes using SDS-PAGE. Mr. Josh Wright, an undergraduate student under my supervision, also took part in this experiment. LPS binds to OmpF so tightly that the native complexes of OmpF and LPS can be observed on SDS-PAGE. Either a ladder or a shift on SDS-PAGE is an indication of LPS binding to OmpF (Holzenburg *et al.*, 1989; Diedrich *et al.*, 1990). Different types of LPS were used to form complexes with OmpF at a 1:5 OmpF/LPS molar ratio in order to observe the shortest LPS molecule that is able to bind to OmpF. In Figure 4.7b, OmpF with added Lipid A, Re-LPS, Rd-LPS, Rc-LPS, Ra-LPS and smooth LPS were run on SDS-PAGE along with LPS-free OmpF. It can be seen that the bands of OmpF with long LPS (Rc, Ra and smooth LPS) formed ladders. The longer the LPS, the longer the ladder. However, even the bands of OmpF with short LPS migrated slower on SDS-PAGE than LPS-free OmpF. This showed that even Lipid A, the shortest form of LPS, binds strongly enough to the OmpF trimer for this to be observable on SDS-PAGE.

In order to discover the number of LPS binding sites on OmpF trimer, the OmpF/LPS complexes were prepared by varying the molar ratio of OmpF:Ra-LPS from 1:1 to 1:10. Ra-LPS was chosen as it is the longest defined LPS and will thus give the largest shift on SDS-PAGE. The number of O-antigen oligosaccharides on smooth LPS can vary and hence smooth LPS is not suitable for this type of experiment. According to Figure 4.7c, all complexes ran as ladders on SDS-PAGE. Increasing the concentration of LPS added to OmpF gave rise to longer ladders with more apparent steps. The inability to saturate the trimers with a clear number of steps meant that the number of LPS binding sites could not be identified by SDS-PAGE because defined complexes cannot be formed. This suggested that there could be additional interactions on top of specific OmpF-LPS interactions since LPS binding to OmpF results in longer, diffuse ladders.

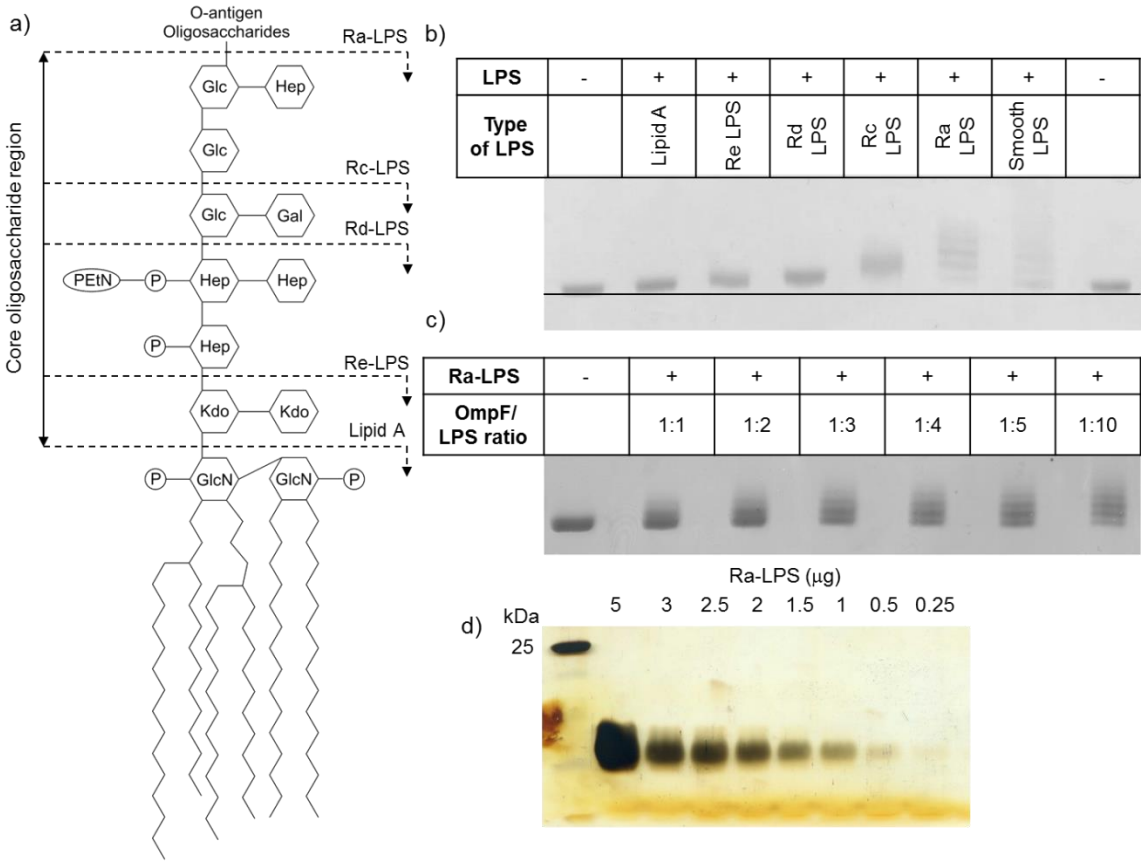

Figure 4.7 *In vitro* study of LPS-free OmpF binding to Ra-LPS. a) The structure of LPS from *E. coli* is adapted from (Chng *et al.*, 2010; Clifton *et al.*, 2013) Gal, D-galactose; Glc, D-glucose; Hep, L-glycero-D-manno-heptose; Kdo, 3-deoxy-D-manno-oct-2-ulosonic acid; P, phosphate; PEtN, phosphoethanolamine. b) SDS-PAGE analysis of OmpF/LPS complexes at 1:5 molar ratio formed by different types of LPS. c) The complexes of OmpF/Ra-LPS at different stoichiometries on SDS-PAGE. d) SDS-PAGE analysis of Ra-LPS alone in the presence of EDTA. The bands correspond to the decreasing loading per well as defined above each lane and were visualised by silver staining.

The variable ladder which appeared on SDS-PAGE could be due to either heterogeneous/impure Ra-LPS or self-association of Ra-LPS. To confirm that the heterogeneous OmpF/LPS complexes were not caused by heterogeneous LPS, SDS-PAGE of Ra-LPS was performed and the gel was stained with silver. LPS samples were prepared in buffer containing 1 mM EDTA and run on 15% SDS-PAGE at different loadings using a running buffer and gel supplemented with 1 mM EDTA. EDTA was used to remove divalent cations such as Ca^{2+} and Mg^{2+} in buffer which might crosslink LPS (Snyder *et al.*, 1999). The SDS-PAGE

of Ra-LPS displayed that Ra-LPS ran as a single band. Therefore, this Ra-LPS sample is homogenous in solution (Figure 4.7d).

The extensive ladder must therefore result from increasing numbers of LPS molecules binding to OmpF trimers and the absence of saturation implies that there is not a defined number of LPS binding sites per trimer. One possible explanation is that there are LPS-LPS interactions occurring and, since LPS would normally repel each other due to their concentrated negative charges, they may be linked via divalent cations. To test this hypothesis, SDS-PAGE was carried out on OmpF/LPS complexes at 1:5 molar ratio supplemented with 5 mM $MgCl_2$, $CaCl_2$ and EDTA. In the presence of divalent cations, the ladder on the gel became longer when compared to the samples in the absence of divalent cations (Figure 4.8a). This suggested that divalent cation linked LPS-LPS interactions build up the ladder on SDS-PAGE. In EDTA one or two "rungs" are seen as well as a strong band which aligns to LPS-Free trimers. We do not know if this lowest band is LPS free but this result does indicate that divalent cations may stabilise the basic LPS-OmpF interaction as well. Figure 4.8b represents the possible OmpF-LPS interaction in the presence of divalent cations. LPS initially binds to OmpF and then LPS link to each other to form the larger complexes via divalent cations.

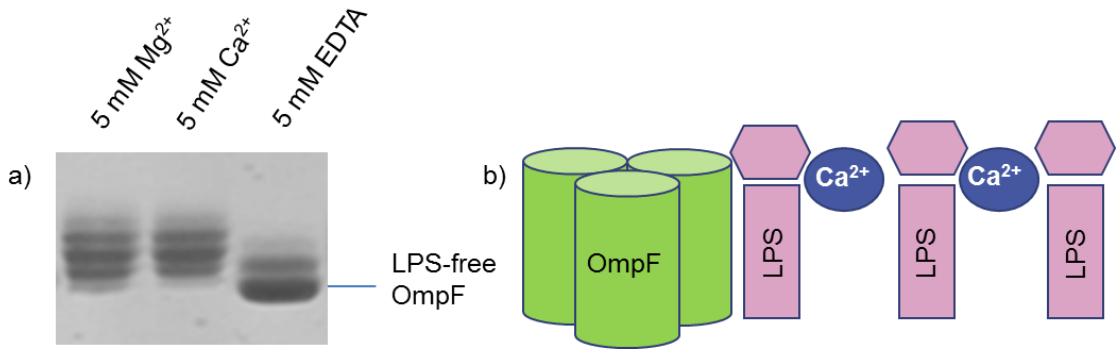

Figure 4.8 Interaction of OmpF with Ra-LPS in the presence and absence of divalent cations a) Comparison of OmpF/Ra-LPS complexes with and without divalent cations on SDS-PAGE. b) Schematic representation of OmpF/Ra-LPS interaction in the presence of divalent cations.

The effect of divalent cations on LPS-LPS interaction studied by dynamic light scattering

The aggregation of LPS was further studied by dynamic light scattering (DLS). Ra-LPS was added to buffer containing no Ca^{2+} and 5 mM Ca^{2+}. According to the size distribution measured by DLS (Figure 4.9b), adding Ra-LPS to the buffer with Ca^{2+} led to the gradual increase in the size of particle in solution. When 30 µg of Ra-LPS were added to 50 µl of buffer, Ra-LPS started to form large aggregates approximately 2000 nm in size and the solution became cloudy. As soon as EDTA was added, the aggregate suddenly disintegrated and the solution became clear. However, adding LPS in the absence of Ca^{2+} did not have an effect on the size of particle (Figure 4.9a). For these reasons, it is obvious that Ca^{2+} plays a role in the aggregation of LPS in solution.

In contrast to Ra-LPS by itself in solution, the size distribution of OmpF/LPS complexes with Ca^{2+} started to aggregate when adding only 10 µg of Ra-LPS to OmpF (the molar ratio of OmpF/LPS is 1 to 10) (Figure 4.9d). The OmpF/LPS aggregates also disappeared in the presence of EDTA but the size of complex in EDTA was still larger than OmpF only. This is probably due to direct OmpF-LPS binding. The OmpF/LPS complexes without Ca^{2+} did not form aggregates in solution even though 30 µg of Ra-LPS was added (Figure 4.9c). Interestingly, the addition of Ca^{2+} promoted the aggregation of complexes and the addition of EDTA broke down the large complexes in the same way as LPS aggregation. These data demonstrated that both Ra-LPS and OmpF/Ra-LPS complexes tend to form large aggregates in the buffer containing divalent cations. OmpF/Ra-LPS complexes accumulated into the large-scale structure more readily than Ra-LPS only. Therefore, OmpF possibly helped the formation of LPS dependent aggregates. Furthermore, the aggregation of complexes depends on the concentration of Ca^{2+} as shown in Figure 4.10. OmpF/Ra-LPS complexes at 1:10 molar ratio were made and supplemented with Ca^{2+}. The higher the concentration of Ca^{2+}, the larger the aggregates.

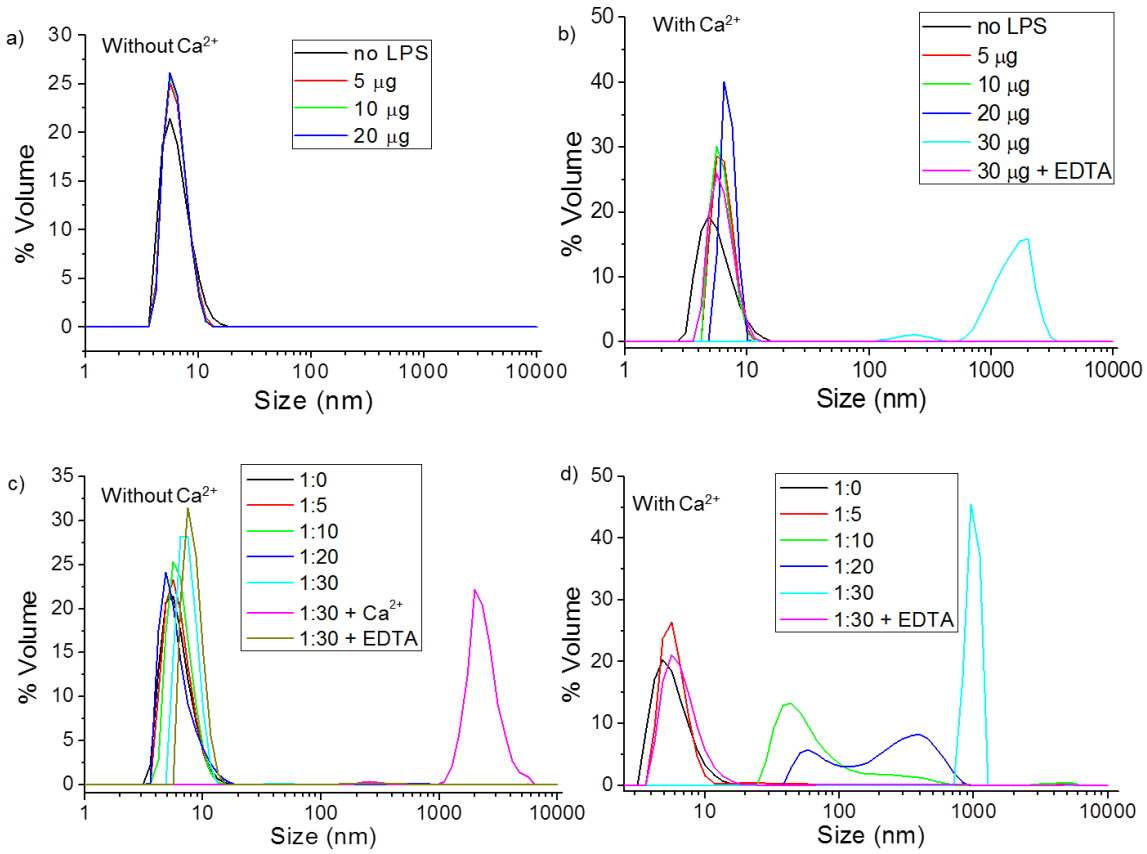

Figure 4.9 Size distribution of OmpF/Ra-LPS and Ra-LPS determined by DLS and expressed by volume in solution with and without divalent cations. a) Ra-LPS without Ca^{2+}, b) Ra-LPS in 5 mM Ca^{2+}, c) OmpF/LPS complexes at the defined OmpF:LPS molar stoichiometry without Ca^{2+}, d) OmpF/LPS complexes at the defined OmpF:LPS molar stoichiometry in 5 mM Ca^{2+}. The measurements were carried out at 25^{o}C using 0.17 mg/ml of OmpF in 20 mM Tris-HCl, pH 7.4, 0.3 M NaCl, 1% (v/v) octyl-POE as the buffer. Total sample volume = 50 µl.

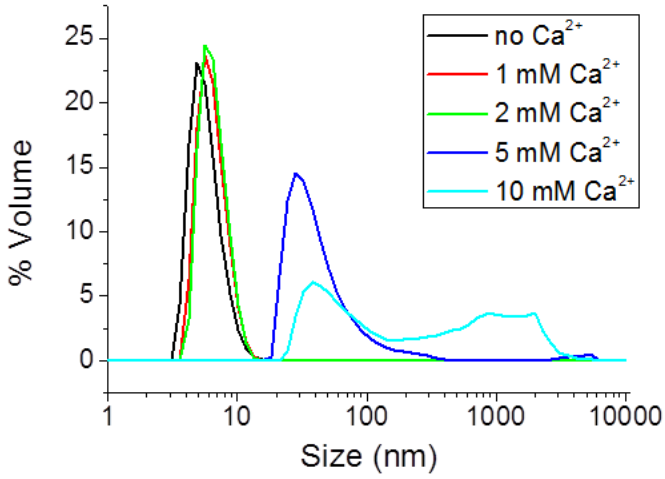

Figure 4.10 Size distribution of OmpF/Ra-LPS in solution by DLS and expressed as volume as a function of Ca^{2+} concentration. Complexes of OmpF and Ra-LPS were prepared at 1:10 OmpF/Ra-LPS molar ratio in the buffer without Ca^{2+}. The measurements were carried out at 25^{o}C using 0.17 mg/ml of OmpF in 20 mM Tris-HCl, pH 7.4, 0.3 M NaCl, 1% (v/v) octyl-POE as the buffer. Total sample volume = 50 µl.

Characterising the OmpF/LPS complex by small-angle x-ray scattering

One method to determine the size and shape of protein complexes is to use small angle x-ray scattering. However, membrane proteins must normally be handled in detergents or lipids. For example, the overall scattering from the sample of membrane protein consists of the scattering of proteins, protein-bound detergent and detergent micelles. Several research groups have developed approaches to exclude the scattering of detergents and model membrane protein-detergent complexes (Berthaud *et al.*, 2012; Calcutta *et al.*, 2012; Koutsioubas *et al.*, 2013).

In this present study, the size of OmpF/LPS complexes in the presence of detergents was determined by SAXS in order to confirm that LPS interacts with OmpF (In collaboration with Dr Alexandra Solovyova). Ra-LPS was added to OmpF at 1:5 OmpF/Ra-LPS molar ratio and then compared with WT-OmpF and LPS-free OmpF. LPS-free OmpF was made as described above by refolding inclusion bodies of OmpF in detergents. WT-OmpF purified from the outer

membrane of *E. coli* K-12 strains has naturally bound rough LPS (similar to Ra-LPS (Muller-Loennies *et al.*, 2003)) attached. The size exclusion chromatography of LPS-free OmpF, Ra-LPS added OmpF and WT-OmpF was performed using Superose 12 column (GE Healthcare) which was previously equilibrated with 10 mM Tris-HCl, pH 8.0, 150 mM NaCl and 0.2% (w/v) DDM. To ensure that the SAXS signal from individual detergent molecules is minimal, detergents used in this experiment must have a low critical micelle concentration (CMC). DDM has very low CMC of 0.2 mM or 0.01% (w/v) hence there is a minimal amount of free DDM in solution (Dupuy *et al.*, 1997). The scattering curves of protein-containing fraction were recorded on the beamline BM29 at ESRF, Grenoble, France (Figure 4.11a). The scattering data of samples were subtracted by the scattering data of buffer with DDM (Figure 4.11d). Therefore, only the scatter of OmpF/LPS and DDM-bound OmpF should be present in the final scattering profiles. The initial analysis and R_g estimation of SAXS data were performed by PRIMUS (Konarev *et al.*, 2003).

The Guinier plots of all samples were linear so all the OmpF samples were homogenous and not aggregated (Figure 4.11c). The agreement of R_g calculated from Guinier and GNOM analysis (Svergun, 1992) also supported the homogeneity of samples. The D_{max} and R_g of samples are summarised in Table 4.1. The P(r) distribution of all samples in Figure 4.11b indicated that the maximum dimension (D_{max}) of LPS-added OmpF and WT-OmpF are approximately 10 Å larger than that of LPS-free OmpF. In addition to D_{max}, the R_g of LPS-added OmpF and WT-OmpF calculated by GNOM are slightly larger but this is not statistically significant. The SAXS data are thus generally in agreement with SDS-PAGE and DLS in showing that LPS has an interaction with OmpF in solution. The final modelling of complexes is still in progress in collaboration with Dr. A. Solovyova.

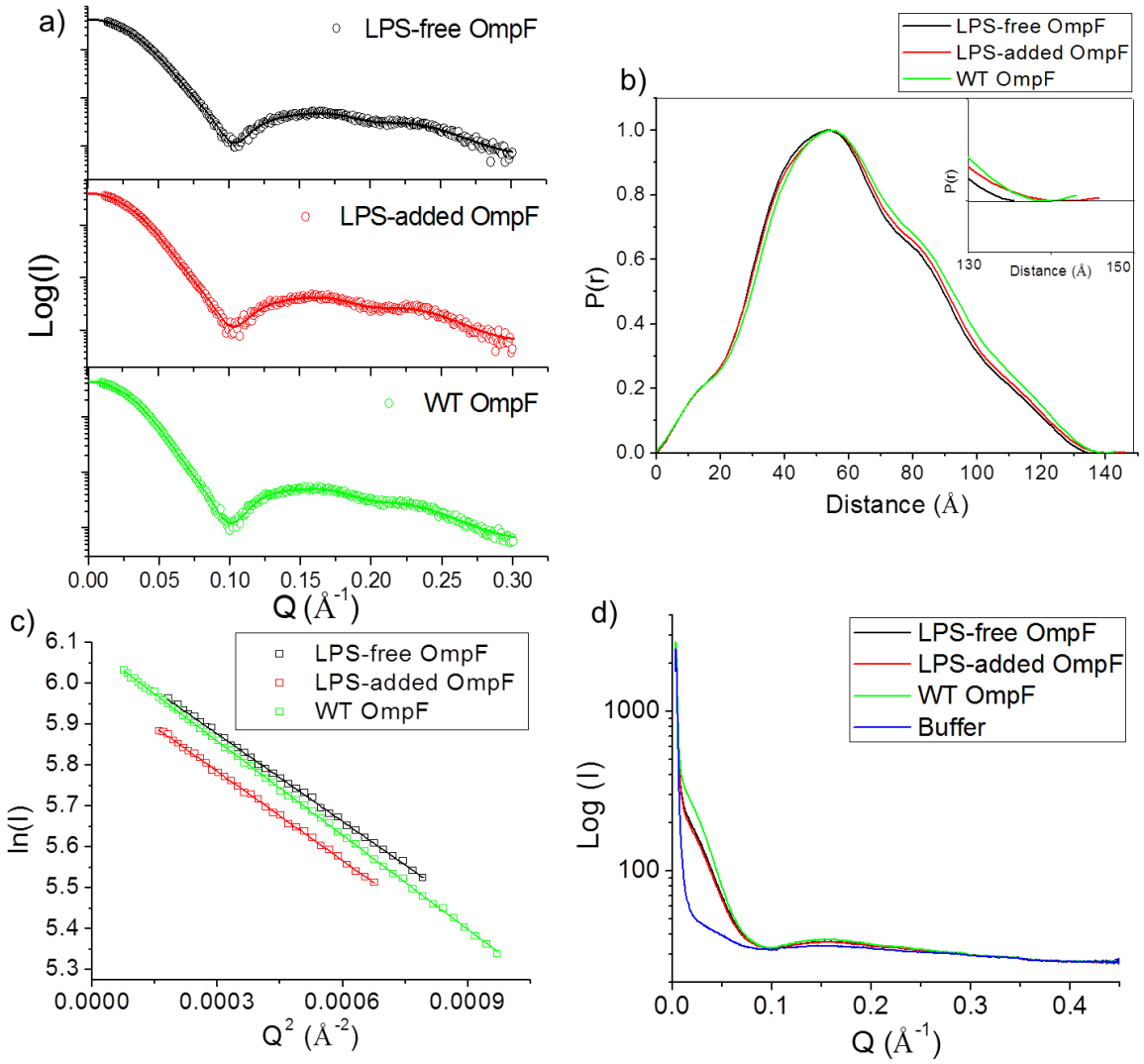

Figure 4.11 Scattering data for OmpF with and without LPS. OmpF was solubilised in buffer containing 0.2% (w/v) DDM. a) Scattering profiles of LPS-free OmpF, LPS-added OmpF and WT-OmpF (symbols). The fitting (lines) generated by GNOM. The samples were purified by size exclusion chromatography. SEC was performed at a flow rate of 0.5 ml/min by using a Superose 12 column equilibrated with 10 mM Tris-HCl, pH 8.0, 150 mM NaCl and 0.2% (w/v) DDM. b) P(r) distribution function calculated by GNOM. The inset shows where D_{max} of samples are c) Guinier plots d) Scattering patterns of the OmpF samples and buffer with DDM before subtraction.

Table 4.1 Summary of all parameters derived from Guinier plot and P(r) function for OmpF and OmpF/LPS complexes in the presence of DDM

Sample	Guinier Analysis $0.4<R_gQ<1.3$	Gnom analysis	
	R_g (Å)	R_g (Å)	D_{max}(Å)
LPS-free OmpF	46.19 ± 0.49	46.3 ± 0.04	136
LPS-added OmpF	46.67 ± 1.18	46.8 ± 0.05	146
WT OmpF	47.91 ± 0.53	47.7 ± 0.03	143

4.2.3 Probing for LPS-binding sites of OmpF

Site-directed mutagenesis on the LPS binding sites of OmpF

In the only published high resolution structure of an LPS-OMPF interaction, LPS binds to FhuA via the charge interaction between the phosphate group of LPS and a group of positively charged residues on FhuA (Ferguson *et al.*, 1998). When examining the crystal structure of OmpF, there are two groups of basic residues (lysine and arginine) located on the extracellular membrane facing side of OmpF. Figure 4.12a displays two possible LPS binding sites which we named as group A (pink) and group B (yellow). The sites were chosen to provide the minimum four basic residues predicted by Ferguson *et al* (Ferguson *et al.*, 2000) and because they appear to form two distinct groups. In order to probe for LPS-binding sites, the mutagenesis of positively-charged residues was carried out by substituting these residues with glutamine. The mutagenesis was done by Mr. Haris Atmoko who was working on this project under my supervision during his summer placement. Replacing basic residues by glutamine removes the charge but maintains the polar side chain behaviour and should result in the specific disruption of the OmpF-LPS interaction. The OmpF mutants were made using QuikChange (Stratagene) site-directed mutagenesis method according to the manufacturer's instructions (see Chapter 2). Single,

double, triple and quadruple mutations were performed to test the prediction that a group of OmpF basic residues are required for LPS binding.

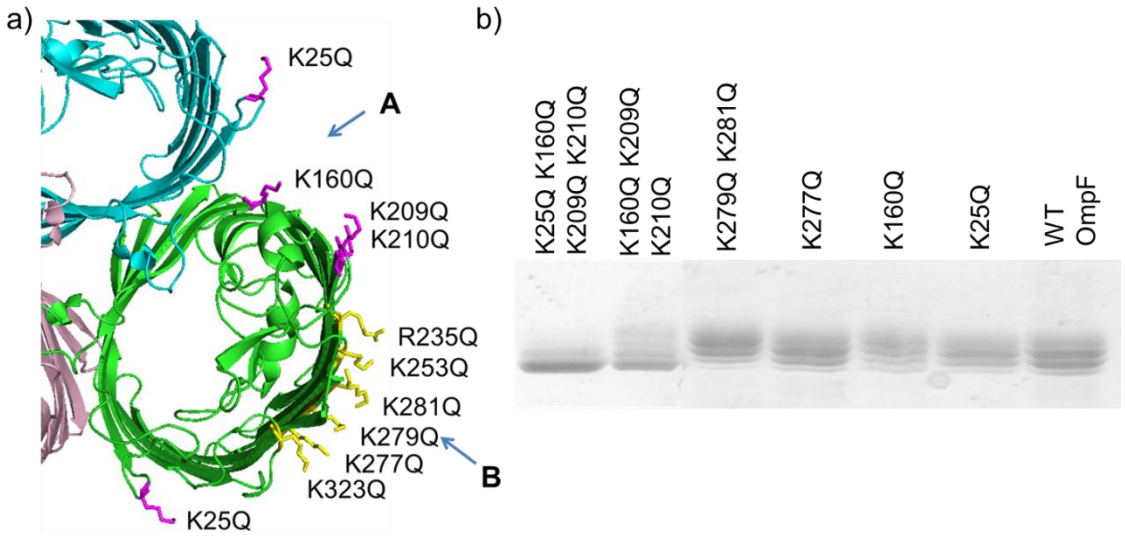

Figure 4.12 Localisation of basic residues on OmpF trimer and SDS-PAGE analysis of OmpF mutants. a) Groups of positively charged residues on extracellular side of the OmpF trimer. The possible LPS binding sites is divided into group A (Cleft) and group B (Perimeter). Viewed from the extracellular side (b) SDS-PAGE analysis of ladder formation by OmpF mutants. All OmpF samples are in the trimeric state.

The list of OmpF mutants in this study is presented in Table 4.2. The pMS119 plasmid containing OmpF gene was transformed into the porin free strain *E. coli* BZB1107. The purification of OmpF WT and mutants from the outer membrane was performed as previously described in the methods chapter. This provides samples that have folded normally in the outer membrane in the presence of LPS and thus reveals the effect of the mutants on this process and natural LPS binding. The protein purification was carried out, under my supervision, by Mr. Danny Newman during his final year project.

Table 4.2 List of OmpF mutants in this study

Binding site	Mutation
A	K25Q
A	K160Q
A	K160Q, K209Q and K210Q
A	K25Q, K160Q, K209Q and K210Q
B	K277Q
B	K279Q and K281Q

To observe LPS bound to OmpF, all OmpF samples were assessed, without boiling, on SDS-PAGE and compared to WT-OmpF purified in an identical manner. As demonstrated above, the ladder on SDS-PAGE is a sign of LPS interaction with OmpF. The number of LPS bound to or associated with OmpF by divalent cations is indicated by the length of the ladder. The samples were not treated with EDTA nor did they have additional divalent cations added, so this data relies upon background levels of ions and is comparable to Figure 4.7. Figure 4.12b illustrates the results for all the OmpF mutants run alongside WT OmpF on SDS-PAGE. It indicated that single and double mutations of positively-charged residues have no discernible effect on LPS-binding as the ladders still existed as in WT OmpF. However, the ladders of triple and quadruple OmpF mutants became shorter than those of WT OmpF meaning that fewer LPS bound to triple and quadruple OmpF mutants. As single and double mutations did not disrupt the OmpF-LPS interaction, this means that LPS binds to OmpF via multiple positively-charged residues. Furthermore LPS still binds to the quadruple mutant in site A as expected if there is another binding site present.

The effect of OmpF mutagenesis on maturation of OmpF in *E. coli*

Due to the fact that several basic residues were essential for LPS interaction, it was decided to mutate the whole group A and group B sites in order to observe clear changes in OmpF-LPS interaction. To achieve several mutations at the same time, we used the “In-Fusion” method (Clonetech) as shown in the

methods section. The lysine and arginine residues at group A and B were replaced by 1) glutamines (a polar uncharged residue), 2) alanines (an uncharged residue) and 3) glutamates (a negatively charged residue). Table 4.3 summarises all mutants made for this study.

Table 4.3 Summary of OmpF mutants created by In-Fusion cloning technique.

OmpF mutants	Replacing Arg and Lys by	Mutation site	Phenotype
Gln A	Gln	A	K25Q, K160Q, K209Q and K210Q
Gln B	Gln	B	R235Q, K253Q, K281Q, K279Q, K277Q and K323Q
Ala A	Ala	A	K25A, K160A, K209A and K210A
Ala B	Ala	B	R235A, K253A, K281A, K279A, K277A and K323A
Ala AB	Ala	A and B	K25A, K160A, K209A, K210A, R235A, K253A, K281A, K279A, K277A and K323A
Glu A	Glu	A	K25E, K160E, K209E and K210E
Glu B	Glu	B	R235E, K253E, K281E, K279E, K277E and K323E
Glu AB	Glu	A and B	K25E, K160E, K209E, K210E, R235E, K253E, K281E, K279E, K277E and K323E

The pMS119 plasmids containing mutated OmpF genes were transformed into *E. coli* BZB1107 as a host. OmpF was expressed and purified from the outer membrane of *E. coli* by Mr. Andrew Dale under my supervision during his summer placement in our laboratory. The samples taken at each step of purification were evaluated on SDS-PAGE for Gln A shown in Figure 4.13. It is evident that Gln A was successfully expressed as the native and heat-

denatured Gln A samples ran at the expected molecular weight of ≈75 kDa and 37 kDa. Trimeric OmpF has an actual MW of ≈ 111 kDa but migrates faster (in a gel dependent manner) due to its compact folded state.

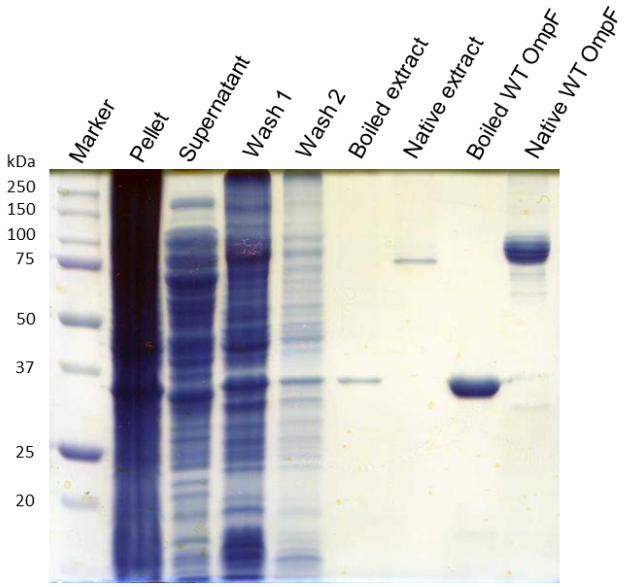

Figure 4.13 SDS-PAGE of GlnA OmpF preparations from *E. coli* BZB1107. Samples loaded on SDS-PAGE were taken from each purification step.

Interestingly, during Gln B preparation, Gln B was successfully expressed in whole cells as the comparison of samples taken before and after induction on SDS-PAGE (Figure 4.14a) displayed the band of OmpF at 37 kDa. When purifying Gln B from the cell pellet, most of the OmpF protein is lost in the wash step as seen on SDS-PAGE (Figure 4.14a). No OmpF band was observed in the extract sample. To ensure that there were no Gln B in the extract, the Gln B samples were concentrated by ethanol precipitation and resuspended in 20 mM Tris-HCl, pH 7.4, 0.3 M NaCl and 1% (v/v) octyl-POE. Figure 4.14b shows the SDS-PAGE analysis of concentrated Gln B. It confirmed that no OmpF band was observed on SDS-PAGE, therefore, Gln B was expressed but did not form a trimer *in vivo*. These results suggested that the mutations of basic residues at site B have an impact on the maturation of OmpF *in vivo*. This effect did not only apply to Gln B as other mutants with B site mutations showed a similar effect to Gln B as shown in Table 4.4.

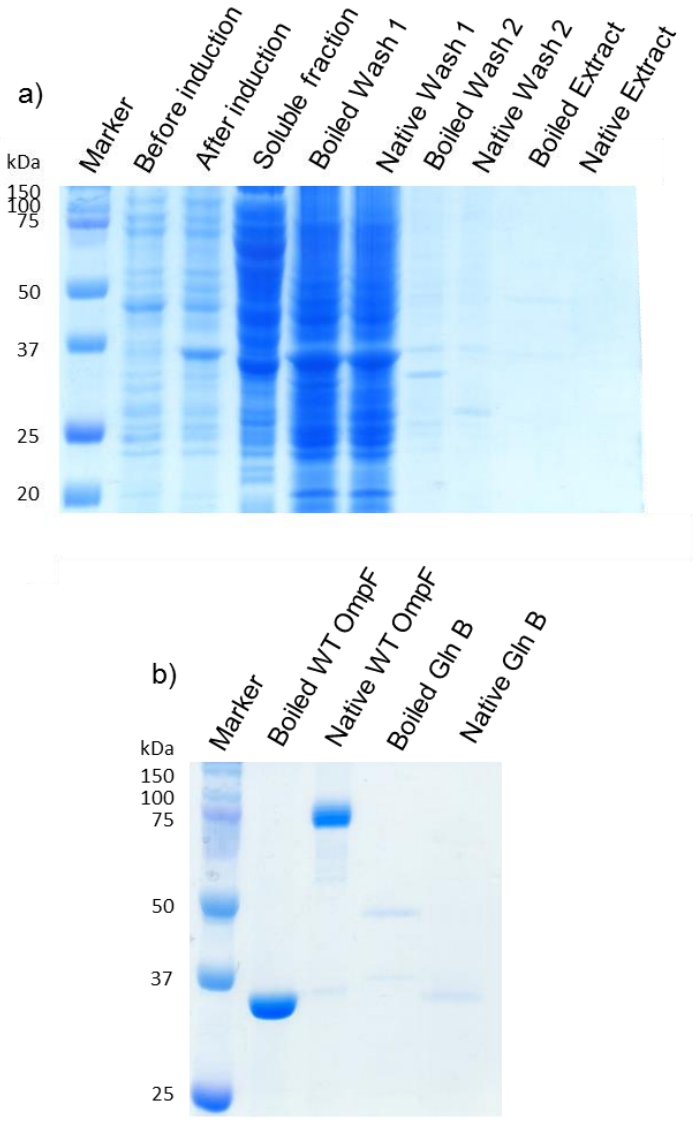

Figure 4.14 SDS-PAGE of Gln B OmpF preparations from *E. coli* BZB1107. a) Samples loaded on SDS-PAGE were taken from each purification step. b) Gln B samples was concentrated by ethanol precipitation and then run alongside WT OmpF.

Table 4.4 Summary of the expression and maturation *in vivo* of OmpF mutants.

OmpF mutants	Expression	Maturation
Gln A	✓	✓
Gln B	✓	X
Glu A	✓	✓
Glu B	✓	X
Glu AB	✓	X
Ala A	✓	✓
Ala B	✓	X
Ala AB	✓	X

To prove that site B is important for OmpF maturation, the OmpF B site mutants were expressed as inclusion bodies and refolded into trimers *in vitro.* Mutant OmpF genes without the signal sequence were subcloned into the pMS119 plasmid using In-Fusion cloning. The lysines and arginines at both A and B sites were replaced by glutamate. Replacement by glutamate was used as it is the charge reversal mutation, thus providing negative charges on OmpF for disrupting the OmpF-LPS interaction and the test of the ability of OmpF to fold. The inclusion bodies were expressed and purified as previously described in Visudtiphole *et al* (Visudtiphole *et al.*, 2005). The purified inclusion bodies were assessed on SDS-PAGE (Figure 4.15a). The inclusion bodies of Glu A, Glu B and Glu AB were expressed, purified and the unfolded proteins were shown to migrate on SDS-PAGE at the expected molecular weight (37 kDa).

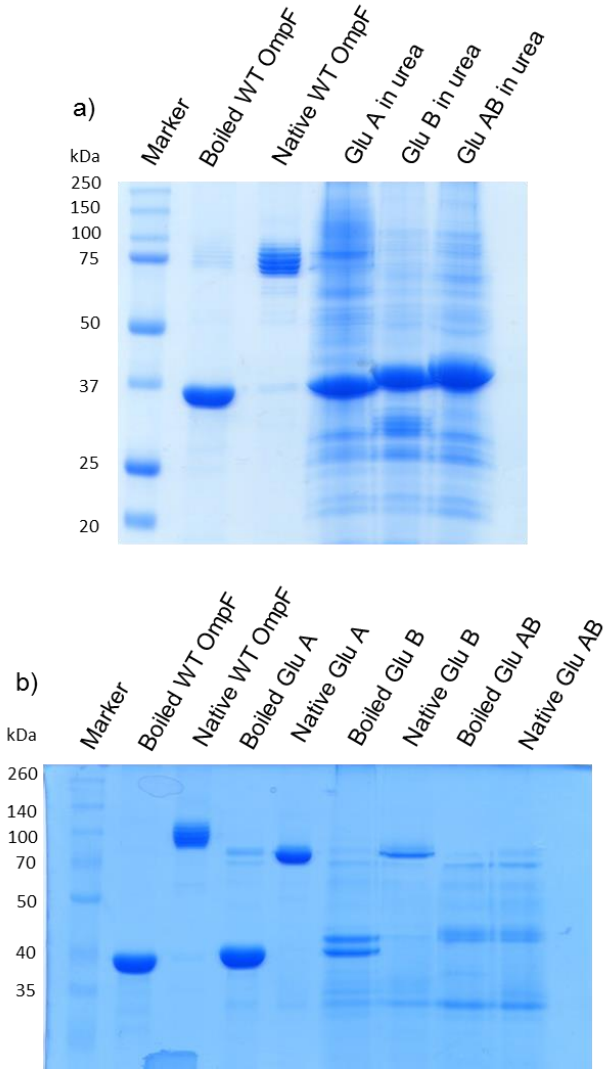

Figure 4.15 SDS-PAGE analysis for OmpF mutants expressed as inclusion bodies. a) OmpF mutants (Glu A, Glu B and Glu AB) purified from inclusion bodies plus a standard of purified WT OmpF. Note the apparent size changes associated with the change in charge. b) Samples of refolded OmpF mutants after 3 days refolding at 37^{o}C; plus a standard of purified WT OmpF with naturally attached LPS. Note how Glu A and B trimers run lower than WT and that Glu B boiled after refolding runs as two bands not seen in a). Glu AB did not refold with good yeild.

The proteins purified from inclusion bodies were then diluted into a buffer containing 1% (v/v) DG and 0.4% (v/v) DDM in order to refold OmpF mutant *in vitro*. Figure 4.15b indicates that only Glu A and Glu B are able to refold efficiently *in vitro* as we observed the bands at ≈37 kDa and ≈70 kDa which corresponds to OmpF monomer and trimer, respectively. This shows that the mutation at B site prevents the folding of OmpF *in vivo* but not *in vitro*, Site A

has no effect on either condition and complete removal of all the basic residues prevents folding in both conditions. Next, the interaction of Ra-LPS with refolded OmpF mutant as well as the effect of divalent cations were studied by adding LPS back to refolded OmpF at a 1:5 OmpF/LPS molar ratio. The Ra-LPS was used in the experiment because it is the largest defined LPS available and, therefore, gives rise to the largest shifts on SDS-PAGE. Glu A and Glu B mutants were studied and compared to WT OmpF. According to Figure 4.16, when adding Ra-LPS back to WT OmpF, Glu A and Glu B, the ladders still presented in all samples. The native samples of Glu A and Glu B ran as a single band in Figure 4.15 so the formation of ladders seen in the samples of OmpF mutants with Ra-LPS should be an indication of LPS binding. This showed that both A and B sites play a vital role in LPS interaction. In the presence of divalent cations, the intensity of the lowest band of OmpF decreased hence the number of high molecular weight species caused by the LPS interaction increased. On the other hand, in the absence of divalent cations (when EDTA is added), the intensity of the lowest band became brighter so fewer Ra-LPS were bound to OmpF. Additionally, the ladders of mutants are simpler than those of WT OmpF and distinct bands on the ladder can be seen in Glu A and Glu B samples. This may indicate fewer bound LPS on the mutants. The OmpF GluB mutant, and therefore the intact site A, appears binds the least LPS.

OmpF	WT			GluA			GluB		
Ca^{2+}	-	+	-	-	+	-	-	+	-
EDTA	-	-	+	-	-	+	-	-	+

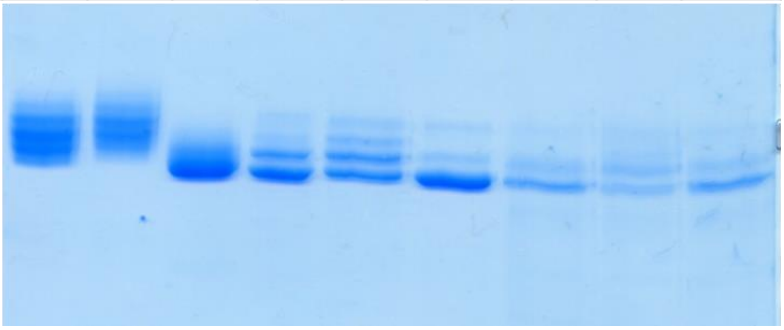

Figure 4.16 SDS-PAGE analysis of OmpF/LPS complexes at 1:5 OmpF/LPS molar ratio in the presence and absence of divalent cations. Ca^{2+} and EDTA were added to sample to promote and disrupt LPS-LPS interaction.

Characterising the OmpF/LPS complex by small-angle neutron scattering

Another approach to investigate the LPS binding site is to study the OmpF/LPS complexes by small-angle neutron scattering. SANS allows us to determine where LPS binds to OmpF by using the contrast variation technique and may be more sensitive than SAXS in the presence of detergent. In this present study, deuterated OmpF (dOmpF) and hydrogenated Ra-LPS were used to form complexes in the mixture of deuterated and hydrogenated SDS (h/d SDS). The details of this SANS technique have been explained in chapter 3. In brief, the neutron scattering is very sensitive to the deuteration of each component in the system. Therefore, we can selectively observe the whole complexes and individual components by changing the H_2O/D_2O content in the sample. To achieve this experiment, the contrast match point (CMP) of each component in the sample must be accurately determined. The CMP of dOmpF and Ra-LPS was 77% and 27% D_2O respectively. Figure 4.17 shows the determination of the CMP of Ra-LPS (For dOmpF see Chapter 3). The scattering curves of Ra-LPS samples at 2.0 mg/ml in 6 different D_2O solutions (20 mM phosphate buffer, pH 7.5, 300 mM NaCl) were recorded. The normalised I(0) obtained from the Guinier analysis of the scattering data were plotted against the D_2O concentration. The CMP of Ra-LPS is the Y=0 intercept of the graph.

The samples for SANS experiment using the contrast variation method were prepared as described in Clifton *et al* (Clifton *et al.*, 2012). dOmpF was passed through a size exclusion column, using a running buffer with EDTA, before use in order to remove the contaminating LPS derived from the outer membrane. Ra-LPS was added back to dOmpF at 1:5 dOmpF/LPS molar ratio. The complexes were then passed through size exclusion column again to remove loosely-bound LPS from the complexes. Finally, the complexes were ready to dialyse into the buffer containing desired H_2O/D_2O contents. The scattering curves of complexes at 3.0 - 3.5 mg/ml in 13%, 27%, 41%, 77% and 100% D_2O buffer (50 mM phosphate buffer, pH7.5, 150 mM NaCl, 0.5% h/d SDS) were recorded at D22 beamline, ILL in Grenoble, France (Figure 4.18a). The initial

manipulation and R_g evaluation of SANS data were performed by PRIMUS (Konarev *et al.*, 2003).

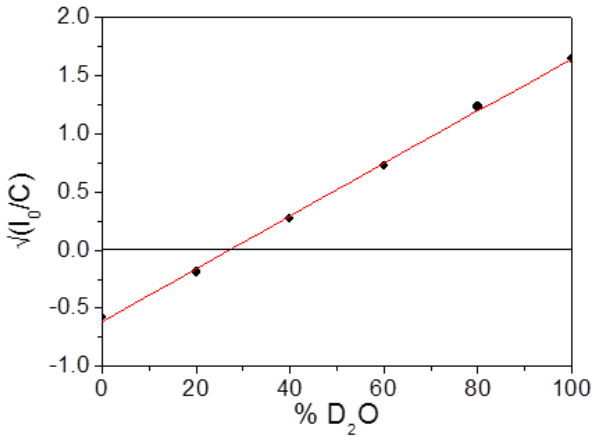

Figure 4.17 Experimental determination of contrast match point of Ra-LPS by SANS. The linear (fitting) of data (symbols) showed the CMP of Ra-LPS (Y=0 intercept) is 27% D_2O.

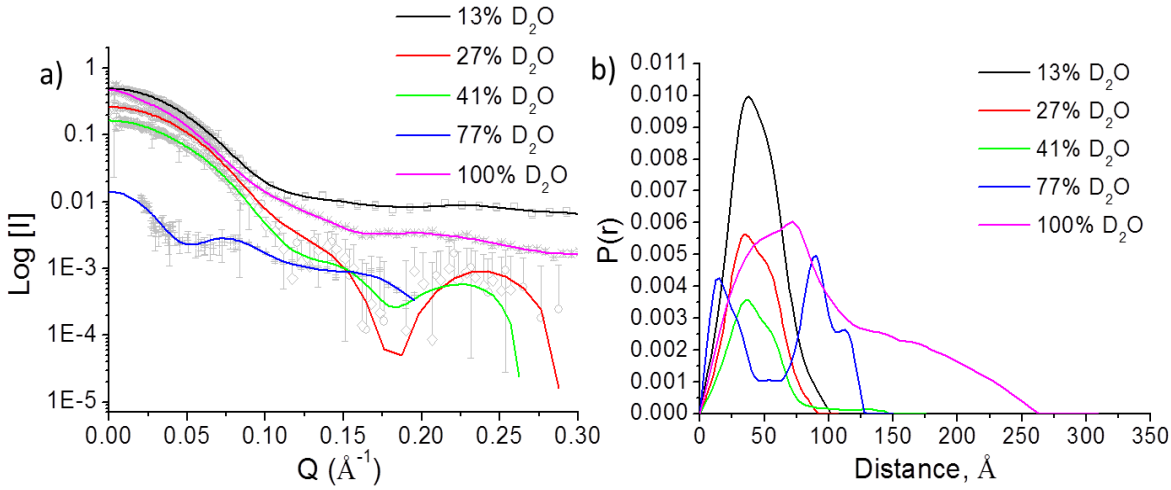

Figure 4.18 SANS data for dOmpF/Ra-LPS complexes in 0.5% h/d SDS. a) SANS data (symbols) and fitting (lines) generated by GNOM. b) Distance distribution function, P(r), calculated by GNOM.

As the CMPs of dOmpF and Ra-LPS are 77% and 27% D_2O, only dOmpF can be seen at 27% D_2O whereas only Ra-LPS can be observed at 77% D_2O. The whole complexes were visible to neutrons in the rest of samples. The P(r) distribution function in Figure 4.18b calculated by GNOM (Svergun, 1992)

indicates that the smallest P(r) was obtained at 27%D_2O (dOmpF only) and the largest P(r) was at 100% D_2O. At 77% D_2O, there are two distinct peaks which correspond to a multi-domain structure as seen with h- colicin N bound to OmpF (Clifton *et al.*, 2012). This suggests that there are more than one LPS bound to the OmpF trimer.

To find out the position of LPS in the complex, the Stuhrmann analysis (Henderson, 1996) was carried out by plotting of R_g^2 against $\frac{1}{\Delta\rho_N}$ and fitting the data to a parabola curve. The MULCh program was utilised to calculate $\Delta\rho_N$ by using I(0) and R_g estimated from Guinier analysis (Whitten *et al.*, 2008). The Stuhrmann plot of OmpF/LPS complexes is illustrated in Figure 4.19. This plot shows the change of R_g as a function of contrast which is given by the Stuhrmann equation (Ibel and Stuhrmann, 1975).

$$R_g^2 = (R_g^2)_{1/\rho\to 0} + \frac{\alpha}{\Delta\rho_N} + \frac{\beta}{\Delta\rho_N^2}$$

The data are rather sparse but do suggest that LPS, which has the lower SLD is located on the outside of the OmpF trimer as the α value obtained from the fit has a negative sign.

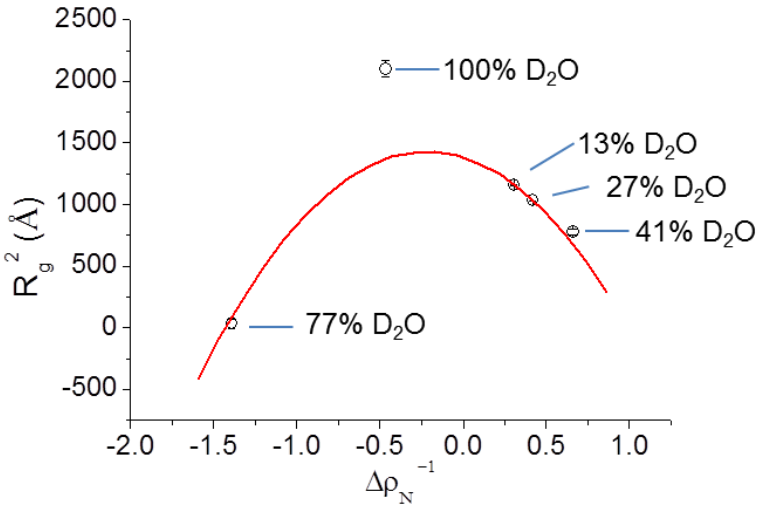

Figure 4.19 Stuhrmann analysis of dOmpF/Ra-LPS complex. The red line is the fitted parabola from the Stuhrmann equation calculated using the programme MULCh. This corresponds to a negative value of α.

According to the study of LPS binding site by mutagenesis, there are two possible binding sites in the cleft and on the perimeter of OmpF. The model of OmpF/LPS complexes were built based on the biochemical data. Three models of the complexes represent in Figure 4.20 where LPS binds to OmpF at a) both A and B site, b) A site only and c) B site only. These models were used to generate the theoretical scattering profile by CRYSON (Svergun *et al.*, 1998). This software then compared this theoretical scattering profile to the experimental one. The goodness of fit was expressed as a chi value (χ). The chi value should be below 1.1 to be considered a good fit. Table 4.5 reported the chi values of the models and WT OmpF when comparing to the experimental data from 5 different D_2O concentrations. It is obvious that model 1 fit the best in all D_2O solutions however none of the models fit well in high D_2O content samples (77% and 100% D_2O).

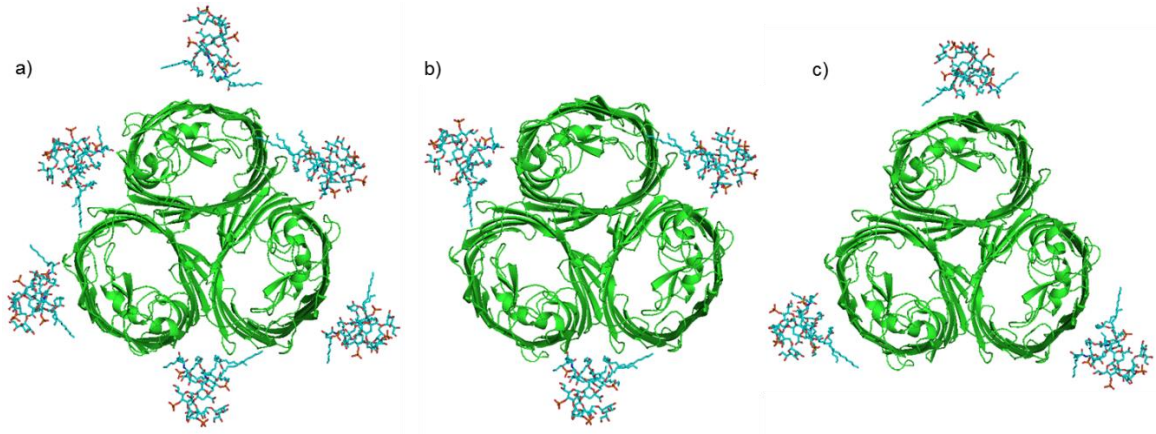

Figure 4.20 Three possible models of OmpF/LPS complexes. OmpF (PDB code: 2OMF) and LPS (PDB code: 3FXI) structures were taken from PDB database. The gaps between the LPS and OmpF result from our use of cartoon and wire frame display rather than space filling representations.

Table 4.5 Summary of goodness of fit of various OmpF/LPS models to experimental data obtained from CRYSON

%D_2O	Goodness of fit (χ)			
	Model 1	Model 2	Model 3	WT OmpF
13	1.283	1.907	1.710	2.396
27	0.515	0.687	0.615	0.909
41	0.539	0.540	0.540	0.545
77	2.202	2.189	2.238	2.234
100	3.879	4.958	4.109	4.951

To improve the fit, the model with LPS bound to both sites was altered slightly. Due to the flexibility of the sugars on LPS molecules, the core oligosaccharides can be bent. The model in Figure 4.21 was made by bending the core oligosaccharide region of LPS and attaching it to OmpF at both A and B sites. Fitting the theoretical curves generated by CRYSON to the experimental data (Figure 4.21) showed that the goodness of fit improved when compared to the previous model. Therefore, this corrected model is currently the best one that represents how LPS binds to OmpF *in vitro*. This result agrees with the biochemical data that there are two possible LPS binding sites on OmpF trimer which are located at the cleft and outside of OmpF trimer.

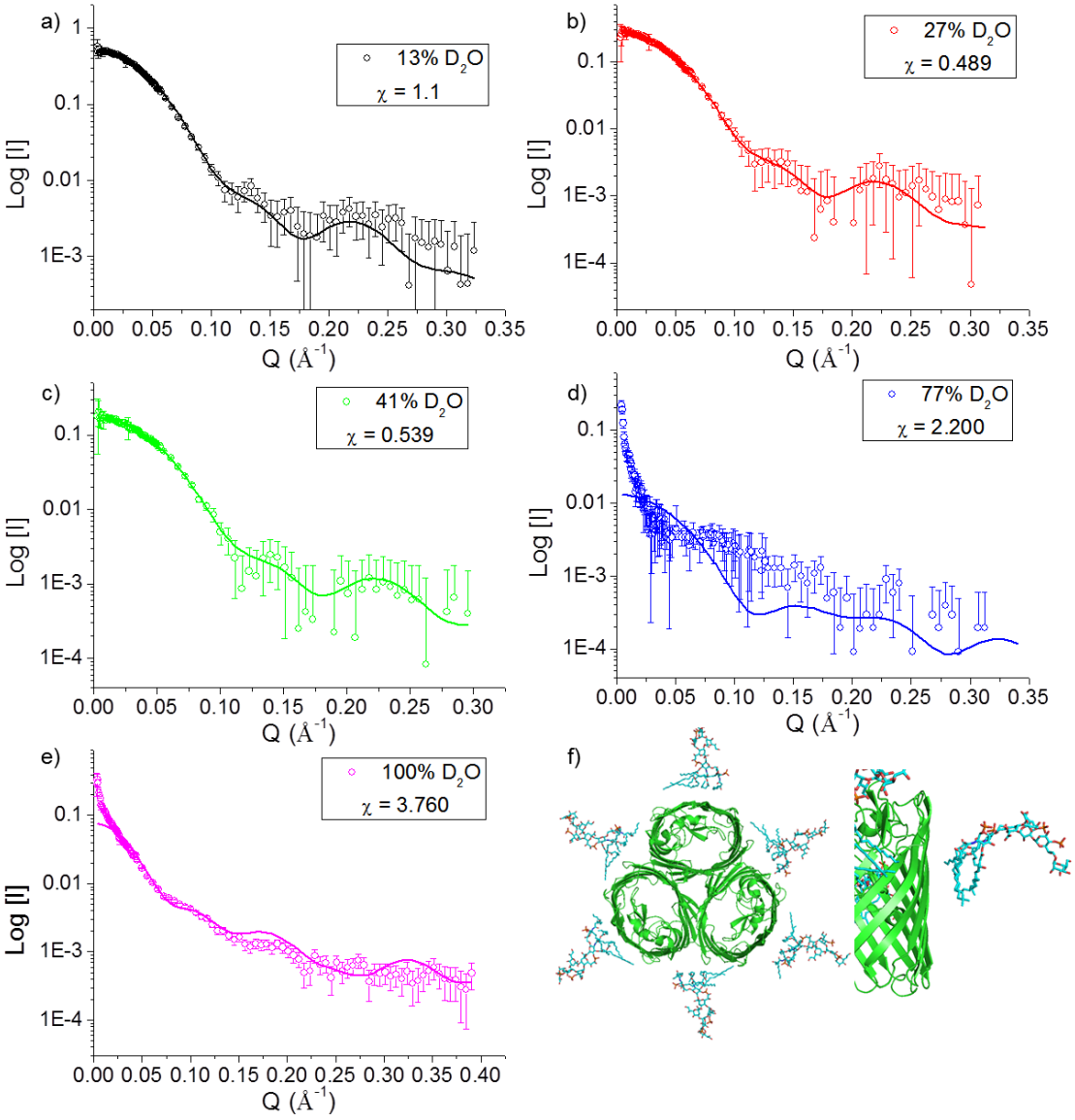

Figure 4.21 Theoretical SANS profiles of OmpF/LPS model generated from CRYSON fitted against the experimental SANS profiles. a-e) Lines and symbols represent CRYSON fitting and SANS data, respectively. f) OmpF/LPS model

4.3 Discussion

The outer membrane (OM) of gram negative bacteria is an asymmetric lipid bilayer containing a phospholipid-rich inner leaflet and LPS in the outer leaflet (Nikaido, 2003). The OM is not only a protective barrier but also extremely permeable as a result of a large number of non-specific channels or porins embedded within OM (Rosenbusch, 1974; Jaroslawski *et al.*, 2009). LPS and porins are major component of the OM, however the interaction between them has not been studied in great detail. OmpF expressed at high levels in *E. coli* is widely used as a laboratory model of porin function.

We have shown by SDS-PAGE that the association of Ra-LPS with LPS-free OmpF caused a slower mobility of OmpF on an SDS-PAGE gel. The multiple banding patterns (a ladder) of OmpF trimer appearing on SDS-PAGE results from the different number of LPS molecules bound to OmpF trimer. Adding more LPS to OmpF results in the formation of longer ladder. Previous work by Holzenburg *et al* has also shown similar effects of LPS association on OmpF migration (Holzenburg *et al.*, 1989). They isolated four forms of OmpF bound to different numbers of LPS using free flow electrophoresis. OmpF with increasing amounts of bound LPS showed a decreasingly lower mobility and an increasing number of bands on SDS-PAGE. Diedrich *et al* studied the interaction of OmpF with smooth and rough LPS (Diedrich *et al.*, 1990). OmpF with bound LPS was purified from *E. coli* strains expressing Rc-LPS, Ra-LPS and smooth LPS. The association of these LPS with OmpF changed the mobility of OmpF trimers on SDS-PAGE. The OmpF associated with smooth LPS migrated slowest. The interaction of OmpF with smooth LPS *in vitro* was also reported by Baboolal *et al* (Baboolal *et al.*, 2008). These results are consistent with the findings presented in this study. It showed that the multiple banding patterns of OmpF trimer on SDS-PAGE results from the LPS binding and depends on the number and type of LPS bound to OmpF trimer. Our findings also revealed that the shortest LPS binding to OmpF is lipid A. It was then concluded that the interaction between OmpF and LPS happens via the lipid A moiety which contains at least two negatively charged phosphate residues. The interaction of

LPS with FhuA from the crystallographic structure also took place at the lipid A moiety via the electrostatic interaction between the cationic side chains and the phosphate groups of lipid A (Ferguson *et al.*, 1998).

LPS is known to bind strongly to divalent cations, which neutralise the negative charges of phosphate groups between neighbouring LPS molecules (Nikaido, 2003). Several studies have shown the tendency of LPS to form a macromolecular structure. In an early study, Galanos *et al* showed the aggregation of LPS in the presence of divalent cations, especially Ca^{2+}, produced large insoluble aggregates (Galanos and Luderitz, 1975). Due to the amphiphilic nature of LPS, LPS has the ability to aggregate into macromolecular structures above a certain concentration in solution. The LPS aggregation behaviour depends on the size of its hydrophilic part, divalent cations, and temperature (Aurell and Wistrom, 1998; Snyder *et al.*, 1999; Garidel *et al.*, 2005). Here we showed that saturated, defined OmpF-LPS complexes could not be observed by SDS-PAGE because LPS-LPS interactions were also involved in the formation of complexes. This result is also supported by DLS. Both LPS and OmpF-LPS complexes aggregated in the presence of Ca^{2+} and the addition of EDTA, a chelating agent of cations, disrupted this interaction. The formation of OmpF-LPS aggregates is easier than that of LPS aggregates. It is likely that OmpF facilitates the LPS aggregation as LPS particles would become more organised upon binding to OmpF. In addition to the aid of OmpF for the LPS association, this process also relies on the concentration of calcium ions in solution. The sheet-like structure of OmpF/LPS complexes in amphipols was also observed by electron microscopy (Arunmanee *et al.*, 2014). This structure was also stabilised by the presence of divalent cations. This data could reflect the organisation of OM in gram negative bacteria.

The solution structure of OmpF with bound LPS was also studied by SAXS in the presence of DDM. Unlike the SANS, using contrast variation techniques in the SAXS experiment is more complicated. To study membrane proteins by SAXS, they should be handled in detergents with low CMC in order to minimise the scattering of free individual detergent molecules (Berthaud *et al.*, 2012).

Detergents with low CMC tend to form the micellar structure rather than being a monomeric form in solution. The structure of membrane proteins are studied in detergent micelles using SAXS while the detergents bound to membrane proteins are present. The scattering of free micelles was subtracted by the scattering of buffer so only detergents bound to membrane proteins were observed by SAXS. We have shown that the R_g and D_{max} of LPS-free OmpF, LPS-added OmpF and WT OmpF in DDM obtained from the SAXS experiment were very similar. This could be due to the fact that the scattering of OmpF-bound DDM was much stronger than that of LPS. The size of LPS molecules is also smaller than the DDM micelles It is more likely to see the proteins in this protein-detergent complexes using SAXS for example the study on the unfolding state of membrane proteins in DDM (Calcutta *et al.*, 2012). These may explain why it is difficult to observe LPS molecules in this system.

In this study, the LPS binding sites of OmpF were identified by mutagenesis and SANS. Replacing two groups of positively charged side chains at the extracellular side of OmpF disrupts the electrostatic interaction between LPS and OmpF. The replacement of cationic side chains to either uncharged or anionic side chains showed the similar effect on the LPS binding so it confirmed the charge interaction is the main interaction between OmpF and LPS. The binding sites are located at the cleft and perimeter of OmpF trimer. The model of OmpF with bound LPS at these two binding sites fitted SANS data in low D_2O content well. The modification of model by bending the core oligosaccharide of LPS improved the fit to the experimental data. This led to an assumption that LPS could be flexible in the complexes therefore a combination of multiple conformations of LPS may fit the data better. However, the 77% and 100% D_2O data are ambiguous due to the upturn at low q-range which is an indication of aggregation. This is not observed at low D_2O % or in pure OmpF samples and indicates that LPS may aggregate in D_2O. The noisy data at 77% D_2O due to the weak scattering of LPS causes a problem in the data fitting as the chi values obtained from the model fitting by CRYSON were almost identical. In contrast to the SAXS study on OmpF/LPS complexes, the SANS study was able to observe the LPS binding on OmpF. Using contrast variation technique in the

SANS experiment allows us to match the scattering of detergents to solvent, thus the small molecules like LPS can be visible. The findings agreed with the crystal structure of FhuA with bound LPS (Ferguson *et al.*, 2000). LPS interacts electrostatically with FhuA via a group of positive charged side chains. The LPS binding site of OmpF at Arg235 proposed by Baboolal *et al* (Baboolal *et al.*, 2008) was also one of the binding sites found in this study. Recently, an unpublished crystal structure of OmpC from *Enterobacter cloacae* elucidated by Van den Berg's research group demonstrated two LPS binding sites located at the cleft and the perimeter of OmpC. This agrees well with our findings by mutagenesis and SANS as OmpF and OmpC share sequence similarity according to the sequence alignment between OmpF from *E. coli* and OmpC from *E. cloacae* in Figure 4.22. Three out of four side chains of OmpC interacting directly with LPS are conserved in OmpF. Figure 4.23 shows these conserved residues on the crystal structure of OmpF. According to the OmpC structure, the lysines at 160 and 210 bind to the same LPS molecule whereas the lysine at 253 interacts with another LPS molecule.

Interestingly, our mutagenesis study revealed the effect of LPS on the trimerisation of OmpF *in vivo*. The mutation of positively charged residues at the perimeter of OmpF prevented the assembly of OmpF *in vivo* as the monomeric form of this OmpF mutant was only observed. During the purification of OmpF, the presence of monomeric OmpF in the wash fractions demonstrated that OmpF somehow associated with the membranes otherwise it would be in the soluble fractions. However, the *in vitro* trimerisation of this mutant in detergents can be achieved. Several studies have also reported that the trimerisation of OmpF is dependent on LPS (Ried *et al.*, 1990; Sen and Nikaido, 1990; Sen and Nikaido, 1991). Laird *et al* also showed that the trimerisation kinetics of OmpF was affected in deep rough LPS mutant of *E. coli* K-12 at the step of a metastable-stable trimer (Laird *et al.*, 1994). However, the role of LPS in the assembly of OmpF is still unclear. Bos *et al* speculated that the influence of LPS on the biogenesis of outer membrane protein is the stabilisation of the trimer after insertion into OM (Bos *et al.*, 2007). Our study has pin pointed that site B is the crucial LPS binding site for OmpF maturation.

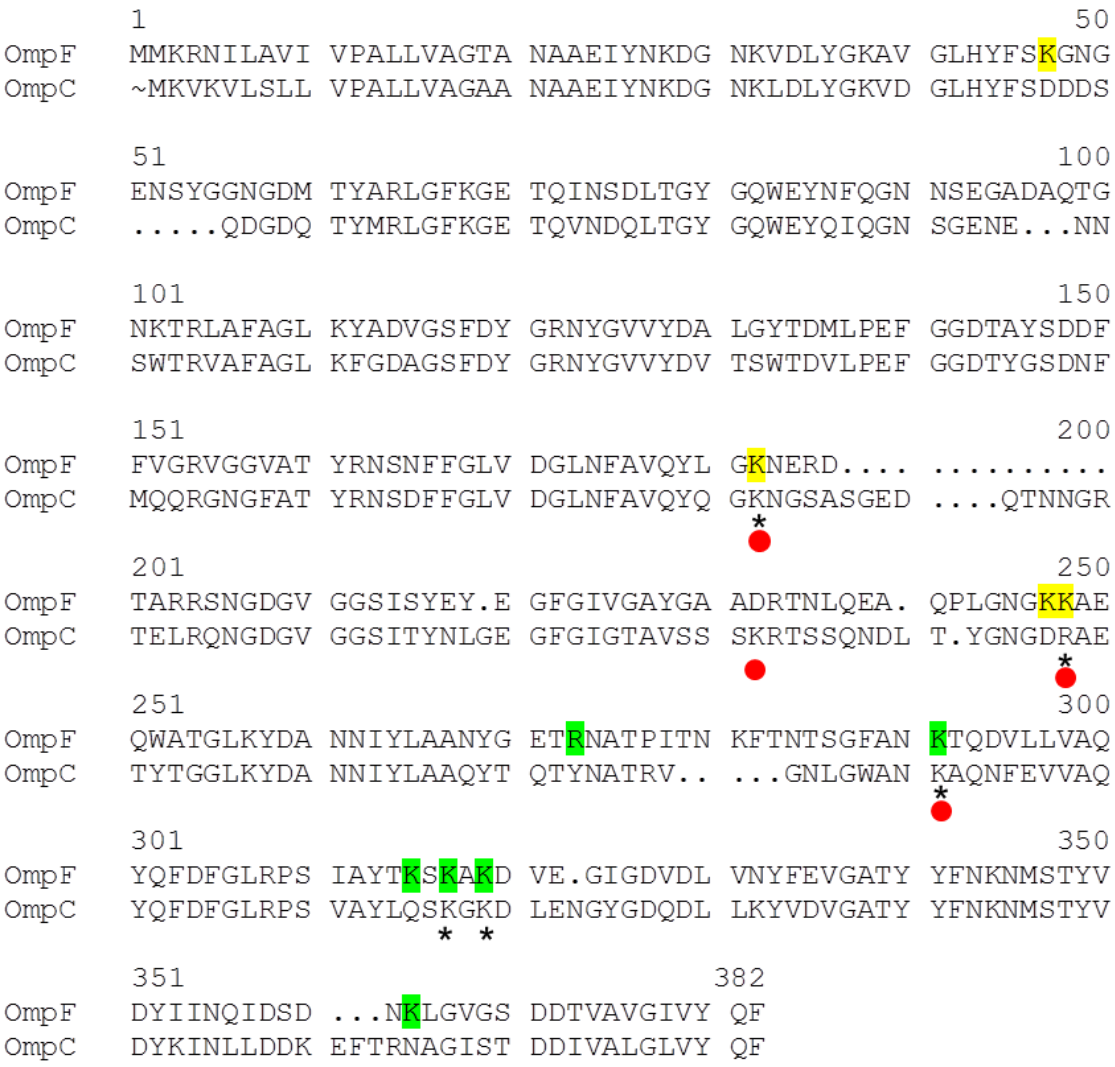

Figure 4.22 Sequence alignment of proteins demonstrating the homology between OmpF from *E. coli* and OmpC from *Enterobacter cloacae.* The predicted LPS binding residues of OmpF are highlighted in yellow for site A and green for site B. Stars underneath the sequences represent conserved residues among 10 predicted residues. The circles underneath the sequences indicate the residues of OmpC having direct contacts with LPS in the crystallographic structure of OmpC (The unpublished data from Van den Berg's group).

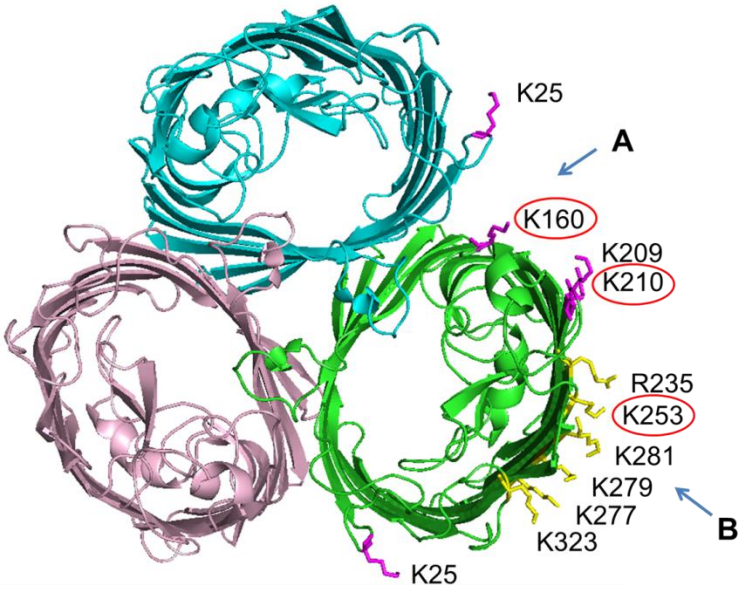

Figure 4.23 Conserved residues of OmpF having a direct contact with LPS. The residues in red circles are conserved basic residues of OmpF (PDB code: 2OMF) corresponding to the crystallographic structure of OmpC from *Enterobacter cloacae* (The unpublished data from Van den Berg's group). K160 and K210 interact with one LPS and K253 interacts with another LPS.

Chapter 5 Using novel approaches to study OmpF in native conditions

5.1 Introduction

Membrane proteins (MP) play a vital role in cell function and many of them, such as GPCRs and ion channels, are exploited as drug targets. Therefore, over the years they have been the target of many structural and functional studies. Conventionally, when extracting MPs from biological membranes, they must be handled in detergents in order to keep them soluble in aqueous solution. It is a formidable task to look for suitable detergents which maintain both structure and function as detergents sometimes destabilise MPs. To overcome this problem, the research groups of J. L. Popot and S. G. Sligar have developed novel approaches to stabilise MP for structural and functional studies of MPs in close to native environments.

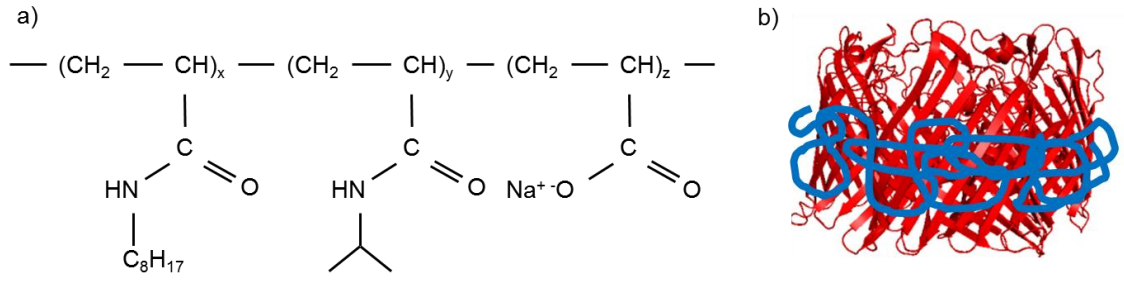

Figure 5.1 Structure of amphipol (A8-35). a) Chemical structure of amphipol (A8-35), a polyacrylate backbone with carboxyl group (z) randomly grafted with octylamine (x), isopropylamine (y) in the ratio x:y:z = 40:25:35. Each polymer contains on average thirty five monomers and weighs ≈ 8 kDa b) Model of OmpF (red) (PDB code: 2OMF) in complex with APol (blue).

J. L. Popot and colleagues invented a new class of detergents which are based upon an amphiphatic polymer called 'Amphipol' (APol) (Tribet *et al.*, 1996). APol comprises a hydrophilic backbone randomly derivatized with hydrophobic groups, octylamine and isopropylamine, as shown in Figure 5.1a. APol makes multiple contacts to a MP hence the affinity of MP for APol is high. Figure 5.1b displays how APols are thought to wrap around OmpF after reconstitution

OmpF into APol. In contrast to conventional detergents, APol is able to solubilise MP in the near absence of free APol (Tribet *et al.*, 1997; J. L. Popot *et al.*, 2003). The structural studies of MP in complex with APol were carried out using several biophysical techniques such as electron microscopy (EM) (Tribet *et al.*, 1998; Flötenmeyer *et al.*, 2007; Gohon *et al.*, 2008; Althoff *et al.*, 2011; Cvetkov *et al.*, 2011; Cao *et al.*, 2013; Liao *et al.*, 2013; Lu *et al.*, 2014), small-angle neutron scattering (SANS)(Gohon *et al.*, 2008), and nuclear magnetic resonance (NMR) (Zoonens *et al.*, 2005; Catoire *et al.*, 2010). Pure APol in solution has recently been studied by neutron scattering (Tehei *et al.*, 2014).

S. G. Sligar and colleagues have developed nanodiscs which are soluble nanoscale phospholipid bilayers surrounded by stabilising proteins (Bayburt *et al.*, 2002). The proteins, called Membrane Scaffold Protein (MSP), are derived from human high-density lipoprotein apoA-I with some modifications (deleting some undesired domains and inserting a polyhistidine tag). MSP consists of amphiphatic α-helices that can wrap around a phospholipid bilayer disc to assemble a disk structure shown in Figure 5.2. The structural studies of several MPs incorporated into nanodiscs were performed using EM (Raschle *et al.*, 2009; Katayama *et al.*, 2010; Frauenfeld *et al.*, 2011), NMR (Raschle *et al.*, 2009; Hagn *et al.*, 2013) and small-angle scattering (SAXS and SANS) (Kynde *et al.*, 2014).

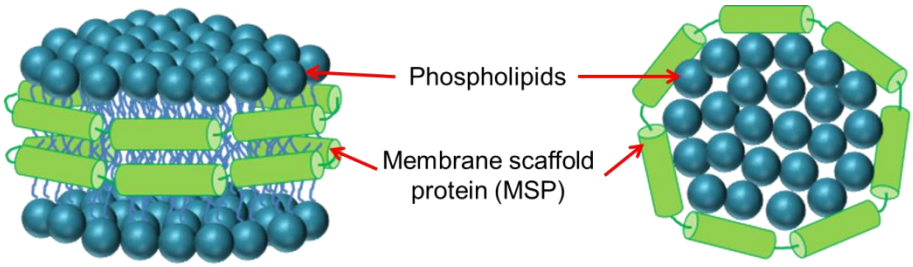

Figure 5.2 Schematic representation of nanodisc structure. A fragment of phospholipid bilayer is surrounded by two molecules of Membrane scaffold protein (MSP; green) as belts.

Here we utilised these alternative platforms to study the structure of OmpF with the aim to ultimately study the interaction of colicin N with OmpF in a native

condition. The OmpF/ColN complexes have previously only been studied in the presence of detergents or lipid monolayers (Clifton *et al.*, 2012). The structures of OmpF reconstituted into APol and nanodiscs were investigated using biophysical techniques such as electron microscopy, small-angle scattering, dynamic light scattering and analytical centrifugation.

5.2 Results

5.2.1 Incorporation of OmpF into Amphipols A8-35

Self-association of OmpF/APol complexes as filaments in the absence of free APol

Amphipol A8-35, commercially available from Anatrace, is widely used to stabilise MPs in aqueous solution. Prior to performing the structural studies, the optimum ratio of OmpF/APol must be determined. OmpF solubilised in octyl-POE was mixed with different OmpF/APol weight ratios (1:1, 1:5 and 1:10). After the removal of detergents by polystyrene beads, the size and dispersity of samples were analysed by size exclusion chromatography (SEC) using Superose 12 previously equilibrated with detergent-free buffer. The elution profiles in Figure 5.3c indicated that the OmpF/APol complexes exiting the column were virtually monodisperse with a very small amount of aggregate. Therefore, OmpF/APol complexes at a 1:10 w/w OmpF/APol ratio (approximately 1:100 molar ratio) is the best condition to solubilise OmpF in the absence of detergents because most of the OmpF samples from 1:1 and 1:5 ratio eluted out at the void volume (V_o = 6 mL) (Figure 5.3a and b). The void volume of the column was determined by running a sample of blue dextran at 2 mg/ml in water (data not shown). When comparing the SEC profile of OmpF/APol complexes to octyl POE-solubilised in OmpF (Figure 5.4a), OmpF/APol complexes are slightly larger (eluted at 9.1 ml) than OmpF in octyl POE (9.8 ml). The elution profiles of APol (Figure 5.3d) showed that APol eluted out at 12 ml hence the final concentration of APol is unknown as a result of the removal of free APol by SEC.

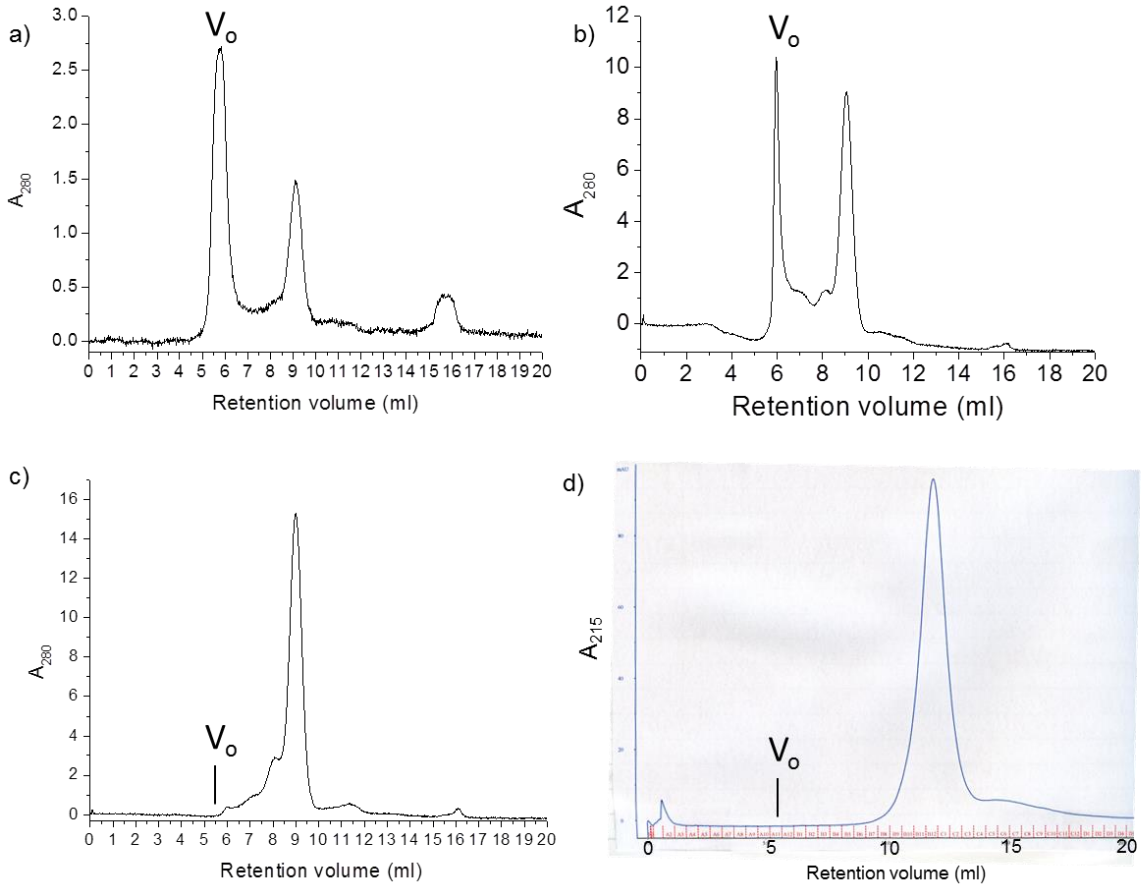

Figure 5.3 Elution profiles of OmpF/APol complexes formed at different OmpF/APol w/w ratios and amphipols A8-35. a) 1:1, b) 1:5, c) 1:10 and d) amphipols. SEC was carried out at a flow rate of 0.5 ml/min using a Superose 12 column equilibrated with 20 mM sodium phosphate, pH 7.9, 100 mM NaCl. V_o stands for the void volume of column where aggregated proteins elute out.

The structure of OmpF/APol complexes taken from the main peak was then investigated using transmission electron microscopy (TEM) with negative stain. According to the crystal structure of OmpF in Figure 5.4b (Cowan *et al.*, 1992), the diameter and height of OmpF are about 10 nm and 6 nm, respectively. Due to the fact that SEC profile of complexes showed only one major peak, the negatively stained TEM images of OmpF/APol complexes were expected to reveal evenly dispersed single particles on the carbon film. OmpF/APol complexes, observed one day after the SEC, formed filaments as illustrated in the TEM image in Figure 5.4c. The filament has a width of ~6 nm which corresponds to the height of OmpF trimer but the length of filament is variable.

The disagreement between SEC and TEM data suggested that the self-association of OmpF/APol complexes took place after performing SEC.

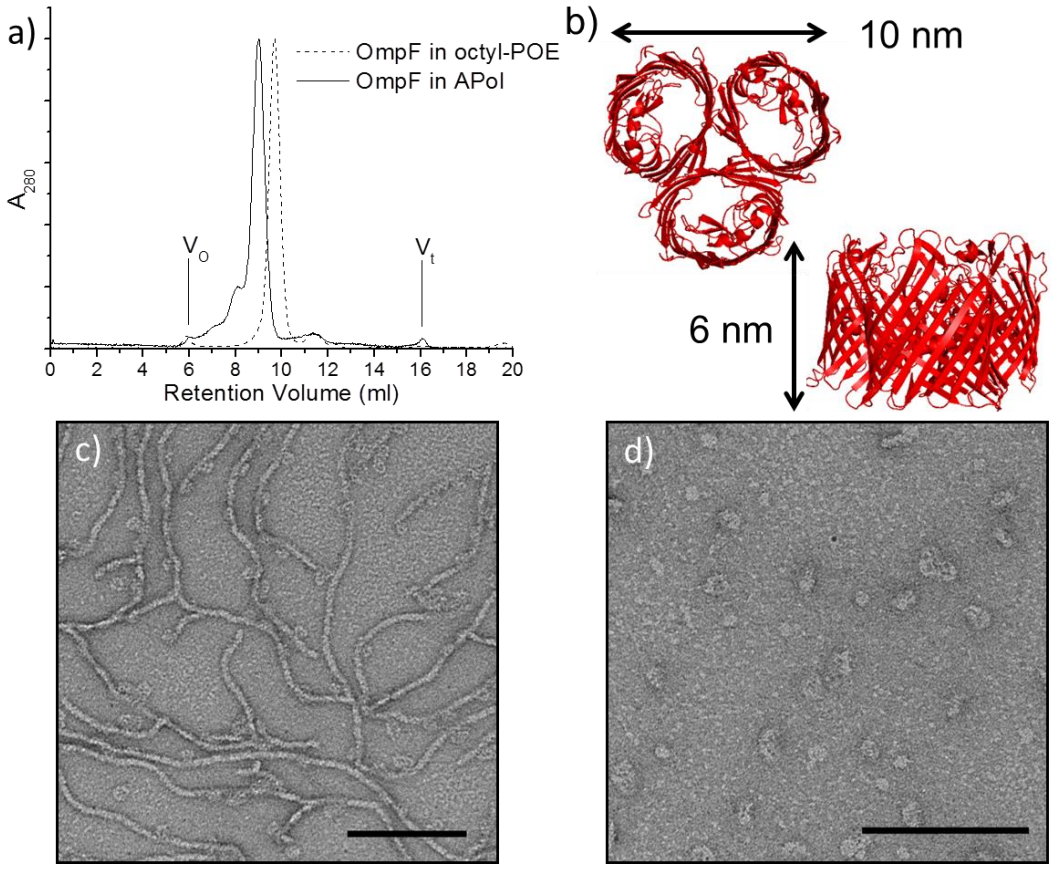

Figure 5.4 Removal of free APol by SEC led to the self-organisation of OmpF/APol complexes as filaments. a) The comparison of size and dispersity between OmpF prepared in APol 1:10 OmpF/APol mass ratio (solid line) and OmpF in 0.5% (v/v) Octyl POE (dash line). OmpF/APol complexes were injected onto Superose 12 column equilibrated with detergent-free buffer while buffer containing octyl-POE was used for OmpF/octyl-POE samples. Profiles have been normalised to the same maximum. b) Top and side view of crystal structure of OmpF trimer (PDB code: 2OMF). The diameter and height of OmpF are about 10 nm and 6 nm, respectively. Electron micrographs of negatively stained OmpF/APol complexes c) OmpF/APol filaments formed one day after removal of free APol by SEC. d) The same batch of complexes after supplementing with free APol at 1:5 OmpF/APol mass ratio. Addition of free APol resulted in dissociation of the filaments. Scale bars = 100 nm (Taken from (Arunmanee *et al.*, 2014))

The long filament structure of bacteriorhodopsin/APol complexes has been previously reported by Gohon *et al* (Gohon *et al.*, 2008). They reasoned that some MP tend to associate as filaments due to the lack of free APol in the samples. Therefore, free APol at a 1:5 OmpF/APol mass ratio was added back to the same SEC treated sample batch and analysed again by TEM. The electron micrograph in Figure 5.4b showed that the filaments with added free APol at a 1:5 OmpF/APol mass ratio disintegrated into individual particles on the carbon film. Thus free APol is essential for the stability of OmpF/APol complexes in solution and removing free APol triggers the self-association of OmpF/APol complexes.

Maturation of OmpF/APol filaments

In the previous experiment, TEM specimens were prepared one day after the removal of free APol by SEC. Therefore, it was unknown how fast the association process of MP/APol complexes in the depletion of free APol is. The bacteriorhodopsin/APol filaments observed by Gohon *et al* appeared after a 6-month storage (Gohon *et al.*, 2008). The rate of self-association was studied by dynamic light scattering (DLS). The size distribution of OmpF/APol samples directly after SEC was monitored at 30^{o}C as a function of time (Figure 5.5a). The size distributions were analysed by intensity as this mode is more sensitive to large particles in the samples. It is evident that the number of single OmpF/APol particles (~10 nm) decreased over time whereas that of large particles (> 10 nm) increased. The formation of large-scale structure can be noticed at 15 min after SEC hence the kinetics of OmpF/APol filament formation are very rapid.

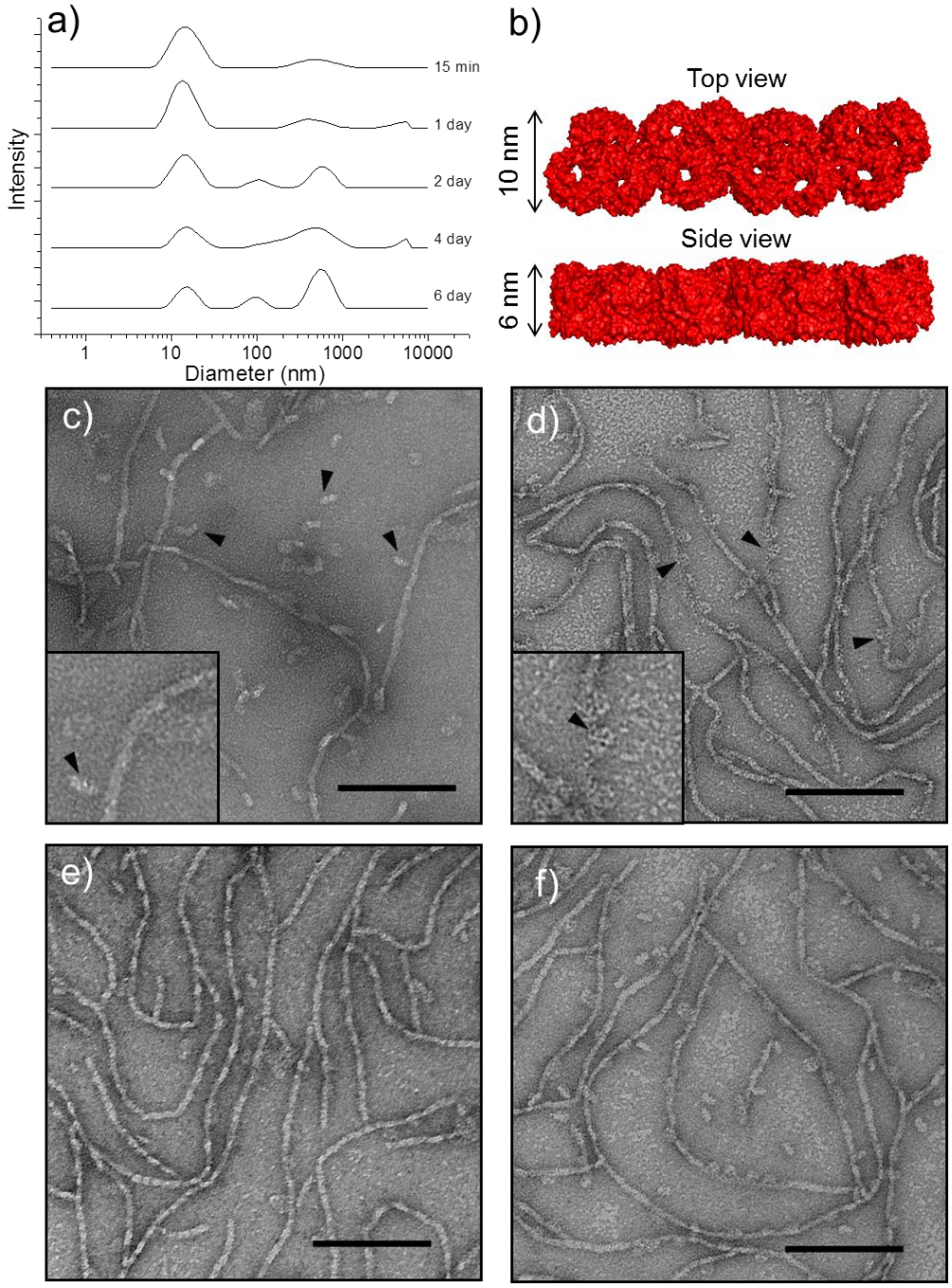

Figure 5.5 Progression of filament formation by OmpF/Apol complexes after depletion of free APol by SEC. a) Size distribution of OmpF/APol complexes by intensity measured at 30^{o}C by dynamic light scattering from 15 min to 6 days after SEC. b) Structural Models of possible OmpF filaments showing “top” and “side” views. Electron microscopy of OmpF/APol studied at different times after SEC. c) after 10 min. Single particles of OmpF trimer (arrowheads) were present. d) after 10 min at different area of the grid. OmpF pores (arrowheads) can be seen on filaments. e) after 1 day. f) after 1 week. Scale bars = 100 nm. The insets in c) and d) were zoomed in 2x higher magnification. (Taken from (Arunmanee *et al.*, 2014))

The results from DLS analysis are in good agreement with EM data. The freshly-prepared, one-day old and one-week old OmpF/APol samples were visualised under an electron microscope. The TEM images of the freshly prepared samples in Figure 5.5 (c and d) look different from those of one-day old and one-week old samples in Figure 5.5 (d and f). The individual particles and filaments of freshly-prepared complexes (arrowheads) were observed. In contrast to the freshly prepared samples, the one-day and one-week old ones contained most filaments with the width of 6 nm. The consistency of filament width indicates that OmpF/APol complexes preferentially absorbed on the carbon film by their side (Figure 5.5b). The filaments in the pre-mature state also show the top view of OmpF/APol particles as the stain-filled pores (arrowheads in Figure 5.5d). Consequently, OmpF/APol complexes in the absence of free APol has a tendency to form filaments confirmed by DLS and TEM and the formation of filaments is very fast.

Uncovering the solution structure of OmpF/APol complexes by SANS

Prior to investigating the structure of OmpF/APol filaments, the solution structure of free APol was carried out using SANS. APol at 10 mg/ml was solubilised in water and then dialysed into 100% D_2O buffer. APol was studied in 100% D_2O buffer as D_2O buffer has low incoherent scattering (low noise) and is far from the CMP of APol. The scattering curve of APol was recorded at SANS2D beamline, ISIS, UK. The initial data analysis by GNOM showed that P(r) distribution function gave a R_g of 16.58 Å and a D_{max} of 47.5 Å (Figure 5.6c). The data were then analysed by FISH modelling suite (Heenan)(in collaboration with Dr Richard Heenan). FISH fits the experimental data with geometric models with a few parameters. These parameters can be changed interactively by users. Here, an oblate ellipsoid, a prolate ellipsoid and a Gaussian coil were the models used to fit free APol. The scattering data and fitting by FISH is illustrated in Figure 5.6a. Oblate ellipsoid with radii, 11, 24.5 and 24.5 Å (Figure 5.6b) fits the experimental data better than the other two models. One particle of APol consists of ~1.3 molecules of 8 kDa APol which allow us to assume 1 molecule per particle.

The structure of OmpF/APol was then studied by SANS using the contrast variation technique as previously described in Chapter 3. Deuteurated OmpF (dOmpF) and hydrogenated APol (hAPol) were used in this experiment. The contrast match point (CMP) of dOmpF has already been determined in the previous experiment and the CMP of APol has been reported by Gohon *et al* (Gohon *et al.*, 2004). The OmpF/APol complexes at a 1:10 OmpF/APol weight ratio were prepared and passed through a size exclusion column using detergent-free buffer. After removing free APol by SEC, the OmpF/APol complexes started assembling as filaments. The protein-containing fractions were collected and then dialysed into APol and detergent-free buffer (20 mM sodium phosphate, pH 7.9, 100 mM NaCl) with 0%, 23.5%, 77% and 100% D_2O. The whole complex is visible to neutrons in 0% and 100% D_2O buffer, only dOmpF is visible in a 23.5% D_2O buffer where APol is matched and only APol is observed at the CMP of OmpF in a 77% D_2O buffer. The final concentration of OmpF in all samples is 2.02 mg/ml however that of APol is unknown (The initial concentration of APol is 20 mg/ml). The scattering data were recorded at beamline SANS2D, ISIS, UK and analysed using FISH programme.

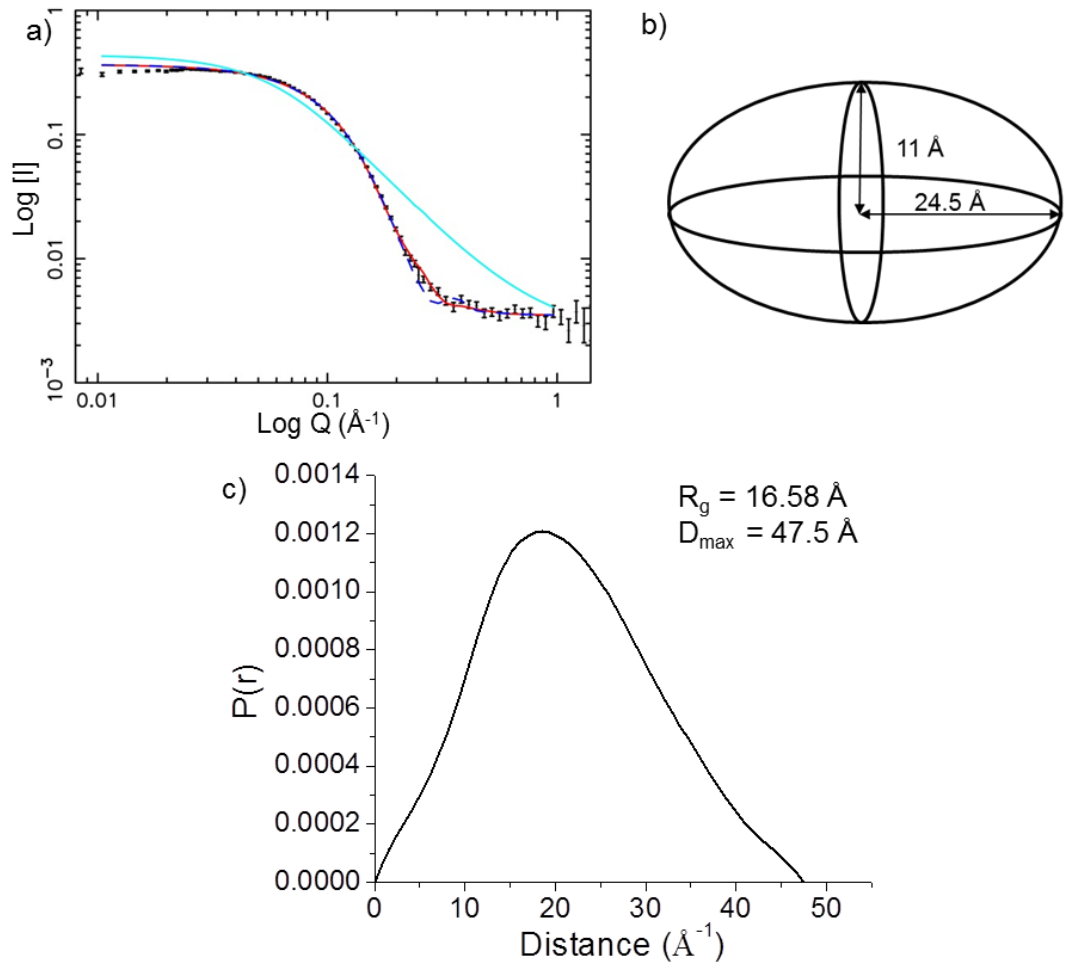

Figure 5.6 SANS data for free hAPol. a) SANS data (symbols) and fitting (lines) by FISH. (red: oblate ellipsoid, blue: prolate ellipsoid and cyan: Gaussian coil) b) the best model of free hAPol. c) P(r) distribution function of free hAPol calculated by GNOM. APol at 10 mg/ml was in 20 mM sodium phosphate, pH 7.9, 100 mM NaCl.

Figure 5.7a shows the scattering curve and fitting of OmpF/APol complexes in 23.5% D_2O where only dOmpF is visible to neutrons. A disk model (Figure 5.7b) was chosen to represent dOmpF. The blue line from a disk with the height of 40 Å fit the experimental data better than the red one from a disk with the height of 60 Å. Although the radius of disk at 38 or 49 Å is ambiguous, the fitting of this simple model to dOmpF is still acceptable. This model also fits to SANS data from d-OmpF in SDS obtained from samples with d/h-SDS matched to the solvent (Data not shown).

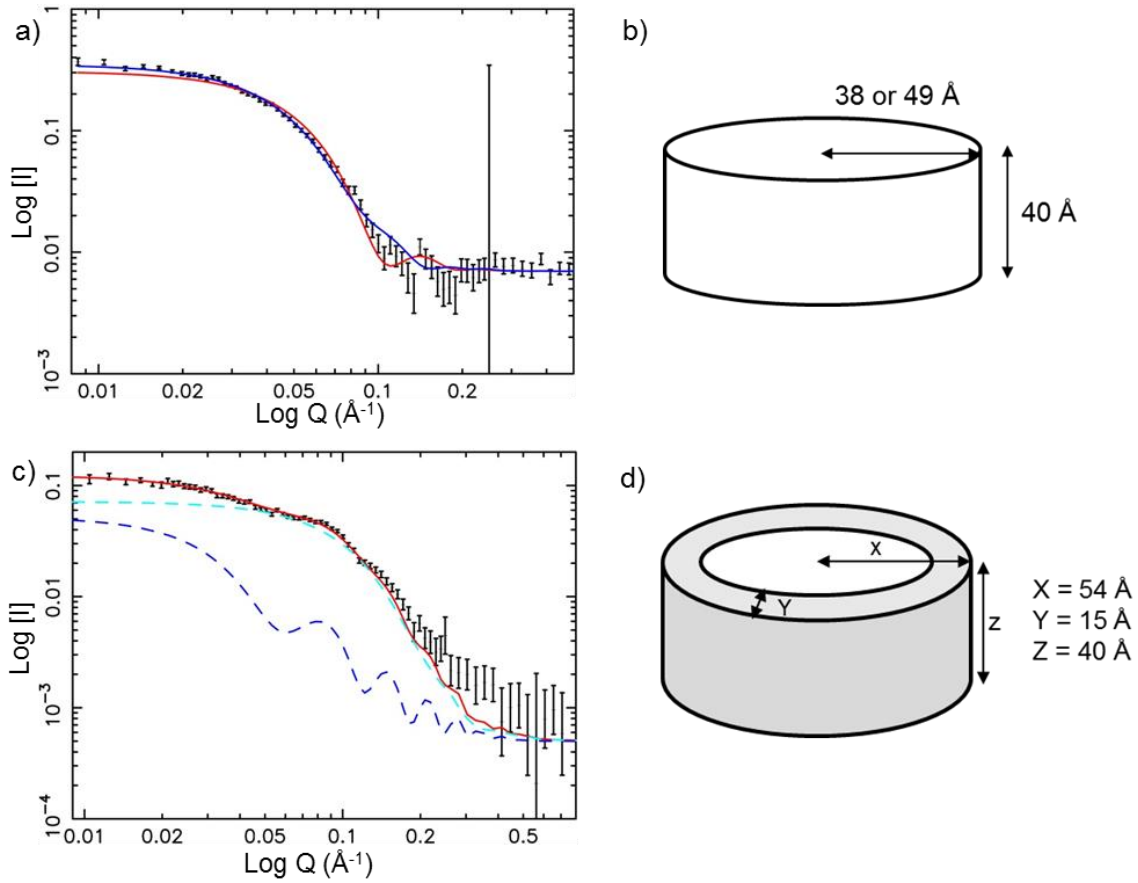

Figure 5.7 SANS data for each component of OmpF/APol complexes after removing free APol by SEC. The scattering data (symbols) and fitting (lines) using the program FISH of a) the sample in 23.5% D_2O where APol is matched. The models are disks with the height of 60 Å (red) and 40 Å (blue) and c) the sample in 77% D_2O where dOmpF is invisible to neutrons. The models are the sum (red lines) of hollow tube (blue dash lines) for complexes and oblate ellipsoids for free APol (cyan dash lines). The best models of OmpF/APol complexes used to fit the experimental data by FISH b) a disk for 23.5% D_2O data and d) a hollow tube for 77% D_2O data.

Next, the structure of APol in complex with OmpF was studied at 77% D_2O where dOmpF is invisible to neutrons. The red fit in Figure 5.7c is a sum of a hollow tube (blue dash line) and oblate ellipsoids (cyan dash line). The hollow tube with outer radius 54 Å, wall thickness 15 Å and height 40 Å (Figure 5.7d) stands for dOmpF whereas oblate ellipsoids represents remaining free APol particles. According to the model, the hollow tube alone does not fit the experimental data thus oblate ellipsoids model must be included in the fitting. This is an indication that free APol is present in the samples. As the free APol

was previously already removed by SEC in the sample preparation, the remaining free APol in the samples must dissociate from the complexes. The SANS method does allow us to estimate that the amount of excess APol present is approximately 4 mg/ml in the 77% D_2O sample. However, there is no sign of the filamentous structure which should appear as the upturn at the low Q range of the scattering data.

When the individual components were determined by SANS, both of them were combined into the whole complex. Therefore, the core/shell tube is used to represent the dOmpF/APol complexes. dOmpF is the core whereas APol is the shell surrounding dOmpF. The scattering data of OmpF/APol in 0% D_2O (Figure 5.8a) was fitted with the core/shell tube but the free APol was not required. The best fit is derived from the model with shell width 15 Å (fixed), outer radius 60 Å and height 40 Å (Figure 5.8b). Excess APol is present up to approximately 0 to 1.5 mg/ml in the 0% D_2O sample.

However, oblate ellipsoids for free APol must be included in the fit for the complexes in 100% D_2O. Figure 5.8c shows the scattering data of complexes in 100% D_2O. The fit is a combination of core/shell tube (blue dash line) and oblate ellipsoids (cyan line) representing OmpF/APol complexes and free APol, respectively. In this case, 5 mg/ml of excess APol is present in the samples and 1.4 mg/ml of APol wrapped 2 mg/ml of dOmpF. The core/shell tube (Figure 5.8d) fitted this 100% D_2O data has shell width of 15 Å, outer radius of 55 Å and height of 40 Å.

The scattering curve of 100% D_2O is the only curve that shows the upturn at small Q region. This is reminiscent of a long-range structure or filament. All in all, the findings from SANS study of OmpF/APol complexes indicated that the complexes were made of OmpF wrapped by APol but the filament structure was only seen in 100% D_2O samples. Moreover, excess APol was found in the samples even though it should have been removed by SEC in the sample preparation. Thus it is likely that only OmpF/Apol complexes elute from the column and then undergo a reequilibration with free Amphipol. The loss of

Amphipol from the individual complexes is compensated by the formation of the filaments where protein-protein interactions may take the place of protein-amphipol. The lack of accurately repetitive structures in the filaments may explain the lack of filament signal in the SANS data.

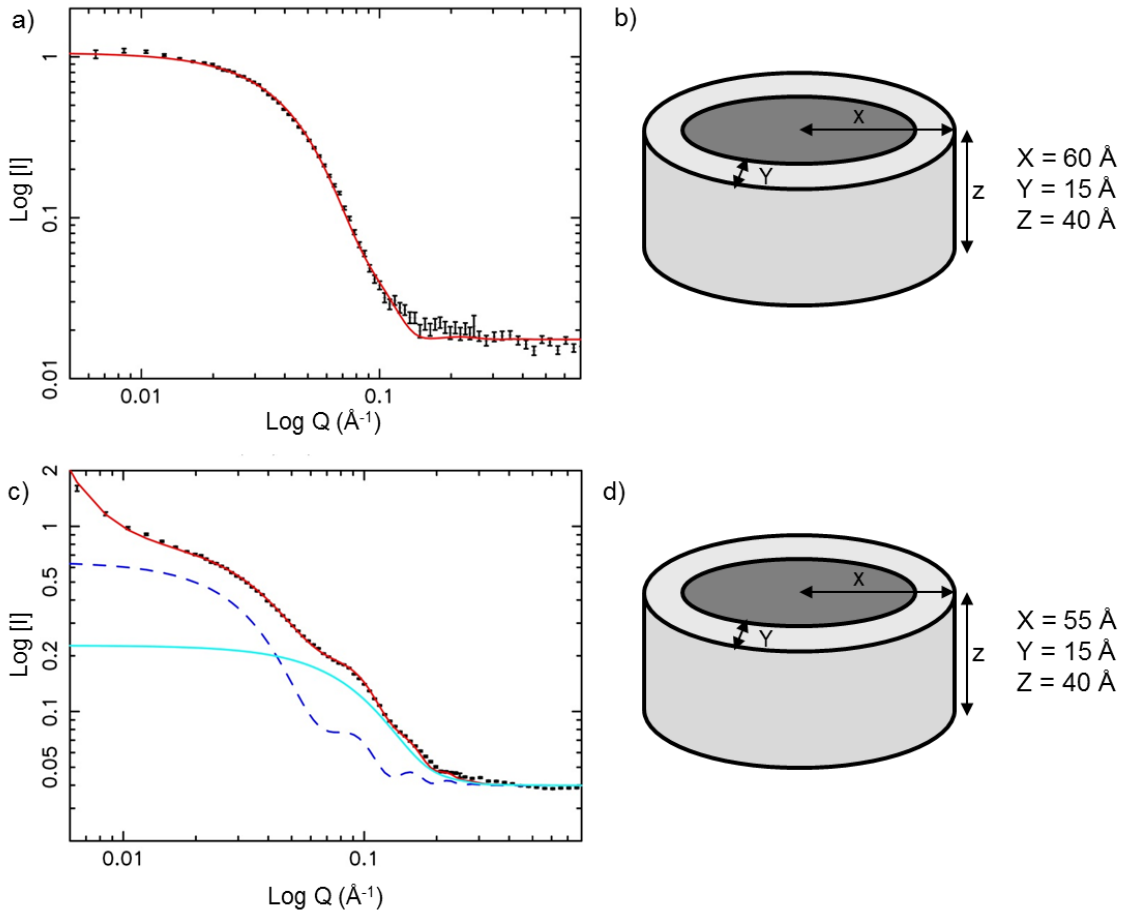

Figure 5.8 SANS data for the whole OmpF/APol complexes after removing free APol by SEC. The scattering data (symbols) and fitting (lines) using the program FISH of a) the sample in 0% D_2O. The model is core/shell tube c) the sample in 100% D_2O. The models are the sum (red line) of core/shell tube (blue dash line) for complexes and oblate ellipsoids for free APol (cyan line). The best models of OmpF/APol complexes used to fit the experimental data by FISH b) 23.5% D_2O data and d) 77% D_2O data.

The effect of LPS on the formation of OmpF/APol filaments

The study on OmpF-LPS interaction in Chapter 4 demonstrated that OmpF-LPS is able to form a large-scale structure in the presence of divalent cations. LPS-LPS molecules link to each other using these cations as a bridge (Schneck *et al.*, 2010). Previously, OmpF/APol complexes were prepared from WT OmpF co-purifying with tightly-bound LPS from the outer membrane (which appear as a ladder on SDS-PAGE in Figure 5.9b). The LPS-LPS interaction could possibly affect the formation of OmpF-APol filaments in the depletion of APol. To clearly investigate the effect of LPS on the lateral association of OmpF, the LPS-free OmpF produced by refolding OmpF from denatured inclusion bodies is used in this study. Three samples of OmpF/APol complexes were prepared 1) LPS-Free OmpF/APol, 2) OmpF+LPS/APol, and 3) OmpF+LPS/APol/EDTA. Ra-LPS was added to OmpF at a 1:5 OmpF/LPS molar ratio prior to incubation with APol. Ra-LPS, lacking O-antigen, is the longest-defined LPS available. The addition of 1 mM EDTA was used to remove divalent cations from the sample and prevent LPS-LPS interaction.

All samples were then studied by SEC and TEM to monitor the size, dispersity and structure of complexes in these three different conditions. Figure 5.9a shows the elution profiles of OmpF/APol complexes obtained from SEC using Superose 12 column equilibrated with detergent-free buffer. As expected, LPS-Free OmpF/APol appeared to be homogenous with a small amount of aggregates. OmpF+LPS/APol aggregated in solution as most complexes eluted from the column at the void volume showing them to be already large aggregates. In contrast to those two samples, OmpF+LPS/APol/EDTA were obviously heterogeneous with various sizes of OmpF/APol particles but the amount of aggregates was significantly decreased.

When looking at these samples fractionated by SEC under the electron microscope using a negative staining technique, the electron micrographs of OmpF/APol complexes (Figure 5.9c, d and e) reveal that OmpF/APol complexes in all samples assemble as filaments. Although LPS-Free OmpF is

used for the formation of complex, the filaments were still observed on the carbon film in the absence of free APol. This confirmed that APol is definitely involved in the formation of filaments. However, the structure of filaments in the presence of LPS looked different. Figure 5.9c reveals that LPS-LPS interaction in the presence of divalent cations disrupted the linear interaction of OmpF/APol. Instead of forming filaments, OmpF+LPS/APol assembled as sheet-like structure which is an indication of 2D interaction. When removing divalent cations by EDTA (Figure 5.9e), a mixture of filamentous and sheet-like structure were observed.

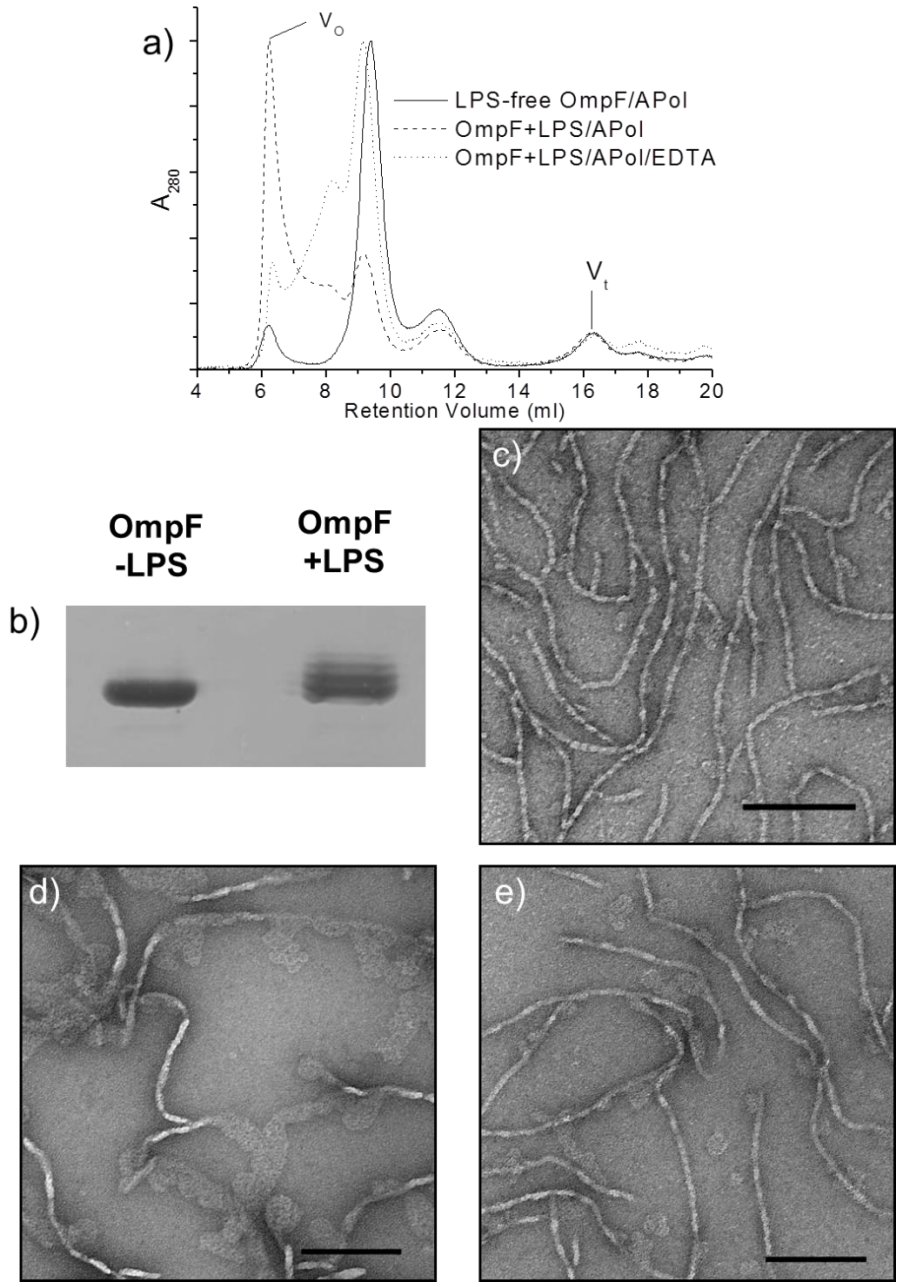

Figure 5.9 Effect of Lipopolysaccharides on the structure of OmpF/APol complexes without free Apol. a) SEC analysis of size and homogeneity of OmpF/APol complexes in various conditions. Solid line, LPS-free OmpF; Dashed line, OmpF+LPS ; Dotted line, OmpF+LPS in 1 mM EDTA. In each case the column was pre-equilibrated with detergent-free buffer. Profiles have been normalised to the same maximum. b) SDS-PAGE analysis of LPS-free OmpF vs. OmpF with added LPS showing characteristic ladder of OmpF bands resulting from LPS binding. The number of additional bands represents the increasing number of LPS attached to OmpF. EM study of OmpF/APol complexes in the presence and absence of LPS. c) LPS-Free OmpF/Apol. d) OmpF+LPS/APol. e) OmpF+LPS/Apol/EDTA. Scale bars = 100 nm. (Taken from (Arunmanee *et al.*, 2014))

Study of the interaction of colicin N with OmpF/APol filaments

WT ColN was added to OmpF/APol complexes to observe the effect of ColN on the self-association of OmpF/APol complexes. The OmpF/APol complexes were formed before adding ColN to the mixture at 3:1 and 1:1 OmpF/ColN molar ratio (one and three ColN per OmpF trimer). The samples were analysed by SEC using detergent-free buffer as the elution buffer. The SEC profiles of both samples show the heterogeneity of complexes (Figure 5.10a and b). Two distinct species of particle are present in the sample.

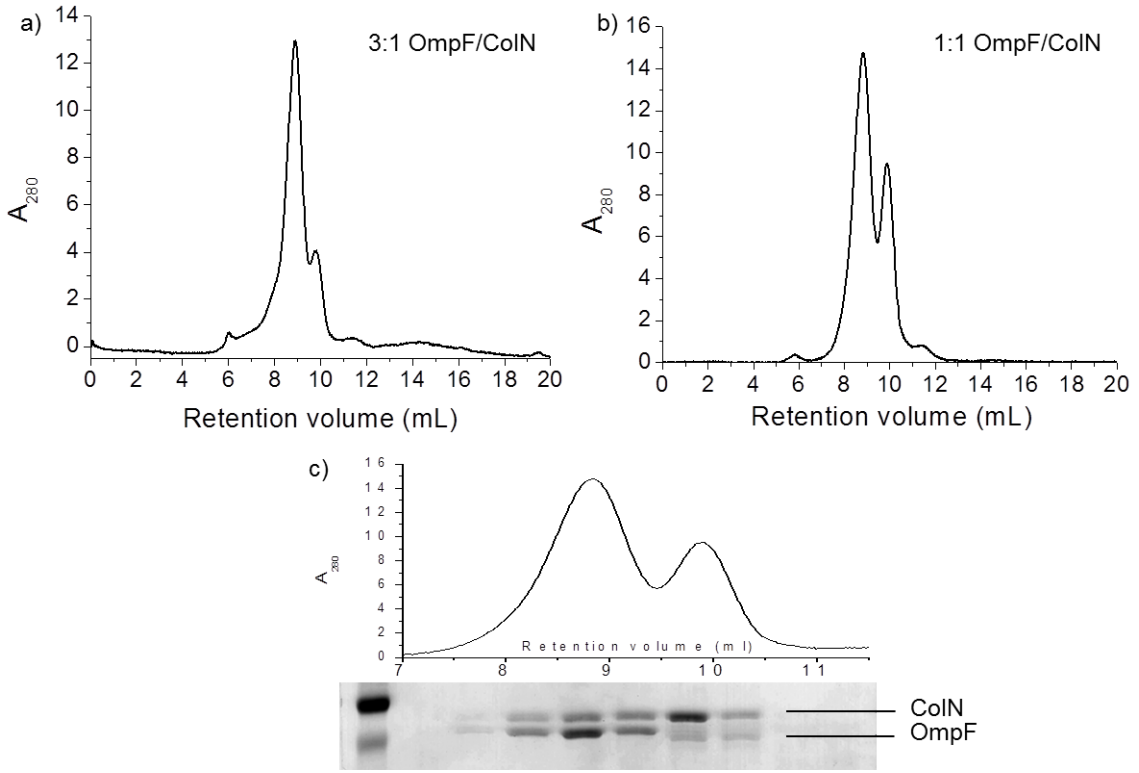

Figure 5.10 SEC profiles of OmpF/ColN/APol complexes at various OmpF/ColN molar ratios. a) 3:1 b) 1:1 c) SDS-PAGE analysis of protein-containing fractions from the fractionation of OmpF/ColN/APol complexes at 3:1 OmpF/ColN molar ratio.

The fractions from SEC were evaluated on SDS-PAGE (Figure 5.10c). The SDS-PAGE analysis indicated that excess WT ColN exiting after OmpF/APol complexes remained in the samples. This suggested that ColN does not bind to OmpF/APol complexes despite adding only one ColN per OmpF trimer. This

result agreed with the EM study in negative stain on OmpF/ColN/APol complexes. The TEM images of OmpF/ColN/APol complexes were recorded before and after removing free APol by SEC. Figure 5.11a shows the structure of OmpF/APol/ColN complexes in the presence of free APol. The complexes were polydisperse with various sizes of particles. On the other hand, the complexes in the absence of free APol (Figure 5.11b) appeared to be a combination of filamentous structure and individual particles. This means the OmpF/APol filament still exists despite adding ColN to disrupt the linear interaction of OmpF/APol.

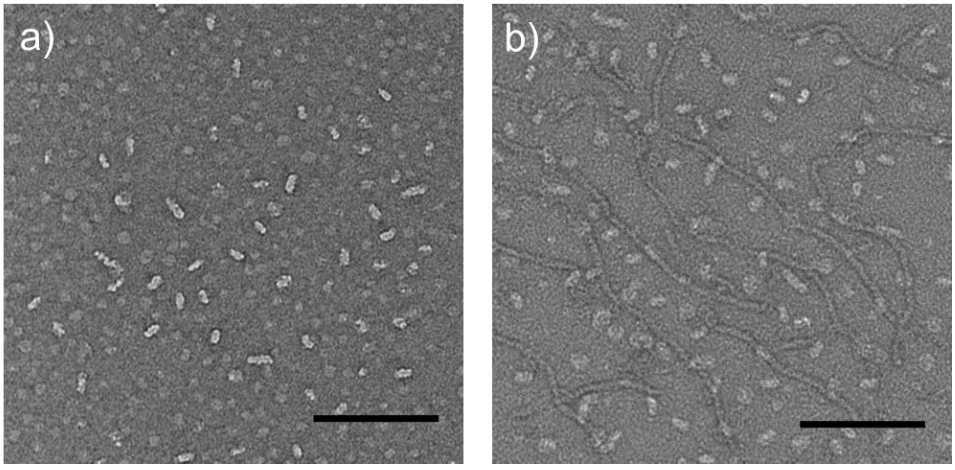

Figure 5.11 EM study of OmpF/ColN/APol complexes at 3:1 OmpF/ColN molar ratio. a) with free APol b) without free APol. The samples were prepared a day before the EM study. Scale bars = 100 nm.

5.2.2 Analysis of OmpF inserted into model membranes, nanodiscs

Expression and purification of membrane scaffold proteins

Membrane scaffold protein (MSP) whose structure is a group of amphipathic α-helices is the key component of making the model nanodiscs. S. G. Sligar and his colleagues have introduced a library of MSP constructs of varying lengths (Denisov *et al.*, 2004). The size of nanodisc is precisely controlled by the length of MSP. In this study, MSP1E3D1 which gives nanodiscs 12.1 nm in diameter was used in the preparation of OmpF nanodiscs as the nanodiscs made from this MSP are large enough for OmpF insertion. MSP1E3D1 with N-terminal his-

tag were expressed using *E. coli* BL21(DE3) as a host. The expression was induced when adding IPTG at the final concentration of 1 mM for 3 h. The cell culture was collected before and after induction. The cell lysates were then evaluated on SDS-PAGE as shown in Figure 5.12a. It confirmed that MSP1E3D1 was successfully expressed as the bands at approximately 30 kDa appeared after induction by IPTG. The theoretical molecular weight of MSP1E3D1 was reported at 32.6 kDa (Ritchie *et al.*, 2009). The MSP1E3D1 were purified using Ni-NTA column. The fractions were collected and loaded on SDS-PAGE to test the protein purity (Figure 5.12b). MSP1E3D1 was relatively clean thus further purification was not required.

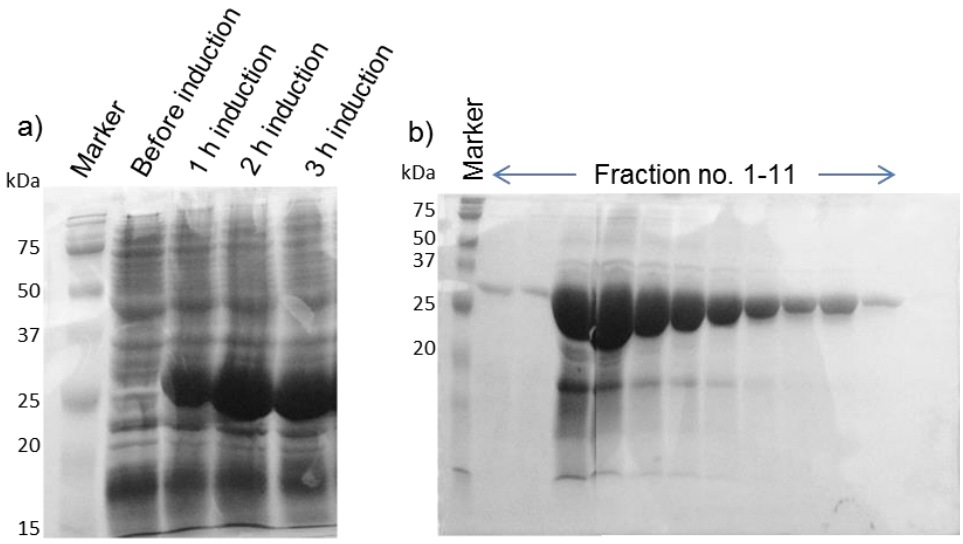

Figure 5.12 SDS-PAGE of MSP1E3D1 expression and purification. a) Cell lysates collected before and after induction by IPTG. The band of expressed MSP1E3D1 appeared at ~30 kDa. b) SDS-PAGE of protein-containing fractions taken from the Ni-NTA column.

A peptide mass fingerprint of proteins by MALDI-TOF MS was performed to identify the expressed MSP1E3D1. The sample in the form of gel slice was sent to Dr Joe Gray at Biological Mass Spectrometry unit (Pinnacle), Newcastle University. The trypsin digestion of proteins was done prior to MALDI-TOF-MS analysis. Figure 5.13 displays the peptide mass fingerprint of expressed MSP1E3D1. The peptide masses were compared with the Swissprot protein database in order to search for potential matches. The results showed that

apoA-I proteins which originated from humans came up with a statistically relevant match. Therefore, it proved that MSP1E3D1 was expressed in *E. coli* because MSP1E3D1 is a derivative of apoA-I protein (Bayburt *et al.*, 2002).

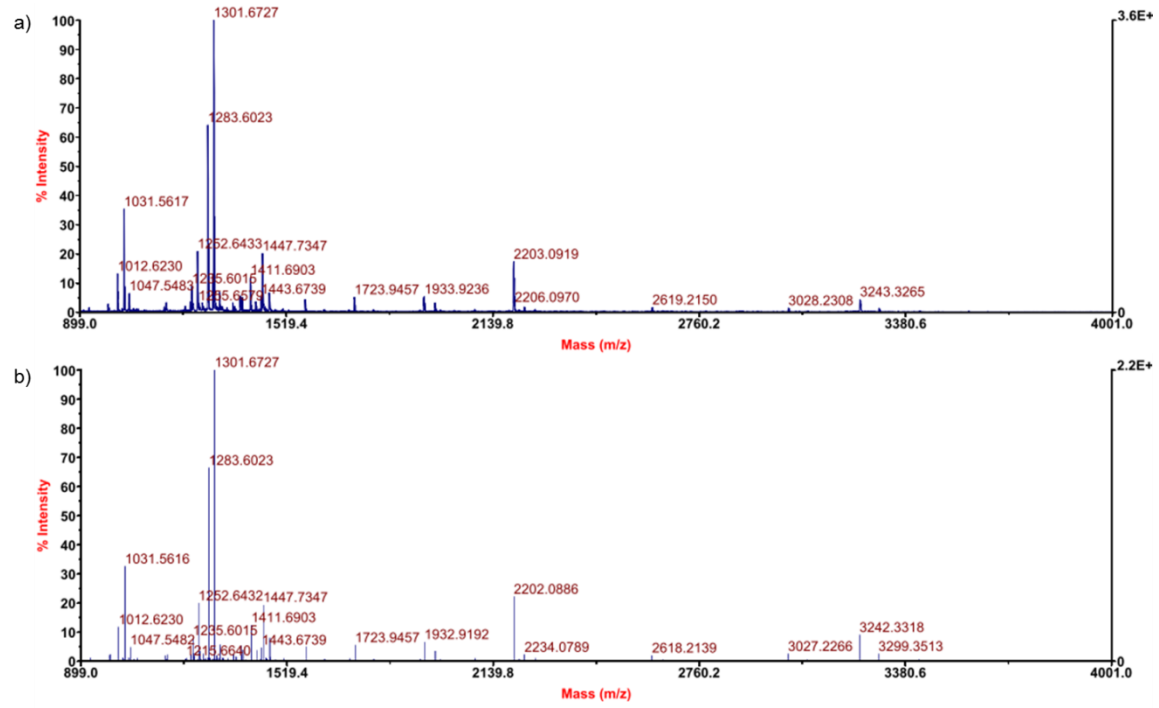

Figure 5.13 MALDI-TOF MS of trypsin digested MSP1E3D1. The expressed proteins were identified using a peptide mass fingerprint technique. a) raw data b) processed peak

The preparation of nanodiscs

Nanodiscs consist of three key components which are MSP, phospholipids and membrane proteins of interest (Bayburt *et al.*, 2002). MSP is added to a mixture of detergent-stabilised phospholipids and membrane protein in an appropriate molar ratio. Once detergents are removed by dialysis or incubation with polystyrene beads, nanodiscs assemble using 2 molecules of MSP1 (Nath *et al.*, 2007). Here, we searched for suitable phospholipids in order to assemble OmpF nanodiscs. OmpF was solubilised in octyl-POE and MSP1E3D1 was used as the molecular belt of the nanodisc. In the case of phospholipids, 1,2-dimyristoyl-sn-glycero-3-phosphocholine (DMPC) and 1,2-dimyristoyl-sn-glycero-3-phospho-(1'-rac-glycerol) (DMPG) were the options as the fatty acyl

chain length (C14) of these lipids matches the hydrophobic region of OmpF well (O'Keeffe *et al.*, 2000). The structures of DMPC and DMPG are similar except their head groups. The zwitterionic head group of DMPC has no overall charge whereas that of DMPG has a single negative charge.

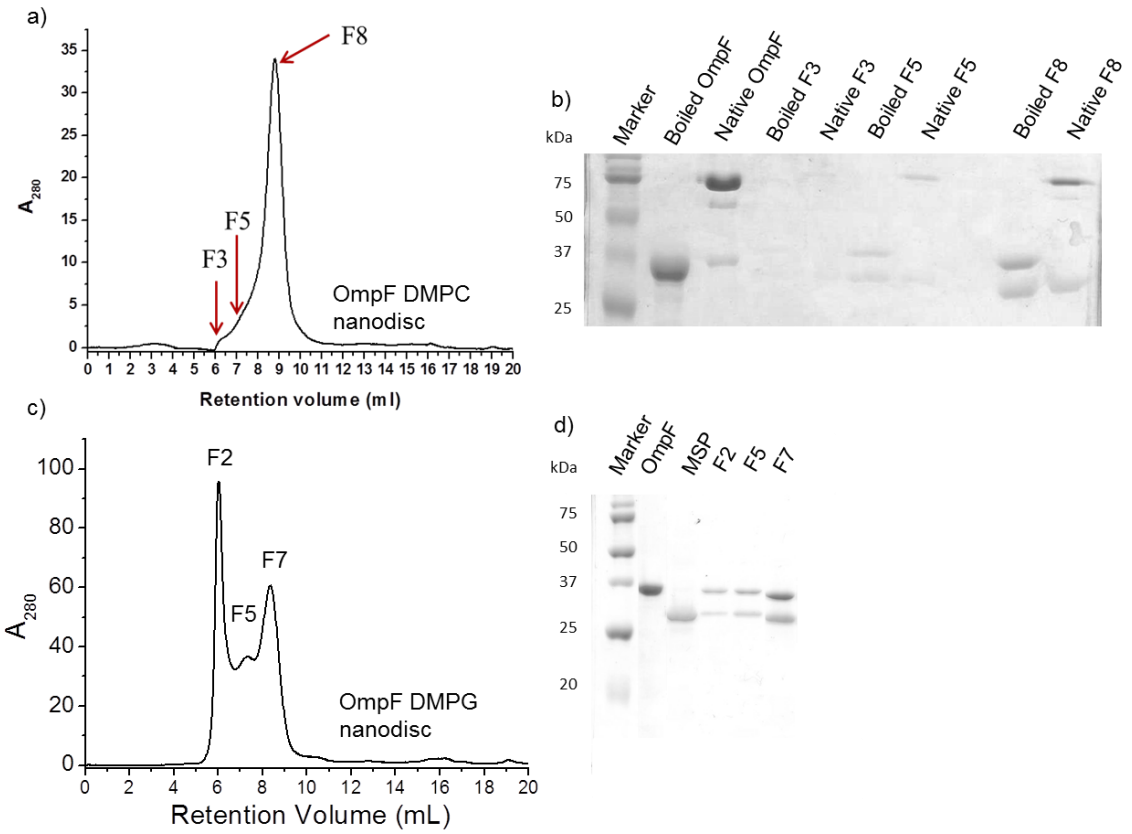

Figure 5.14 Analysis of OmpF-inserted nanodisc by gel filtration and SDS-PAGE. SEC profiles of OmpF incorporated into nanodisc using a) DMPC and c) DMPG. SEC was performed at a flow rate of 0.5 ml/min using a Superose 12 column equilibrated with 20 mM Tris-HCl pH 7.4, 0.1 M NaCl, 0.5 mM EDTA. The protein-containing fractions collected from SEC were tested on SDS-PAGE for OmpF in b) DMPC nanodiscs and d) DMPG nanodiscs (heat denatured samples).

The suitable molar ratio of making DMPC nanodisc has been reported at 1:140 MSP1E3D1:DMPC molar ratio hence we used the same ratio for DMPG (Bayburt *et al.*, 2002; Denisov *et al.*, 2004; Bayburt *et al.*, 2006). OmpF stabilised in octyl-POE was added to the mixture of MSP1E3D1 and lipids at 3:2 OmpF/MSP1E3D1 molar ratio. The mixture was incubated at 30^{o}C above the

phase transition temperature of DMPC and DMPG for 1 h. Detergents were removed by mixing with Bio-beads SM-2 for 3 h. The size and dispersity of OmpF nanodiscs were studied by SEC using detergent-free buffer. The elution profiles of OmpF in DMPC and DMPG nanodiscs are displayed in Figure 5.14a and c, respectively. OmpF in DMPC nanodiscs contained heterogeneous populations as there were some large particles exiting the column before the main peaks. OmpF in DMPG nanodiscs were also heterogeneous but most proteins came out at the void volume (fraction no. 2). The fractions of these two nanodiscs were evaluated by SDS-PAGE in order to test whether OmpF and MSP1E3D1 co-eluted out. Figure 5.14b shows the SDS-PAGE analysis of OmpF in DMPC nanodisc. All fractions contained both OmpF and MSP1E3D1 so this indicated that OmpF was incorporated into nanodiscs. Likewise, both OmpF and MSP1E3D1 were present in all fractions of OmpF in DMPG nanodiscs. (Figure 5.14d)

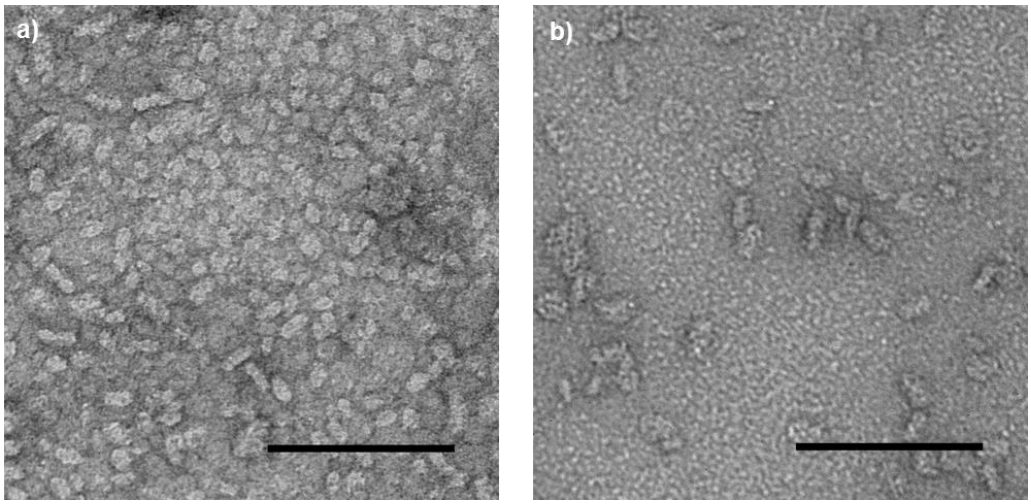

Figure 5.15 TEM images of OmpF-loaded nanodiscs. Nanodiscs made from a) DMPC (fraction no 8) and b) DMPG (fraction no 7). Scale bar = 100 nm.

The structures of OmpF nanodiscs were further investigated by EM with negative staining as previously described in Chapter 2. The negative-stained nanodiscs were loaded onto the carbon films. According to the electron micrograph of OmpF in DMPC nanodiscs in Figure 5.15a, the individual particles were scarcely observed due to the fact that nanodiscs associated to

formed large aggregates or nanodiscs were overloaded on the carbon film. However, in the case of OmpF in DMPG nanodiscs (Figure 5.15b), nanodiscs were evenly spread onto the carbon film. The size of nanodisc particle determined by JMicro Vision program is approximately 20 nm in diameter. Therefore, making OmpF nanodiscs from DMPG is better as the individual nanodiscs can be observed. This may be due to the repulsion between the negatively charged particles.

Examining the structure of OmpF reconstituted into nanodiscs

In order to understand OmpF-inserted nanodisc, the structure of OmpF nanodiscs in solution was examined using SEC, DLS, AUC and small-angle scattering in comparison with empty DMPG nanodiscs. Both nanodiscs were made from MSP1E3D1 and DMPG using the same ratio as previously explained in section 1.3.2. Once nanodiscs assembled after the removal of detergent, SEC was utilised to purify the nanodiscs. The elution profiles of empty and OmpF nanodiscs in Figure 5.16 (a and b) indicated that the size of OmpF nanodisc eluted at 8.2 ml was slightly larger than that of empty nanodiscs exiting the column at 8.5 ml. This is in good agreement with the DLS study. The samples of both types of nanodiscs were taken from the protein-containing fractions collected at the main peak. The nanodisc samples were previously assessed by SDS-PAGE to verify that each nanodisc sample consisted of OmpF and MSP1E3D1 (data not shown). The size distribution of empty nanodisc compared to OmpF nanodiscs in Figure 5.16 (c) also confirmed that the size of OmpF nanodisc is larger.

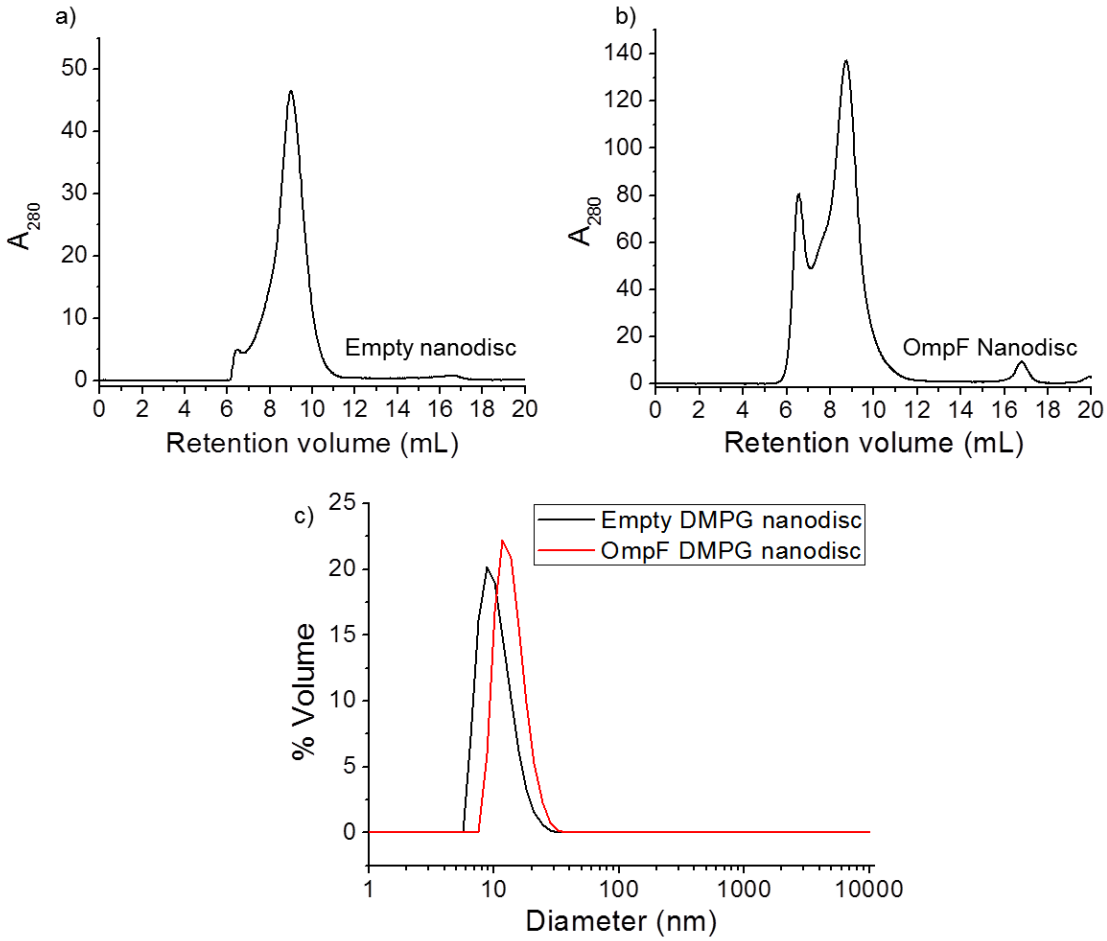

Figure 5.16 Analysis of nanodiscs by SEC and DLS. The elution profiles of a) DMPG nanodiscs compares to that of b) OmpF in DMPG nanodisc. c) The size distribution of empty and OmpF DMPG nanodiscs by volume observed by DLS.

Furthermore, the same nanodisc samples used in DLS experiment were investigated under electron microscope. The TEM images (in negative stain) of nanodiscs are shown in Figure 5.17. Both samples spread evenly on the carbon films even though most nanodiscs absorbed onto the carbon films by their side. OmpF moleclues were mostly embedded within nanodiscs therefore it is difficult to observe inserted OmpF by EM. The size of nanodiscs was determined using JMicro Vision software; OmpF nanodiscs with approximately 20 nm diameters are larger than empty nanodiscs which are approximately 14 nm in diameter. This suggested that MSP1E3D1 is flexible as it can extend to make a larger nanodisc if it encloses a large protein, in this case OmpF.

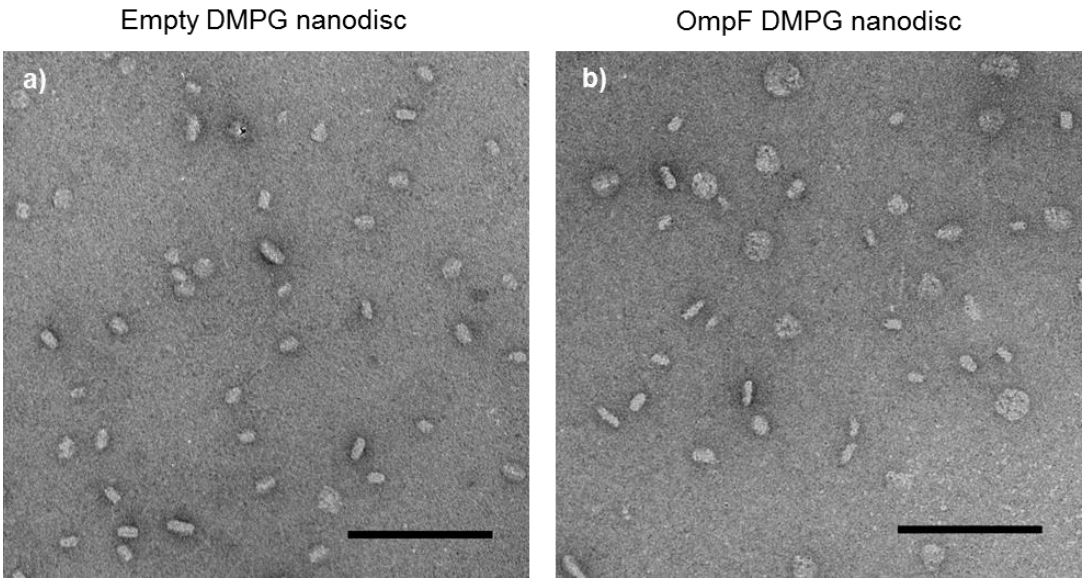

Figure 5.17 Study on empty and OmpF DMPG nanodiscs by EM. Scale bar = 100 nm.

In order to confirm that OmpF was successfully inserted into nanodiscs, the nanodisc samples were studied by AUC. Due to the fact that the density of lipid is less than that of protein, OmpF nanodiscs sediment much faster than empty nanodisc. This is because phospholipids in nanodisc were replaced by OmpF. Additionally, AUC provides the information about the size and dispersity of samples. The nanodisc samples, after fractionation by SEC, were sent to Dr A. Solovyova. The AUC experiment was performed at room temperature. The sedimentation velocity experiment (Figure 5.18) revealed that both types of nanodiscs were relatively homogenous with a small amount of large particles. There are some empty nanodiscs remaining in the OmpF nanodisc samples. As expected, the s value of empty nanodiscs is much lower when compared to OmpF nanodiscs. This result verified that OmpF has actually incorporated into the nanodiscs.

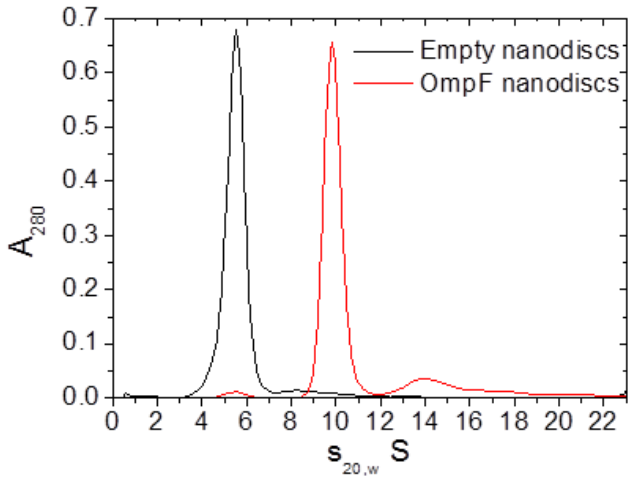

Figure 5.18 Sedimentation coefficient distribution c(s) of nanodiscs.

Recently, the research group of Lise Arleth in Copenhagen has developed a strategy to study the structure of membrane proteins in nanodiscs using small-angle scattering. (Kynde *et al.*, 2014) In brief, the freshly-prepared nanodiscs purified by SEC were studied by SAXS and SANS. The combined use of SAXS and SANS provides the scattering curves in two different contrast situations. The scattering data obtained by these two techniques is then fitted to a model represented by simple geometrical objects. Here, we characterised the structure of empty and OmpF nanodiscs by SAXS and SANS. The SAXS and SANS experiment were performed at beamline B21, Diamond, UK and beamline SANS2D, ISIS, UK. The samples were freshly prepared on site using the same approach as described before.

SAXS curves of empty DMPG nanodiscs (Figure 5.19a) were acquired at two different temperatures (4 and 25^{o}C) which are below and above the phase transition temperature of DMPG (21^{o}C). The pair-distribution function, P(r), calculated by indirect Fourier transform with GNOM (Figure 5.19b) showed a sign of disc structure with a minimum at 30 Å and yielded D_{max} and R_g as summarised in Table 5.1. The minimum at 30 Å is derived from the negative contrast of phospholipid tails. The R_g estimated by GNOM is consistent with Rg obtained from the Guinier approximation by PRIMUS (Figure 5.19c) (Svergun, 1992; Konarev *et al.*, 2003). The agreement of R_g value between two

approaches and the linear Guinier plots supported the lack of aggregation in samples.

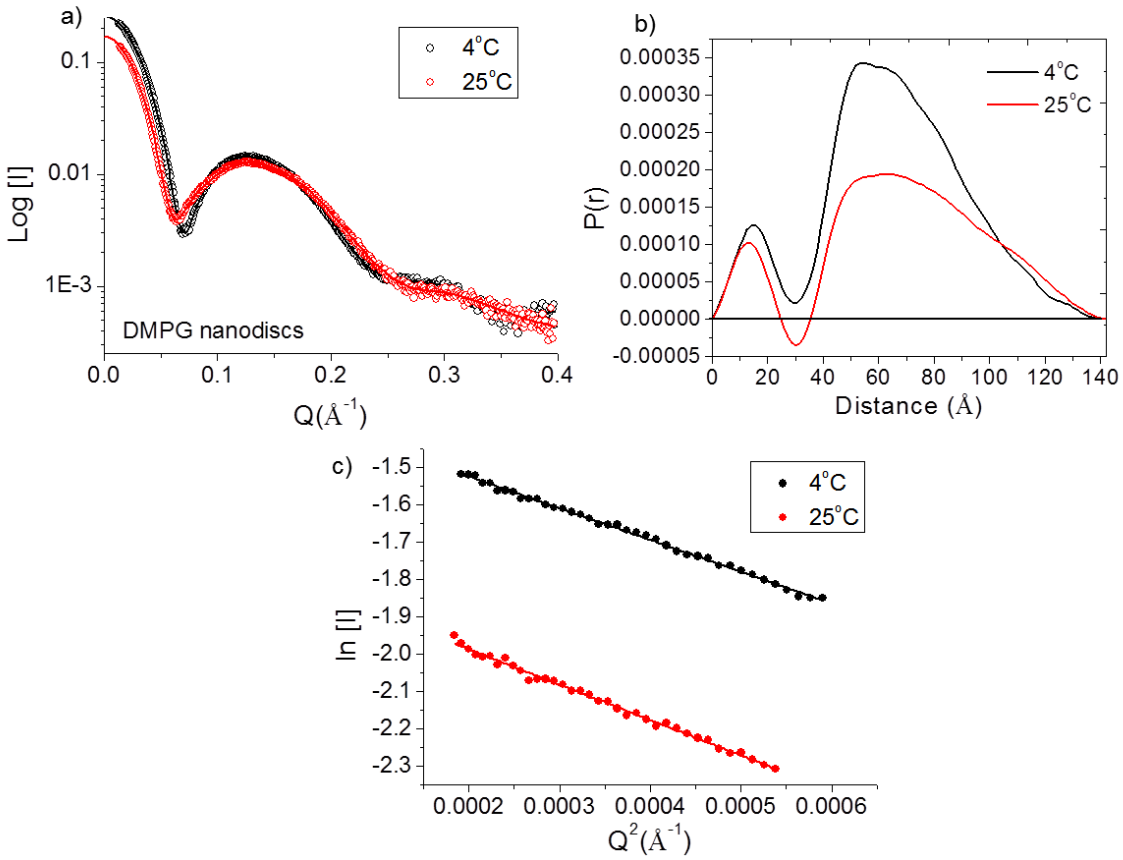

Figure 5.19 SAXS data for empty DMPG nanodiscs. a) SAXS data (symbols) and fitting (line) by GNOM. b) Distance distribution functions, P(r), calculated using GNOM. c) Guinier analysis

When comparing the SAXS data of empty nanodiscs to OmpF nanodiscs, P(r) of OmpF nanodiscs in Figure 5.20b gave much larger D_{max} and R_g as shown in Table 5.1. The consistency of R_g value and the straight line of Guinier plot (Figure 5.20c) confirm the homogeneity of the OmpF nanodiscs. This is in a good agreement with SEC, DLS and AUC data showing that DMPG nanodiscs became larger when OmpF was inserted into them. Furthermore, the P(r) showed OmpF definitely reconstituted into nanodiscs as the minimum of the curve at 30 Å, thought to be due to the lipid component, disappeared in the OmpF nanodisc samples.

Table 5.1 Summary of SAXS structural parameters for empty and OmpF nanodiscs by Guinier approximation and P(r) function.

Sample	Guinier Analysis $0.4<R_gQ<1.3$	GNOM analysis	
	R_g (Å)	R_g (Å)	D_{max}(Å)
Empty nanodisc at 4°C	50.152 ± 1.049	49.48 ± 0.022	140
Empty nanodisc at 25°C	53.607 ± 1.017	53.89 ± 0.036	143
OmpF nanodisc at 4°C	68.77 ± 0.536	69.02 ± 0.114	252
OmpF nanodisc at 25°C	67.343 ± 0.404	68.5 ± 0.129	243

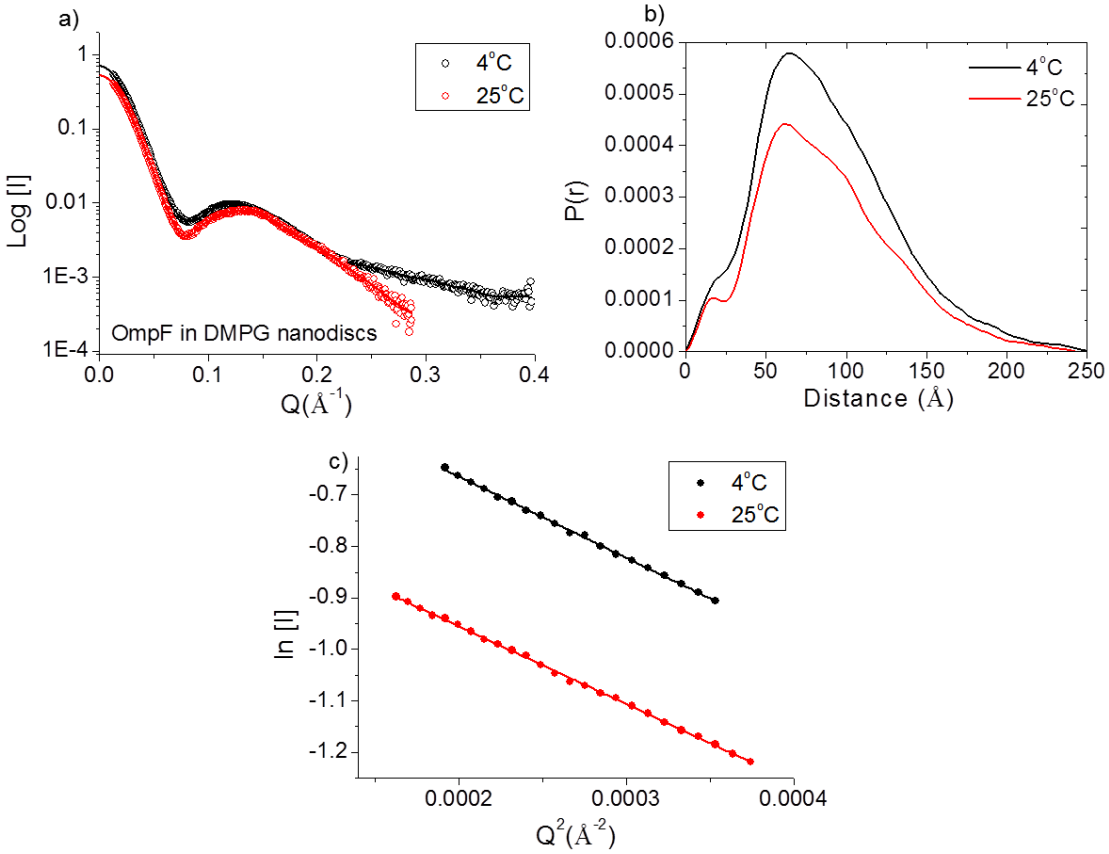

Figure 5.20 SAXS data for OmpF in DMPG nanodiscs. a) SAXS data (symbols) and fitting (line) by GNOM. b) Distance distribution functions, P(r), calculated using GNOM. c) Guinier analysis

Regarding the SANS study, the nanodisc samples were also freshly prepared onsite but the buffer was exchanged to 100% D_2O using SEC. The purpose of performing the experiment using 100% D_2O is to reduce the incoherent scattering of the buffer. This leads to the low background signal. The nanodisc samples were tested on SAXS beamline beforehand in order to confirm that the samples were free of aggregates caused by solubilising the sample in D_2O. The SANS curve of empty and OmpF nanodiscs were recorded at 25^{o}C as shown in Figure 5.21a. The P(r) generated by GNOM shows a similar result to the SAXS experiment (Figure 5.21b). It yielded the higher values of D_{max} and R_g for OmpF nanodiscs in comparison with empty nanodiscs (Table 5.2). These values between Guinier and GNOM analysis are also consistent with each other. This confirmed that there was no aggregate present in either sample. The data is currently being modelled in the group of Lise Arleth using the published methods and we hope that this will lead to a clearer understanding of how nanodiscs adapt to the inclusion of large proteins.

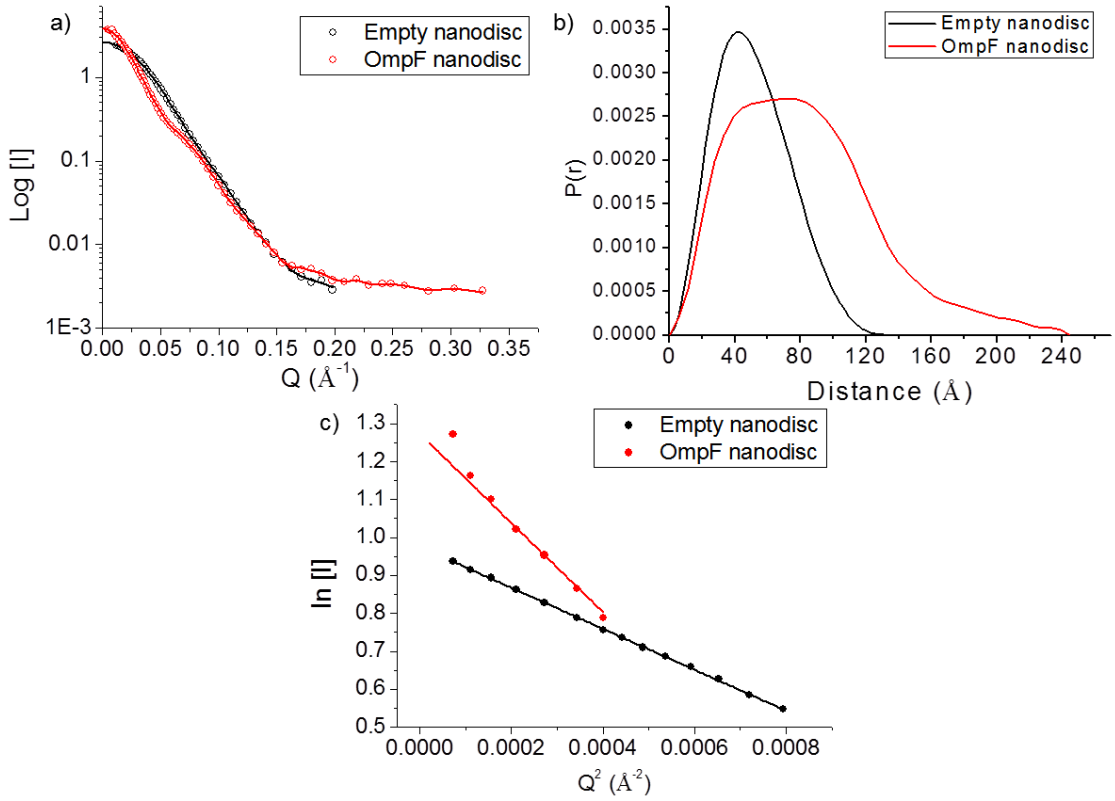

Figure 5.21 SANS data for empty and OmpF DMPG nanodiscs. a) SANS data (symbols) and fitting (lines) generated from GNOM analysis. b) Distance distribution functions calculated by GNOM. c) Guinier analysis

Table 5.2 Summary of SANS structural parameters for empty and OmpF nanodiscs by Guinier approximation and P(r) function.

Sample	Guinier Analysis $0.4<R_gQ<1.3$	GNOM analysis	
	R_g (Å)	R_g (Å)	D_{max}(Å)
Empty nanodisc at 25°C	39.091 ± 0.224	39.6 ± 0.113	137
OmpF nanodisc at 25°C	64.800 ± 0.016	66.18 ± 0.34	245

5.3 Discussion

The difficulty in studying membrane proteins (MP) is to find a suitable platform which can solubilise and stabilise MP in solution at the same time. This explains why fewer MP structures have been resolved compared to soluble proteins (White, 2009). In general, MP is handled in detergents but finding detergents for MP is a demanding task. In this chapter, novel approaches were used to study MP in solutions; OmpF is the MP studied in these experiments.

APol, a new class of detergents, has been used for a number of structural studies including NMR, SANS, EM etc (Zoonens *et al.*, 2005; Gohon *et al.*, 2008; Liao *et al.*, 2013; Lu *et al.*, 2014). OmpF were reconstituted into APol with the aim to solubilise and stablilise OmpF in solution for molecular interaction studies. The OmpF/APol complexes were studied by SEC, DLS, TEM and SANS. Unexpectedly, instead of forming individual particles in solution, TEM data indicated that OmpF/APol assembled as filaments automatically after removal of free APol by SEC. This self-association of MP/APol complexes when lacking free APol were also reported by Zoonens *et al* and Gohon *et al* (Zoonens *et al.*, 2007; Gohon *et al.*, 2008). This suggested that free APol is essential for the stability of MP/APol complexes. The SANS experiment on OmpF/APol complexes confirmed that some APol bound to OmpF dissociated from the complex after performing SEC. Once APol are removed from complexes, the remaining APol is not enough to keep OmpF soluble. Eventually, the filaments started to assemble very rapidly in one direction. The model generated from SANS data revealed that APol wraps around OmpF in a similar way to conventional detergents. The SANS also showed that free Amphipol is present meaning that a new equilibrium between free and bound Amphipol is established. The SANS experiment on these complexes was unable to give a clear evidence for the filamentous structure of complexes. The upturn at low Q region is an indication of the filamentous structure but this was observed in the sample in 100% D_2O only. The lack of this feature could be due to the fact that the scattering of free APols is stronger than that of filaments or it is difficult to see them in the Q range of SANS2D instrument. However, the

formation of filaments are easily disrupted by adding LPS to OmpF/APol complexes. A sheet-like 2D structure was formed in the presence of LPS rather than filamentous structure. This is reminiscent of the outer membrane of *E. coli* comprising OmpF and LPS and may even be a method to create 2D crystals for structural studies (Baboolal *et al.*, 2008; Arunmanee *et al.*, 2014).

OmpF was also reconstituted into nanodiscs which is an alternative approach to study MP in lipid environments. In this study, DMPG and MSP1E3D1 were chosen to prepare OmpF nanodisc because 1) the TEM data showed that making nanodiscs with DMPG gave soluble particles. 2) DMPG with negative charge mimics LPS in the outer membrane of *E. coli.* 3) MSP1E3D1 yielded a large nanodisc that is suitable for the size of OmpF trimer. The OmpF DMPG nanodiscs were studied in comparison with empty DMPG using SEC, DLS, AUC and small-angle scattering. The findings from these methods suggested that the size of OmpF-inserted nanodisc is much larger than that of empty nanodisc. However, previous studies have shown that the size of MP-inserted nanodiscs increased slightly. For example, the nanodisc of bacteriorhodopsin trimers has a hydrodynamic radius of 2 - 4 nm larger than the empty nanodiscs (Bayburt *et al.*, 2006) and cytochrome P450 nanodiscs studied by SAXS demonstrated a 3 nm increase in size (Baas *et al.*, 2004). The increase in the size of MP-inserted nanodiscs may be caused by the hydrophilic domain of MP extending into the aqueous environment. In the case of OmpF, most of the OmpF molecule consists of a large hydrophobic region that is embedded within the lipid bilayers hence the larger size was derived from the extension of MSP1E3D1. Several channel-forming MPs like OmpF have been studied in nanodiscs such as OmpX (Hagn *et al.*, 2013), FhuA (Mills *et al.*, 2014), and VDAC-1(Raschle *et al.*, 2009) but OmpF is one of the large membrane proteins which was incorporated into nanodiscs. It is concluded that the membrane scaffold protein is flexible as a larger nanodisc can be formed. It is known that a nanodisc consists of two molecules of MSP (Bayburt *et al.*, 2002) so it is likely that there are more than two MSPs in a large nanodiscs of OmpF. Consequently, studying MP in APol and nanodisc is a promising way for characterising the structure of MP. Here, we were able to incorporate OmpF

into these two platforms. It is the starting point of investigation into the structure of OmpF in complex with the bacterial toxin, colicin N, in nearly native conditions.

Chapter 6 Conclusions and Future work

Structural studies of the Colicin N translocon complex by small-angle neutron scattering

The solution structure of truncated colicin N containing translocation and receptor binding domains (ColN-TR) was investigated by small angle x-ray scattering (SAXS) and analytical ultracentrifugation (AUC). This study revealed the structure of the first 90 amino acids of the translocation domain which were absent from the crystallographic structure of ColN (Vetter *et al.*, 1998). The solution structure of ColN-TR modeled from SAXS data has three main species with different degrees of compactness but AUC shows that there is only one compact species of ColN-TR. The species will probably be in equilibrium so the AUC data may be dominated by the faster sedimenting species. Previous studies of the OmpF-ColN interaction in SDS indicated that the pore-forming domain is responsible for OmpF binding and that this is likely to reflect the later pore inserting stage (Dover *et al.*, 2000; Clifton *et al.*, 2012). According to an ITC study on the binding of different ColN constructs to OmpF in neutral detergents (Johnson *et al.*, 2013), the interaction of ColN with OmpF in these conditions is driven by the translocation domain. Therefore, we have studied the solution structure of OmpF/ColN-TR in mild detergents (OG) by small angle neutron scattering (SANS) which more likely reflects the early stage of ColN translocation. The previously extended ColN-TR structure became more compact upon binding at the perimeter of OmpF. However, an accurate molecular reconstruction of OmpF/ColN-TR cannot be achieved because of the underestimation of the contrast match point of OG.

The study of TolA II-III in solution was carried out by SAXS and AUC due to its flexibility. The extended structure of TolA II-III also confirmed by SAXS and AUC and its structure was found to be more extended that TolA II-III from *P aeruginosa* (Witty *et al.*, 2002). Interestingly, in TolA II-III complexes with OmpF in SDS studied by SANS, TolA II-III is much more compact. The observed D_{max} of TolA II-III in the complexes obtained from SANS is 110 Å while the D_{max} of

TolA II-III in solution derived from SAXS ranges from 120 to 350 Å. Results obtained from the SDS-PAGE and SANS studies showed that TolA II-III interacts with the perimeter of OmpF at the periplasmic side. We speculated that the structure of this complex may be similar to the structure of TolC (Koronakis *et al.*, 2000) as ColE1 uses TolC for its translocation (Schendel *et al.*, 1997). OmpF and TolA II-III may act as the β-barrel domain and α-helical barrel of TolC, respectively.

OmpF/LPS binding studies

The *in vitro* binding of OmpF to LPS, studied by SDS-PAGE, demonstrated that the binding of LPS to OmpF caused a slower mobility and a characteristic ladder of OmpF on a SDS-PAGE gel. OmpF in complex with different lengths of LPS, analysed by SDS-PAGE, revealed that the minimal Lipid A structure is able to bind to OmpF. Dynamic light scattering experiments showed that the aggregation of both OmpF/LPS and LPS was facilitated by calcium ions but OmpF/LPS aggregation occured more easily. It is known that calcium ions link LPS to adjacent LPS and neutralise the negative charges of LPS. The formation of OmpF/LPS complexes was a simple model of the organisation of the gram negative bacterial outer membrane which mostly contains LPS and porins. The mutagenesis and SANS study uncovered two LPS-binding sites of OmpF in its cleft and at its perimeter. Substituting the basic residues of OmpF at the extracellular side by uncharged or negatively-charged residues disrupted the OmpF-LPS interaction. The lack of any effect of single mutations showed that the negatively charged LPS interacts, via electrostatic interactions, with a group of positively charged side chains of OmpF. This finding agrees with the previous studies on the FhuA-LPS interaction (Ferguson *et al.*, 1998; Ferguson *et al.*, 2000). Interestingly, the perimeter binding site is essential for OmpF assembly *in vivo* but not *in vitro*. It indicated that LPS is involved in the pathway of OmpF biogenesis. OmpF may use the Skp/DegP pathway for its assembly since a putative LPS binding site of Skp has been discovered in the crystal structure of Skp (Walton and Sousa, 2004).

Using novel approaches to study OmpF in native conditions.

The structural studies of OmpF were carried out in two new platforms, amphipols (APol) and nanodiscs. The OmpF stablilised in APol unexpectedly assembled as filaments. The self-association of OmpF/APol complexes was observed in the depletion of free APol. The complexes interacted side by side and this led to the formation of filamentous structures seen by TEM. The filaments have a consistent width of 6 Å but are variable in length. The self-assembled filaments formed very rapidly after the removal of free APol by gel filtration. It is possible that, after free APols were removed, some APol dissociated from OmpF/APol complexes to reach a new equilibrium. This dissociation of APol from complexes was confirmed by a SANS study. These free APols must dissociate after the gel filtration step that removes the preexisting free APol. The one dimensional interaction of OmpF/APol complexes was easily disrupted by adding LPS to the complexes because LPS bound to OmpF tightly and specifically. The addition of LPS resulted in the formation of sheet-like structure especially in the presence of calcium ions. This two dimensional interaction, forming two dimensional arrays, is similar to the assembly of the gram-negative outer membrane. Previously, a similar association of OmpF has been shown in natural gram negative outer membrane (Hoenger *et al.*, 1993; Jaroslawski *et al.*, 2009).

OmpF was inserted into nanodiscs prepared from DMPC and DMPG. The electron micrograph of OmpF in DMPG nanodiscs showed evenly spread homogeneous nanodiscs on the carbon film but OmpF in DMPC nanodiscs was aggregated. This could be due to the electrostatic repulsion of the negatively charged DMPG head groups. Structural studies of OmpF in DMPG nanodiscs were performed and compared to empty DMPG nanodiscs. The findings from SEC, DLS, AUC and small angle scattering confirmed the insertion of OmpF into nanodiscs. The size of OmpF nanodiscs was larger than that of empty nanodiscs. This suggested that membrane scaffold proteins (MSP) could extend to form larger nanodiscs and that the number of MSP per disk may vary. It is known that a nanodisc contains two MSPs (Bayburt *et al.*, 2002).

Future work

Due to the underestimation of the contrast match point of OG, there remained a scatter of OG micelles which interfered with the scattering profile of OmpF/ColN-TR complexes. A new data collection of these complexes by SANS is required using the correct CMP of OG. Furthermore, we wish to study the interaction of ColN with OmpF-LPS complexes as recent studies reported that LPS also plays a role in ColN entry to gram negative bacteria (Sharma *et al.*, 2009; Johnson *et al.*, 2014). The binding studies will be performed by SPR or ITC and the structural study will be carried out by small angle scattering.

To gain a better understanding of outer membrane organization, the integrity of the native outer membrane in the presence and absence of porins or in cells expressing OmpF mutants should be studied by a SDS sensitivity assay. Additionally, the binding affinity of LPS to porins should be determined. This may explain why some porins such as FhuA can co-crystallise with LPS. Finally, the role of LPS in the assembly of outer membrane proteins should be studied in more detail.

The presence of free APols in the sample of OmpF/APol filaments will be confirmed by AUC as the SANS study only showed the individual particles of OmpF/APol complex and free APol. We could hardly observe the scatter of OmpF/APol filaments because of much stronger signal of free APol.

References

Althoff, T., Mills, D. J., Popot, J.-L. and Kuehlbrandt, W. (2011) 'Arrangement of electron transport chain components in bovine mitochondrial supercomplex I1III2IV1', *EMBO J.*, 30(22), pp. 4652-4664.

Anderluh, G., Gokce, I. and Lakey, J. H. (2004) 'A natively unfolded toxin domain uses its receptor as a folding template', *J. Biol. Chem.*, 279(21), pp. 22002-22009.

Anderluh, G., Hong, Q., Boetzel, R., MacDonald, C., Moore, G. R., Virden, R. and Lakey, J. H. (2003) 'Concerted folding and binding of a flexible colicin domain to its periplasmic receptor TolA', *J. Biol. Chem.*, 278(24), pp. 21860-21868.

Artero, J. B., Hartlein, M., McSweeney, S. and Timmins, P. (2005) 'A comparison of refined X-ray structures of hydrogenated and perdeuterated rat gamma E-crystallin in H_2O and D_2O', *Acta. Crystallogr. D.*, 61, pp. 1541-1549.

Arunmanee, W., Harris, J. R. and Lakey, J. H. (2014) 'Outer Membrane Protein F Stabilised with Minimal Amphipol Forms Linear Arrays and LPS-Dependent 2D Crystals', *J. Membr. Biol.*, 247(9-10), pp. 949-56.

Aurell, C. A. and Wistrom, A. O. (1998) 'Critical aggregation concentrations of gram-negative bacterial lipopolysaccharides (LPS)', *Biochem. Biophys. Res. Commun.*, 253(1), pp. 119-123.

Baas, B. J., Denisov, I. G. and Sliger, S. G. (2004) 'Homotropic cooperativity of monomeric cytochrome P450 3A4 in a nanoscale native bilayer environment', *Arch. Biochem. Biophys.*, 430(2), pp. 218-228.

Baboolal, T. G., Conroy, M. J., Gill, K., Ridley, H., Visudtiphole, V., Bullough, P. A. and Lakey, J. H. (2008) 'Colicin N binds to the periphery of its receptor and translocator, outer membrane protein F', *Structure*, 16(3), pp. 371-379.

Bainbridge, G., Armstrong, G. A., Dover, L. G., Whelan, K. F. and Lakey, J. H. (1998) 'Displacement of OmpF loop 3 is not required for the membrane translocation of colicins N and A *in vivo*', *FEBS Lett.*, 432(3), pp. 117-122.

Basle, A., Rummel, G., Storici, P., Rosenbusch, J. P. and Schirmer, T. (2006) 'Crystal structure of osmoporin OmpC from E-coli at 2.0 angstrom', *J. Mol. Biol.*, 362(5), pp. 933-942.

Bayburt, T. H., Grinkova, Y. V. and Sligar, S. G. (2002) 'Self-assembly of discoidal phospholipid bilayer nanoparticles with membrane scaffold proteins', *Nano Lett.*, 2(8), pp. 853-856.

Bayburt, T. H., Grinkova, Y. V. and Sligar, S. G. (2006) 'Assembly of single bacteriorhodopsin trimers in bilayer nanodiscs', *Arch. Biochem. Biophys.*, 450(2), pp. 215-222.

Bernado, P., Mylonas, E., Petoukhov, M. V., Blackledge, M. and Svergun, D. I. (2007) 'Structural characterization of flexible proteins using small-angle X-ray scattering', *J. Am. Chem. Soc.*, 129(17), pp. 5656-5664.

Berthaud, A., Manzi, J., Perez, J. and Mangenot, S. (2012) 'Modeling Detergent Organization around Aquaporin-0 Using Small-Angle X-ray Scattering', *J. Am. Chem. Soc.*, 134(24), pp. 10080-10088.

Bitto, E. and McKay, D. B. (2003) 'The periplasmic molecular chaperone protein SurA binds a peptide motif that is characteristic of integral outer membrane proteins', *J. Biol. Chem.*, 278(49), pp. 49316-49322.

Bitto, E. and McKay, D. B. (2004) 'Binding of phage-display-selected peptides to the periplasmic chaperone protein SurA mimics binding of unfolded outer membrane proteins', *FEBS Lett.*, 568(1-3), pp. 94-98.

Bos, M. P., Robert, V. and Tommassen, J. (2007) 'Biogenesis of the gram-negative bacterial outer membrane', *Annu. Rev. Microbiol.*, 61, pp. 191-214.

Braun, V., Patzer, S. I. and Hantke, K. (2002) 'Ton-dependent colicins and microcins: modular design and evolution', *Biochimie*, 84(5-6), pp. 365-380.

Bredin, J., Simonet, V., Iyer, R., Delcour, A. H. and Pages, J. M. (2003) 'Colicins, spermine and cephalosporins: a competitive interaction with the OmpF eyelet', *Biochem. J.*, 376, pp. 245-252.

Bulieris, P. V., Behrens, S., Holst, O. and Kleinschmidt, J. H. (2003) 'Folding and insertion of the outer membrane protein OmpA is assisted by the chaperone Skp and by lipopolysaccharide', *J. Biol. Chem.*, 278(11), pp. 9092-9099.

Calcutta, A., Jessen, C. M., Behrens, M. A., Oliveira, C. L. P., Renart, M. L., Gonzalez-Ros, J. M., Otzen, D. E., Pedersen, J. S., Malmendal, A. and Nielsen, N. C. (2012) 'Mapping of unfolding states of integral helical membrane proteins by GPS-NMR and scattering techniques: TFE-induced unfolding of KcsA in DDM surfactant', *BBA-Biomembranes*, 1818(9), pp. 2290-2301.

Cao, E., Liao, M., Cheng, Y. and Julius, D. (2013) 'TRPV1 structures in distinct conformations reveal activation mechanisms', *Nature*, 504(7478), pp. 113-+.

Cascales, E., Buchanan, S. K., Duche, D., Kleanthous, C., Lloubes, R., Postle, K., Riley, M., Slatin, S. and Cavard, D. (2007) 'Colicin biology', *Microbiol. Mol. Biol. Rev.*, 71(1), pp. 158-229.

Catoire, L. J., Zoonens, M., van Heijenoort, C., Giusti, F., Guittet, E. and Popot, J.-L. (2010) 'Solution NMR mapping of water-accessible residues in the transmembrane beta-barrel of OmpX', *Eur. Biophys. J. Biophy.*, 39(4), pp. 623-630.

Chen, R. and Henning, U. (1996) 'A periplasmic protein (Skp) of Escherichia coli selectively binds a class of outer membrane proteins', *Mol. Microbiol.*, 19(6), pp. 1287-1294.

Chng, S.-S., Ruiz, N., Chimalakonda, G., Silhavy, T. J. and Kahne, D. (2010) 'Characterization of the two-protein complex in *Escherichia coli* responsible for lipopolysaccharide assembly at the outer membrane', *Proc. Natl. Acad. Sci. U. S. A.*, 107(12), pp. 5363-5368.

Christie, M. P., Whitten, A. E., King, G. J., Hu, S.-H., Jarrott, R. J., Chen, K.-E., Duff, A. P., Callow, P., Collins, B. M., James, D. E. and Martin, J. L. (2012) 'Low-resolution solution structures of Munc18:Syntaxin protein complexes indicate an open binding mode driven by the Syntaxin N-peptide', *Proc. Natl. Acad. Sci. U. S. A.*, 109(25), pp. 9816-9821.

Clifton, L. A., Johnson, C. L., Solovyova, A. S., Callow, P., Weiss, K. L., Ridley, H., Le Brun, A. P., Kinane, C. J., Webster, J. R. P., Holt, S. A. and Lakey, J. H. (2012) 'Low Resolution Structure and Dynamics of a Colicin-Receptor Complex Determined by Neutron Scattering', *J. Biol. Chem.*, 287(1), pp. 337-346.

Clifton, L. A., Skoda, M. W. A., Daulton, E. L., Hughes, A. V., Le Brun, A. P., Lakey, J. H. and Holt, S. A. (2013) 'Asymmetric phospholipid: lipopolysaccharide bilayers; a Gram-negative bacterial outer membrane mimic', *J. R. Soc. Interface*, 10(89).

Cowan, S. W., Schirmer, T., Rummel, G., Steiert, M., Ghosh, R., Pauptit, R. A., Jansonius, J. N. and Rosenbusch, J. P. (1992) 'Crystal-structures explain functional-properties of two *Escherichia coli* porins', *Nature*, 358(6389), pp. 727-733.

Cvetkov, T. L., Huynh, K. W., Cohen, M. R. and Moiseenkova-Bell, V. Y. (2011) 'Molecular Architecture and Subunit Organization of TRPA1 Ion Channel Revealed by Electron Microscopy', *J. Biol. Chem.*, 286(44), pp. 38168-38176.

Dalbey, R. E., Wang, P. and Kuhn, A. (2011) 'Assembly of Bacterial Inner Membrane Proteins', *Annu. Rev. Biochem.*, 80, pp. 161-187.

de la Torre, J. G., Huertas, M. L. and Carrasco, B. (2000) 'Calculation of hydrodynamic properties of globular proteins from their atomic-level structure', *Biophys. J.*, 78(2), pp. 719-730.

Death, A., Notley, L. and Ferenci, T. (1993) 'Derepression of LamB protein facilitates outer membrane permeation of carbohydrates into *Escherichia coli* under conditions of nutrient stress', *J. Bacteriol.*, 175(5), pp. 1475-1483.

deCock, H. and Tommassen, J. (1996) 'Lipopolysaccharides and divalent cations are involved in the formation of an assembly-competent intermediate of outer-membrane protein PhoE of E-coli', *EMBO J.*, 15(20), pp. 5567-5573.

Demot, R. and Vanderleyden, J. (1994) 'The C-terminal sequence conservation between OmpA-related outer membrane proteins and MotB suggests a common function in both gram-positive and gram-negative bacteria, possibly in the interaction of these domains peptidoglycan', *Mol. Microbiol.*, 12(2), pp. 333-336.

Denisov, I. G., Grinkova, Y. V., Lazarides, A. A. and Sligar, S. G. (2004) 'Directed self-assembly of monodisperse phospholipid bilayer nanodiscs with controlled size', *J. Am. Chem. Soc.*, 126(11), pp. 3477-3487.

Denoncin, K., Schwalm, J., Vertommen, D., Silhavy, T. J. and Collet, J.-F. (2012) 'Dissecting the *Escherichia coli* periplasmic chaperone network using differential proteomics', *Proteomics*, 12(9), pp. 1391-1401.

Deprez, C., Lloubes, R., Gavioli, M., Marion, D., Guerlesquin, F. and Blanchard, L. (2005) 'Solution structure of the E. coli TolA C-terminal domain reveals conformational changes upon binding to the phage g3p N-terminal domain', *J. Mol. Biol.*, 346(4), pp. 1047-1057.

Derouiche, R., Gavioli, M., Benedetti, H., Prilipov, A., Lazdunski, C. and Lloubes, R. (1996) 'TolA central domain interacts with Escherichia coli porins', *EMBO J.*, 15(23), pp. 6408-6415.

Derouiche, R., Lloubes, R., Sasso, S., Bouteille, H., Oughideni, R., Lazdunski, C. and Loret, E. (1999) 'Circular dichroism and molecular modeling of the E-coli TolA periplasmic domains', *Biospectroscopy*, 5(3), pp. 189-198.

Diedrich, D. L., Stein, M. A. and Schnaitman, C. A. (1990) 'Associations of *Escherichia coli* K-12 OmpF trimers with rough and smooth lipopolysaccharides', *J. Bacteriol.*, 172(9), pp. 5307-5311.

Dipadova, F. E., Brade, H., Barclay, G. R., Poxton, I. R., Liehl, E., Schuetze, E., Kocher, H. P., Ramsay, G., Schreier, M. H., McClelland, D. B. L. and Rietschel, E. T. (1993) 'A broadly cross-protective monoclonal-antibody binding to *Escherichia coli* and *Salmonella* lipopolysaccharides', *Infect. Immun.*, 61(9), pp. 3863-3872.

Dover, L. G., Evans, L. J. A., Fridd, S. L., Bainbridge, G., Raggett, E. M. and Lakey, J. H. (2000) 'Colicin pore-forming domains bind to Escherichia coli trimeric porins', *Biochemistry*, 39(29), pp. 8632-8637.

Driessen, A. J. M. and Nouwen, N. (2008) 'Protein translocation across the bacterial cytoplasmic membrane', *Annu. Rev. Biochem.*, 77, pp. 643-667.

Dupuy, C., Auvray, X. and Petipas, C. (1997) 'Anomeric effects on the structure of micelles of alkyl maltosides in water', *Langmuir*, 13(15), pp. 3965-3967.

Durand, D., Vives, C., Cannella, D., Perez, J., Pebay-Peyroula, E., Vachette, P. and Fieschi, F. (2010) 'NADPH oxidase activator P67(phox) behaves in solution as a multidomain protein with semi-flexible linkers', *J. Struct. Biol.*, 169(1), pp. 45-53.

Elkins, P., Bunker, A., Cramer, W. A. and Stauffacher, C. V. (1997) 'Structure-function relationships in the channel forming domain of colicin E1', *Biophys. J.*, 72(2).

Elkouhen, R., Fierobe, H. P., Scianimanico, S., Steiert, M., Pattus, F. and Pages, J. M. (1993) 'Characterization of the receptor and translocator domains of colicin N', *Eur. J. Biochem.*, 214(3), pp. 635-639.

Evans, L. J. A., Cooper, A. and Lakey, J. H. (1996a) 'Direct measurement of the association of a protein with a family of membrane receptors', *J. Mol. Biol.*, 255(4), pp. 559-563.

Evans, L. J. A., Labeit, S., Cooper, A., Bond, L. H. and Lakey, J. H. (1996b) 'The central domain of colicin N possesses the receptor recognition site but not the binding affinity of the whole toxin', *Biochemistry*, 35(48), pp. 15143-15148.

Ferguson, A. D., Hofmann, E., Coulton, J. W., Diederichs, K. and Welte, W. (1998) 'Siderophore-mediated iron transport: Crystal structure of FhuA with bound lipopolysaccharide', *Science*, 282(5397), pp. 2215-2220.

Ferguson, A. D., Welte, W., Hofmann, E., Lindner, B., Holst, O., Coulton, J. W. and Diederichs, K. (2000) 'A conserved structural motif for lipopolysaccharide recognition by procaryotic and eucaryotic proteins', *Struct. Fold. Des.*, 8(6), pp. 585-592.

Flötenmeyer, M., Weiss, H., Tribet, C., Popot, J. L. and Leonard, K. (2007) 'The use of amphipathic polymers for cryo electron microscopy of NADH:ubiquinone oxidoreductase (complex I)', *J. Microsc.*, 227(3), pp. 229-235.

Frauenfeld, J., Gumbart, J., van der Sluis, E. O., Funes, S., Gartmann, M., Beatrix, B., Mielke, T., Berninghausen, O., Becker, T., Schulten, K. and Beckmann, R. (2011) 'Cryo-EM structure of the ribosome-SecYE complex in the membrane environment', *Nat. Struct. Mol. Biol.*, 18(5), pp. 614-U127.

Gabel, F., Lensink, M. F., Clantin, B., Jacob-Dubuisson, F., Villeret, V. and Ebel, C. (2014) 'Probing the Conformation of FhaC with Small-Angle Neutron Scattering and Molecular Modeling', *Biophys. J.*, 107(1), pp. 185-196.

Galanos, C. and Luderitz, O. (1975) 'Electrodialysis of lipopolysaccharides and their conversion to uniform salt forms', *Eur. J. Biochem.*, 54(2), pp. 603-610.

Garavito, R. M. and Rosenbusch, J. P. (1986) 'Isolation and crystallization of bacterial porin', *Methods Enzymol.*, 125, pp. 309-328.

Garidel, P., Rappolt, M., Schromm, A. B., Howe, J., Lohner, K., Andra, J., Koch, M. H. J. and Brandenburg, K. (2005) 'Divalent cations affect chain mobility and aggregate structure of lipopolysaccharide from Salmonella minnesota reflected in a decrease of its biological activity', *BBA-Biomembranes*, 1715(2), pp. 122-131.

Gasteiger, E., Gattiker, A., Hoogland, C., Ivanyi, I., Appel, R. D. and Bairoch, A. (2003) 'ExPASy: the proteomics server for in-depth protein knowledge and analysis', *Nucleic Acids Res.*, 31(13), pp. 3784-3788.

Gohon, Y., Dahmane, T., Ruigrok, R. W. H., Schuck, P., Charvolin, D., Rappaport, F., Timmins, P., Engelman, D. M., Tribet, C., Popot, J. L. and Ebel, C. (2008) 'Bacteriorhodopsin/Amphipol complexes: Structural and functional properties', *Biophys. J.*, 94(9), pp. 3523-3537.

Gohon, Y., Pavlov, G., Timmins, P., Tribet, C., Popot, J. L. and Ebel, C. (2004) 'Partial specific volume and solvent interactions of amphipol A8-35', *Anal. Biochem.*, 334(2), pp. 318-334.

Gokce, I., Raggett, E. M., Hong, Q., Virden, R., Cooper, A. and Lakey, J. H. (2000) 'The TolA-recognition site of colicin N. ITC, SPR and stopped-flow fluorescence define a crucial 27-residue segment', *J. Mol. Biol.*, 304(4), pp. 621-632.

Graham, L. L., Harris, R., Villiger, W. and Beveridge, T. J. (1991) 'Freeze-substitution of gram-negative eubacteria - general cell morphology and envelope profiles', *J. Bacteriol.*, 173(5), pp. 1623-1633.

Guihard, G., Benedetti, H., Besnard, M. and Letellier, L. (1993) 'Phosphate efflux through the channels formed by colicins and phage T5 in *Escherichia coli* cells is responsible for the fall in cytoplasmic ATP', *J. Biol. Chem.*, 268(24), pp. 17775-17780.

Hagn, F., Etzkorn, M., Raschle, T. and Wagner, G. (2013) 'Optimized Phospholipid Bilayer Nanodiscs Facilitate High-Resolution Structure Determination of Membrane Proteins', *J. Am. Chem. Soc.*, 135(5), pp. 1919-1925.

Harris, J. R. (1997) *Negative Staining and Cryoelectron Microscopy*. Oxford, UK: Bios Scientific Publishers Ltd.

Hecht, O., Ridley, H., Boetzel, R., Lewin, A., Cull, N., Chalton, D. A., Lakey, J. H. and Moore, G. R. (2008) 'Self-recognition by an intrinsically disordered protein', *FEBS Lett.*, 582(17), pp. 2673-2677.

Hecht, O., Ridley, H., Lakey, J. H. and Moore, G. R. (2009) 'A Common Interaction for the Entry of Colicin N and Filamentous Phage into Escherichia coli', *J. Mol. Biol.*, 388(4), pp. 880-893.

Heenan, R. K. *FISH*. Available at: http://www.diamond.ac.uk/Beamlines/Soft-Condensed-Matter/small-angle/SAXS-Software/CCP13/FISH.html (Accessed: 27/01/2015).

Heffernan, E. J., Wu, L., Louie, J., Okamoto, S., Fierer, J. and Guiney, D. G. (1994) 'Specificity of the complement resistance and cell association phenotypes encoded by the outer-membrane protein genes rck from *Salmonella typhimurium* and ail from *Yersinia enterocolitica*', *Infect. Immun.*, 62(11), pp. 5183-5186.

Henderson, S. J. (1996) 'Monte Carlo modeling of small-angle scattering data from non-interacting homogeneous and heterogeneous particles in solution', *Biophys. J.*, 70(4), pp. 1618-1627.

Hennecke, G., Nolte, J., Volkmer-Engert, R., Schneider-Mergener, J. and Behrens, S. (2005) 'The periplasmic chaperone SurA exploits two features characteristic of integral outer membrane proteins for selective substrate recognition', *J. Biol. Chem.*, 280(25), pp. 23540-23548.

Hilsenbeck, J. L., Park, H., Chen, G., Youn, B., Postle, K. and Kang, C. H. (2004) 'Crystal structure of the cytotoxic bacterial protein colicin B at 2.5 angstrom resolution', *Mol. Microbiol.*, 51(3), pp. 711-720.

Hoenger, A., Ghosh, R., Schoenenberger, C. A., Aebi, U. and Engel, A. (1993) 'Direct in situ structural analysis of recombinant outer membrane porins expressed in an OmpA-deficient mutant *Escherichia coli* strain', *J. Struct. Biol.*, 111(3), pp. 212-221.

Hoenger, A., Gross, H., Aebi, U. and Engel, A. (1990) 'Localization of the lipopolysaccharides in metal-shadowed reconstituted lipid porin membranes', *J. Struct. Biol.*, 103(2), pp. 185-195.

Holzenburg, A., Engel, A., Kessler, R., Manz, H. J., Lustig, A. and Aebi, U. (1989) 'Rapid isolation of OmpF porin LPS complexes suitable for structure-function studies', *Biochemistry*, 28(10), pp. 4187-4193.

Housden, N. G., Hopper, J. T. S., Lukoyanova, N., Rodriguez-Larrea, D., Wojdyla, J. A., Klein, A., Kaminska, R., Bayley, H., Saibil, H. R., Robinson, C. V. and Kleanthous, C. (2013) 'Intrinsically Disordered Protein Threads Through the Bacterial Outer-Membrane Porin OmpF', *Science*, 340(6140), pp. 1570-1574.

Housden, N. G., Wojdyla, J. A., Korczynska, J., Grishkovskaya, I., Kirkpatrick, N., Brzozowski, A. M. and Kleanthous, C. (2010) 'Directed epitope delivery across the Escherichia coli outer membrane through the porin OmpF', *Proc. Natl. Acad. Sci. USA*, 107(50), pp. 21412-21417.

Ibel, K. and Stuhrmann, H. B. (1975) 'Comparison of neutron and x-ray-scattering of dilute myoglobin solutions', *J. Mol. Biol.*, 93(2), pp. 255-265.

Ito, Y., Harada, M., Ohta, S., Kagawa, Y., Aono, O., Schefer, J. and Schoenborn, B. P. (1990) 'Small-angle neutron-scattering from the reconstituted TF_1 of H^+-ATPase from thermophilic bacterium-PS3 with deuterated subunits', *J. Mol. Biol.*, 213(2), pp. 289-302.

Jacques, D. A. and Trewhella, J. (2010) 'Small-angle scattering for structural biology-Expanding the frontier while avoiding the pitfalls', *Protein Sci.*, 19(4), pp. 642-657.

Jacrot, B. (1976) 'Study of biological structures by neutron-scattering from solution', *Reports on Progress in Physics*, 39(10), pp. 911-953.

Jakes, K. S. (2014) 'Daring to be different:colicin N finds another way', *Mol. Microbiol.*, 92(3), pp. 435-439.

Jakes, K. S. and Cramer, W. A. (2012) 'Border Crossings: Colicins and Transporters', *Annu. Rev. Genet.*, 46, pp. 209-231.

Jakes, K. S. and Finkelstein, A. (2010) 'The colicin Ia receptor, Cir, is also the translocator for colicin Ia', *Mol. Microbiol.*, 75(3), pp. 567-578.

Jaroslawski, S., Duquesne, K., Sturgis, J. N. and Scheuring, S. (2009) 'High-resolution architecture of the outer membrane of the Gram-negative bacteria Roseobacter denitrificans', *Mol. Microbiol.*, 74(5), pp. 1211-1222.

Jeanteur, D., Lakey, J. H. and Pattus, F. (1991) 'The bacterial porin superfamily - sequence alignment and structure prediction', *Mol. Microbiol.*, 5(9), pp. 2153-2164.

Jeanteur, D., Schirmer, T., Fourel, D., Simonet, V., Rummel, G., Widmer, C., Rosenbusch, J. P., Pattus, F. and Pages, J. M. (1994) 'Structural and functional alterations of a colicin-resistant mutant of OmpF porin from Escherichia-coli ', *Proc. Natl. Acad. Sci. USA*, 91(22), pp. 10675-10679.

Johnson, C. L., Ridley, H., Marchetti, R., Silipo, A., Griffin, D. C., Crawford, L., Bonev, B., Molinaro, A. and Lakey, J. H. (2014) 'The antibacterial toxin colicin N binds to the inner core of lipopolysaccharide and close to its translocator protein', *Mol. Microbiol.*, 92(3), pp. 440-452.

Johnson, C. L., Ridley, H., Pengelly, R. J., Salleh, M. Z. and Lakey, J. H. (2013) 'The unstructured domain of colicin N kills *Escherichia coli*', *Mol. Microbiol.*, 89(1), pp. 84-95.

Kamio, Y. and Nikaido, H. (1976) 'Outer membrane of *Salmonella typhimurium* - accessibility of phospholipid head groups to phospholipase-c and cyanogen-bromide activated dextran in external medium', *Biochemistry*, 15(12), pp. 2561-2570.

Katayama, H., Wang, J., Tama, F., Chollet, L., Gogol, E. P., Collier, R. J. and Fisher, M. T. (2010) 'Three-dimensional structure of the anthrax toxin pore inserted into lipid nanodiscs and lipid vesicles', *Proc. Natl. Acad. Sci. U. S. A.*, 107(8), pp. 3453-3457.

Kim, K. H., Aulakh, S. and Paetzel, M. (2012) 'The bacterial outer membrane ss-barrel assembly machinery', *Protein Sci.*, 21(6), pp. 751-768.

Kim, S., Malinverni, J. C., Sliz, P., Silhavy, T. J., Harrison, S. C. and Kahne, D. (2007) 'Structure and function of an essential component of the outer membrane protein assembly machine', *Science*, 317(5840), pp. 961-964.

Kim, Y. C., Tarr, A. W. and Penfold, C. N. (2014) 'Colicin import into E. coli cells: A model system for insights into the import mechanisms of bacteriocins', *BBA-Mol. Cell. Res.*, 1843(8), pp. 1717-1731.

Kleanthous, C. (2010) 'Swimming against the tide: progress and challenges in our understanding of colicin translocation', *Nat. Rev. Microbiol.*, 8(12), pp. 843-848.

Knowles, T. J., Scott-Tucker, A., Overduin, M. and Henderson, I. R. (2009) 'Membrane protein architects: the role of the BAM complex in outer membrane protein assembly', *Nat. Rev. Microbiol.*, 7(3), pp. 206-214.

Koebnik, R. (1995) 'Proposal for a peptidoglycan-associating alpha-helical motif in the C-terminal regions of some bacterial cell-surface proteins', *Mol. Microbiol.*, 16(6), pp. 1269-1270.

Koebnik, R., Locher, K. P. and Van Gelder, P. (2000) 'Structure and function of bacterial outer membrane proteins: barrels in a nutshell', *Mol. Microbiol.*, 37(2), pp. 239-253.

Konarev, P. V., Volkov, V. V., Sokolova, A. V., Koch, M. H. J. and Svergun, D. I. (2003) 'PRIMUS: a Windows PC-based system for small-angle scattering data analysis', *J. Appl. Crystallogr.*, 36, pp. 1277-1282.

Koronakis, V., Sharff, A., Koronakis, E., Luisi, B. and Hughes, C. (2000) 'Crystal structure of the bacterial membrane protein TolC central to multidrug efflux and protein export', *Nature*, 405(6789), pp. 914-919.

Koutsioubas, A., Berthaud, A., Mangenot, S. and Perez, J. (2013) '*Ab Initio* and All-Atom Modeling of Detergent Organization around Aquaporin-0 Based on SAXS Data', *J. Phys. Chem. B.*, 117(43), pp. 13588-13594.

Kynde, S. A. R., Skar-Gislinge, N., Pedersen, M. C., Midtgaard, S. R., Simonsen, J. B., Schweins, R., Mortensen, K. and Arleth, L. (2014) 'Small-angle scattering gives direct structural information about a membrane protein inside a lipid environment', *Acta. Crystallogr. D.*, 70, pp. 371-383.

Laemmli, U. K. (1970) 'Cleavage of Structural Proteins during the Assembly of the Head of Bacteriophage T4', *Nature*, 227(5259), pp. 680-685.

Laird, M. W., Kloser, A. W. and Misra, R. (1994) 'Assembly of LamB and OmpF in deep rough lipopolysaccharide mutants of *Escherichia coli* K-12', *J. Bacteriol.*, 176(8), pp. 2259-2264.

Laue, T. M., Shah, B. D., Ridgeway, T. M. and Pelletier, S. L. (1992) *Analytical ultracentrifugation in biochemistry and polymer science*. Royal Society of Chemistry.

Lazar, S. W. and Kolter, R. (1996) 'SurA assists the folding of Escherichia coli outer membrane proteins', *J. Bacteriol.*, 178(6), pp. 1770-1773.

Lebowitz, J., Lewis, M. S. and Schuck, P. (2002) 'Modern analytical ultracentrifugation in protein science: A tutorial review', *Protein Sci.*, 11(9), pp. 2067-2079.

Li, M. Z. and Elledge, S. J. (2007) 'Harnessing homologous recombination in vitro to generate recombinant DNA via SLIC', *Nat. Methods*, 4(3), pp. 251-256.

Liao, M., Cao, E., Julius, D. and Cheng, Y. (2013) 'Structure of the TRPV1 ion channel determined by electron cryo-microscopy', *Nature*, 504(7478), pp. 107-+.

Lu, P., Bai, X.-c., Ma, D., Xie, T., Yan, C., Sun, L., Yang, G., Zhao, Y., Zhou, R., Scheres, S. H. W. and Shi, Y. (2014) 'Three-dimensional structure of human gamma-secretase', *Nature*, 512(7513), pp. 166-+.

Lubkowski, J., Hennecke, F., Pluckthun, A. and Wlodawer, A. (1999) 'Filamentous phage infection: crystal structure of g3p in complex with its coreceptor, the C-terminal domain of TolA', *Struct. Fold. Des.*, 7(6), pp. 711-722.

Luckey, M. and Nikaido, H. (1980) 'Specificity of diffusion channels produced by lambda-phage receptor protein of *Escherichia coli*', *Proc. Natl. Acad. Sci-Biol.*, 77(1), pp. 167-171.

Lupi, N., Bourgois, A., Bernadac, A., Laboucarie, S. and Pages, J. M. (1989) 'Immunological analysis of porin polymorphism in *Escherichia coli* B and K-12', *Mol. Immunol.*, 26(11), pp. 1027-1036.

McMorran, L. M., Brockwell, D. J. and Radford, S. E. (2014) 'Mechanistic studies of the biogenesis and folding of outer membrane proteins in vitro and in vivo: What have we learned to date?', *Arch. Biochem. Biophys.*, 564, pp. 265-280.

Meilleur, F., Weiss, K. L. and Myles, D. A. A. (2009) 'Deuterium labeling for neutron structure-function-dynamics analysis', *Methods in molecular biology (Clifton, N.J.)*, 544, pp. 281-92.

Merdanovic, M., Clausen, T., Kaiser, M., Huber, R. and Ehrmann, M. (2011) 'Protein Quality Control in the Bacterial Periplasm', *Annu. Rev. Microbiol.*, 65, pp. 149-+.

Mertens, H. D. T. and Svergun, D. I. (2010) 'Structural characterization of proteins and complexes using small-angle X-ray solution scattering', *J. Struct. Biol.*, 172(1), pp. 128-141.

Mills, A., Le, H.-T., Coulton, J. W. and Duong, F. (2014) 'FhuA interactions in a detergent-free nanodisc environment', *BBA-Biomembranes*, 1838(1), pp. 364-371.

Milne, J. L. S., Borgnia, M. J., Bartesaghi, A., Tran, E. E. H., Earl, L. A., Schauder, D. M., Lengyel, J., Pierson, J., Patwardhan, A. and Subramaniam, S. (2013) 'Cryo-electron microscopy - a primer for the non-microscopist', *FEBS J.*, 280(1), pp. 28-45.

Mogensen, J. E. and Otzen, D. E. (2005) 'Interactions between folding factors and bacterial outer membrane proteins', *Mol. Microbiol.*, 57(2), pp. 326-346.

Muhlradt, P. F. and Golecki, J. R. (1975) 'Asymmetrical distribution and artifactual reorientation of lipopolysaccharide in outer membrane bilayer of *Salmonella typhimurium*', *Eur. J. Biochem.*, 51(2), pp. 343-352.

Muller-Loennies, S., Lindner, B. and Brade, H. (2003) 'Structural analysis of oligosaccharides from lipopolysaccharide (LPS) of *Escherichia coli* K12 strain W3100 reveals a link between inner and outer core LPS biosynthesis', *J. Biol. Chem.*, 278(36), pp. 34090-34101.

Nakae, T. (1976) 'Outer membrane of *Salmonella* - isolation of protein complex that produces transmembrane channels', *J. Biol. Chem.*, 251(7), pp. 2176-2178.

Nath, A., Atkins, W. M. and Sligar, S. G. (2007) 'Applications of phospholipid bilayer nanodiscs in the study of membranes and membrane proteins', *Biochemistry*, 46(8), pp. 2059-2069.

Nikaido, H. (2003) 'Molecular basis of bacterial outer membrane permeability revisited', *Microbiol. Mol. Biol. Rev.*, 67(4), pp. 593-+.

Noinaj, N., Kuszak, A. J., Balusek, C., Gumbart, J. C. and Buchanan, S. K. (2014) 'Lateral Opening and Exit Pore Formation Are Required for BamA Function', *Structure*, 22(7), pp. 1055-1062.

Noinaj, N., Kuszak, A. J., Gumbart, J. C., Lukacik, P., Chang, H., Easley, N. C., Lithgow, T. and Buchanan, S. K. (2013) 'Structural insight into the biogenesis of beta-barrel membrane proteins', *Nature*, 501(7467), pp. 385-+.

O'Keeffe, A. H., East, J. M. and Lee, A. G. (2000) 'Selectivity in lipid binding to the bacterial outer membrane protein OmpF', *Biophys. J.*, 79(4), pp. 2066-2074.

Osborn, M. J., Gander, J. E., Parisi, E. and Carson, J. (1972a) 'Mechanism of assembly of outer membrane of *Salmonella typhimurium* - isolation and characterization of cytoplasmic and outer membrane', *J. Biol. Chem.*, 247(12), pp. 3962-&.

Osborn, M. J., Parisi, E. and Gander, J. E. (1972b) 'Mechanism of assembly of outer membrane of *Salmonella typhimurium* - site of synthesis of lipopolysaccharide', *J. Biol. Chem.*, 247(12), pp. 3973-&.

Parker, M. W., Pattus, F., Tucker, A. D. and Tsernoglou, D. (1989) 'Structure of the membrane-pore-forming fragment of colicin A', *Nature*, 337(6202), pp. 93-96.

Penfold, C. N., Li, C., Zhang, Y., Vankemmelbeke, M. and James, R. (2012) 'Colicin A binds to a novel binding site of TolA in the Escherichia coli periplasm', *Biochem. Soc. Trans.*, 40, pp. 1469-1474.

Petoukhov, M. V., Franke, D., Shkumatov, A. V., Tria, G., Kikhney, A. G., Gajda, M., Gorba, C., Mertens, H. D. T., Konarev, P. V. and Svergun, D. I. (2012) 'New developments in the ATSAS program package for small-angle scattering data analysis', *J. Appl. Crystallogr.*, 45, pp. 342-350.

Phale, P. S., Philippsen, A., Kiefhaber, T., Koebnik, R., Phale, V. P., Schirmer, T. and Rosenbusch, J. P. (1998) 'Stability of trimeric OmpF porin: The contributions of the latching loop L2', *Biochemistry*, 37(45), pp. 15663-15670.

Phale, P. S., Philippsen, A., Widmer, C., Phale, V. P., Rosenbusch, J. P. and Schirmer, T. (2001) 'Role of charged residues at the OmpF porin channel constriction probed by mutagenesis and simulation', *Biochemistry*, 40(21), pp. 6319-6325.

Popot, J.-L. (2010) 'Amphipols, Nanodiscs, and Fluorinated Surfactants: Three Nonconventional Approaches to Studying Membrane Proteins in Aqueous Solutions', in Kornberg, R. D., Raetz, C. R. H., Rothman, J. E. and Thorner, J. W. (eds.) *Annual Review of Biochemistry, Vol 79*. pp. 737-775.

Popot, J. L., Berry, E. A., Charvolin, D., Creuzenet, C., Ebel, C., Engelman, D. M., Flotenmeyer, M., Giusti, F., Gohon, Y., Herve, P., Hong, Q., Lakey, J. H.,

Leonard, K., Shuman, H. A., Timmins, P., Warschawski, D. E., Zito, F., Zoonens, M., Pucci, B. and Tribet, C. (2003) 'Amphipols: polymeric surfactants for membrane biology research', *Cell. Mol. Life Sci.*, 60(8), pp. 1559-1574.

Pratt, L. A., Hsing, W. H., Gibson, K. E. and Silhavy, T. J. (1996) 'From acids to osmZ: Multiple factors influence synthesis of the OmpF and OmpC porins in Escherichia coli', *Mol. Microbiol.*, 20(5), pp. 911-917.

Qu, J., Behrens-Kneip, S., Holst, O. and Kleinschmidt, J. H. (2009) 'Binding Regions of Outer Membrane Protein A in Complexes with the Periplasmic Chaperone Skp. A Site-Directed Fluorescence Study', *Biochemistry*, 48(22), pp. 4926-4936.

Qu, J., Mayer, C., Behrens, S., Holst, O. and Kleinschmidt, J. H. (2007) 'The trimeric periplasmic chaperone skp of *Escherichia coli* forms 1 : 1 complexes with outer membrane proteins via hydrophobic and electrostatic interactions', *J. Mol. Biol.*, 374(1), pp. 91-105.

Raetz, C. R. H. and Whitfield, C. (2002) 'Lipopolysaccharide endotoxins', *Annu. Rev. Biochem.*, 71, pp. 635-700.

Raggett, E. M., Bainbridge, G., Evans, L. J. A., Cooper, A. and Lakey, J. H. (1998) 'Discovery of critical tol A-binding residues in the bactericidal toxin colicin N: a biophysical approach', *Mol. Microbiol.*, 28(6), pp. 1335-1343.

Rambo, R. P. and Tainer, J. A. (2011) 'Characterizing Flexible and Intrinsically Unstructured Biological Macromolecules by SAS Using the Porod-Debye Law', *Biopolymers*, 95(8), pp. 559-571.

Rapoport, T. A. (2007) 'Protein translocation across the eukaryotic endoplasmic reticulum and bacterial plasma membranes', *Nature*, 450(7170), pp. 663-669.

Raschle, T., Hiller, S., Yu, T.-Y., Rice, A. J., Walz, T. and Wagner, G. (2009) 'Structural and Functional Characterization of the Integral Membrane Protein VDAC-1 in Lipid Bilayer Nanodiscs', *J. Am. Chem. Soc.*, 131(49), pp. 17777-17779.

Reumann, S., Maier, E., Benz, R. and Heldt, H. W. (1995) 'The membrane of leaf peroxisomes contains a porin-like channel', *J. Biol. Chem.*, 270(29), pp. 17559-17565.

Reumann, S., Maier, E., Benz, R. and Heldt, H. W. (1996) 'A specific porin is involved in the malate shuttle of leaf peroxisomes', *Biochem. Soc. Trans.*, 24(3), pp. 754-757.

Reumann, S., Maier, E., Heldt, H. W. and Benz, R. (1998) 'Permeability properties of the porin of spinach leaf peroxisomes', *Eur. J. Biochem.*, 251(1-2), pp. 359-366.

Ricci, D. P., Hagan, C. L., Kahne, D. and Silhavy, T. J. (2012) 'Activation of the Escherichia coli beta-barrel assembly machine (Bam) is required for essential components to interact properly with substrate', *Proc. Natl. Acad. Sci. U. S. A.*, 109(9), pp. 3487-3491.

Ried, G., Hindennach, I. and Henning, U. (1990) 'Role of lipopolysaccharide in assembly of *Escherichia coli* outer-membrane proteins OmpA, OmpC, and OmpF', *J. Bacteriol.*, 172(10), pp. 6048-6053.

Rietschel, E. T., Kirikae, T., Schade, F. U., Mamat, U., Schmidt, G., Loppnow, H., Ulmer, A. J., Zahringer, U., Seydel, U., Dipadova, F., Schreier, M. and Brade, H. (1994) 'Bacterial, endotoxin - molecular relationships of structure to activity and function', *FASEB J.*, 8(2), pp. 217-225.

Rigel, N. W., Ricci, D. P. and Silhavy, T. J. (2013) 'Conformation-specific labeling of BamA and suppressor analysis suggest a cyclic mechanism for beta-barrel assembly in Escherichia coli', *Proc. Natl. Acad. Sci. U. S. A.*, 110(13), pp. 5151-5156.

Ritchie, T. K., Grinkova, Y. V., Bayburt, T. H., Denisov, I. G., Zolnerciks, J. K., Atkins, W. M. and Sligar, S. G. (2009) 'Reconstitution of membrane proteins in phospholipid bilayer nanodiscs', in Duzgunes, N. (ed.) *Methods Enzymol.*, pp. 211-231.

Rizzitello, A. E., Harper, J. R. and Silhavy, T. J. (2001) 'Genetic evidence for parallel pathways of chaperone activity in the periplasm of Escherichia coli', *J. Bacteriol.*, 183(23), pp. 6794-6800.

Rosenbusch, J. (1974) 'Characterization of major envelope protein from *Escherichia coli* - regular arrangement on peptidoglycan and unusual dodecyl-sulfate binding', *J. Biol. Chem.*, 249(24), pp. 8019-8029.

Roy, A., Kucukural, A. and Zhang, Y. (2010) 'I-TASSER: a unified platform for automated protein structure and function prediction', *Nat. Protoc.*, 5(4), pp. 725-738.

Ruiz, N., Kahne, D. and Silhavy, T. J. (2009) 'TIMELINE Transport of lipopolysaccharide across the cell envelope: the long road of discovery', *Nat. Rev. Microbiol.*, 7(9), pp. 677-683.

Salvay, A. G., Communie, G. and Ebel, C. (2012) 'Sedimentation velocity analytical ultracentrifugation for intrinsically disordered proteins', *Methods in molecular biology (Clifton, N.J.)*, 896, pp. 91-105.

Sanderson, K. E., Macalist, T., Costerton, J. W. and Cheng, K. J. (1974) 'Permeability of lipopolysaccharide-deficient (rough) mutants of *Salmonella typhimurium* to antibiotics, lysozyme, and other agents', *Can. J. Microbiol.*, 20(8), pp. 1135-1145.

Schafer, U., Beck, K. and Muller, M. (1999) 'Skp, a molecular chaperone of gram-negative bacteria, is required for the formation of soluble periplasmic intermediates of outer membrane proteins', *J. Biol. Chem.*, 274(35), pp. 24567-24574.

Schein, S. J., Colombini, M. and Finkelstein, A. (1976) 'Reconstitution in planar lipid bilayers of a voltage-dependent anion-selective channel obtained from paramecium mitochondria', *J. Membr. Biol.*, 30(2), pp. 99-120.

Schendel, S. L., Click, E. M., Webster, R. E. and Cramer, W. A. (1997) 'The TolA protein interacts with colicin E1 differently than with other group A colicins', *J. Bacteriol.*, 179(11), pp. 3683-3690.

Schirmer, T., Keller, T. A., Wang, Y. F. and Rosenbusch, J. P. (1995) 'Structural basis for sugar translocation through maltoporin channels at 3.1-angstrom resolution', *Science*, 267(5197), pp. 512-514.

Schneck, E., Schubert, T., Konovalov, O. V., Quinn, B. E., Gutsmann, T., Brandenburg, K., Oliveira, R. G., Pink, D. A. and Tanaka, M. (2010) 'Quantitative determination of ion distributions in bacterial lipopolysaccharide membranes by grazing-incidence X-ray fluorescence', *Proc. Natl. Acad. Sci. U. S. A.*, 107(20), pp. 9147-9151.

Schuck, P. (2000) 'Size-distribution analysis of macromolecules by sedimentation velocity ultracentrifugation and Lamm equation modeling', *Biophys. J.*, 78(3), pp. 1606-1619.

Sen, K. and Nikaido, H. (1990) '*In vitro* trimerization of OmpF porin secreted by spheroplasts of *Escherichia coli*', *Proc. Natl. Acad. Sci. U. S. A.*, 87(2), pp. 743-747.

Sen, K. and Nikaido, H. (1991) 'Lipopolysaccharide structure required for *in vitro* trimerization of *Escherichia coli* OmpF porin', *J. Bacteriol.*, 173(2), pp. 926-928.

Sharma, O., Datsenko, K. A., Ess, S. C., Zhalnina, M. V., Wanner, B. L. and Cramer, W. A. (2009) 'Genome-wide screens: novel mechanisms in colicin import and cytotoxicity', *Mol. Microbiol.*, 73(4), pp. 571-585.

Sklar, J. G., Wu, T., Kahne, D. and Silhavy, T. J. (2007) 'Defining the roles of the periplasmic chaperones SurA, Skp, and DegP in Escherichia coli', *Genes Dev.*, 21(19), pp. 2473-2484.

Snyder, S., Kim, D. and McIntosh, T. J. (1999) 'Lipopolysaccharide bilayer structure: Effect of chemotype, core mutations, divalent cations, and temperature', *Biochemistry*, 38(33), pp. 10758-10767.

Studier, F. W., Rosenberg, A. H., Dunn, J. J. and Dubendorff, J. W. (1990) 'Use of T7 RNA-polymerase to direct expression of cloned genes', *Methods Enzymol.*, 185, pp. 60-89.

Svergun, D. I. (1992) 'Determination of the regularization parameter in indirect-transform methods using perceptual criteria', *J. Appl. Crystallogr.*, 25, pp. 495-503.

Svergun, D. I., Barberato, C. and Koch, M. H. J. (1995) 'CRYSOL - A program to evaluate x-ray solution scattering of biological macromolecules from atomic coordinates', *J. Appl. Crystallogr.*, 28, pp. 768-773.

Svergun, D. I., Richard, S., Koch, M. H. J., Sayers, Z., Kuprin, S. and Zaccai, G. (1998) 'Protein hydration in solution: Experimental observation by x-ray and neutron scattering', *Proc. Natl. Acad. Sci. U. S. A.*, 95(5), pp. 2267-2272.

Tamaki, S., Sato, T. and Matsuhas.M (1971) 'Role of lipopolysaccharides in antibiotic resistance and bacteriophage adsorption of *Escherichia coli* K-12', *J. Bacteriol.*, 105(3), pp. 968-&.

Tehei, M., Perlmutter, J. D., Giusti, F., Sachs, J. N., Zaccai, G. and Popot, J.-L. (2014) 'Thermal fluctuations in amphipol a8-35 particles: a neutron scattering and molecular dynamics study', *J. Membr. Biol.*, 247(9-10), pp. 897-908.

Tommassen, J. and Lugtenberg, B. (1982) 'Pho-regulon of *Escherichia coli* K12 - a minireview', *Ann. Microbiol. (Paris).* A133(2), pp. 243-249.

Tormo, A., Almiron, M. and Kolter, R. (1990) 'SurA, an *Escherichia coli* gene essential for survival in stationary phase', *J. Bacteriol.*, 172(8), pp. 4339-4347.

Tribet, C., Audebert, R. and Popot, J.-L. (1996) 'Amphipols: Polymers that keep membrane proteins soluble in aqueous solutions', *Proc. Natl. Acad. Sci. USA*, 93(26), pp. 15047-15050.

Tribet, C., Audebert, R. and Popot, J. L. (1997) 'Stabilization of hydrophobic colloidal dispersions in water with amphiphilic polymers: Application to integral membrane proteins', *Langmuir*, 13(21), pp. 5570-5576.

Tribet, C., Mills, D., Haider, M. and Popot, J. L. (1998) 'Scanning transmission electron microscopy study of the molecular mass of amphipol cytochrome b(6)f complexes', *Biochimie*, 80(5-6), pp. 475-482.

Vaara, M. (1993) 'Antibiotic-supersusceptible mutants of *Escherichia coli* and *Salmonella typhimurium*', *Antimicrob. Agents Chemother.*, 37(11), pp. 2255-2260.

Vandergoot, F. G., Didat, N., Pattus, F., Dowhan, W. and Letellier, L. (1993) 'Role of acidic lipids in the translocation and channel activity of colicin A and colicin N in *Escherichia coli* cells', *Eur. J. Biochem.*, 213(1), pp. 217-221.

Velkov, T., Thompson, P. E., Nation, R. L. and Li, J. (2010) 'Structure-Activity Relationships of Polymyxin Antibiotics', *J. Med. Chem.*, 53(5), pp. 1898-1916.

Vetter, I. R., Parker, M. W., Tucker, A. D., Lakey, J. H., Pattus, F. and Tsernoglou, D. (1998) 'Crystal structure of a colicin N fragment suggests a model for toxicity', *Structure*, 6(7), pp. 863-874.

Visudtiphole, V., Thomas, M. B., Chalton, D. A. and Lakey, J. H. (2005) 'Refolding of Escherichia coli outer membrane protein F in detergent creates LPS-free trimers and asymmetric dimers', *Biochem. J.*, 392, pp. 375-381.

Voulhoux, R., Bos, M. P., Geurtsen, J., Mols, M. and Tommassen, J. (2003) 'Role of a highly conserved bacterial protein in outer membrane protein assembly', *Science*, 299(5604), pp. 262-265.

Walton, T. A. and Sousa, M. C. (2004) 'Crystal structure of Skp, a prefoldin-like chaperone that protects soluble and membrane proteins from aggregation', *Mol. Cell*, 15(3), pp. 367-374.

Weiss, M. S., Abele, U., Weckesser, J., Welte, W., Schiltz, E. and Schulz, G. E. (1991) 'Molecular architecture and electrostatic properties of a bacterial porin', *Science*, 254(5038), pp. 1627-1630.

Weiss, M. S. and Schulz, G. E. (1992) 'Structure of porin refined at 1.8 angstrom resolution', *J. Mol. Biol.*, 227(2), pp. 493-509.

White, S. H. (2009) 'Biophysical dissection of membrane proteins', *Nature*, 459(7245), pp. 344-346.

Whitten, A. E., Cai, S. and Trewhella, J. (2008) 'MULCh: modules for the analysis of small-angle neutron contrast variation data from biomolecular assemblies', *J. Appl. Crystallogr.*, 41, pp. 222-226.

Wiener, M., Freymann, D., Ghosh, P. and Stroud, R. M. (1997) 'Crystal structure of colicin Ia', *Nature*, 385(6615), pp. 461-464.

Witty, M., Sanz, C., Shah, A., Grossmann, J. G., Mizuguchi, K., Perham, R. N. and Luisi, B. (2002) 'Structure of the periplasmic domain of Pseudomonas aeruginosa TolA: evidence for an evolutionary relationship with the TonB transporter protein', *EMBO J.*, 21(16), pp. 4207-4218.

Zalman, L. S., Nikaido, H. and Kagawa, Y. (1980) 'Mitochondrial outer-membrane contains a protein producing nonspecific diffusion channels', *J. Biol. Chem.*, 255(5), pp. 1771-1774.

Zimorski, V., Ku, C., Martin, W. F. and Gould, S. B. (2014) 'Endosymbiotic theory for organelle origins', *Curr. Opin. Microbiol.*, 22(0), pp. 38-48.

Zoonens, M., Catoire, L. J., Giusti, F. and Popot, J. L. (2005) 'NMR study of a membrane protein in detergent-free aqueous solution', *Proc. Natl. Acad. Sci. U. S. A.*, 102(25), pp. 8893-8898.

Zoonens, M., Giusti, F., Zito, F. and Popot, J.-L. (2007) 'Dynamics of membrane Protein/Amphipol association studied by forster resonance energy transfer: Implications for in vitro studies of amphipol-stabilized membrane proteins', *Biochemistry*, 46(36), pp. 10392-10404.

Appendix : Publications

J Membrane Biol (2014) 247:949–956
DOI 10.1007/s00232-014-9640-5

Outer Membrane Protein F Stabilised with Minimal Amphipol Forms Linear Arrays and LPS-Dependent 2D Crystals

Wanatchaporn Arunmanee · J. Robin Harris · Jeremy H. Lakey

Received: 13 December 2013 / Accepted: 11 February 2014 / Published online: 1 March 2014

Abstract Amphipols (APol) are polymers which can solubilise and stabilise membrane proteins (MP) in aqueous solutions. In contrast to conventional detergents, APol are able to keep MP soluble even when the free APol concentration is very low. Outer membrane protein F (OmpF) is the most abundant MP commonly found in the outer membrane (OM) of *Escherichia coli*. It plays a vital role in the transport of hydrophilic nutrients, as well as antibiotics, across the OM. In the present study, APol was used to solubilise OmpF to characterize its interactions with molecules such as lipopolysaccharides (LPS) or colicins. OmpF was reconstituted into APol by the removal of detergents using Bio-Beads followed by size-exclusion chromatography (SEC) to remove excess APol. OmpF/APol complexes were then analysed by SEC, dynamic light scattering (DLS) and transmission electron microscopy (TEM). TEM showed that in the absence of free APol–OmpF associated as long filaments with a thickness of ~6 nm. This indicates that the OmpF trimers lie on their sides on the carbon EM grid and that they also favour side by side association. The formation of filaments requires APol and occurs very rapidly. Addition of LPS to OmpF/APol complexes impeded filament formation and the trimers form 2D sheets which mimic the OM. Consequently, free APol is undoubtedly required to maintain the homogeneity of OmpF in solutions, but 'minimum APol' provides a new phase, which can allow weaker protein–protein and protein–lipid interactions characteristic of native membranes to take place and thus control 1D–2D crystallisation.

Keywords OmpF · Lipopolysaccharides · Amphipol · Transmission electron microscopy · Dynamic light scattering · SEC

W. Arunmanee · J. R. Harris · J. H. Lakey (✉)
Institute for Cell and Molecular Biosciences, Newcastle University, Framlington Place, Newcastle upon Tyne NE2 4HH, UK
e-mail: jeremy.lakey@ncl.ac.uk

J. R. Harris
Institute of Zoology, University of Mainz, 55099, Mainz, Germany

Introduction

Escherichia coli are gram-negative bacteria which are a normal but minor commensal in the human gut. Most *E. coli* strains are harmless to humans, however, some strains can cause food poisoning, meningitis, or septicaemia. Like all gram-negative bacteria, the cell envelope of *E. coli* is surrounded by two membranes. The additional, so called outer membrane (OM), is highly asymmetric, consisting of tightly-packed lipopolysaccharides (LPS) located in the outer leaflet and phospholipids located in the inner leaflet. This OM acts as a defensive barrier but is also extremely permeable as a result of a large number of channel-forming proteins associated with the OM (Rosenbusch 1974; Jaroslawski et al. 2009). The nonspecific channel-forming proteins in the OM are termed porins and are responsible for the influx of hydrophilic solutes and nutrients, as well as the excretion of waste products (Nakae 1976; Nikaido 2003).Outer membrane protein F (OmpF) which is the major porin of *E. coli* OM is a trimeric protein, each monomer forming a 16-stranded β-barrel channel which allows the diffusion of small hydrophilic molecules of less than ~600 kDa through its channel across the hydrophobic OM (Cowan et al. 1992). OmpF is also a receptor and a translocator of colicins, bacterial toxins

produced by *E. coli* (Evans et al. 1996; Cascales et al. 2007). Therefore, OmpF is a potential target for the design of new antibiotics (Johnson et al. 2013).

To study membrane proteins (MP) in vitro, they require detergents to stabilise them in aqueous solutions whilst remaining as native structures. It is often a demanding task to find suitable detergents to stabilise MPs outside their lipid bilayer environment. This partly explains why, relative to soluble proteins, so few high-resolution unique structures of MPs have been resolved (White 2009). To provide an alternative technology to overcome this problem, Popot and colleagues developed a novel class of detergent called *Amphipol* (APol), an amphipathic polymer comprising a hydrophilic backbone randomly grafted with hydrophobic chains. This structure enables APol to stabilise MP in detergent-free aqueous solutions (Tribet et al. 1996; Popot 2010). As APol forms multiple contacts with hydrophobic surface of MP, the rate of dissociation of APol from proteins is slow (Popot et al. 2003). Theoretically, APol can solubilise MPs in a near absence of free APol (Tribet et al. 1997; Popot et al. 2003). Since its introduction almost 20 years ago, the reconstitution of MP into APol has become a promising approach to investigate the structure and function of MP. To date, structural studies on several MP stabilised by APol have been carried out using biophysical techniques such as electron microscopy (EM) (Tribet et al. 1998; Flötenmeyer et al. 2007; Gohon et al. 2008; Althoff et al. 2011; Cvetkov et al. 2011; Cao et al. 2013; Liao et al. 2013), nuclear magnetic resonance (NMR) (Zoonens et al. 2005; Catoire et al. 2010) and small-angle neutron scattering (Gohon et al. 2008).

However, although the multiple contacts of APol to MP ensure the high affinity of APol association, less is known about the importance of free APol to the long-term stability of MP Apol complexes. Unexpectedly, Zoonens et al. (2007) reported that the removal of free APol gave rise to the association of MP/APol complexes from an initially homogenous state. Likewise, the preparation of bacteriorhodopsin/APol complexes using an approach which completely removed free APol, led to the self-organisation over months or years of bacteriorhodopsin/APol particles into long filaments. This worm-like structure observed by EM was constructed by linear association of monomeric particles (Gohon et al. 2008).

Here, we report our observations of OmpF in complex with APol A8-35 in the absence of free APol. Initially, OmpF/APol complexes were prepared with the aim to study the interaction of the bacterial toxin Colicin N with OmpF (Clifton et al. 2012). However, in the absence of APol, the OmpF/APol complexes had a tendency to form long filaments, similar to those observed by Gohon et al. (2008) for bacteriorhodopsin but much more rapidly. Consequently, we studied the structure and assembly kinetics of these filaments by transmission electron microscopy (TEM) and dynamic light scattering (DLS). The effect of the OM specific lipopolysaccharide on the self-association of the OmpF/APol complexes was also examined.

Materials and Methods

Chemicals Specialist chemicals were purchased from the following suppliers octyl-polyoxyethylene (POE); Enzo, R_a-Lipopolysaccharide (R_a-LPS); Sigma Aldrich, BugBuster protein extraction reagent; Novagen, *n*-dodecyl-*β*-D-glucopyranoside (DG); Anatrace, and *n*-dodecyl-*β*-D-maltoside; Melford. Bio-Beads SM2 were from Bio-Rad. Amphipol A8-35 (APol) was a kind gift from J.L. Popot.

Expression and Purification of Wild-Type OmpF

Wild-type OmpF was produced from *E. coli* BE3000. Cells were grown in LB (Luria–Bertani) medium in a 10-l Bioflo 3000 bioreactor (New Brunswick Scientific) and growth was monitored by measuring OD_{600}. When OD_{600} reached 10.0–15.0, cells were harvested by centrifugation at 8,000×*g* at 4 °C for 10 min. WT OmpF was purified as described previously by (Lakey et al. 1985). OmpF was then precipitated in cold ethanol and resuspended in 20 mM sodium phosphate, pH 7.9, 100 mM NaCl, 0.5 % (v/v) octyl-POE.

Expression and Purification of OmpF Inclusion Bodies

OmpF inclusion bodies were overexpressed from *E. coli* BZB1107 with the plasmid pMS119 in which the *ompF* signal sequence (residues 1–22) plus the initial alanine residue are replaced by a single methionine residue (Visudtiphole et al. 2005). Transformed cells were grown at 37 °C in LB medium in flasks supplemented with 0.05 % (w/v) glucose, 100 μg/ml Ampicillin and 30 μg/ml Kanamycin. When OD_{600} reached 0.6, isopropyl *β*-D-1-thiogalactopyranoside was added to give a final concentration of 1 mM. After incubation at 37 °C for 3 h, cells were harvested by centrifugation at 8,000×*g* at 4 °C for 10 min. Inclusion bodies were purified using BugBuster protein extraction reagent, solubilised with the denaturation buffer (50 mM sodium phosphate, pH 8.0, 300 mM NaCl, and 6 M guanidinium HCL) and dialysed into 50 mM sodium phosphate, pH 8.0, 300 mM NaCl, and 6 M urea at room temperature.

Refolding OmpF in Mixed Detergents

The OmpF from solubilised inclusion bodies was refolded by a 20× dilution in 50 mM Tris/HCl, pH 8.0, 1 mM

dithiothreitol and 0.1 mM EDTA containing a mixture of 1 % (w/v) *n*-dodecyl-*β*-D-glucopyranoside (DG) and 0.4 % (w/v) *n*-dodecyl-*β*-D-maltoside (DM) following the procedure of Visudtiphole et al. 2005 with some changes. After incubation at 37 °C for 3 days, the refolding buffer was exchanged with 20 mM Tris/HCl, pH 7.4, 0.5 % (v/v) octyl POE, on 1-ml HiTrap Q Sepharose column. OmpF was then precipitated in cold ethanol and resuspended in 20 mM sodium phosphate, pH 7.9, 100 mM NaCl, 0.5 % (v/v) octyl-POE.

Reconstitution of OmpF into Amphipol A8-35

The reconstitution of OmpF into APol was carried out as previously described by Zoonens et al. 2005. APol A8-35 was added to OmpF in 20 mM sodium phosphate, pH 7.9, 100 mM NaCl, 0.5 % (v/v) octyl-POE at 1:10 protein/APol weight ratio. After incubation for 15 min at room temperature, the wet polystyrene beads (Bio-Beads SM2), prewashed with methanol and water, were added to remove octyl-POE at a 1:10 detergent/beads weight ratio and then incubated for 2 h at room temperature on a roller mixer. The beads were removed by using an Eppendorf 5424 benchtop microcentrifuge at maximum speed for 1 min.

Lipopolysaccharide Preparation

R_a-LPS was dissolved in 20 mM sodium phosphate, pH 7.9, 100 mM NaCl to give a final concentration of 2 mg/ml. The LPS solution was then sonicated in a water bath for 20 min and temperature cycled 6 times between 4 and 70 °C. The resulting solution was kept at 4 °C overnight before use.

Size-Exclusion Chromatography

Size-exclusion chromatography (SEC) was performed using an ÄKTA purification system (GE Healthcare). All buffers were filtered through a 0.22 µm filter and 100 µl samples were injected into a Superose 12 10/300 GL column which was previously equilibrated with 20 mM sodium phosphate, pH 7.9, 100 mM NaCl until a stable baseline was reached. Elution at a flow rate of 0.5 ml/min was carried out at room temperature and the proteins were detected using optical absorption at 280 nm.

Dynamic Light Scattering

DLS measurements were carried out using a Zetasizer Nano (Malvern instrument Ltd.) on 50 µl samples at 0.1–0.5 mg/ml OmpF in a quartz cuvette (Hellma 105.251-QS) at 30 °C. The size measurements and the data analysis were carried out using Zetasizer software.

Transmission Electron Microscopy

Negatively stained specimens were prepared using the single-droplet Parafilm procedure as described in (Harris 1997). Samples were adsorbed to glow-discharged carbon-coated grids and individually negatively stained with uranyl acetate (2.0 % w/v). After 30-s incubation, the excess of protein, washing and staining solution was blotted away with filter paper (Whatman No.1), and the grids air dried for a further 1–2 s. Electron micrographs were recorded at 100 kV from a Philips CM100 transmission electron microscope as digital images, using an Optronics 1824 × 1824 pixel CCD camera with an AMT40 version 5.42 image capture engine, supplied by Deben UK. From the calibrated images, feature sizes were determined within JMicroVision v1.27.

Results and Discussion

OmpF/APol Complexes Associate as Filaments in the Absence of Free APol

Native trimeric OmpF purified from *E. coli* OM was reconstituted into Amphipol 8-35 at a ratio of 1 OmpF/10 APol by weight (since the MW of an A8-35 polymer is approximately 4.3 kDa and the MW of OmpF is 37 kDa this ratio is roughly a 1 OmpF/100 APol molar ratio). The size and dispersity of the OmpF–APol complexes were then analysed by SEC in APol-free buffer. The SEC elution profiles shown in Fig. 1a indicated that the OmpF/APol complexes exiting the column were virtually monodisperse with a very small amount of aggregate, which eluted at the void volume. When comparing the SEC chromatogram of OmpF/APol complexes to that of OmpF/octyl-POE complexes eluted in octyl-POE containing buffer, the OmpF/APol particles eluted at 9.1 ml, while OmpF/octyl-POE complexes eluted at 9.8 ml indicating that the OmpF/APol particles are slightly larger than OmpF in octyl-POE.

The OmpF/APol complexes taken from the main peak were presumably free of unbound APol, but the final ratio of the two components in this sample is unknown. These complexes were negatively stained and then studied by TEM. According to the published high-resolution structure of OmpF, illustrated in Fig. 1b (Cowan et al. 1992), OmpF forms a trimer with a height of approximately 6 nm and a maximum diameter of about 10 nm. Since the SEC elution profile revealed a homogeneous population of OmpF–APol complexes marginally larger in diameter than detergent solubilised trimers, the negatively stained TEM images of OmpF/APol complexes were expected to reveal evenly dispersed single particles on the carbon film. Surprisingly, the electron micrographs (Fig. 1c) demonstrated that

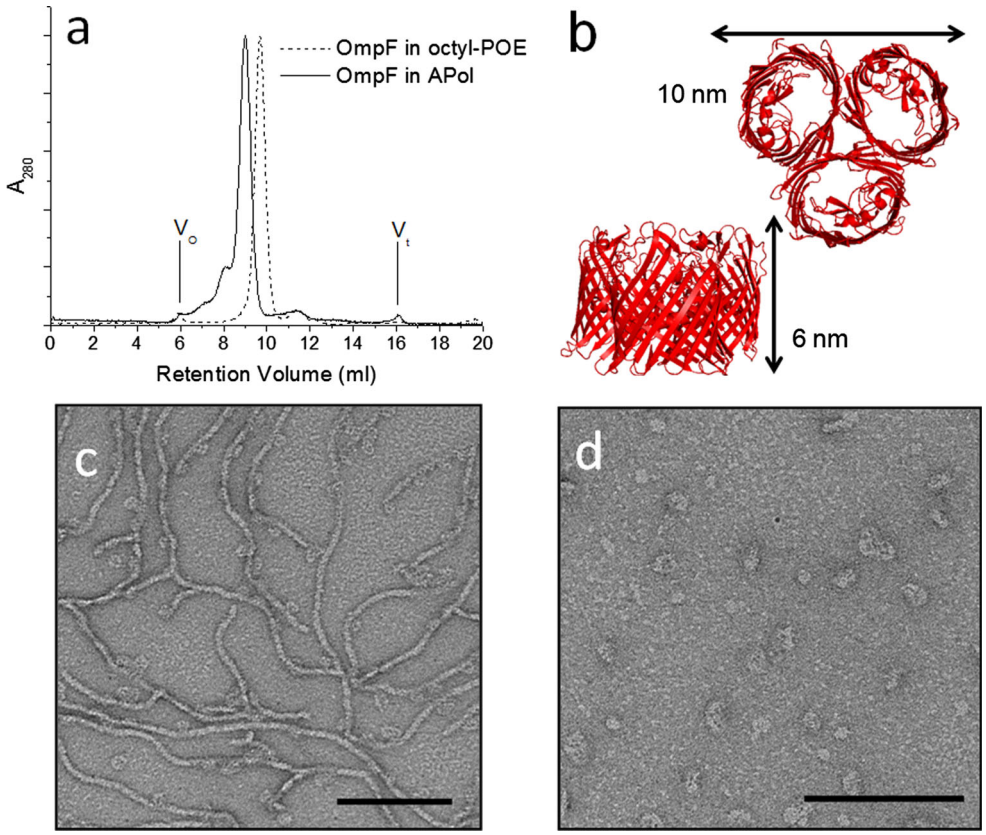

Fig. 1 Removal of free APol by SEC leads to the formation OmpF/APol filaments. **a** The comparison of size and dispersity between OmpF prepared in APol 1:10 OmpF/APol mass ratio (*solid line*) and OmpF in 0.5 % (v/v) octyl POE (*dash line*). OmpF/APol complexes were injected onto Superose 12 column equilibrated with detergent-free buffer, while buffer containing octyl-POE was used for OmpF/octyl-POE samples. Profiles have been normalised to the same maximum. **b** Top and side view of crystal structure of OmpF trimer (PDB code: 2OMPF). The diameter and height of OmpF are about 10 and 6 nm, respectively. Electron micrographs of negatively stained OmpF/APol complexes. **c** OmpF/APol filaments formed 1 day after removal of free APol by SEC. **d** The same batch of complexes after supplementing with free APol at 1:5 OmpF/APol mass ratio. Addition of free APol resulted in dissociation of the filaments. *Scale bars* 100 nm

OmpF/APol complexes formed long filaments with a characteristic width of ~6 nm. This width corresponds to the minimum dimension of OmpF, the height of the trimer, and suggests that they absorbed edge-on to the carbon film. Thus, the width of the filaments is rather constant, whereas, in contrast, the length of the long filaments is highly variable. The characteristic three pores which traverse the OmpF trimer show up as stain filled pits in negatively stained TEM images but were rarely seen within the filaments, thus supporting the suggestion that the hydrophobic edge of the filament preferentially absorbs onto the carbon film. OmpF without detergent forms large aggregates, so APol must still be present and involved in the filament structures which are stable in solution for at least a week with a complete absence of aggregates seen after centrifugation. Furthermore, filament formation by OmpF/APol complexes is reversed when adding free APol at 1:5 OmpF/APol weight ratio back to the same batch of OmpF/APol complexes containing filaments (Fig. 1d).

LPS Inhibits Self-Association of OmpF/APol Complexes

Conventionally expressed, in vivo folded, OmpF is purified from the OM of *E. coli* which contains tightly-packed LPS in the outer leaflet. OmpF extracted from this membrane often co-purifies with the significant amounts of tightly bound LPS. This OmpF–LPS interaction is stable enough to be observed by SDS-PAGE analysis of native OmpF trimers and reveals a ladder pattern of LPS-bound OmpF bands (Fig. 2a) (Baboolal et al. 2008). The number of additional bands indicates the relative amount of LPS attached to the OmpF trimers. In the initial study, above, the samples had a low LPS content but were not conclusively LPS free. Since LPS molecules cross-link to adjacent LPS via divalent cations such as Ca^{2+} and Mg^{2+} (Schneck et al. 2010), the OmpF–LPS interaction may promote lateral OmpF association. In order to clearly investigate the effect of LPS on the formation of filaments,

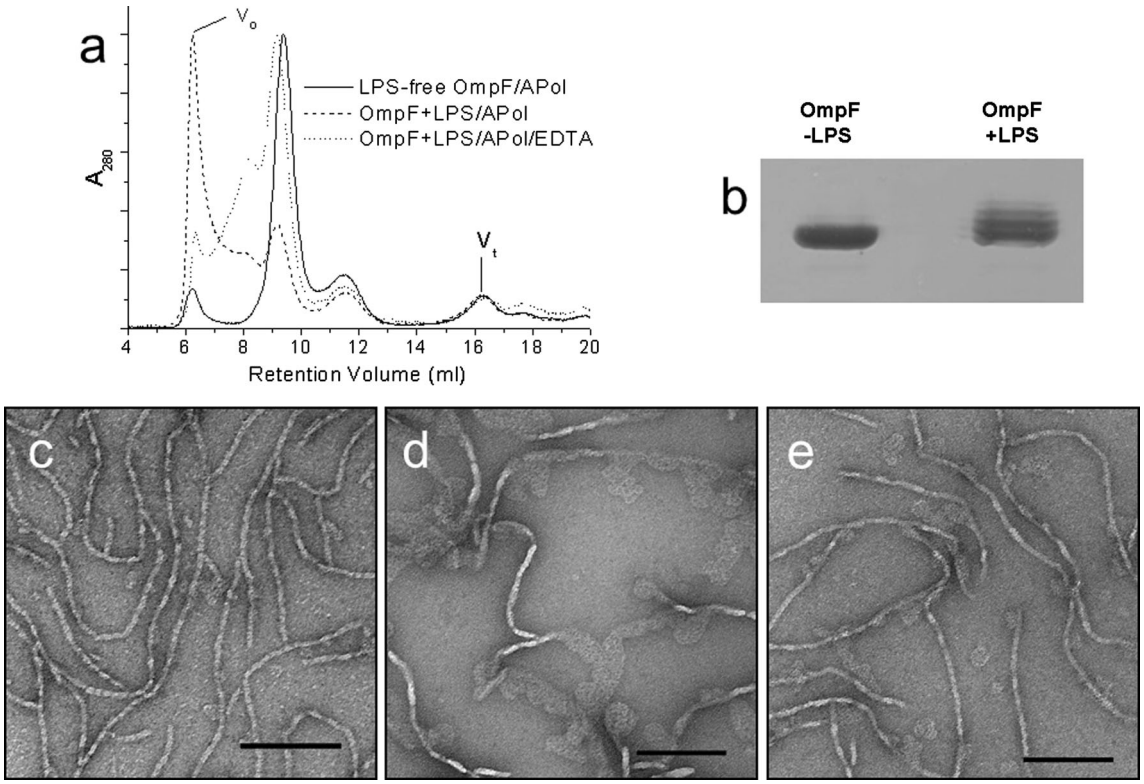

Fig. 2 Effect of lipopolysaccharides on the structure of OmpF/APol complexes. **a** SEC analysis of size and homogeneity of OmpF/APol complexes in various conditions. (*Solid line*) LPS-free OmpF, (*dashed line*) OmpF+LPS, (*dotted line*) OmpF+LPS in 1 mM EDTA. In each case, the column was pre-equilibrated with detergent-free buffer. Profiles have been normalised to the same maximum. **b** SDS-PAGE analysis of LPS-free OmpF versus OmpF with added LPS showing characteristic ladder of OmpF bands resulting from LPS binding. The number of additional bands represents the increasing number of LPS attached to OmpF. EM study of OmpF/APol complexes in the presence and absence of LPS. **c** LPS-free OmpF/Apol. **d** OmpF+LPS/APol. **e** OmpF+LPS/APol/EDTA. *Scale bars* 100 nm

LPS-free OmpF was produced by refolding OmpF from denatured inclusion bodies. In the present study, LPS-free OmpF, OmpF+LPS and OmpF+LPS in EDTA were reconstituted into APol, and the complexes were fractionated by SEC. We used 'rough' Ra-LPS lacking the outer core and O-antigen to limit the interactions to the membrane region of OmpF and this was added to LPS-free OmpF at 1:5 OmpF/LPS molecular ratio prior to incubation with APol. The addition of 1 mM EDTA removed divalent cations from the buffer to inhibit LPS–LPS association. According to SEC elution profiles shown in Fig. 2b, LPS-free OmpF/APol complexes appeared to be monodisperse with a small amount of aggregate present, whereas the bulk of the OmpF+LPS/APol sample eluted as large aggregates at the void volume. Furthermore, when OmpF+LPS/APol complexes were formed in, and eluted in SEC column buffer containing EDTA, the amount of aggregates significantly decreased leaving a mixture of OmpF/APol particles with various sizes.

The structure of OmpF/APol complexes was further studied by TEM. Using LPS-free OmpF, the filaments of OmpF/APol still appeared in the absence of free APol (Fig. 2c). However, they clearly showed a beaded structure which probably corresponds to the repetitive pattern of OmpF trimers along the chain. OmpF/APol complexes in the presence of LPS assembled as sheet-like structures rather than filaments (Fig. 2e) and this led to small areas of apparent 2D crystallisation. In fact, the filament-like structure observed in samples of OmpF+LPS/APol were, in reality, folded sheets of OmpF. Once divalent cations were chelated by EDTA, a combination of small sheet-like and filamentous structure was observed (Fig. 2d). These results indicate that LPS disrupts the linear (1D) filaments of OmpF stabilised by APol and provokes a 2D behaviour reminiscent of the natural membrane and also in vitro crystals formed by OmpF–Lipid mixtures (Hoenger et al. 1993b; Schabert and Engel 1994; Baboolal et al. 2008). Thus, the OmpF/APol structure stabilises a unique interaction where a simple, side by side, linear association of trimers is preferred over all other forms. However, this stability is easily disrupted by LPS to form 2D sheets or by excess APol to form isolated complexes. In the presence of a carbon grid surface used for EM it appears that one membrane face of the linear filament, normally stabilised

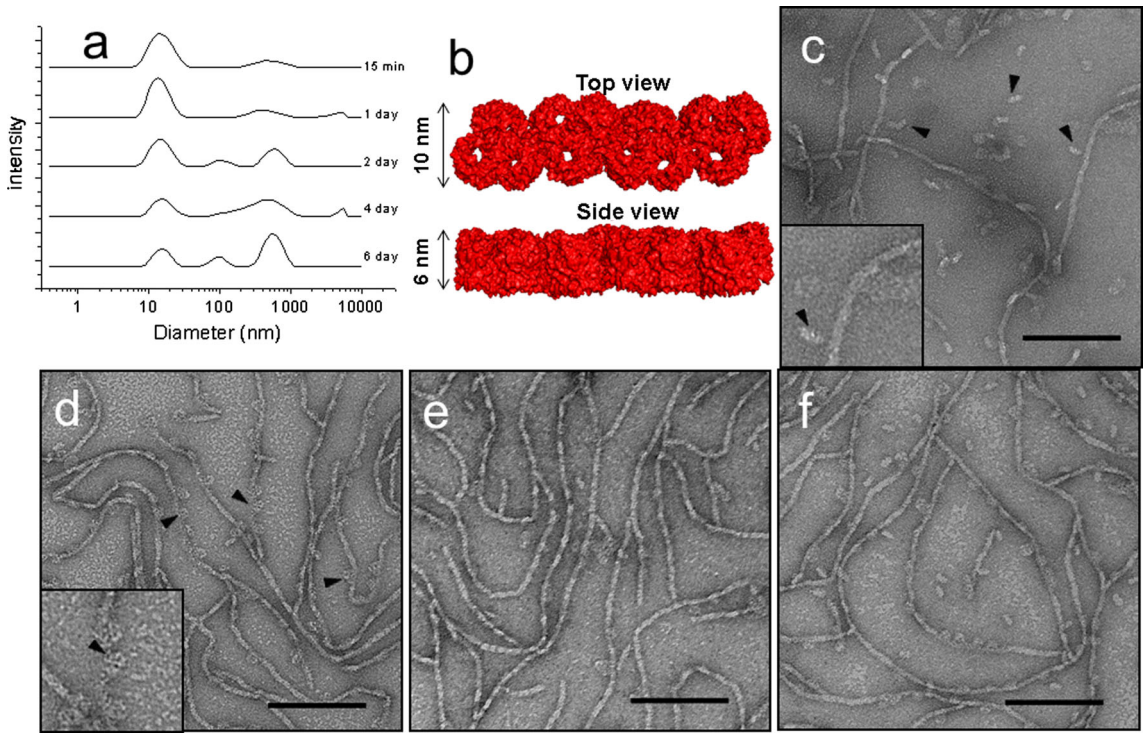

Fig. 3 Progression of filament formation by OmpF/APol complexes. **a** Size distribution of OmpF/APol complexes by intensity measured at 30 °C by DLS from 15 min to 6 days after SEC. **b** Structural models of possible OmpF filaments showing 'top' and 'side' views. Electron microscopy of OmpF/APol studied at different times after SEC. **c** After 10 min. Single particles of OmpF trimer (*arrowheads*) were present. **d** After 10 min. OmpF pores (*arrowheads*) can be seen on filaments. **e** After 1 day. **f** After 1 week. *Scale bars* 100 nm. The *insets* in **c**, **d** are at ×2 higher magnification

by APol, is adsorbed onto that surface. Thus, the APol–OmpF filaments are marginally stable and highly dynamic such that they can be influenced by small changes in their environment. They may thus be useful starting points for crystallisation studies of OmpF complexes.

Maturation of OmpF/APol Filaments

In the previous experiments, all complexes for TEM study were prepared the day before, and thus the rate of formation of OmpF/APol complexes was unknown. To measure the kinetics of OmpF/APol filament formation after the removal of free APol, the size distribution of LPS-free OmpF/APol complexes after SEC was monitored by DLS at 30 °C as a function of time. The size distributions were analysed by intensity as this mode is more sensitive to large particles in the samples. The size of OmpF trimer in conventional detergents measured by DLS is approximately 10 nm (data not shown). DLS size distribution data of OmpF/APol complexes suggested that the number of particles with sizes above 10 nm increased over time while the number of single OmpF trimers/APol decreased (Fig. 3a). Even though we measured freshly prepared complexes, a small amount of large particles was already present after 15 min. Therefore, it is evident that self-association of OmpF in the absence of free APols occurred very rapidly.

The findings from the DLS experiment are in a good agreement with an electron microscopic study on LPS-free OmpF/APol complexes. The images of negatively stained complexes were recorded at different times after SEC. The TEM images of freshly prepared complexes 10 min after filament removal of APol by SEC revealed that there was the mixture of short and long filaments, as well as individual particles of OmpF trimers (Fig. 3c, d). Groups of OmpF trimers starting to join up with the filaments can also be observed in these early samples. Interestingly, the top view of OmpF, with stain filled pores, can be occasionally seen only in freshly prepared samples, whereas this was very rarely seen with mature filaments in older samples. These measurements make it clear that single Apol stabilised OmpF trimers behave like OmpF/APol filaments in preferably attaching to the carbon film on their membrane interacting face. The 1-day-old filaments extended further after (Fig. 3e) 1 week's total incubation (Fig. 3f). In accordance with these results, it can concluded that the filaments consist of OmpF trimers bound side by side and mostly seen on their side on the EM grid as in the model shown in Fig. 3b with the long axis of the trimer arranged in line with the filament.

Conclusion

The results reveal a hierarchy of OmpF self-association which has not been observed in conventional detergents. The SEC almost certainly removes all but directly bound APol from the OmpF trimer, and this is apparently a metastable state. Rather than forming large insoluble aggregates, which form a distinct pellet when centrifuged, the resulting structures are linear filaments of fixed width. The easiest way to imagine how such an array would form is by head to tail stacking of OmpF trimers, but this clearly cannot account for the 6 nm width which corresponds to the height of a trimer. The 10 nm diameter of the trimer most likely lies in the long axis of the filament, and this is supported by the higher resolution LPS-free filaments where a significant beading is observed with an approximate 10 nm repeat. Thus, we propose that the filaments are one dimensional arrays of OmpF linked by their normally membrane exposed surfaces, but why this does not progress to 2D arrays is not clear. Is there a point of specific strong interaction between trimers that overcomes the solubility afforded by APol or does filament formation release enough APol to satisfy the need to stabilise the filaments? The filaments would appear to pre-exist in solution but on contact with the reactive carbon film on the EM grid, preferentially adsorb with one hydrophobic membrane face downwards. Thus, the first step of stabilisation in minimal APol is specific self-association, and the second one we observe is the possible displacement of APol from one face of the filament via contact with the surface. Finally, the OmpF–APol complexes reveal much about the role of LPS in OmpF association. It is known that LPS binds tightly and specifically to OmpF, but here it is shown to strongly favour the assembly of 2D crystals especially in the presence of calcium-induced cross-links. Our previous AFM experiments revealed limited ordered self-association of OmpF in octyl-POE (Cisneros et al. 2006) but the use of APol has revealed a subtlety of interaction which was suppressed by the more conventional detergents. This lateral association into quasi-crystalline arrays has been seen in natural gram-negative OMs by both electron and atomic force microscopy (Hoenger et al. 1993a; Jaroslawski et al. 2009). It suggests that reconstitution of weakly associated membrane complexes may be achieved by careful control of free APol levels.

Acknowledgments This work was supported by a Royal Thai Government Scholarship to WA and the Wellcome Trust (Grant number 093581). We thank the Newcastle University Biomedical Electron Microscopy Unit and Dr. Helen Ridley for her technical assistance. We thank Jean-Luc Popot and Christophe Tribet for advice and amphipol samples.

References

Althoff T, Mills DJ, Popot J-L, Kuehlbrandt W (2011) Arrangement of electron transport chain components in bovine mitochondrial supercomplex I1III2IV1. EMBO J 30(22):4652–4664

Baboolal TG, Conroy MJ, Gill K, Ridley H, Visudtiphole V, Bullough PA, Lakey JH (2008) Colicin N binds to the periphery of its receptor and translocator, outer membrane protein F. Structure 16(3):371–379

Cao E, Liao M, Cheng Y, Julius D (2013) TRPV1 structures in distinct conformations reveal activation mechanisms. Nature 504(7478):113

Cascales E, Buchanan SK, Duché D, Kleanthous C, Lloubès R, Postle K, Riley M, Slatin S, Cavard D (2007) Colicin biology. Microbiol Mol Biol Rev 71(1):158–229

Catoire LJ, Zoonens M, Van Heijenoort C, Giusti F, Guittet É, Popot JL (2010) Solution NMR mapping of water-accessible residues in the transmembrane β-barrel of OmpX. Eur Biophys J 39(4):623–630

Cisneros DA, Muller DJ, Daud SM, Lakey JH (2006) An approach to prepare membrane proteins for single-molecule imaging. Angew Chem Int Ed Engl 45(20):3252–3256

Clifton LA, Johnson CL, Solovyova AS, Callow P, Weiss KL, Ridley H, Le Brun AP, Kinane CJ, Webster JRP, Holt SA, Lakey JH (2012) Low resolution structure and dynamics of a colicin-receptor complex determined by neutron scattering. J Biol Chem 287(1):337–346

Cowan SW, Schirmer T, Rummel G, Steiert M, Ghosh R, Paupit RA, Jansonius JN, Rosenbusch JP (1992) Crystal structures explain functional properties of two *E. coli* porins. Nature 358:727–733

Cvetkov TL, Huynh KW, Cohen MR, Moiseenkova-Bell VY (2011) Molecular architecture and subunit organization of TRPA1 ion channel revealed by electron microscopy. J Biol Chem 286(44):38168–38176

Evans LJA, Cooper A, Lakey JH (1996) Direct measurement of the association of a protein with a family of membrane receptors. J Mol Biol 255(4):559–563

Flötenmeyer M, Weiss H, Tribet C, Popot JL, Leonard K (2007) The use of amphipathic polymers for cryo electron microscopy of NADH:ubiquinone oxidoreductase (complex I). J Microsc 227(3):229–235

Gohon Y, Dahmane T, Ruigrok RWH, Schuck P, Charvolin D, Rappaport F, Timmins P, Engelman DM, Tribet C, Popot J-L, Ebel C (2008) Bacteriorhodopsin/amphipol complexes: structural and functional properties. Biophys J 94(9):3523–3537

Harris JR (1997) Negative staining and cryoelectron microscopy. Bios Scientific Publishers Ltd., Oxford

Hoenger A, Ghosh R, Schoenenberger CA, Aebi U, Engel A (1993a) Direct in-situ structural-analysis of recombinant outer-membrane porins expressed in an OmpA-deficient mutant *Escherichia coli* strain. J Struct Biol 111(3):212–221

Hoenger A, Pagès J-M, Fourel D, Engel A (1993b) The orientation of porin OmpF in the outer membrane of *Escherichia coli*. J Mol Biol 233(3):400–413

Jaroslawski S, Duquesne K, Sturgis JN, Scheuring S (2009) High-resolution architecture of the outer membrane of the Gram-negative bacteria *Roseobacter denitrificans*. Mol Microbiol 74(5):1211–1222

Johnson CL, Ridley H, Pengelly RJ, Salleh MZ, Lakey JH (2013) The unstructured domain of colicin N kills *Escherichia coli*. Mol Microbiol 89(1):84–95

Lakey JH, Watts JP, Lea EJA (1985) Characterization of channels induced in planar bilayer-membranes by detergent solubilized *Escherichia coli* porins. Biochim Biophys Acta 817(2):208–216

Liao M, Cao E, Julius D, Cheng Y (2013) Structure of the TRPV1 ion channel determined by electron cryo-microscopy. Nature 504(7478):107

Nakae T (1976) Outer membrane of *Salmonella*. Isolation of protein complex that produces transmembrane channels. J Biol Chem 251(7):2176–2178

Nikaido H (2003) Molecular basis of bacterial outer membrane permeability revisited. Microbiol Mol Biol Rev 67(4):593

Popot J-L (2010) Amphipols, nanodiscs, and fluorinated surfactants: three nonconventional approaches to studying membrane proteins in aqueous solutions. In: Kornberg RD, Raetz CRH, Rothman JE, Thorner JW (eds) Annual review of biochemistry, vol 79., pp 737–775

Popot JL, Berry EA, Charvolin D, Creuzenet C, Ebel C, Engelman DM, Flotenmeyer M, Giusti F, Gohon Y, Herve P, Hong Q, Lakey JH, Leonard K, Shuman HA, Timmins P, Warschawski DE, Zito F, Zoonens M, Pucci B, Tribet C (2003) Amphipols: polymeric surfactants for membrane biology research. Cell Mol Life Sci 60(8):1559–1574

Rosenbusch JP (1974) Characterisation of the major envelope protein fron *Escherichia coli*. J Biol Chem 249:8019–8029

Schabert FA, Engel A (1994) Reproducible acquisition of *Escherichia coli* porin surface topographs by atomic-force microscopy. Biophys J 67(6):2394–2403

Schneck E, Schubert T, Konovalov OV, Quinn BE, Gutsmann T, Brandenburg K, Oliveira RG, Pink DA, Tanaka M (2010) Quantitative determination of ion distributions in bacterial lipopolysaccharide membranes by grazing-incidence X-ray fluorescence. Proc Natl Acad Sci USA 107(20):9147–9151

Tribet C, Audebert R, Popot J-L (1996) Amphipols: polymers that keep membrane proteins soluble in aqueous solutions. Proc Natl Acad Sci USA 93(26):15047–15050

Tribet C, Audebert R, Popot JL (1997) Stabilization of hydrophobic colloidal dispersions in water with amphiphilic polymers: application to integral membrane proteins. Langmuir 13(21): 5570–5576

Tribet C, Mills D, Haider M, Popot JL (1998) Scanning transmission electron microscopy study of the molecular mass of amphipol cytochrome b(6)f complexes. Biochimie 80(5–6):475–482

Visudtiphole V, Thomas MB, Chalton DA, Lakey JH (2005) Refolding of *Escherichia coli* outer membrane protein F in detergent creates LPS-free trimers and asymmetric dimers. Biochem J 392:375–381

White SH (2009) Biophysical dissection of membrane proteins. Nature 459(7245):344–346

Zoonens M, Catoire LJ, Giusti F, Popot JL (2005) NMR study of a membrane protein in detergent-free aqueous solution. Proc Natl Acad Sci USA 102(25):8893–8898

Zoonens M, Giusti F, Zito F, Popot J-L (2007) Dynamics of membrane protein/amphipol association studied by forster resonance energy transfer: implications for in vitro studies of amphipol-stabilized membrane proteins. Biochemistry 46(36): 10392–10404

doi:10.1017/S1431927614007776
Microsc. Microanal. 20 (Suppl 3), 2014

One and Two Dimensional Arrays of Membrane Proteins Stabilized by Amphipol

Wanatchaporn Arunmanee[1], J. Robin Harris[1,2] and Jeremy H Lakey[1]

1. Institute for Cell and Molecular Biosciences, Newcastle University, Framlington Place, Newcastle upon Tyne NE2 4HH, United Kingdom
2. Institute of Zoology, University of Mainz, D-55099 Mainz, Germany

All living cells are sounded by a lipid bilayer which forms the cell membrane and separates the aqueous intra- and extra cellular compartments. The lipid bilayer itself creates a five nanometer thick environment which is hydrophobic at its center and hydrophilic where it meets the bounding environments (Fig1). As throughout the rest of the cell, the membrane contains a repertoire of proteins which confer on it active functions such as transport, metabolism or molecular recognition. However, unlike the water soluble proteins found in the cytoplasm, the membrane proteins are highly hydrophobic where they are buried in the bilayer but hydrophilic where they face the compartments on either side. Because of this the study of purified membrane proteins is complicated by the need to recreate the mixed environment of the membrane. In some cases membranes containing only one type of protein are found in nature and one of these, the purple membrane from photosynthetic bacteria, was used to obtain the first molecular structure of a membrane protein using electron microscopy by Henderson and Unwin [1].
In most cases the membranes contain low levels of the required protein in a mixture with others and thus the protein needs to be extracted from the original membrane and purified before it can be studied in a reductionist way. To extract the protein from the membrane workers generally use detergents which dissolve the membrane and from a protective micelle around the hydrophobic regions of the membrane protein (Fig.1). Whilst the basis of many successful studies, detergents have negative aspects and, in particular, they need to be present at a concentration above that needed to from micelles. Under these conditions a complex mixture exists of protein containing micelles, empty micelles and free detergent. Furthermore the micelle is dynamic and does not recreate the surface pressure of the bilayer and can be destabilizing.

To provide an alternative technology to overcome this problem, Popot and colleagues developed a novel class of detergent called Amphipol (APol), an amphipathic polymer comprising a hydrophilic backbone randomly grafted with hydrophobic chains. This structure enables APol to stabilize MP in detergent-free aqueous solutions [2, 3].As APol forms multiple contacts with hydrophobic surface of MP (Fig1), the rate of dissociation of APol from proteins is slow [3] Theoretically, APol can solubilise membrane proteins in a near absence of free APol [2, 3]. Since its introduction almost 20 years ago structural studies on several MP stabilized by APol have been carried out using electron microscopy (EM) [4-10]

Here we show that the removal of free amphipol from purified preparations of the bacterial outer membrane protein OmpF results in the formation of linear arrays of individual protein trimers (Fig1). These filaments have been imaged by electron microscopy using negative staining [11] and reveal that the proteins lie on their hydrophobic face on the carbon grid. This appears to show that there is a preferred intermolecular interface which promotes the use of long linear arrangements of the protein. This regular arrangement may provide the basis of new approaches to use crystallinity to enhance the resolution of membrane protein structures [12, 13].

OmpF is originates from the outer membrane of *Escherichia coli* bacteria [14] which have a very asymmetric lipid bilayer comprising phospholipids on the inside and lipopolysaccharide (LPS) on the outer [12] (Fig1). LPS protects the cells from the external environment and consists of a sugar headgroup attached to a lipid tail. It is known that OmpF interacts strongly with LPS and we wished to recreate this condition in the minimal amphipol solubilized samples. The effect was striking since the addition of LPS caused the linear arrays to break down resulting in the formation of two dimensional crystals of OmpF (Fig. 1). This confirms that minimal amphipol is a "gentle" solubilizing system which does not inhibit weak interactions between membrane proteins. It suggests that reconstitution of weakly associated membrane complexes may be achieved by careful control of free Apol levels [15].

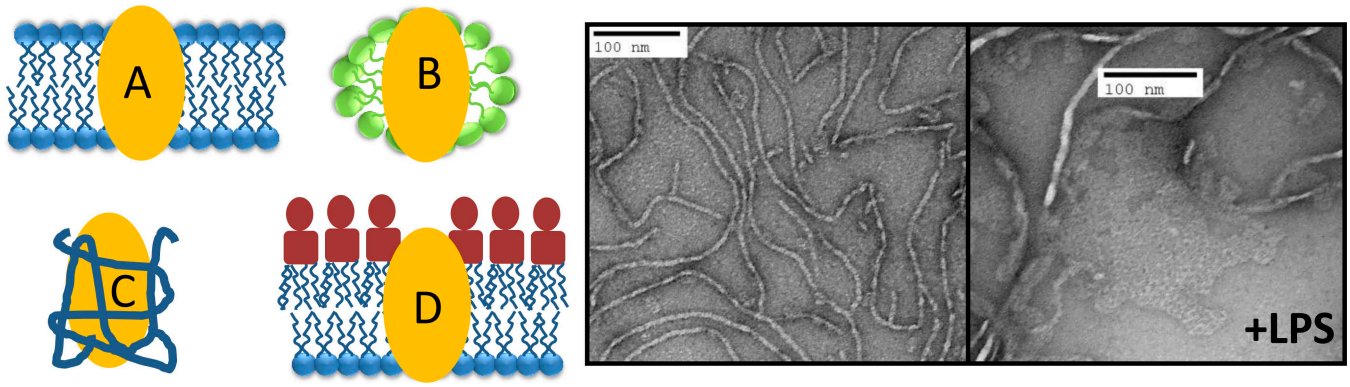

Figure 1. Left; cartoons of proteins in (A) lipid bilayer, (B) detergent micelles,(C)Amphipol, (D) E coli outer membrane with LPS shown in red. Right Negative stained EM comparison of OMPF protein in minimal APol (filaments) and with added LPS where the linear filaments break down to form 2D crystals.

1. R. Henderson and P. N. T. Unwin, *Nature,* 1975, **257**, 28-32.
2. C. Tribet, et al., *Proceedings of the National Academy of Sciences of the United States of America,* 1996, **93,** 15047-15050.
3. J. L. Popot, et al., *Cellular and Molecular Life Sciences,* 2003, **60**, 1559-1574.
4. C. Tribet, et al., *Biochimie,* 1998, **80,** 475-482.
5. M. Flötenmeyer, et al., *Journal of Microscopy,* 2007, **227**, 229-235.
6. Y. Gohon, et al., *Biophysical Journal,* 2008, **94**, 3523-3537.
7. T. Althoff, et al., *Embo Journal,* 2011, **30**, 4652-4664.
8. T. L. Cvetkov, et al., *Journal of Biological Chemistry,* 2011, **286,** 38168-38176.
9. E. Cao, et al., *Nature,* 2013, **504**, 113.
10. M. Liao, et al., *Nature,* 2013, **504**, 107.
11. J. R. Harris, *Negative Staining and Cryoelectron Microscopy,* Bios Scientific Publishers Ltd, Oxford, UK, 1997.
12. T. G. Baboolal, et al., *Structure,* 2008, **16**, 371-379.
13. L. A. Clifton, et al., *Journal of Biological Chemistry,* 2012, **287**, 337-346.
14. J. H. Lakey, et al., *Biochimica Et Biophysica Acta,* 1985, **817**, 208-216.
15. WA thanks the Royal Thai Government for a Scholarship. We thank Helen Ridley for technical assistance.